Universidade do Minho
Escola de Engenharia

Mariana Peixoto Gomes

Computational modeling of storm surges

Mariana Peixoto Gomes Computational modeling of storm surges

UMinho | 2014

outubro de 2014

Universidade do Minho
Escola de Engenharia

Mariana Peixoto Gomes

Computational modeling of storm surges

Dissertação de Mestrado
Ciclo de Estudos Integrados Conducentes ao
Grau de Mestre em Engenharia Civil

Trabalho efetuado sob a orientação do
Professor Doutor José Luís da Silva Pinho

outubro de 2014

ACKNOWLEDGEMENTS

For the development of this dissertation, a product of long months of work, several people were instrumental, to whom I express deep gratitude.

First of all, my thanks to the Department of Civil Engineering, especially the Hydraulic Engineering professors, for always inspiring and encouraging their students.

To Dr. José Luis Silva Pinho for being my advisor. Thank you for motivating me toward computational modeling, and introducing a field completely unknown to me. They say, "Choose a job you love, and you will never have to work a day in your life." Like him, I hope to continue to enclose the same eagerness.

To my colleagues, my thanks for the continued incentive, the shared wisdom, and the friendships created over the course of these five years.

To my closest friends, a great thank you for believing in me. Even with non-coinciding schedules, no matter how long the absence, things start right back where they left off!

To my aunt and uncle, Palmira and Boaventura, and my cousins, André and Bruno, for allowing me to become a part of their family system. It would not have been the same, without a doubt. Thank you for my home away from home.

To my parents, Tina and Antonio, and my brother, Tiago, for enduring five long years of absence. To them, my greatest 'thank you' for the unconditional support.

Lastly, a special 'thank you' to Carlos, a true best friend, for accompanying me through this dissertation and being my greatest motivation. An eternal 'thank you' for the patience, the affection, and the endless conversations.

RESUMO

A importância ambiental e socioeconómica das zonas costeiras é amplamente reconhecida, mas atualmente as zonas costeiras enfrentam graves enfraquecimentos e situações de alto risco. A crescente ocupação populacional e o aumento da pressão nas zonas costeiras têm contribuído para agravar essas fraquezas. Atualmente, em todo o mundo, em países com zonas costeiras, os incidentes de inundações costeiras são frequentes. Inundações costeiras são causadas por tempestades, principalmente devido à ação de ventos muito fortes. A propagação destas tempestades à costa induz a grandes aumentos de níveis de água. Numa primeira fase deste trabalho, trajetórias de tempestades previamente registadas e intensidades são caracterizadas para a Bacia do Atlântico Norte em termos da sua probabilidade de ocorrência, especificamente na região nordeste do litoral dos Estados Unidos e da região noroeste do litoral Português. Numa seguinte etapa, várias tempestades são geradas utilizando uma ferramenta específica, Delft Dashboard, para o software Delft3D-FLOW. Modelos hidrodinâmicos implementados são utilizados para simular os efeitos das tempestades gerados sobre as correntes e os níveis de água nas costas e, posteriormente, comparados com os resultados observados. Para ambos os casos, a costa nordeste dos Estados Unidos (englobando a área de The Battery, New York) e a costa noroeste Portuguesa (abrangendo a área entre o Porto e Viana do Castelo), são considerados domínios regionais altamente refinados.

É previsto que os fenómenos de alterações climáticas irão contribuir para a intensificação das tempestades costeiras. Neste contexto, uma estimativa dos riscos das inundações costeiras é de grande importância para o planeamento e gestão das zonas costeiras. Uma contribuição para a preservação e a sustentabilidade das zonas costeiras constitui o principal objetivo deste trabalho. Assim, numa segunda fase, a realização de uma série de situações hipotéticas de tempestades e análise dos seus impactos através de modelação numérica, o método conhecido como *ensemble forecasting*, é de primordial interesse em termos de decisões de planeamento costeiro. Com base em dados estatísticos e modelação numérica, são realizadas avaliações do impacto das tempestades nestas duas áreas de estudo.

Palavras-chave: tempestades; modelação numérica; avaliação de risco; *ensemble forecasting*

-

ABSTRACT

The environmental and socio-economic importance of coastal areas is widely recognized, but at present these areas face severe weaknesses and high-risk situations. The increased demand and growing human occupation of coastal zones have greatly contributed to exacerbating such weaknesses. Today, throughout the world, in countries with coastal zones, episodes of coastal flooding are frequent. Flooding is caused by coastal storms primarily due to the action of very strong winds. The propagation of these storms towards the coast induces high water levels. In a first phase of this work, historical storm tracks and intensities are characterized for the Northern Atlantic Basin, specifically the northeastern region of United States coast and the northwestern region of the Portuguese coast, in terms of their probability of occurrence. Several chosen tropical storm events are generated using a specific tool of Delft Dashboard interface for the Delft3D-FLOW software. Implemented hydrodynamic models are then used to simulate the generated storms' effects on currents and coastal water levels and subsequently compared with observed results. For both the United States' northeastern coast case (surrounding the area of The Battery, New York) and the northwestern Portuguese coast case (encompassing the area between the cities of Porto and Viana do Castelo), highly refined regional domains are considered.

It is expected that climate change phenomena will contribute to the intensification of coastal storms. In this context, an estimation of coastal flooding hazards is of paramount importance for the planning and management of coastal zones. A contribution to the preservation and sustainability of coastal zones constitutes the main aim of this work. Consequently, in a second phase, carrying out a series of hypothetical storm scenarios and analyzing their impacts through numerical modeling, known as ensemble forecasting, is of prime interest to coastal decision-makers. Based on statistical data and numerical modeling, reviews of the impact of coastal storms to these two different study areas are performed.

Keywords: Storm surges; numerical modeling; hazard assessment; ensemble forecasting

INDEX

INDEX OF FIGURES

INDEX OF TABLES

LIST OF SYMBOLS

α	-	artificial compression coefficient
$\hat{c}$	mg/L	average concentration of passive constituent A
c'	mg/L	fluctuation of the concentration relative to the temporal average
C	m/s	celerity or wave speed
C_{2D}	$m^{1/2}/s$	2D Chézy coefficient
D	m	diameter
D_H	m^2/s	horizontal eddy diffusivity coefficient
D_V	m^2/s	vertical eddy diffusivity coefficient
d	m	depth below the free surface
E	m/s	evaporation
F	(kg·m)/s	viscous force
F_ξ	m/s^2	turbulent momentum flux in ξ-direction
F_η	m/s^2	turbulent momentum flux in η-direction
Fr	-	Froude number
f	1/s	Coriolis parameter (inertial frequency)
$\sqrt{G_{\xi\xi}}$	m	coefficient used to transform curvilinear to rectangular coordinates
$\sqrt{G_{\eta\eta}}$	m	coefficient used to transform curvilinear to rectangular coordinates
g	m/s^2	acceleration due to gravity
h	m	water depth
H	m	total water depth ($H = d + \zeta$)
κ	m	Von Kármán constant ($\approx 0{,}41$)
k	m^2/s^2	turbulent kinetic energy
k_s	m	Nikuradse roughness length
L	m	wavelength
L	m	mixing length
L	$(kg·m^2)/s$	angular momentum
m	kg	mass

M_ξ	m/s^2	source or sink momentum in ξ-direction
M_η	m/s^2	source or sink momentum in η-direction
n	m$^{-1/3}$/s	Manning's coefficient
O	-	local truncation error
P	kg/(ms^2)	pressure
P	m/s	precipitation
P_ξ	kg/(m^{2}s^2)	gradient hydrostatic pressure in ξ-direction
P_η	kg/(m^{2}s^2)	gradient hydrostatic pressure in η-direction
Q	J/(m^{2}s)	heat transferred
Q	m/s	global source or sink per unit area
q_{in}	1/s	local source per unit volume
q_{out}	1/s	local sink per unit volume
r	m	distance (separation) between objects
R	m	Earth's radius
Re	-	Reynolds number
Ri	-	gradient Richardson's number
s	ppt	salinity
s	J/(K·kg)	specific entropy or entropy per unit of mass
T	°C	temperature
T	K	temperature
t	s	time
$\left\vert\vec{U}\right\vert$	m/s	magnitude of depth-averaged horizontal velocity vector (U,V)^T
u	m/s	flow velocity in the x- or ξ-direction
$\hat{u}$	m/s	temporal average of flow velocity in the x- or ξ-direction
u'	m/s	fluctuations of the flow velocity in the x- or ξ-direction
u_*	m/s	friction velocity due to currents or due to current and waves
v	m/s	flow velocity in the y- or η-direction
$\hat{v}$	m/s	temporal average of flow velocity in the y- or η-direction
v'	m/s	fluctuations of the flow velocity in the y- or η-direction

v	m/s	velocity
w	m/s	flow velocity in the z-direction
$\widehat{w}$	m/s	temporal average of flow velocity in the z-direction
w'	m/s	fluctuations of the flow velocity in the z-direction
z	-	vertical coordinate in physical space
z_0	m	bed roughness length
z_{0n}	m	roughness length normal to the boundary
δ_{ij}	-	Kronecker delta
$\Delta x^{(m,n)}$	m	cell width in the x-direction, held at the v-point of cell (m,n)
$\Delta y^{(m,n)}$	m	cell width in the y-direction, held at the u-point of cell (m,n)
ε_m	m^2/s	molecular viscosity coefficient
ε_{ti}	m^2/s	turbulent viscosity coefficient in the i-direction
ϕ	deg	latitude coordinate in spherical coordinates
λ	m^2/s	second viscosity coefficient
λ	deg	longitude coordinate in spherical coordinates
ν	m^2/s	kinematic viscosity
ν_H	m^2/s	horizontal eddy viscosity
ν_V	m^2/s	vertical eddy viscosity
η	(kg·m)/s	dynamic viscosity
η	-	horizontal curvilinear coordinate
μ_B	m^2/s	bulk viscosity
ρ	km/m^3	water density
ρ_a	km/m^3	air density
ρ_0	km/m^3	reference water density
σ	-	scaled vertical coordinate; $\sigma = \frac{z-\zeta}{d+\zeta}$
		(surface, σ = 0; bed level, σ = -1)
$\tau_{b\xi}$	$kg/(ms^2)$	bed shear stress in the ξ-direction
$\tau_{b\eta}$	$kg/(ms^2)$	bed shear stress in the η-direction

ω	m/s	velocity in the σ-direction in the σ-coordinate system
ξ	-	horizontal curvilinear coordinate

1. INTRODUCTION

1.1. Scope

Coastal flooding, derived from the occurrence of storms, constitute hazards to property and coastal populations, intensified by the growing occupation of coastal regions in recent years. These flood events are the most frequent, costly, and deadly dangers that impact coastal communities. Coastal flooding mainly results from storms and storm surges, but it also can be caused by sea level rise as a result of climate change or tsunami waves.

Coastal storms, i.e. tropical cyclones, are a common occurrence in the North Atlantic Basin. Tropical cyclones are atmospheric phenomena made up of precipitation and thunderstorms that arise over warm tropical water. They are categorized in terms of their wind speeds, as tropical depressions, tropical storms, or hurricanes. A storm surge is an irregular rise in sea level generated by tropical cyclone wind, waves, and low atmospheric pressure, measured above the normal predicted astronomical tide. A storm tide is defined as the height of the sea level, affected by a storm surge, measured above mean sea level. When coinciding with a region's high tide, a storm surge can elevate the water level significantly, resulting in disastrous effects.

Climate change is another factor when considering the causes of coastal flooding. According to the Intergovernmental Panel on Climate Change, satellite observations show that from 1993 to 2010, sea level has been rising at a rate of about 3,2 millimeters per year, a significantly higher rate than the average observed in the previous half century (Gregory, 2014). It is also expected that storms will also increase in terms of frequency and intensity which means that the coastal flooding will be a significant issue.

The third possible cause of flooding, tsunami waves, are waves of tremendous energy capable of transporting an enormous quantity of water. Tsunamis have very long wavelengths and small amplitudes which go unnoticed in deep water. The most common cause of tsunami

waves are undersea earthquakes. In the open ocean, the waves don’t lose much energy, but once they approach the coast, the steepness increases resulting in waves of great heights.

Historically, storm surges, which can sometime reach heights of up to 10 meters, have been responsible for some of the largest losses of life associated with hurricane occurrences. In the United States, the Great Galveston Hurricane of 1900 (responsible for an estimated 8000 deaths), the Miami Hurricane of 1926, the Lake Okeechobee Hurricane of 1928, the Florida Keys Labor Day Hurricane of 1935, the New England Hurricane of 1938, Hurricane Camille of 1969, and Hurricane Katrina of 2005 are all unforgettable catastrophes where the victims drowned in wind-driven flooding (NWS National Hurricane Center, 2012).

The forces caused by a cyclone's wind and waves induce currents in the water. The currents produced while the hurricane is in deep water produces little storm surge because converging water and the current's "piling up" is compensated by currents at greater depths moving water away. As the hurricane travels towards the shore onto the continental shelf, making landfall, the compensating currents are eliminated by the slope of the shelf, and the converging water rises (Rappaport & Fernandez-Partagas, 1995).

Three of the abovementioned catastrophes have dominate the United States mortality due to hurricanes record. Galveston in 1900, Lake Okeechobee in 1928 and Katrina in 2008 claimed a total of 12.000 lives. Two of these hurricanes along with 11 other deadly seasons (resulting in over 100 deaths) have struck before 1970. From 1970 to 2004 the annual average loss of life was of 21 (Willoughby, 2012). The great decrease in mortality is a result of better forecasts and warnings, which is a significant achievement in the face of the continually growing population at risk.

In this dissertation, storm surge occurrences in the North Atlantic Basin will be studied. There will be detailed analyses made of historic tropical cyclones affecting the northeastern United States' coast and the northwestern Portuguese coast. The ongoing population increase along the coast, verified in both the United States’ eastern coast and the Iberian Peninsula's western coast only exacerbates the importance of the effects of eventual coastal flooding resulting from storm surges. Much of the United States’ populated Atlantic and Gulf Coast lies in less than three meters above the mean sea level (Weather Underground, 2014). Over 75% of tropical cyclones that form in the Atlantic basin originate from tropical easterly waves that typically emerge three to four days from the coast of Africa; the other 25% of tropical cyclones typically form along the trailing ends of cold fronts or can occasionally even develop

from upper-level lows in the atmosphere (Holweg, 2000). Typically, six out of ten tropical storms that develop over the Atlantic Ocean, Caribbean Sea, and Gulf of Mexico develop into hurricanes (Dinis & Tavares, 2005). Also, about 42% of the Portuguese coast is located at low levels resulting in set of transition systems and beaches, where dunes are the sole natural defense against storms (Dinis & Tavares, 2005). In many areas, due to erosion, there has been great degradation of frontal dunes systems, leaving urban areas exposed and increasing potential flood areas. The risk of coastal flooding is so high that its quantification is essential for the establishment of proper planning and management of the coastal resources in the future.

This dissertation seeks to indentify and analyze the impact of historic tropical systems that affected both ends of the Northern Atlantic Basin. The characteristics and pathways of tropical cyclones will be explored as well as an assessment of their associated weather conditions. Numerical modeling systems are essential for a correct forecasting of the impact of coastal storms. Studying important aspects like the wind speed, water levels and possible flood regions make it possible to define the most vulnerable areas.

At present, there are hydrodynamic tools available to allow for the simulation of storms effects, provided that one knows their associated wind and atmospheric characteristics. They can be estimated based on the prediction of the velocity, atmospheric pressures, and trajectory of the storm's center. With this, it is then possible to establish proper planning and management of the coastal areas in the future. It is important to study various scenarios to identify the more susceptible areas and manage existing coastal resources for long term planning. Due to climate changes these scenarios can be exacerbated.

1.2. Objectives

The proposed research for this dissertation deals with the use of practical applications as the main objective of generating useful knowledge for advancements in the hydrodynamic modeling of storm surges. Hydrodynamic modeling is used as a representation of the motion of liquids. Two classes are common in hydrodynamic models: structured grid approaches (primarily finite difference algorithms) and unstructured grid approaches (including finite element and finite volume methods). The numerical methods deal with the domain by separating it into numerous components through a discretization process that produces a

model grid. Structured grid models tend to use quadrilateral grid cells that limit the grid's flexibility in resolving the complex shoreline but are characterized by their straightforward and efficient algorithms (NOAA Office of Coast Survey, 2014). Unstructured grid models have much more flexibility in their grid resolution by employing variable triangular elements, but tend to be more time consuming to run and more sensitive to numerical errors (NOAA Office of Coast Survey, 2014). Both types of numerical methods can been applied to high performance computing systems, enabling the simulation of complex coastal regions at high spatial and temporal resolutions. (NOAA Office of Coast Survey, 2014). The accuracy of the coastal model is very closely related to the bathymetry and the meteorological data, such as the wind velocity and atmospheric pressure. A good definition of boundary conditions, such as river inflow or tidal signals are important to be able to produce good quality outputs. The difficulty in this task lies in the attainment of quality data. Common outputs of hydrodynamic modeling are predictions in water levels, tidal currents, and waves resulting from tidal currents, meteorological and density forces.

In this dissertation, the application of Delft Dashboard and Delft3D-FLOW will be explored for the simulation of the effect of storms on the surface elevation of the water along the coast. The creation of models for storm simulations is possible with the Delft Dashboard software based on the grid generation, definition of the corresponding boundary conditions, generation of the trajectory's wind field and the storm's center wind speed. Models of historical storms, affecting the US's northeastern coast (encompassing the Hudson River mouth) and the northwestern Portuguese coast (encompassing the Douro and Lima River mouths), will be simulated and results compared to the storms' recorded values.

Additionally, the definition and subsequent simulation of probabilistic ensemble forecasts will be created to assess the vulnerability of the coast to storminess. These hypothetical scenarios are to be considered resulting from a geographical shift of typical trajectories of historic tropical storms. By comparing the different possible outcomes, one can examine how likely a particular weather event will be, and better analyze its consequences so as to better prepare coastal emergency plans, for example.

1.3. Dissertation contents

The present dissertation is organized in five chapters. The first chapter provides a general description of the theme of this dissertation, expressing the importance and value the topic has in today's society. The objectives of the dissertation are also presented.

In the second chapter, a generalized literature review will be given on some of the basics of coastal engineering. Also, the generation, classification, and the general climatology of storms will be presented. With this chapter, a better understanding of how tropical systems behave in the North Atlantic Basin, both on its eastward and westward extremities, will be given.

In the third chapter, the foundation of computational hydrodynamic models, i.e. the set of equations that describe the motion of fluids are presented and briefly explained. The descriptions of the programs utilized in the development of this dissertation will be presented, with a greater emphasis given to the pre-processing program - Delft Dashboard.

The fourth chapter will present the two analyzed case studies. First, the historical tropical systems that have occurred in the two locations will be produced and compared with observed data. Then, the vulnerability of the two same locations to storminess will be assessed with the aid of probabilistic ensemble forecasting. A methodology will be presented that considers hypothetical scenarios resulting from shifts of the already generated historical tropical systems. A Microsoft Excel sheet will be created which will randomly define values for the values of the various variables necessary in into Delft Dashboard. These values: latitude, longitude, maximum velocity, radius of maximum winds, and pressure drop, will be generated based on typically observed figures. The principal goal is to create a large range of trajectories that demonstrate correlations between one another, but at the same time produce different results.

Lastly, in the final chapter, the main conclusions of the analyzed results are presented, as well as, suggestions for future challenges.

2. LITERATURE REVIEW

In this chapter, brief descriptions will be given about the different types of waves, the reason for their generations, and their subsequent intensification or general growth. Also, a short explanation on storms will be given, particularly their formation and tendencies in terms of occurrences in the North Atlantic Basin. Because of the nature of this dissertation, the greatest threat to life and property when dealing with tropical cyclones, that is, storm surges, will also be specifically addressed.

2.1. Wave types

Surface water is variable in space and time and its shape can be described by waves that have various origins. There are four types of waves: wind-generated, tides, seiches, and tsunami. The main elements of a wave are its height and length, as represented in Figure 2-1.

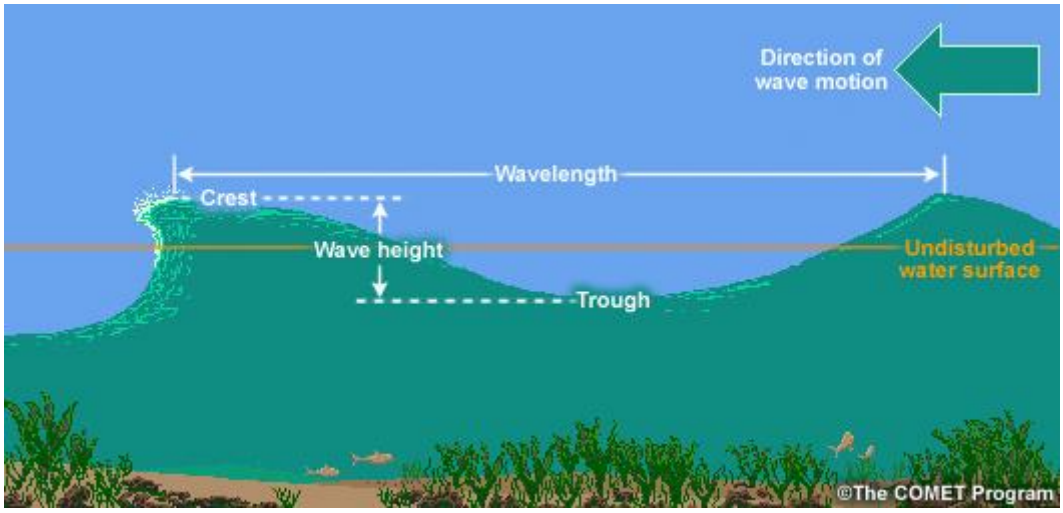

Figure 2-1 - Basic Wave Characteristics (COMET, 2003).

Wind-generated waves, or gravity waves, essentially want to restore equilibrium. The wind has a very important impact in the development of waves. The process of energy transfer from the air to water begins with a capillary wave, that is, a wave with a wavelength of less than 1,73 centimeters (COMET, 2003). It is the water's response to wind waves that typically has the greatest impact on small crafts, ships, coastal structures, and people engaging in

recreational activities in the water and along coastlines. It is important to refer that for wave growth to occur, the wind speed must be greater than the wave speed (COMET, 2003).

When considering wind-wave generation, there are two mechanisms that force growth once a wave is bigger than a capillary wave. They are form drag and frictional drag. Form drag occurs when the eddy creates a localized low pressure on the sheltered side from the wind of the wave which allows for the increase in wave height on the leading side of the wave crest. On the contrary, as localized high pressure is created, frictional drag occurs on the windward side of the leading wave, pushing down the leading edge of the wave trough, thus decreasing its height. The leading edge of the wave crest is elevated while the leading edge of the wave trough is pushed downward. On the whole, the wave height is augmented, as depicted in Figure 2-2 (COMET, 2005).

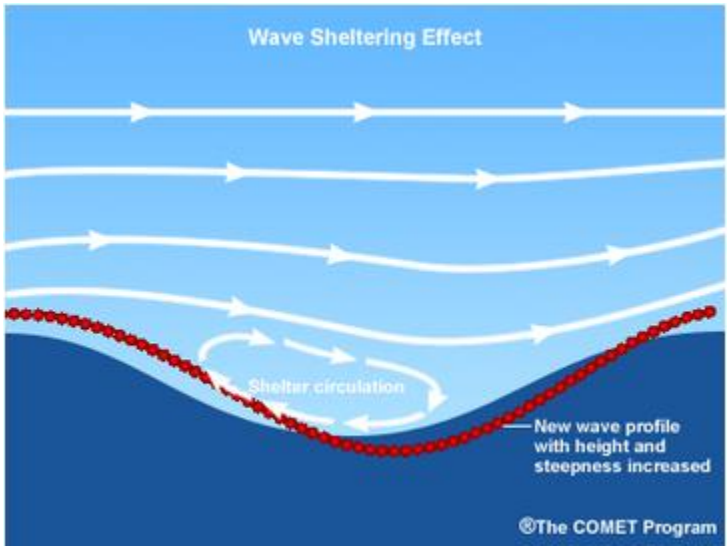

Figure 2-2 - Wave Sheltering Effect (COMET, 2005).

The direction of a wave and the magnitude of the currents depend on the frictional forces between the atmosphere and the hydrosphere. The process of energy transfer from wind to wave is complex. The wind exerts a force or stress on the ocean's surface, proportional to the square of the wind speed. The movement this causes the surface layer is not in the direction of the force, but rather at an angle to it, creating a sort of "spiral" movement across the surface layer. This is due to a Coriolis force, a deflection of a moving object when relative to a rotating reference frame. The Coriolis force acts in a direction perpendicular to the rotation of axis and to the velocity of the body in the rotating frame and is proportional to the objects speed in the rotating frame (Gordon, 2004).

The abovementioned surface layer is known as the Ekman layer and extends to about 50 to 200 meters in depth. The mean transport is 90º towards the right of the wind in the northern hemisphere and 90º to the left of the wind in the southern hemisphere. A typical surface current is approximately 3% of the wind speed, meaning that about 10 m/s wind speed gives rise to a surface current by 0,3 m/s (Gordon, 2004).

Tides, on the other hand, are essentially produced by the gravitational pull of the Sun and Moon due to the inertial and centrifugal force produced by the Earth rotating with these bodies. A tide is basically the rise and fall of the sea level. The Moon produces approximately twice the tidal effect that the Sun produces. Essentially, the body of water facing the moon results in a high tide, while the opposite side experiences a low tide. When the Sun and Moon are in line, the Sun's effect is more evident and the highest high tides and lowest low tides are observed. They are referred to as "spring tides." When the Sun and Moon are perpendicular to each other, the variation is at its lowest. These tides are usually called "neap tides." These two phenomena are portrayed in Figure 2-3 (COMET, 2003).

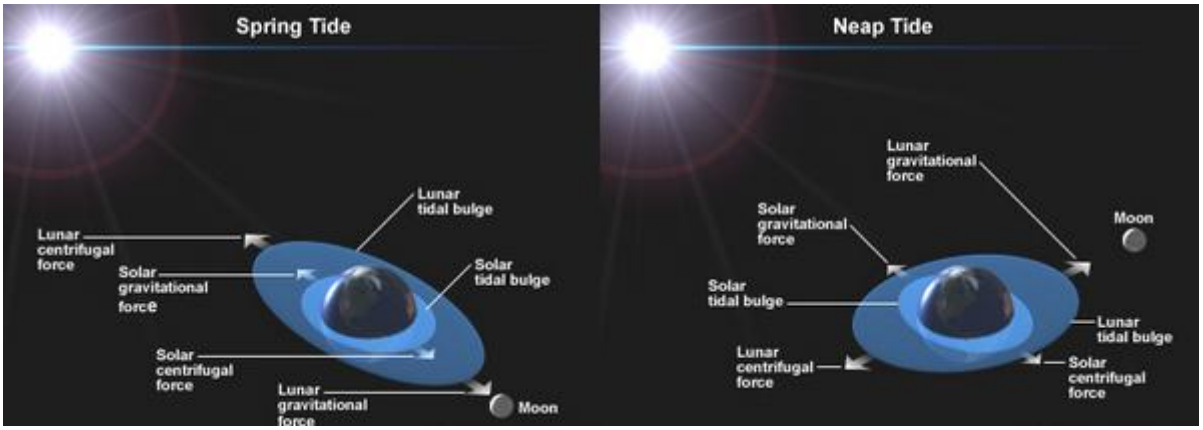

Figure 2-3 - Spring and Neap Tides (COMET, 2003).

Seiche waves are produced by earthquakes, landslides, changes of the wind, wave interaction, change in pressure, etc. Seiche waves can be described as a sloshing of water back and forth starting with a strong wind blowing down a long axis of a large body of water. When the wind settles, the water is "released" as a seiche wave. The wave then decreases due to friction. Flooding and erosion can occur at one end, while a decrease in depth on the other end can cause hazards to ships (COMET, 2003).

Lastly, tsunami waves are a series of long-period waves generated by an impulsive disturbance that displaces massive amounts of water, such as an earthquake occurring on or near the ocean floor. As the tsunami reaches the shore, the waves can become extremely large

in height, reaching tens of meters as they approach the shoreline. The effects are further amplified where a bay, harbor, or lagoon funnels the waves. The amount of water and energy contained in a tsunami can have devastating effects on coastal areas (COMET, 2003).

Tsunamis have very long wavelengths and small amplitudes which go unnoticed in deep water. In the open ocean the waves won't lose much energy. Once it travels towards the shore, the steepness increases causing the formation of waves of great heights and energy. A wave that in the open ocean measures about 0.5 meters, when encountering the shore can reach up to 30 meters in height (COMET, 2010).

At sea, water molecules move in elliptical and circular orbits as waves pass by. Near shore they move not only in ellipses but with a small net forward movement as it approaches the shore. This forward movement is called current. As waves move into shallower water, rising bottom slows the wave and shorten the wave length while increasing its height. As a tsunami wave approaches the shore, the wave speed decreases as the current speed increases. When the tsunami surges over land the two speeds are equal (COMET, 2010).

A tsunami wave is characterized as a shallow water wave. A wave is considered shallow when the quotient of the water depth and the wave length is very small. While wind-generated wave have periods of five to twenty seconds and a wavelength of 100 to 200 meters, a tsunami wave can have periods in the range of ten minutes to two hours and wavelengths greater than 500 km! The rate at which a wave loses energy is inversely proportional to its wavelength. Because tsunami wavelengths can have wavelengths greater than 500 km, it will not lose much energy as it propagates. This is why in very deep water, a tsunami can travel at very high speeds with little loss of energy. For example, at an ocean's depth of 6100 meters, a tsunami can travel about 890 km/h (Nelson, 2012)!

The most common cause of tsunami waves is undersea earthquakes. An uplift or down drop of rock and sediments above a fault results in vertical displacement of sea's floor that can extend along hundreds of kilometers along the length of the rupture. The water above the seas floor travels with it, causing a disturbance which results in dangerous radiating waves (COMET, 2010).

In order to predict which coasts are in danger of tsunami waves, seismic data, deep sea and coastal sea level data, bathymetric data, tsunami models, and DART buoys are used. This data is run through models where different numerical techniques are used to solve tsunami

propagation equations. They forecast wave height. The models solve three equations for three unknowns. Tsunamis are shallow water waves; therefore, vertical particle velocity is considered to be zero. Only the two horizontal equations of motion need to be solved with the equation of continuity. Although solutions are not exact, tsunami model output includes, forecast amplitudes, forecast currents, time traveled, inundation effects, and energy maps (COMET, 2010).

2.2. Wind-wave growth

The three major components of wave growth are wind speed, fetch length, and duration. Wind speed is the measure of motion of the air with respect to a surface of the earth covering a unit of distance over time. The fetch is the distance over which the wind blows generally from a constant direction at a constant speed, and duration is the time in which the wind affects that distance. A fully developed sea can be defined as sea state in which the wave's characteristics are not changing. Provided that the growth is not limited by fetch length, duration, the wave growth reaches an equilibrium where the energy given to the waves by the wind equals the energy dissipated by the waves through dispersion and breaking. Wave growth is ultimately determined by the wind speed, which is normally limited by the fetch length and wind duration for strong wind speed (COMET, 2005). The faster the wind, the longer the wind blows, and the bigger the area over which the wind blows, the bigger the waves (Stewart, 2006).

Wave speed, or celerity, is the speed at which an individual wave moves through water (COMET, 2003). The following equation describes wave speed for all wavelengths and wave depths.

$$C \cong \sqrt{\frac{gL}{2\pi}\tanh\left(\frac{2\pi h}{L}\right)} \quad (1)$$

As waves transition from deep ocean water waves towards the coast, they eventually get steeper. Steepness is the quotient between the wave height and the wavelength. The wave speed equation can be simplified separately for deep and shallow water use. Wave depth transitioning is depicted in Figure 2-4.

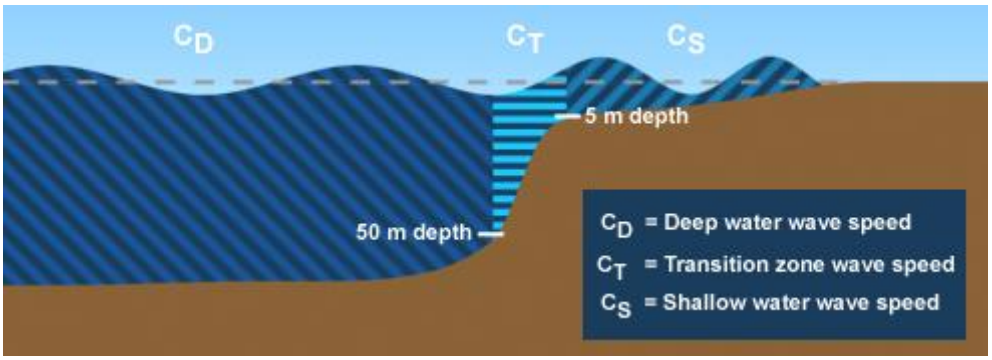

Figure 2-4 - Wave Depth Overview (COMET, 2003).

Waves are considered deep water waves when its wave height exceeds half the wavelength. Deep water wave speed, C_d, is dependent solely on wavelength, as seen in the equation below,

$$C_d = \sqrt{\frac{g \times L}{2 \times \pi}} = 2{,}26 \times \sqrt{L} \tag{2}$$

in which, g corresponds to the gravity and L corresponds to the wavelength. On the other hand, a wave is considered to be shallow as long as the wave depth is less than half the wavelength. The equation for shallow water waves can be simplified as the following,

$$C_s = \sqrt{g \times h} \tag{3}$$

in which, again, g is the gravity and h corresponds to the water depth. In this case, the wave speed is directly dependent on the depth. As the water approaches the coast, the decreasing depth causes a decrease in wave speed. In shallow water conditions, the waves are steeper and the wavelengths shorter. The transition zone is defined in terms of wavelength. In this region, the full wave equation, Equation (1), would ideally be necessary to determine the wave speed (COMET, 2003). In most realistic situations, however, the transition zone is very abrupt, and typically a wave is either considered deep or shallow.

The second most influential wave growth factor is the fetch. The fetch is the distance over which wind blows generally from a constant direction and at a constant speed, exemplified in Figure 2-5. The application of a wave nomogram can be used to find the maximum height waves in the new fetch. The timing of the height is greatly dependent on the height of the waves entering the fetch. Normally, fetch size is constrained by land masses and wind area. Comprehending how a fetch region changes and knowing if more than one region exists is essential in determining whether numerical models are correct in their forecasts (COMET, 2005).

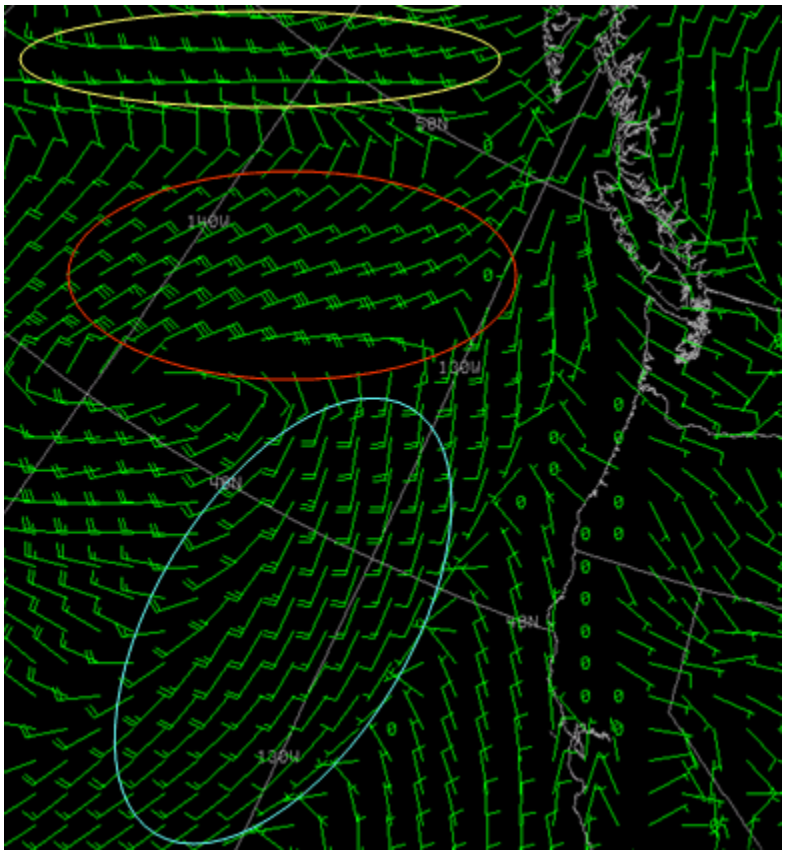

Figure 2-5 - Examples of Fetch Regions (COMET, 2005).

Within a fetch, energy is transferred between waves, helping build larger waves. In most cases, wider fetches result in bigger waves, making the turning of winds less significant. The amount lost as a percentage of the fetch's total energy is larger when the fetch is narrower. Waves that move in the same direction as the storm can experience dynamic fetch, shown in Figure 2-6 as the purple rectangle. The distance at which the waves actually grow is called the dynamic fetch (COMET, 2005).

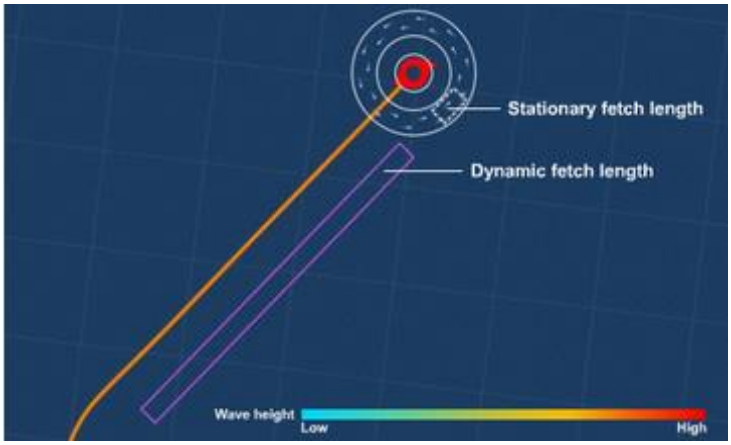

Figure 2-6 - Typical Tropical Cyclone Path (COMET, 2005).

In order to evaluate wave growth in a dynamic fetch, it is important to know the duration of the waves remaining in harmony with the wind system. The waves found inside the stationary fetch length are the waves that are affected by the fetch winds the longest. Besides the three known stationary storm factors (wind speed, duration, and fetch), the assessment of the dynamic fetch requires knowledge of the translation speed, storm speed, and wave-generating cyclone. The forecasting becomes difficult because the relationships between these factors are non-linear (COMET, 2005).

Wave and storm acceleration do not have to be the same for a dynamic fetch to occur. In the case of tropical cyclones, studies have shown that the dynamic fetch waves at the leading edge of hurricane travel 30 to 150% faster than the storm itself (COMET, 2005). Optimal dynamic fetch situations result from waves originating at the leading edge of the storm, then losing ground to the more quickly advancing system, then speeding up before the trailing edge of the fetch passes them by, and finally accelerating back through the fetch to the leading edge once again. It is important to remember that dynamic fetch waves are preceded by much smaller waves, giving little warning of the arrival of the larger dynamic fetch waves (COMET, 2005).

Last of the wave growth components is the wind duration, which is the time which affects the fetch. In a case of very high wind speeds, with a long fetch length and a long duration, the larger the wave growth (COMET, 2005).

The Wave Analysis and Forecasting Nomogram, seen in Figure 2-7, illustrates the relationship between wind speed, wind duration, fetch length, and wave growth. The X-axis indicates the fetch length in nautical miles, the Y-axis indicates the wind speed in knots, and the contour lines represent the wind duration, wave height and wave period. A nautical mile corresponds to 1,852 kilometer. A knot is a unit of speed equivalent to one nautical mile, or 1,852 kilometer per hour. While each of these three aspects are significant, their relationships to wave height is not the same. The effect on wave height is the greatest and most sensitive to changes in wind speed. When analyzing areas of significant wave generation, wind speed is the most important factor to consider (COMET, 2005).

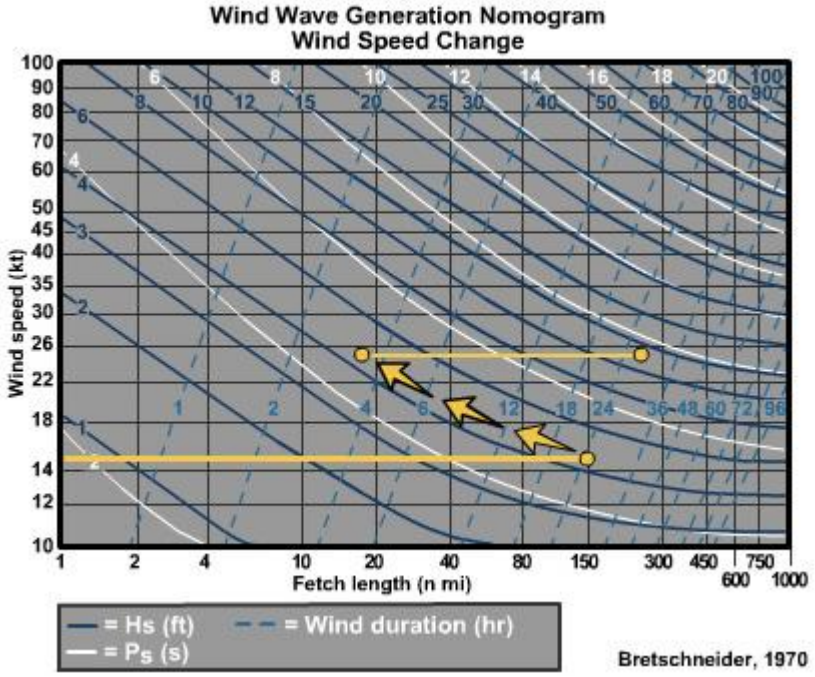

Figure 2-7 - Wave Analysis and Forecasting Nomogram (COMET, 2005).

Apply the nomogram shown in Figure 2-7, when wind over a fetch blows for 24 hours at 15 knots (27,78 km/h), by simply intersecting the wind speed (Y-axis) with the blue solid line (representing the wave height), one concludes that a wave height of 4,5 feet (1,37 meter) will be reached. This also corresponds to a wave period of 5 seconds (represented by the white solid line). To see what happens when the wave moves into an area with a wind speed of 25 knots (46,3 km/h) for another 24 hours, one should follow the wave height line (4,5 feet) represented by the arrows until it reaches the 25 knot limit. Next, that line should be followed across for 24 hours. Because the starting point is at about 3,5 hours, represented by the blue dotted line, applying the said 24 hours, the final durations will be of 28 hours. This would increase the wave height to about 11 feet, or 3,35 meters. This demonstrates the fact that a wave grows when moving into an area in which the wind speed is greater than the wave speed. A decreasing wind speed has no effect on wave creation. If waves move into an area where the wind speed is less than 25 knots (46,3 km/h), it would continue to have a wave height of 4,5 meters (COMET, 2005).

The previous concept of "fully developed seas" was proposed by Pierson and Moskowitz. The Pierson-Moskowitz spectra assumes that if the wind blows steadily for a long enough time over a large area, the waves would come in equilibrium with the wind (Stewart, 2006). The Pierson-Moskowitz spectra is an empirical relationship that defines that distribution with the frequency of the ocean. This spectrum was developed with measurements of waves made by

accelerometers on British weather ships in the North Atlantic (Stewart, 2006). In (Hasselmann, et al., 1973) during the Joint North Sea Wave Project (JONSWAP) Spectrum, it was found that the wave spectrum is never actually fully developed. This spectrum is a form of the Pierson-Moskowitz spectrum, except that the waves continue to grow with distance or time and it is multiplied by an extra "peak enhancement factor" (Stewart, 2006). This peak is important because it leads to enhanced non-linear interactions and a spectrum that changes in time.

Observations of wind waves are taken by satellite scatterometry, buoy, coastal-marine stations and ships. Scatterometry uses microwave remote sensing of the ocean surface to determine the wind speed, as well as the direction. There are several websites that offer both active and passive scatterometry based on real time wind data. The National Data Buoy Center provides hourly observations from a network of about 70 buoys and 60 Coastal-Marine Network stations (Holweg, 2000). These stations measure wind speed, direction, gusts, barometric pressure, air temperature, sea surface temperature, significant wave heights, and dominant wave periods. There is also a Voluntary Observing Ship or VOS Program that obtains weather and oceanographic observations from moving ships.

2.3. Storms

Coastal storms, better known as tropical cyclones, often affect the United States' eastern coast and sometimes Western Europe. Tropical cyclones are areas made up of precipitation and thunderstorms that arise over warm tropical water.

2.3.1. Thunderstorm Formation

The formation of thunderstorms is of particular importance for a better understanding of essentially, the source of a storm surge and subsequently the flooding and its damaging consequences. A thunderstorm can be defined as a local storm with *cumulonimbus* clouds that generates thunder, lightening, gust, heavy rain, and even hail. A local storm, as defined by the US National Weather Service, produces one or more of the following: tornadoes, winds of at least 92,60 km/h, and hail of at least 2,54 centimeters (COMET, 2013).

An ordinary or single-cell thunderstorm's progression can be described in three phases, seen in Figure 2-8. The first, the *cumulus* phase, occurs when the moist air is warmer than the surrounding environment, i.e. large bodies of water, and the air rises due to its lower density value. Once the rising air is cooled to a saturated point, cumulous clouds are formed. These clouds appear white with slightly darker bases and have a noticeable vertical development (COMET, 2013).

The second phase is the maturing stage. During this stage, the clouds appear to have an "anvil shape" in which the updraft spreads. It is during this stage that the convection is most vigorous, with very dark bases. In this stage, the rainfall creates a downdraft. This downdraft mixed with lower drier air creates a strong evaporating cooling, spreading out like a gust front (COMET, 2013).

Lastly, throughout the dissipating phase, the storm and clouds decay. The downdraft cuts off the supply of rising, moist air and the rainfall decreases. This kind of thunderstorm usually lasts between 20 to 30 minutes (COMET, 2013).

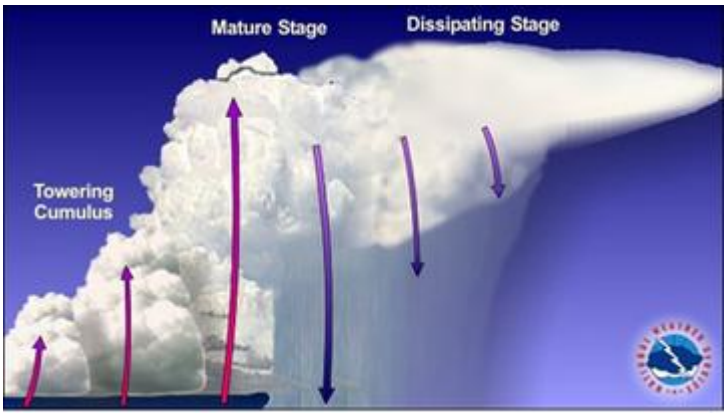

Figure 2-8 - Thunderstorm's Lifecycle (COMET, 2013).

The intensity of the thunderstorms is measured by stability indices. They are its lifted index (LI), and the amount of convective available potential energy (CAPE), released. The lifted index is the difference between observed temperature at 500 hPa and temperature of parcel lifted without heat transfer from near the surface to 500 hPa. The CAPE studies the amount of buoyant energy available to a parcel accelerating upward. It represents the area between the level of free convection and the equilibrium level. It defines how vigorous the updrafts of the storm are. The larger the CAPE, the greater is the probability of thunderstorm occurrence (COMET, 2013).

Another important factor when addressing thunderstorms is shear. Shear is the difference in wind speed and wind direction in the atmosphere. The shear defines what occurs as the downdraft develops. The Bulk Richardson Number (BRN) was developed to link the shear parameter and the convective available potential energy, CAPE. The BRN is directly proportional to the CAPE and inversely proportional to the shear. The BRN basically determines whether the convection is free or forced (Weather FAQs, 2008).

High values of BRN represent an unstable or weak shear. The shear is not strong enough to stop the downdraft from moving quickly away from the updraft. As the cells form, they spread away from the original cells and the precipitation falls into a saturated environment. Because of this, there is no danger of having an extensive downdraft. For moderate BRN values, the shear now plays an important part in distorting the updraft by slanting the cloudy environment. This allows for the precipitation to fall into unsaturated air and the evaporating cooling will cause a cold downdraft. The updraft essentially separates the downdraft. The downdraft hits the surface and spreads, like a "gust front", generating new cells away from the original cells. The old or original cells will mature and dissipate (Weather FAQs, 2008). This is fundamentally the development of multi-cellular thunderstorms. Essentially, multicellular thunderstorms are a group of ordinary thunderstorms at varying stages in their lifecycle, portrayed in Figure 2-9. They can last for a few hours (COMET, 2013).

Figure 2-9 - Schematics of a Multicellular Storm in Easterly Shear (COMET, 2013).

With low BRN values, the shear is strong and the value of the CAPE is high. These are good indicators for the development of super-cell thunderstorms. A super-cell thunderstorm is an intense thunderstorm that produces severe weather lasting for several hours. Since the shear is so strong, both its speed and most importantly, its directional component, are significant factors. In this case, the thunderstorm updraft slants the horizontal vorticity upwards forming a rotating updraft. This rotating updraft is also known as a mesocyclone. The super-cell thunderstorm creates a strong forward downdraft, where a shelf cloud spreads and heavy rain

ensues. The mesocyclone creates a high potential for tornado formation, most possibly observed along the boundary created by the rear downdraft (COMET, 2013).

2.3.2. Storm Surges

The United States' National Oceanic and Atmospheric Administration defines a tropical cyclone as a rotating, organized system of clouds and thunderstorms that originates over tropical or subtropical water and have closed low-level circulation. The term tropical cyclone refers to this type of systems occurring over the Atlantic Ocean. A very strong tropical cyclone occurring in the Atlantic Ocean is called a hurricane. The terms hurricane, cyclone and typhoon correspond to the same weather phenomenon (very strong tropical cyclone). In the Atlantic and Northwestern Pacific, the term “hurricane” is used. The same kind of occurrence in the Northwest Pacific is called a typhoon and in the South Pacific and the Indian Ocean, they are referred to as cyclones (NOAA - Hurricane Research Division, 2014). In the western North Pacific, the term "super typhoon" is used for tropical cyclones with sustained winds exceeding 240 km/h (NOAA - National Hurricane Center, 2013).

Storms can be categorized as tropical depressions, tropical storms, or hurricanes. A tropical depression is a low pressure region belonging to a stage of cyclone formation sustaining a maximum of winds of up to 62 km/h. A tropical storm is able to sustain winds from 62 to 118 km/h. A hurricane is a much more intense tropical weather system, sustaining winds of 119 km/h or greater. A hurricane is further classified, according to its intensity, i.e. the wind speed. This intensity is categorized using the Saffir-Simpson Hurricane Scale, SSHS. The scale estimates potential property damage (NOAA - National Hurricane Center, 2013). As seen in Table 2-1, a Category 1 hurricane represents a hurricane with the lowest wind speed, while the fastest wind speed corresponds to a Category 5 hurricane. A classification of Category 3 or higher is considered a major hurricane (Federal Emergency Management Agency Review, 2014). Hurricanes reaching Category 3 are considered major because of their potential for significant loss of life and damage. Even so, a Category 1 or 2 hurricane is still considered dangerous and still require preventative measures (NOAA - National Hurricane Center, 2013).

Table 2-1 - Saffir-Simpson Hurricane Scale, SSHS (NOAA - National Hurricane Center, 2013).

Category	Sustained Winds	Types of Damage Due to Hurricane Winds
1	74-95 mph 64-82 kt 119-153 km/h	**Very dangerous winds will produce some damage:** Well-constructed frame homes could have damage to roof, shingles, vinyl siding and gutters. Large branches of trees will snap and shallowly rooted trees may be toppled. Extensive damage to power lines and poles likely will result in power outages that could last a few to several days.
2	96-110 mph 83-95 kt 154-177 km/h	**Extremely dangerous winds will cause extensive damage:** Well-constructed frame homes could sustain major roof and siding damage. Many shallowly rooted trees will be snapped or uprooted and block numerous roads. Near-total power loss is expected with outages that could last from several days to weeks.
3 (major)	111-129 mph 96-112 kt 178-208 km/h	**Devastating damage will occur:** Well-built framed homes may incur major damage or removal of roof decking and gable ends. Many trees will be snapped or uprooted, blocking numerous roads. Electricity and water will be unavailable for several days to weeks after the storm passes.
4 (major)	130-156 mph 113-136 kt 209-251 km/h	**Catastrophic damage will occur:** Well-built framed homes can sustain severe damage with loss of most of the roof structure and/or some exterior walls. Most trees will be snapped or uprooted and power poles downed. Fallen trees and power poles will isolate residential areas. Power outages will last weeks to possibly months. Most of the area will be uninhabitable for weeks or months.
5 (major)	157 mph or higher 137 kt or higher 252 km/h or higher	**Catastrophic damage will occur:** A high percentage of framed homes will be destroyed, with total roof failure and wall collapse. Fallen trees and power poles will isolate residential areas. Power outages will last for weeks to possibly months. Most of the area will be uninhabitable for weeks or months.

The greatest threat to life and property when dealing with hurricanes is the effects of storm surges. The strongest winds associated with a cyclone are concentrated along the center of the circulation, generally along its right side. The winds flow cyclonically, or counter clockwise, around the surface resulting in very elevated values of sea heights. With the force of the winds moving cyclonically around the storm, the water is then pushed onto the shore.

A storm surge is an irregular rise in sea level generated by tropical cyclone wind, waves, and low atmospheric pressure, measured above the normal predicted astronomical tide. A storm tide is defined as the height of the sea level, affected by a storm surge, measured above mean sea level (Weather FAQs, 2008). The difference between a storm tide and a storm surge is portrayed below in Figure 2-10. When the storm surge matches the high tide, drastic water level rises can result. For example, in a location where the high tide is about 1 meter above mean sea level, a 3-meter storm surge would cause a 4-meter storm tide if the hurricane hit at the time of its high tide. In some cases, storm tides can reach up to 6 meters or more (NOAA - National Hurricane Division, 2014).

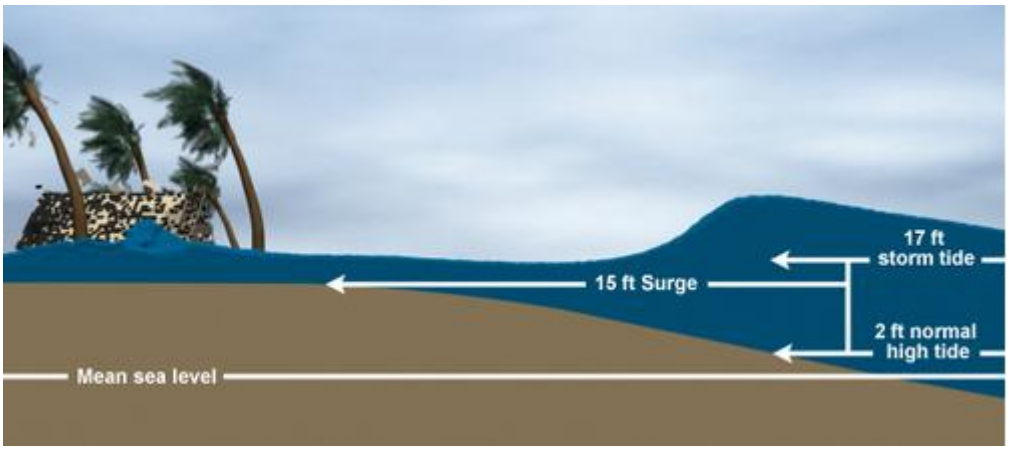

Figure 2-10 - Storm Surge vs. Storm Tide (NOAA - National Hurricane Division, 2014).

Storm surges are sensitive to numerous factors, such as, the storm intensity, forward speed, radius of maximum winds, angle in which it approaches the coast, the proximity of the storm trajectory, pressure, bathymetry, and the shape and characteristics of the coast being considered. The coastal characteristics, its width and the slope of the continental shelf, can influence the size of the storm surge. Steeper slopes will produce a smaller surge compared to a shallower slope. For example, a Category 4 storm hitting the Louisiana coastline, which has a very wide and shallow continental shelf, may produce a 6-meter surge, while the same hurricane in a place like Miami Beach, Florida, where the continental shelf drops off very quickly, might see a 2,5 or 3-meter storm surge (NOAA - National Hurricane Division, 2014). Figure 2-11 demonstrates the wind and pressure components, verified as the most influential aspects of a storm surge.

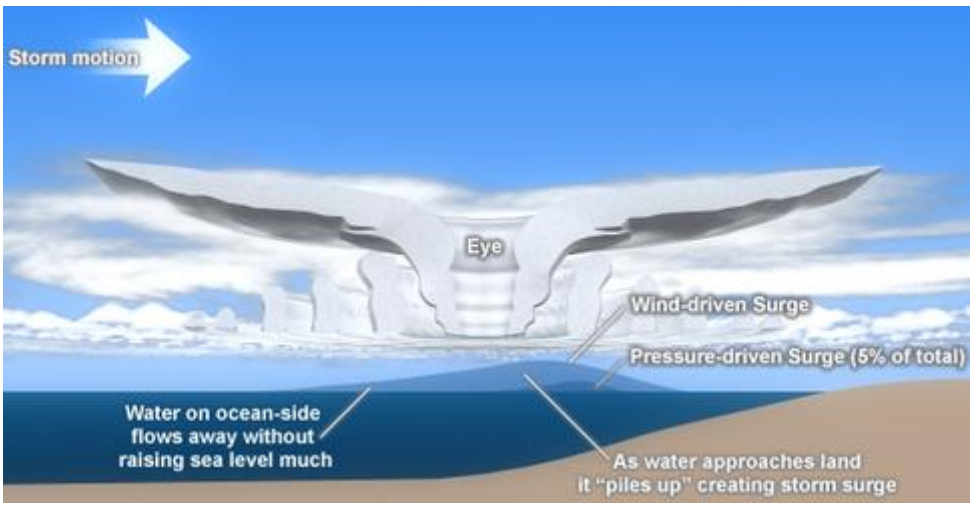

Figure 2-11 - Wind and Pressure Components of Hurricane Storm Surges (NOAA - National Hurricane Division, 2014).

Most of the surge occurs when the force of the wind pushes water towards the shore. For hurricanes in the Northern Hemisphere, this effect creates the largest storm surge in the right-forward quadrant of the storm due to the combination of the storm's counter-clockwise rotation and forward motion. In the Southern Hemisphere, clockwise rotation of storms means the largest surge is in the left-forward motion (NOAA - National Hurricane Division, 2014).While the wind is the primary contributor to the surge, the storm's atmospheric pressure increases the height of the surge as the pressure falls. This aspect is secondary compared to the wind. Atmospheric pressure, force exerted by the weight of air in the Earth's atmosphere, is higher at the edges of a cyclone than it is at the center. This pushes down the water in the outer parts of the storm, causing the water to bulge at the eye and the eye wall (National Geographic, 2014).

Fast moving storms cause higher surges over open coasts and lower surges in protected estuaries, while slower moving storms usually result in greater flooding in estuaries and smaller values of flooding along the coast (NOAA - National Hurricane Division, 2014). Besides its speed, the direction of the storm is also an important factor when evaluating the issue of flooding. Evidently, a tropical cyclone that hits the coast in a perpendicular fashion will result in much greater critical impacts and consequently bigger storm surges, compared to a tropical cyclone with the same intensity that passes parallel to the same coast.

2.3.3. Tropical Cyclone Climatology

The essential components of a tropical cyclone are a pre-existing instability in the weather, warm ocean waters, moist atmospheric layers, light winds, and a northward/southward formation of approximately 5°N/5ºS latitude in the northern hemisphere. This northward formation of about 5°N is required to produce a minimum of Coriolis force required in the development of a tropical cyclone. The Coriolis effect is when objects traveling in a straight path veer to the left or right. The centrifugal force proceeds to swerve outward in the radial direction, proportional to the distance the object is to the axis of the rotating source, the Earth (Landsea & Goldenberg, 2004). This phenomenon is explained in detail in Section 3.3.3. Tropical cyclones typically form between 5°N and 30°N latitude, usually moving toward the west with slight polarward movement. When reaching 30°N, due to the existence of the North American continent, they often move northwest. The Atlantic “hurricane season” runs from

June 1st to November 30th (Landsea & Goldenberg, 2004). The climatological areas of origin and typical hurricane tracks by month during "hurricane season" are depicted in Figure 2-12 for the Northern Atlantic. A peak of tropical cyclones is observed from August to October.

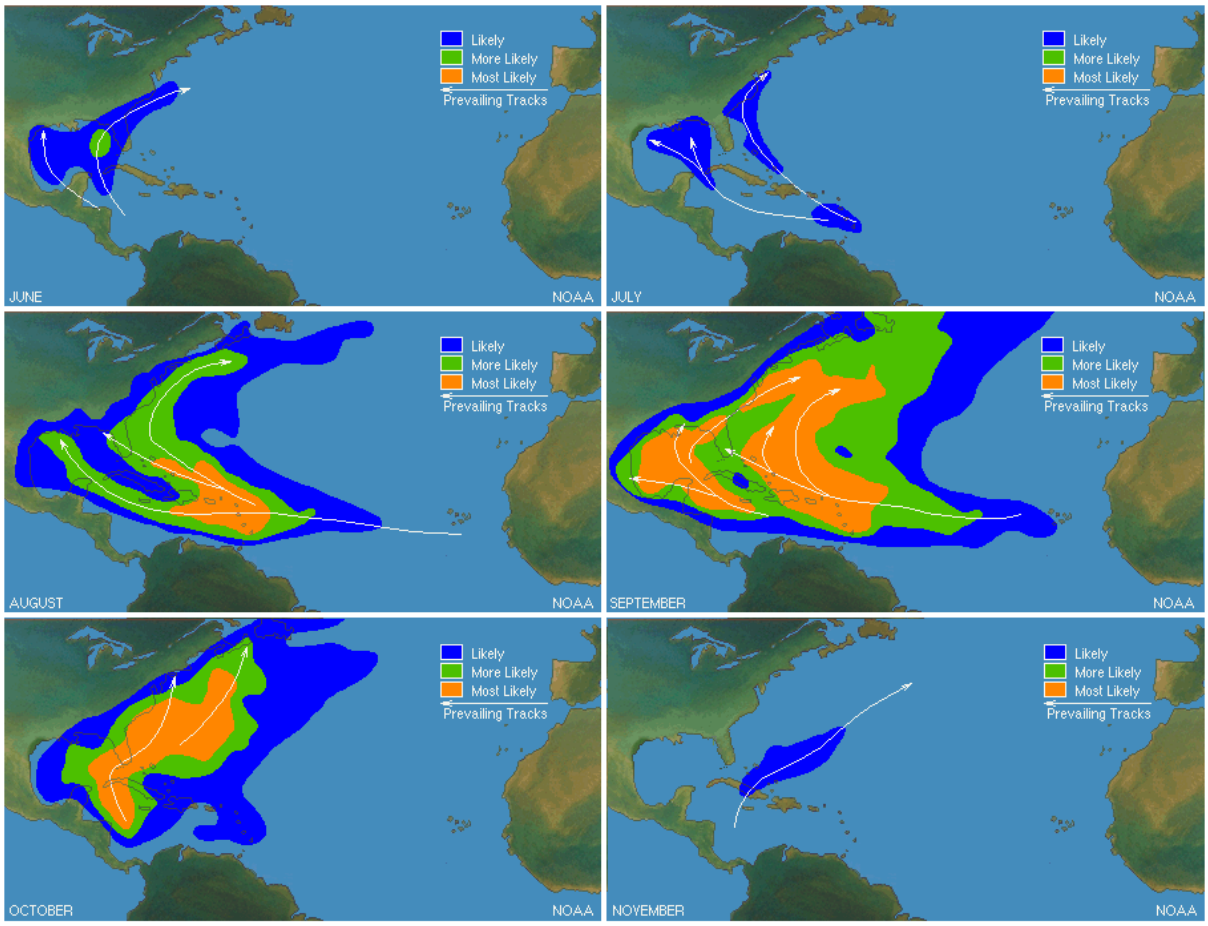

Figure 2-12 - Climatological Areas of Origin and Typical Hurricane Tracks by Month (Tropical Cyclone Climatology, 2014).

A reason for this movement is because of an axis of high pressure called the subtropical ridge, seen in Figure 2-13, that extends east-west polarward of the storm.

Figure 2-13 - Subtropical Ridge of the North Atlantic Basin (National Weather Service, 2011).

In the cases where the subtropical ridge is weak, due to a trough in the jet stream, the tropical cyclone may turn polarward and then curve towards the east, affecting the eastern shore of the United States coast. These are the westerly winds that typically move cold and warm fronts from west to east, sometimes changing the structure of the tropical systems arriving at the lower United States coast (Landsea, 2014).

The winds typically move from west to east in jet streams, but the flow shifts to the north and south. A jet stream can be defined as a narrow band of strong wind in the upper levels of the atmosphere. Usually, jet streams are stronger during the winter because of the more pronounced hot and cold boundaries (National Weather Service, 2011). The path of jet streams can steer cyclonic storm systems at lower levels which means it is an influential aspect in weather forecasting. The Earth's rotation is divided into three cells: Polar Cell, Ferrel Cell, and Hadley Cell. The motion of the air is affected by the momentum the air has as it moves away from the equator. The momentum the air has as it travels around the Earth is conserved, meaning that as the air that is over the equator starts moving towards one of the poles, it keeps its eastward motion constant. However, the Earth below the air moves slower as that air travels towards the poles (National Weather Service, 2011). This results in the air moving faster and faster in an easterly direction the farther it moves from the equator, depicted in Figure 2-14.

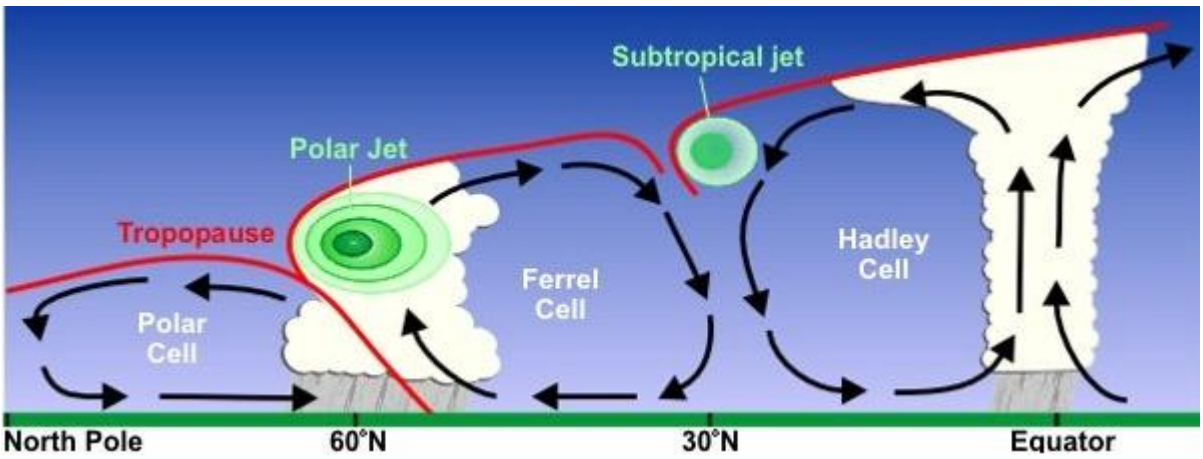

Figure 2-14 - Three-cell circulation (NWS JetStream - Types of Thunderstorms, 2014).

Another important aspect to consider when studying the formation of tropical cyclones is the ocean currents themselves. The Gulf Stream is an ocean current system that could quite possibly be one of the most important in the northern hemisphere. The Gulf Stream is an intense, warm ocean current system in the western North Atlantic Ocean which moves from Florida and then turns eastward off North Carolina, flowing northeast across the Atlantic,

reaching northwestern Europe. It is the main conveyor of heat from south to north in the Atlantic Ocean. The Gulf Stream flows at a rate of nearly 300 times faster than the typical flow of the Amazon River off the coast of eastern United States. The average speed of the Gulf Stream is 6,4 km/h. The velocity of the current is fastest near the surface, with the maximum speed typically about 9 km/h (National Ocean Service, 2014).

The Gulf Stream is very narrow, only 80 km wide, and carries water at about 25ºC. The North Atlantic Drift, one of the branches of the tail of the Gulf Stream, widens considerably to about 1000 kilometers, slows to less than 2 km/h and splits in to several sub-currents. Off the British Isles it splits into two branches, one going south towards what is called the Canary Current, and the other going north along the coast of western and northern Europe. The relatively warm waters of the North Atlantic Drift are responsible for moderating the climate of western Europe, so that winters are less cold than would otherwise be expected at its latitude. Without this steady stream of warmth, the British Isles, for example, are estimated to be more than 5ºC, bringing the average December temperature in London to about 2ºC (Weather Online, 2014). The different ocean currents discussed are represented below in Figure 2-15.

The two main driving forces behind these phenomena are the prevailing southwesterly trade winds and circulation of the water far below the ocean's surface, i.e. the North Atlantic Deep Water (NADW) circulation. The water in the North Atlantic sinks because it is dense, which is increased by both salinity and temperature. Deep water flows to the Gulf of Mexico until it warms enough to resurface and flow back north as the Gulf Stream (Weather Online, 2014).

Figure 2-15 - Depiction of the Gulf Stream, North Atlantic Drift, and Canary Current (Weather Online, 2014).

As the said "hurricane season" progresses, the landfalling of tropical cyclones becomes less and less frequent. Tropical cyclone landfalling makes it more probable for the cyclone to

undergo transitioning due to the increased frequency of the troughs and the baroclinicity over land, later on in the season (Hart & Evans, 2000). A tropical transition is referred to as a tropical cyclone that moves over colder water and into stronger shear at higher latitudes (Hart & Evans, 2000). The term 'extratropical' means that there is polarward displacement of the cyclone and the conversion of its primary energy from the release of latent heat of condensation develops to baroclinic. Baroclinicity refers to atmosphere in which its density depends on both temperature and pressure. The cyclone's source of energy becomes baroclinic, meaning it is obtained from horizontal temperature contrasts between cold and warm air. With the three-cell circulation cells previously mentioned, the regions around 30°N, and between 50° and 60°N are areas where the temperature changes are the greatest. As the difference in temperature between two locations increases, the strength of the wind increases. regions around 30°N, and between 50° and 60°N are regions where the wind is the strongest (National Weather Service, 2011).

The probability of cyclone's transitioning is during the months of September and October, when 50% of all Atlantic tropical cyclones transition (Hart & Evans, 2000). Currently there is no definition for the transitioning, but according to subjective examination by the National Hurricane Center, the transitioning is due to two factors: the underlying sea surface temperature, SST, and satellite interpretation of storm structure and asymmetry. The seasonal distribution of the tracks of extratropically transitioning cyclones can be broken down into three periods: a low-latitude quiet early season, a high-latitude active mid season, and a mid-latitude active late season. In May and June, there is already a transitioning in the lower latitudes. By July there is a transition shift northward (about 5° latitude) into the mid-latitudes. Between July and August, tropical cyclone transitioning occurs between the 40° and 45°N, and lastly from September to October there is another drastic shift with a shift southward of 4° (Hart & Evans, 2000).

The sudden change from tropical to extratropical cyclones means a sudden change to the structure of the cyclone. Drastic variations of storm speed, direction, and position are a result of this structural change. As the systems become extratropical, rapid fluctuations of a storm's wind field intensity and an outward expansion of storm force is associated. The transformation of tropical cyclones to extratropical cyclones, and vice versa, is in fact a challenging forecasting problem. This is the most challenging aspect of simulating the tropical systems of the chosen case study areas, located in the Northern Atlantic Basin.

3. HYDRODYNAMIC MODELING OF COASTAL ZONES – CONCEPTUAL DESCRIPTION

Hydrodynamic modeling is a representation of the motion of liquids. It can be used for solving problems relating to oceanic movement. Before the arrival of widely available computer systems, a hydrodynamic model was a physical model built to scale. Nowadays, nearly all models used are computational numerical models (NOAA Office of Coast Survey, 2014).

The numeric model has the common basis of governing equations of conservation of momentum and mass in the fluid. The foundation of computational hydrodynamic models lies upon a set of equations that describe the motion of fluids: the Navier-Stokes equations. For hydrodynamic modeling, the Navier Stokes equations are simplified by the specific properties of the ocean's coastal zone. The resulting equations are referred to as shallow water equations. This is because the scale of features in the horizontal plane is much greater than the vertical one. Oceans and estuaries are much larger in length and width than in depth, and motions within them are predominantly horizontal (tides and currents). The shallow water equations allow for more efficient numerical solution of flow in this setting (NOAA Office of Coast Survey, 2014).

The use of the Navier-Stokes equations can be applied to many different ecological problems with the use of different model configurations and forcing. The models can be used in efficient depth averaged two-dimensional application or in a full three-dimensional form. For well-mixed systems, the effects of density variations due to temperature and salinity can be ignored and the model runs in barotropic mode. The baroclinic effects can also be included if necessary by solving for temperature and salinity forcing (NOAA Office of Coast Survey, 2014). Equations describing transport and fate of the constituents can also be coupled to the hydrodynamic equations.

The Delft3D-FLOW program uses nonlinear 2DH (depth-averaged) and 3D shallow water equations. Shallow water equations are derived by integrating the full Navier-Stokes equations in the vertical direction. The main assumption made to derive these equations is that

the horizontal scale is much bigger than the vertical one; therefore, the three dimensional shallow water equations suffice. This is the case of the σ-coordinate system. Vertical accelerations are presumed to be very small in comparison to the gravitational acceleration. This assumption reduces the vertical momentum equation to a hydrostatic pressure equation. Delft3D-FLOW solves the Navier-Stokes equations for an incompressible fluid, under shallow water and the Boussinesq assumptions (Deltares, 2011). For cases when the previous assumption is invalid, Delft3D provides the option of applying the "non-hydrostatic pressure" model in the Z-model. For more details one should refer to (Deltares, 2011). The output of such models result in the time history of many different features, such as, the water level, atmospheric pressure, current velocity, temperature, salinity, etc. The results can be verified by comparing them to observational data. The use of these models can be very helpful in providing forecast guidance. The prediction of water levels and water currents can be critical to maritime communities in case of planning safe navigation or evacuation.

3.1. Navier-Stokes Equations

The Navier-Stokes equations can be viewed as an application of Newton's second law, in which the force is equal to the product of the mass and the acceleration. These equations basically describe the action of force applied fluid that is the resulting changes in flow. When dealing with fluids, its acceleration is dependent on the force exerted per unit of mass. This is the property of conservation of momentum. Computational hydrodynamics also imposes the continuity principle which states that mass and energy are conserved until they pass out of the domain (NOAA Office of Coast Survey, 2014).

The Navier-Stokes equations are extensions of the Euler equations and include the effects of viscosity flow. Even though they could, in theory, be solved by applying calculus methods, in practice they are very difficult to solve analytically. With the use of computers, employing for example, the finite difference method, the problems are easy to solve using approximations to the equations. To better explain the foundation of the Navier-Stokes equations the description given by (Weisstein, 2014) will be described here.

The Navier-Stokes equations are the fundamental partial differential equations that describe the flow of incompressible fluids. Using the rate of stress and rate of strain tensors, the components F_j of a viscous force, F, in a non-rotating frame are given by,

$$\frac{F_i}{V} = \frac{\delta}{\delta x_j}\left[\eta\left(\frac{\delta u_i}{\delta x_j} + \frac{\delta u_j}{\delta x_i}\right) + \lambda\delta_{ij}\nabla\cdot u\right] = \frac{\delta}{\delta x_j}\left[\eta\left(\frac{\delta u_i}{\delta x_j} + \frac{\delta u_j}{\delta x_i} - \frac{2}{3}\delta_{ij}\nabla\cdot u\right) + \mu_B\delta_{ij}\nabla\cdot u\right] \quad (4)$$

where η is the dynamic viscosity, λ is the second viscosity coefficient, δ_{ij} is the Kronecker delta, $(\nabla\cdot u)$ is the divergence, μ_B is the bulk viscosity, and the Einstein summation has been used to sum over j = 1, 2, and 3.

For an incompressible fluid, the divergence is equal to zero, so the lambda term is eliminated. Considering the dynamic viscosity to be constant in space, the previous equation is rewritten as the following,

$$\frac{F_{viscous}}{V} = \eta\nabla^2 u \quad (5)$$

The pressure force is an additional force acting on the fluid parcels,

$$\frac{F_{pressure}}{V} = -\nabla P \quad (6)$$

where P is the pressure and the so-called body force is,

$$F = \frac{F_{body}}{V} \quad (7)$$

Adding Equations 5, 6, and 7, and equating them to Newton's law for fluids, the following equation is obtained,

$$\rho\frac{\delta u}{\delta t} + \rho u\cdot\nabla u = -\nabla P + \eta\nabla^2 u + \mathrm{F} \quad (8)$$

Dividing this equation by the water density, ρ, following vector equations for the irrotational Navier-Stokes equations are given,

$$\frac{\delta u}{\delta t} + u\cdot\nabla u = -\frac{\nabla P}{\rho} + v\nabla^2 u + \frac{\mathrm{F}}{\rho} \quad (9)$$

where the kinematic viscosity, v, is defined by,

$$v = \frac{\eta}{\rho} \quad (10)$$

When combined with the continuity equations of fluid flow, the Navier-Stokes equations yield four equations in four unknowns. Besides cases of very simple geometries, these equations cannot be solved exactly and approximations have to be made. As previously

mentioned, the Navier-Stokes equations must satisfy the conservation of mass, momentum, and energy.

Mass conservation is included implicitly through the continuity equation,

$$\frac{\delta\rho}{\delta t} = -\nabla \cdot \varphi_{mass} = -\nabla \cdot (\rho u) = -u \cdot \nabla\rho - \rho\nabla \cdot u \tag{11}$$

For an incompressible fluid,

$$\frac{\delta\rho}{\delta t} = -\rho\nabla \cdot \mathrm{u} \tag{12}$$

Conservation of momentum requires,

$$\frac{momentum}{mass} = [mass] + [pressure] + [body\ force] + [viscosity]$$

Therefore,

$$\frac{\delta u}{\delta t} = (u \cdot \nabla)u - \frac{1}{\rho}\nabla P + \frac{F}{\rho} + v\nabla^2 u \tag{13}$$

Lastly, conservation of energy follows from,

$$\frac{\delta s}{\delta t} = -u \cdot \nabla s + \frac{Q}{T} \tag{14}$$

where s is the entropy per unit of mass, Q is the heat transferred, and T is the temperature.

Considering the Navier-Stokes equations in Cartesian coordinates with velocity components given by $u = (u, v, w)$, the continuity equation is given by,

$$\frac{\delta u}{\delta x} + \frac{\delta v}{\delta y} + \frac{\delta w}{\delta z} = 0 \tag{15}$$

And the resulting Navier-Stokes equations are given by,

$$inerctial\ terms = pressure\ gradient + viscous\ terms + body\ force\ terms$$

$$\rho\left(\frac{\delta u}{\delta t} + u\frac{\delta u}{\delta x} + v\frac{\delta u}{\delta y} + w\frac{\delta u}{\delta z}\right) = -\frac{\delta P}{\delta x} + \eta\left(\frac{\delta^2 u}{\delta x^2} + \frac{\delta^2 u}{\delta y^2} + \frac{\delta^2 u}{\delta z^2}\right) + F_x \tag{16}$$

$$\rho\left(\frac{\delta v}{\delta t} + u\frac{\delta v}{\delta x} + v\frac{\delta v}{\delta y} + w\frac{\delta v}{\delta z}\right) = -\frac{\delta P}{\delta y} + \eta\left(\frac{\delta^2 v}{\delta x^2} + \frac{\delta^2 v}{\delta y^2} + \frac{\delta^2 v}{\delta z^2}\right) + F_y \tag{17}$$

$$\rho\left(\frac{\delta w}{\delta t} + u\frac{\delta w}{\delta x} + v\frac{\delta w}{\delta y} + w\frac{\delta w}{\delta z}\right) = -\frac{\delta P}{\delta z} + \eta\left(\frac{\delta^2 w}{\delta x^2} + \frac{\delta^2 w}{\delta y^2} + \frac{\delta^2 w}{\delta z^2}\right) + F_z \tag{18}$$

Considering spherical coordinates with the components of the velocity vector given by $u = (u_r, u_\theta, u_\varphi)$, the continuity equation is as follows,

$$\frac{\delta u_r}{\delta r} + \frac{2u_r}{r} + \frac{1}{r}\frac{\delta u_\theta}{\delta \theta} + \frac{u_\theta cot\theta}{r} + \frac{1}{rsin\theta}\frac{\delta u_\varphi}{\delta \varphi} = 0 \tag{19}$$

And the resulting Navier-Stokes equations are given by,

$$\rho\left(\frac{\delta u_r}{\delta t} + u_r\frac{\delta u_r}{\delta r} + \frac{u_\theta}{r}\frac{\delta u_r}{\delta \theta} + \frac{u_\varphi}{rsin\theta}\frac{\delta u_r}{\delta \varphi} - \frac{u_\theta^2}{r} - \frac{u_\varphi^2}{r}\right) = -\frac{\delta P}{\delta r} + \eta\left(\frac{\delta^2 u_r}{\delta r^2} + \frac{2}{r}\frac{\delta u_r}{\delta r} - \frac{2u_\varphi}{r^2} + \frac{1}{r^2}\frac{\delta^2 u_\varphi}{\delta \theta^2} + \frac{cot\theta}{r^2}\frac{\delta u_r}{\delta \theta} + \frac{1}{r^2 sin^2\theta}\frac{\delta^2 u_\varphi}{\delta \varphi^2} - \frac{2}{r^2}\frac{\delta u_\theta}{\delta \theta} - \frac{2u_\theta cot\theta}{r^2} - \frac{2}{r^2 sin\theta}\frac{\delta u_\varphi}{\delta \varphi}\right) + F_r \tag{20}$$

$$\rho\left(\frac{\delta u_\theta}{\delta \theta} + u_r\frac{\delta u_\theta}{\delta r} + \frac{u_r u_\theta}{r} + \frac{u_\theta}{r}\frac{\delta u_\theta}{\delta \theta} + \frac{u_\varphi}{r\,sin\theta}\frac{\delta u_\theta}{\delta \varphi} - \frac{u_\varphi^2 cot\theta}{r}\right) = -\frac{1}{r}\frac{\delta P}{\delta \theta} + \eta\left(\frac{\delta^2 u_\theta}{\delta r^2} + \frac{2}{r}\frac{\delta u_\theta}{\delta r} - \frac{u_\theta}{r^2 sin^2\theta} + \frac{1}{r^2}\frac{\delta^2 u_\theta}{\delta \theta^2} + \frac{cot\theta}{r^2}\frac{\delta u_\theta}{\delta \theta} + \frac{1}{r^2 sin^2\theta}\frac{\delta^2 u_\theta}{\delta \varphi^2} + \frac{2}{r^2}\frac{\delta u_r}{\delta \theta} - \frac{2cot\theta}{r^2 sin\theta}\frac{\delta u_\varphi}{\delta \varphi}\right) + F_\theta \tag{21}$$

$$\rho\left(\frac{\delta u_\varphi}{\delta t} + u_r\frac{\delta u_\varphi}{\delta r} + \frac{u_r u_\theta}{r} + \frac{u_\theta}{r}\frac{\delta u_\varphi}{\delta \theta} + \frac{u_\theta u_\varphi cot\theta}{r} + \frac{u_\varphi}{r\,sin\theta}\frac{\delta u_\varphi}{\delta \varphi}\right) = -\frac{1}{rsin\theta}\frac{\delta P}{\delta \varphi} + \eta\left(\frac{\delta^2 u_\varphi}{\delta r^2} + \frac{2}{r}\frac{\delta u_\varphi}{\delta r} - \frac{u_\varphi}{r^2 sin^2\theta} + \frac{1}{r^2}\frac{\delta^2 u_\varphi}{\delta \theta^2} + \frac{cot\theta}{r^2}\frac{\delta u_\varphi}{\delta \theta} + \frac{1}{r^2 sin^2\theta}\frac{\delta^2 u_\varphi}{\delta \varphi^2} + \frac{2}{r^2 sin\theta}\frac{\delta u_\varphi}{\delta \varphi} + \frac{2cot\theta}{r^2 sin\theta}\frac{\delta u_\theta}{\delta \varphi}\right) + F_\varphi \tag{22}$$

3.2. Turbulent Flow

Turbulence is a flow property that is characterized by recirculation, eddies, and is defined as being very random, very much significant when dealing with coastal modeling. Turbulence is represented via the Reynolds number. The Reynolds number represents the ratio between inertial and viscous forces.

$$Re = \frac{\rho UD}{\mu} \tag{23}$$

The smaller the number, the more orderly the flow is with parallel streamlines. As the number increases, the flow loses its "laminar" characteristics. As the number grows, the flow structure becomes characterized as having large-scaled eddies. The more turbulent areas are found close to solid boundaries, called the boundary layer, shown in Figure 3-1 (Sayma, 2009).

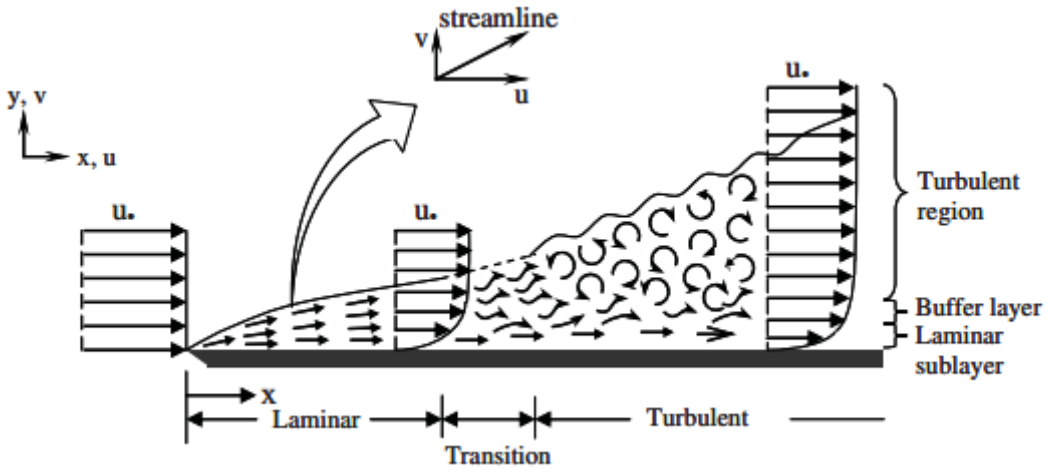

Figure 3-1 - Boundary Layer over Flat Plate (Sayma, 2009).

To explain this phenomenon, suppose there is a free stream flow with a velocity, U_∞, approaching a flat plate, as seen in Figure 3-1. The flow doesn't have any velocity at the wall due to friction, while at a distance from the wall, the flow has a velocity of U_∞. As the flow approaches the wall, the supposed boundary layer forms. As the flow reached the wall, the Reynolds number increases and so the inertial forces begin to dominate, thus forming a development of instability in the boundary layer. (Sayma, 2009)

Present study focuses in investigating the main principles of turbulence modeling, including examination of the physics of turbulence, closure models, and application to specific flow conditions. Turbulent flow usually involves computational fluid dynamics. It is three dimensional and time-dependent, and a great deal of information is necessary is required to describe all of the mechanics of the flow. The complexity of the mathematical models increases with the amount of information required about the flow field. Turbulence can be modeled from simple mixing length models to the solution of full Navier Stokes equations (Celik, 1999).

In the case of highly turbulent flows, variation in time is random and its detailed variation is not of interest. The average quantity is useful in engineering aspects. This average is obtained by averaging over an interval large enough to filter small scale variations, but small enough so that meaningful large scale time variations are maintained. The Reynolds equations are derived from the abovementioned Navier-Stokes equations, replacing the instantaneous velocity value by adding a temporal average value with a random fluctuation. These equations characterize the moving average, temporal average, of a particle of fluid (Pinho, 2000).

The derivations of these equations are known as,

$$\rho\left(\frac{\delta\hat{u}}{\delta t}+u\frac{\delta(\hat{u}\hat{u})}{\delta x}+v\frac{\delta(\hat{u}\hat{v})}{\delta y}+w\frac{\delta(\hat{u}\hat{w})}{\delta z}\right)=\rho F_x-\frac{\delta\hat{p}}{\delta x}+\mu\left(\frac{\delta^2\hat{u}}{\delta x^2}+\frac{\delta^2\hat{u}}{\delta y^2}+\frac{\delta^2\hat{u}}{\delta z^2}\right)-\frac{1}{\rho}\left(\frac{\delta}{\delta x}\overline{u'u'}+\frac{\delta}{\delta y}\overline{u'v'}+\frac{\delta}{\delta z}\overline{u'w'}\right) \quad (24)$$

$$\rho\left(\frac{\delta\hat{v}}{\delta t}+u\frac{\delta(\hat{v}\hat{u})}{\delta x}+v\frac{\delta(\hat{v}\hat{v})}{\delta y}+w\frac{\delta(\hat{v}\hat{w})}{\delta z}\right)=\rho F_y-\frac{\delta\hat{p}}{\delta y}+\mu\left(\frac{\delta^2\hat{v}}{\delta x^2}+\frac{\delta^2\hat{v}}{\delta y^2}+\frac{\delta^2\hat{v}}{\delta z^2}\right)-\frac{1}{\rho}\left(\frac{\delta}{\delta x}\overline{v'u'}+\frac{\delta}{\delta y}\overline{v'v'}+\frac{\delta}{\delta z}\overline{v'w'}\right) \quad (25)$$

$$\rho\left(\frac{\delta\hat{w}}{\delta t}+u\frac{\delta(\hat{w}\hat{u})}{\delta x}+v\frac{\delta(\hat{w}\hat{v})}{\delta y}+w\frac{\delta(\hat{w}\hat{w})}{\delta z}\right)=\rho F_z-\frac{\delta\hat{p}}{\delta z}+\mu\left(\frac{\delta^2\hat{w}}{\delta x^2}+\frac{\delta^2\hat{w}}{\delta y^2}+\frac{\delta^2\hat{w}}{\delta z^2}\right)-\frac{1}{\rho}\left(\frac{\delta}{\delta x}\overline{w'u'}+\frac{\delta}{\delta y}\overline{w'v'}+\frac{\delta}{\delta z}\overline{w'w'}\right) \quad (26)$$

In which, $\hat{u}, \hat{v}, and\ \hat{w}$ are temporal averages of the velocity components (m/s), $\hat{p}$ is the temporal average of the pressure (Pa), and $u', v', and\ w'$ are fluctuations of the velocity components (m/s) (Pinho, 2000). This is very useful for numerical modeling because, with the spatial and temporal variations, the user can wind up with very fine grids and very small time steps that are very difficult to solve; therefore, the use of averaged quantities requires coarser grids, and larger time steps making it much easier to compute.

The abovementioned system of equations can be broadened with a scalar transport equation. The mass balance of a passive constituent A, introduced into a fluid characterized as turbulent is characterized by the following equation (Pinho, 2000),

$$\frac{\partial\hat{c}}{\partial t}+\frac{\partial(\hat{c}\,\hat{u})}{\partial x}+\frac{\partial(\hat{c}\,\hat{v})}{\partial y}+\frac{\partial(\hat{c}\,\hat{w})}{\partial z}=\varepsilon_m\left(\frac{\partial^2\hat{c}}{\partial x^2}+\frac{\partial^2\hat{c}}{\partial y^2}+\frac{\partial^2\hat{c}}{\partial z^2}\right)+\frac{\partial}{\partial x}\left(\varepsilon_{tx}\frac{\partial\hat{c}}{\partial x}\right)+\frac{\partial}{\partial y}\left(\varepsilon_{ty}\frac{\partial\hat{c}}{\partial y}\right)+\frac{\partial}{\partial z}\left(\varepsilon_{tz}\frac{\partial\hat{c}}{\partial z}\right) \quad (27)$$

assuming that,

$$-\varepsilon_{tx}\frac{\partial\hat{c}}{\partial x}=(\overline{u'c'})\,,-\varepsilon_{ty}\frac{\partial\hat{c}}{\partial y}=(\overline{v'c'}),-\varepsilon_{tz}\frac{\partial\hat{c}}{\partial z}=(\overline{w'c'}), \quad (28)$$

in which $\hat{c}$ is the average concentration of the passive constituent, c' is the fluctuation of the concentration relative to the temporal average, e_m is the molecular viscosity coefficient, and $e_{ti}$is the turbulent viscosity coefficient in the i-direction.

The molecular mass diffusivity remains constant, $\varepsilon_m = Cte$. The turbulent mass diffusivity, $\overline{\overline{\varepsilon_t}} = (\varepsilon_{tx}, \varepsilon_{ty}, \varepsilon_{tz})$ depends on its local flow properties, its value being $\varepsilon_{tx} = \varepsilon_{ty} = \varepsilon_{tz}$, in the case of isotropic turbulence (Pinho, 2000).

The parts which involve the fluctuations of velocity components relative to the average are called Reynolds stresses. In turbulent flow, Reynolds stresses are predominant when compared to stresses related to kinematic viscosity, with the exception of layers found near the borders where the average velocity gradient is much higher and the transversal fluctuations are practically annulled (Pinho, 2000).

Adopting the Boussinesq hypothesis, the Reynolds stresses are proportional to the gradient average velocities as seen in the equation below (Pinho, 2000),

$$-\overline{u_i' u_j'} = v_t \left(\frac{\partial u_i}{\partial x_j} + \frac{\partial u_j}{\partial x_i}\right) - \frac{2}{3}\delta_{ij} K; i, j = 1,2,3 \tag{29}$$

in which δ_{ij} is the Kronecker delta and $K = \frac{1}{2}\left(\overline{u'^2} + \overline{v'^2} + \overline{w'^2}\right)$ is the turbulent kinetic energy per mass unit.

The Reynolds equations in a 3D form and the continuity equation established in terms of mean values of $\hat{u}$, $\hat{v}$, $\hat{w}$, $\hat{p}$, and $\hat{c}$ are the starting point for the study of real flow. In coastal zones, these equations must undergo the necessary adjustments to the consideration of their particularities: shallow depths and prevailing consideration of other applied forces, such as the Coriolis effect, variations of atmospheric pressure, friction on the surface due to wind, and the influence of density gradients causes by the presence of substances like salts and pollutants (Pinho, 2000).

It is important to refer that for three dimensional shallow water flow, the stress and diffusion tensor are anisotropic. The horizontal eddy viscosity coefficient, v_H, and eddy diffusivity coefficient, D_H, are much larger than the vertical coefficients v_V and D_V, i.e. $v_H \gg v_V$ and $D_H \gg D_V$. The horizontal coefficients are assumed to be a superposition of three parts: a part due to molecular viscosity, a part due to 2D-turbulence and a part due to 3D-turbulence (Deltares, 2011). The two dimensional part is associated with the contribution of horizontal motions and forcing that cannot be resolved by the horizontal grid (Reynolds averaged computations). The three dimensional part is referred to as the three dimensional turbulence and is computed by following a turbulence closure model. In the case of 2D depth-averaged simulations, the horizontal eddy viscosity and eddy diffusivity coefficient should also contain

a contribution due to the vertical variation of the horizontal flow, i.e. Taylor shear dispersion (Deltares, 2011).

The turbulence closure models implemented to determine ν_V and D_V applied in Delft3D-FLOW are the constant coefficient, Algebraic Eddy viscosity closure Model (AEM), the *k*-L turbulence model, and the *k*-ε turbulence model. The turbulence models differ in their prescription of the turbulent kinetic energy *k*, the dissipation rate of turbulent kinetic energy ε, and/or the mixing length *L* (Deltares, 2011).

The first turbulence closure model is based on a constant value. This model will lead to parabolic vertical velocity profiles, otherwise known as laminar flow. The second model, the algebraic eddy viscosity model, does not involve transport equations for the turbulent quantities. It is a combination of two algebraic formulations and uses analytical formulas to determine *k* and *L*. The turbulent kinetic energy *k* depends on the friction velocities or velocity gradients, and for the mixing length L, the following function of depth is taken (Deltares, 2011),

$$L = \kappa\,(z+d)\sqrt{1-\frac{z+d}{H}} \tag{30}$$

with κ the Von Kármán constant, $\kappa \approx 0{,}41$. For a homogeneous flow this leads to a logarithmic velocity profile. In the cases of vertical density gradients, the mixing length must be corrected due to the fact that the turbulent exchanges are limited by buoyancy forces. Stratification stability can be described in the interaction between gravitational forces and turbulent shear production. It is characterized by the Richardson number, Ri, defined by (Deltares, 2011),

$$Ri = \frac{-g\frac{\partial \rho}{\partial z}}{\rho\left[\left(\frac{\partial u}{\partial z}\right)^2+\left(\frac{\partial v}{\partial z}\right)^2\right]} \tag{31}$$

in which, for $R_i \geq 0$, the stratification is stable and for $R_i < 0$, the stratification is unstable. Stable stratification leads to damping of turbulent mixing and unstable stratification leads to higher mixing. This damping function is dependent on the Richardson number as can be seen by the following equation (Deltares, 2011),

$$L = \kappa\,(z+d)\sqrt{1-\frac{z+d}{H}}\;F_L(Ri) \tag{32}$$

In Delft3D-FLOW, the algebraic eddy viscosity model is extended to stratified flows by the following formulation (Deltares, 2011),

$$F_L(Ri) = \begin{cases} e^{-2,3Ri}, & Ri \geq 0 \\ (1 - 14Ri)^{0,25}, & Ri < 0 \end{cases} \quad (33)$$

The third model involves one transport equation for *k* and is called a first order turbulence closure scheme. The mixing length *L* is prescribed analytically and the same formulation, including damping functions, is used as for the AEM turbulence model. Nevertheless, to find the kinetic energy *k*, a transport equation is solved. This model is known as the *k*-*L* model.

The fourth turbulence closure model is *k*-ε turbulence model, a second order turbulence model, in which both the turbulence energy *k* and dissipation rate of turbulent kinetic energy ε are calculated by a transport equation. From *k* and ε, the mixing length *L* and viscosity are determined. The mixing length is now a property of the flow, and in the case of stratification no damping functions are needed. For more details on any of these models, one can refer to the Delft3D-FLOW Manual.

3.3. Pre-processing – Delft Dashboard

Delft Dashboard, seen in Figure 3-2, is a software distributed by Open Earth, a free and open source initiative mainly dealing with marine and coastal earth science and engineering projects. Open Earth provides a platform to archive, host, and disseminate high quality data, state-of-the-art model systems and well-tested tools for practical analysis (Deltares, 2014). Delft Dashboard is a pre-processing information system developed by Deltares, aimed at facilitating the use of data and expert knowledge in coastal problems, by supporting modelers as much as possible in the efforts needed to set up new models and manage and use existing ones enabling researchers to quickly try out innovative approaches by advanced prototyping (Deltares, 2014). The general layout of Delft Dashboard consists of a Top menu, describing the most common functions, a Delft3D menu, and a Map View, as seen in Figure 3-2. The Deflt3D menu is similar to the FLOW modeling suite interface; however, it includes a number of Toolbox Tabs, that can be used directly within waves, hydrodynamics, morphodynamics, or water quality calculations.

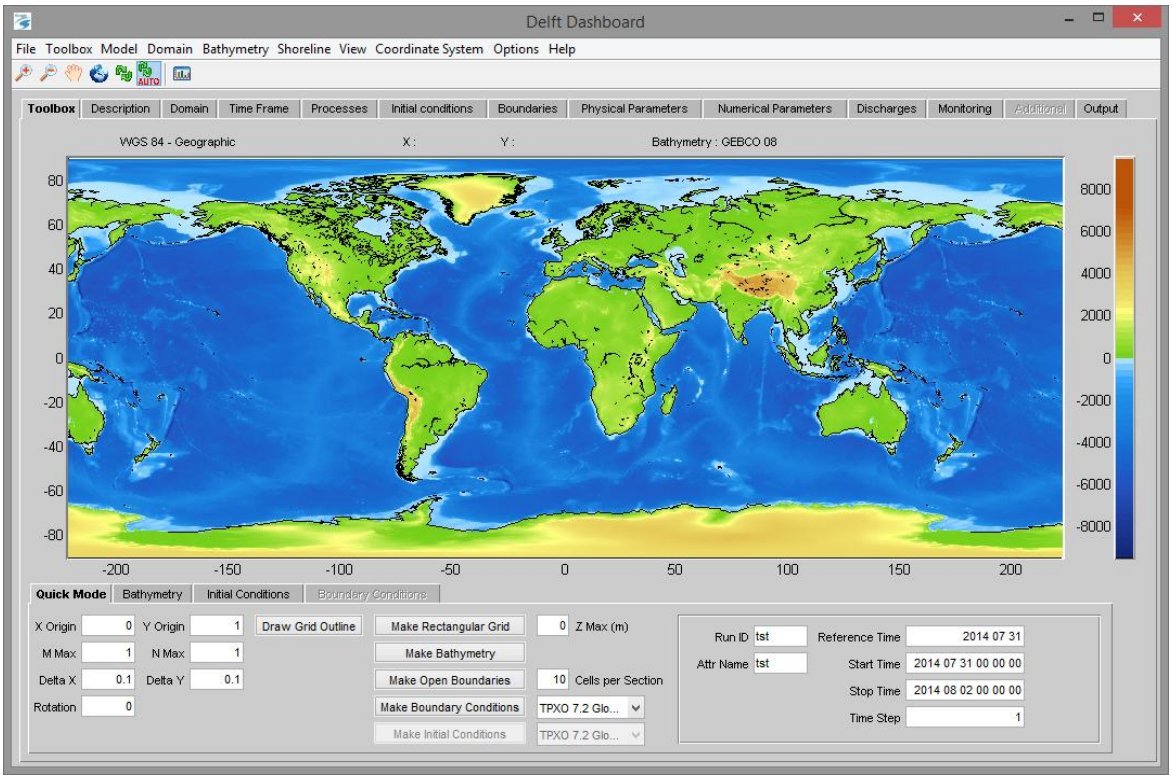

Figure 3-2 - Delft Dashboard Graphical User Interface (Deltares, 2014).

In the case of Delft Dashboard, it is a Matlab based interface coupled with many toolboxes, specified in Table 3-1, to allow for easy data preparation (Deltares, 2014). It is an application, focused on supporting modelers in easy model generation. The set up of a model that once took weeks of work, can be executed in a matter of minutes, for any location in the world.

Table 3-1 - Delft Dashboard Toolboxes and respective Functionalities (Deltares, 2014).

Toolbox	Functionality
Model Maker	Construction or refinement of an existing model.
Bathymetry	Import, export and merge bathymetry data.
Domain Decomposition	Refinement of a coarser grid and set up of a simulation using domain decomposition technique.
Geo Image	Download satellite images to be used as model output background.
Navigation Charts	*Under development:* download data from navigation charts.
Nesting	Set-up a simulation using nested models.
Nourishments	*Under development:* compute spatial advection and diffusion of a nourishment.
Observation Stations	*Under development:* download real-time observations.
Shoreline	Download and export of shoreline data.
Tide Database	Download and export 2D tidal astronomical constituents on a predefined grid.
Tide Stations	Download water level time series derived using astronomical constituents for a selected tidal station.
Tiling	To add bathymetry data to Delft Dashboard after tiling
Tropical Cyclone	Computes wind field and pressure drop generated by a cyclone.
Tsunami	Computes water level initial displacement induced by an earthquake.

3.3.1. Master Definition File

The first feature to refer to when discussing flow simulation for Deflt3D-FLOW is the Master Definition or MDF-file. The MDF-file is an input file of all the simulation's data. It is the file that retains all the necessary, pre-defined information for the model and for running the model in Delft3D-FLOW. It is an ASCII-file, each line containing a maximum of 300 characters, where one can attribute files where important data is stored. The MDF-file contains only relevant input parameters and references to these attribute files. With the selection of an already existing MDF-file (*.mdf), one can also load into memory and display all the attribute files and their respective data (Deltares, 2011).

Attribute files contain input quantities, such as time dependent input data, for example, wind intensity when defining a tropical cyclone. The names of the main attribute files are free, but their extension is mandatory, indicated in Table 3-2.

Table 3-2 - Main Attribute Files (Deltares, 2011).

Quantity	Filename and mandatory extension
Bathymetry or depth	<name.dep>
Grid	<name.grd>
Flow boundary conditions (astronomic)	<name.bca>
Flow boundary conditions (harmonic)	<name.bch>
Flow boundary conditions (QH-relation)	<name.bcq>
Flow boundary conditions (time-series)	<name.bct>
Grid enclosure	<name.enc>
Initial conditions	<name.ini>
Open boundaries	<name.bnd>
Wind	<name.wnd>

Many different types of information are needed in order to correctly execute a flow simulation, like the extent of the model being considered, its bathymetry, its boundary conditions, and so forth. A numerical grid is then created in which all location-based parameters are defined. According to the (Ormondt, 2012), the following are the basic steps one should take before defining the input file:

1. Selection of the extent of the area to be modeled
2. Definition of the location and extent of open boundaries and the type of boundaries to be prescribed, i.e. water level, velocities or discharges
3. Definition of the land (-water) boundaries

4. Generation of the numerical grid
5. Generation of the bathymetry defined on the numerical grid
6. Definition of the many different grid related quantities, such as open boundaries, monitoring points, etc.
7. Definition of the time frame of the scenario in question, i.e. start and stop time and various time functions,, such as open boundary conditions, wind speed and direction, discharges, and salinity concentrations or other substances transported by the flow.

In the following section, a more in depth description of how to set up a simulation will be described.

3.3.2. Setup

Before the start of setting-up a simulation, the coordinate system must first be selected because this will eliminate any previous model setting. A warning message will pop-up before choosing a new coordinate system: “All model and Toolbox window will be discarded! Continue?”. If "Yes" is chosen, a new model will be set up from scratch, based on the newly selected coordinate system (Deltares, 2014).

The next step is the definition of the simulation's time frame. The time frame defines the relationship between the real world time axis and that of the simulation. The time frame input can be defined as [dd mm yyyy hh mm ss]. The "Reference Data" is the arbitrary t=0 time for the time series being simulated. The "Start Time" and the "Stop Time" define the start and end of the simulation, respectively, and the forcing of all processes in the simulation. The "Time Step" is defined as the time interval for which the results of the simulation is set. As a default, the time interval is set to 1 minute.

In Delft Dashboard's Output Tab, one can input the “Start Time”, “Stop Time”, “Time Step” at which point, the output data will be stored in the Map and Communication output files. Maps are snapshots of the computed quantities of the entire area. In the Communication file, data required for other modules of Delft3D can be stored. Seeing that the results must be stored in all grid points, a Communication file can be quite large. Again, the Time Steps are both set in minutes. The first several time steps result in water level at zero meters. This is

because initially, the model is at rest ("cold start"). Short waves will progress from the open boundaries until reaching the shore (Deltares, 2011).

Once the time frame is defined, one should proceed to the definition of the grid. As default, Delft Dashboard starts with the Model Maker Toolbox, seen in Figure 3-3. This tool allows the user to create or improve a computational grid (*.grd file). It is also possible to extract and interpolate bathymetry data (*.dep file) and boundary conditions (*.bnd file) from open source online databases on the grid. The numerical method of Delft3D-FLOW is based on finite differences. Delft Dashboard allows for the generation of rectangular grids. Although the creation of curvilinear grids is not possible with Delft Dashboard, the program does support operations that have been created separately with Delft3D-RGFGRID for Delft3D-FLOW.

There are two kinds of grid coordinate systems supported by Delft3D-FLOW. They are the Cartesian coordinate system and the spherical coordinate system. The Cartesian coordinate system demands that the latitude of the model area be specified so that it may be used to calculate the Coriolis force for the entire area. For the spherical grid, the Coriolis force is calculated from the latitude coordinates in the grid file and therefore varies in the latitude direction. Spherical grids are usually applied to larger, regional models (Deltares, 2011).

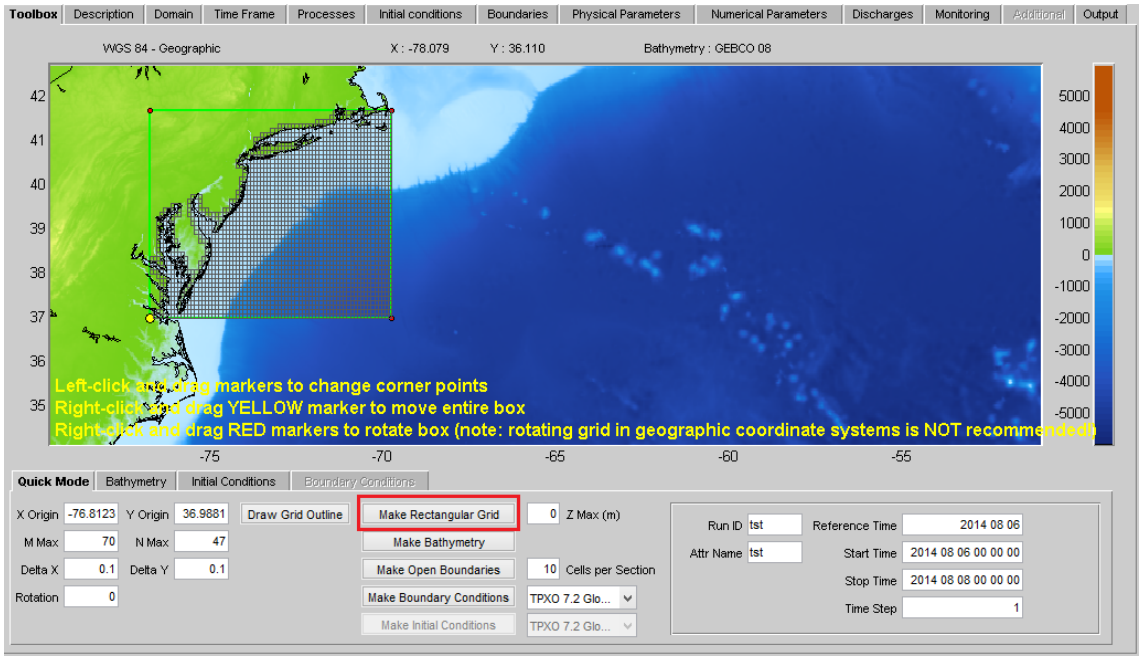

Figure 3-3 - Model Maker Toolbox - Grid Generation (Deltares, 2014).

Once the rectangular grid is defined with the "Draw Grid Outline" option, one can automatically generate the grid file, as well as, the grid enclosure file by selecting the "Make Rectangular Grid" option on the Model Maker Toolbox, Figure 3-3. The M max dimension represents the number of grid points in the x-direction and the N max dimension represents the number of grid points in the y-direction. The Delta X and Delta Y values correspond to the desired horizontal grid resolution. The Z max value is the altitude that one wants to cut out the grid above that value, in reference to the mean sea level. In the defined grid file, the type of coordinate system is stored along with the number of grid points in both directions and the coordinates of the grid points. The grid enclosure file (*.enc) represents a closed polygon specified on a grid through water level points. Its functions are to define the active (wet) or potentially active computational cells in the domain and to locate the open and closed boundaries (Deltares, 2011).

In Figure 3-4, a prototype of a grid applied in Delft3D-FLOW is shown, in which the closed boundaries are defined by the u- or v- points, and the open boundaries defined by either u-, v-, or water level (ζ) points depending on the type of boundary condition (Deltares, 2011). A more detailed description of the nature of the type of grid applied in Delft3D-FLOW can be found in the next chapter in Section 3.4.1.2.

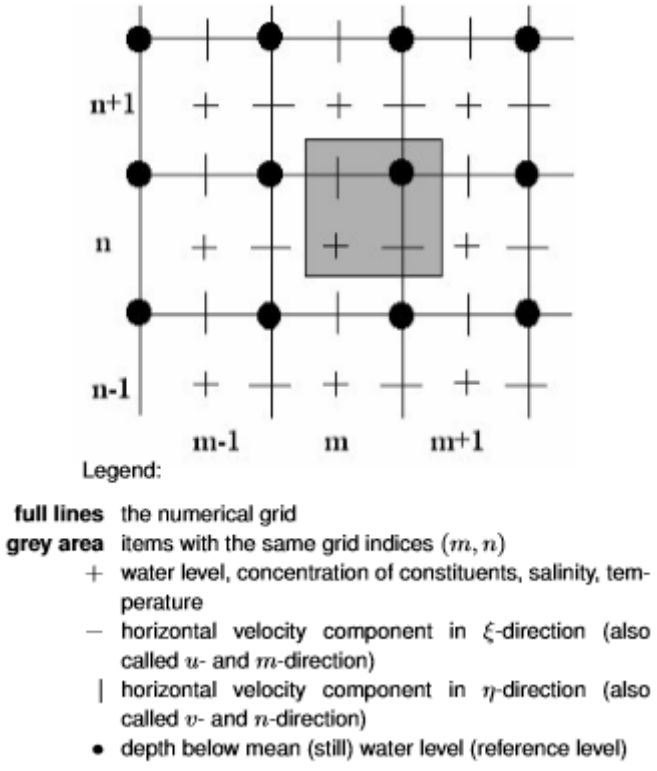

Figure 3-4 - Staggered grid applied in Delft3D-FLOW (Deltares, 2011).

The accuracy of the designed coastal model is very closely related to the bathymetry and the meteorological data. A good definition of boundary conditions, such as river inflow or tidal signals are important to be able to produce an output of good quality. Delft Dashboard's Map View shows the map with the bathymetry and topography used in the model's construction. In Figure 3-5, different types of bathymetry accessed by Delft Dashboard are shown. When selecting the "Make Bathymetry" option, the bathymetry selected is defined for the model.

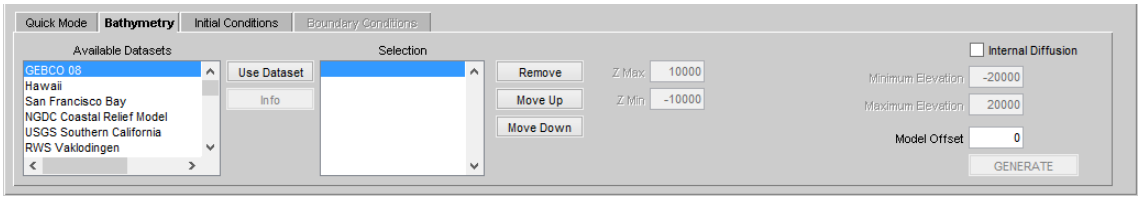

Figure 3-5 - Model Maker Toolbox - Bathymetry Generation (Deltares, 2014).

The various bathymetry databases accessible in Delft Dashboard are:

- GEneral Bathymetry Chart of the Ocean (GEBCO)
- National Geophysical Data Center (NGDC) Coastal Relief Model
- Shuttle Radar Topography Mission (SRTM) v4.1 (Only Land Data)
- United State Geological Survey (USGS) - Hawaii
- USGS - San Francisco Bay
- USGS Southern California
- Rijks Water Staat
- Southeastern Universities Research Association (SURA) -Gulf of Mexico
- European Marine Observation and Data Network (EMODnet) - Adriatic Sea - Ionian Sea - Central Mediterranean
- EMODnet - Aegean Sea - Levantine Sea
- EMODnet - Bay of Biscay - Iberian Coast
- EMODnet - Celtic Seas
- EMODnet - Greater North Sea
- EMODnet - Western Mediterranean
- Marine Scotland - West of Lewis

Each bathymetry is associated to a specific reference system. The Delft Dashboard default setting is the GEBCO 2008 world bathymetry (Deltares, 2014). It is also possible to add one's own bathymetry dataset. Again, it is crucial to remember that before setting-up a simulation, a

coordinate system must be is selected. Delft Dashboard's default coordinate system is the WGS84 coordinate system.

Then, proceeding to the definition of the grid's boundaries, one selects the "Make Open Boundaries" option for the definition of the open boundaries (*.bnd), followed by the "Make Boundary Conditions" for the definition of the closed boundaries (*.bca, *.bch, *.bcq, or *.bct). The open boundary represents the conditions of the "outer world", meaning the area that goes beyond the model area. They are artificial "water-water" boundaries in which flow and transport conditions are required. They should be situated as far away from the study area as possible. Closed boundaries, on the other hand, are natural "land-water" boundaries. A more detailed description of the specific boundary conditions for the 3D or 2D depth-averaged shallow water or long-wave equations applied in Delft3D can be found in the next chapter in Section 3.4.1.3 (Deltares, 2011).

The open boundaries are divided into sections, identified by its "Name" (North, East, South, and West), with start and end coordinates designated as ("M1","N1") and ("M2","N2") respectively, and an associated reflection coefficient ("Alpha"), portrayed in Figure 3-6. The reflection parameter indicates how much one wants to make the open boundary less reflective for short wave disturbances.

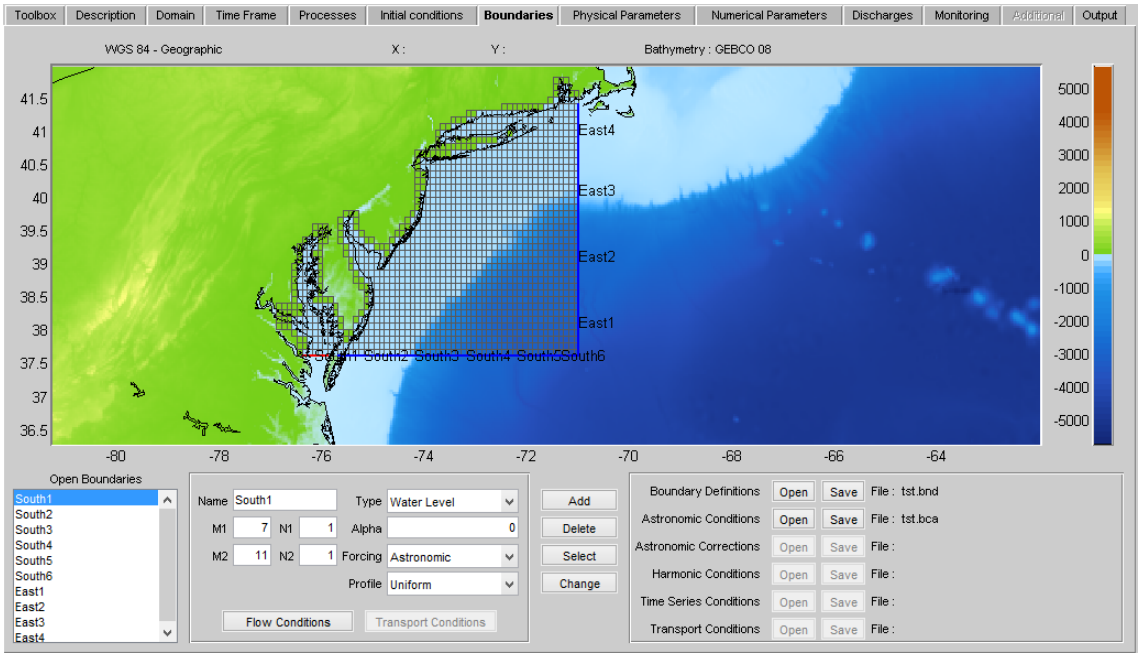

Figure 3-6 - Model Maker Toolbox - Boundary Condition Definition (Deltares, 2014).

The following boundary condition types in Delft Dashboard are available:

- Water level
- Velocity
- Neumann (water level gradient)
- Discharge or flux (total or per grid cell)
- Riemann or weakly reflective boundaries

Hydrodynamic forcing can be prescribed using harmonic or astronomical components, or time-series. Water level forcing can be specified in terms of QH-relations. Lastly, the transport of salinity, temperature, and constituents are prescribed be specifying the inflow concentrations.

Astronomic boundary flow conditions are defined in terms of astronomical components, like tidal constituents, amplitudes, and phases. Each nodal amplitude and phase are determined at the beginning of the simulation and updated at every time interval. These components are obtained from a tidal analysis program. Harmonic flow conditions are similar to the astronomical flow conditions, but have the added benefit of its parameters being user defined. The harmonic component's frequency, amplitude, and phase must be defined. This grows to be a lengthy activity, seeing as ten of components can be prescribed. Time-series flow conditions are specified in terms of the values of the selected kind, such as water level, Neumann, etc. Last of all, QH-relation flow conditions states the relation between the computed outflow discharge and the water level at the boundary. Intermediate vales are calculated through linear interpolation (Deltares, 2011). The vertical profile for hydrodynamics can be selected between one of them: “Uniform”, “Logarithmic”, “Per Layer”. This last choice does not apply for “Water Level” or “Neumann: controlled boundary sections, neither for a depth-averaged simulation (Deltares, 2014).

Once all the discussed parameters are defined and associated to their respective attribute files, one can then proceed to the definition of the tropical cyclone.

3.3.3. Tropical Cyclone Toolbox

The wind field of a tropical cyclone can be characterized by rapidly rotating air around a center of circulation, while also flowing radially inwards causing the air to rotate cyclonically in order to conserve angular momentum. Due to the Coriolis effect, the cyclonic rotation is in

the counterclockwise direction in the northern hemisphere and in the clockwise direction in the southern hemisphere. The cause of the Coriolis effect is mainly due to the rotation of the Earth. As the Earth spins in a counterclockwise direction, anything flowing above the Earth's surface is deflected. As the latitude increases, the speed of the Earth's rotation also increases and as a result, the Coriolis effect increases. Essentially, an object moving along the equator (tropical cyclone) would be able to continue moving directly along the equator without any apparent deflection; however, a little to the north or to the south, the object is drawn away. The further from the equator, i.e. the poles, the most deflection is experienced (Briney, 2014).

The abovementioned "object" executing motion around a point possesses a magnitude called angular momentum which can be quantified with the following equation,

$$L = mvr \tag{26}$$

where L is the angular momentum, m is the mass of the object, v is the magnitude of its velocity, and r is the separation between the objects (University of Tennessee, 2014). This is a simplified form of its quantification, neglecting the effect of the center of mass. This simplified form can be rewritten as the following,

$$v = L/(mr) \tag{27}$$

in which L represents a constant for an isolated system, the velocity v and the separation r are inversely correlated. Thus, conservation of angular momentum requires that a decrease in separation, r, be accompanied by an increase in the velocity, v, and vice versa. This is an important concept that carries over to more complicated systems, such as rotating bodies. An example of this is tropical cyclones. If the radius decreases (air flowing inwardly), the cyclone must spin faster in order to conserve angular momentum. This "radius" corresponds to the inner radius of the eyewall known as the radius of maximum winds, Rmax. This is the area in which the most severe weather occurs (University of Tennessee, 2014).

Radial inflow is typically maximized within the boundary layer. Weaker inflow is observed into the middle troposphere. When reaching the eyewall, the radial inflow rapidly decelerates and the resulting convergence leads to the ascending motion over a deep vertical layer within the eyewall. Once the system is sufficiently aloft, the air flows away from the storm's center producing a shield of *cirrus* clouds. *Cirrus* clouds are clouds that form in very high elevations and often mark the start of a warm front, an indication of bad weather.

Delft Dashboard's Tropical Cyclone Toolbox computes the wind field and pressure drop generated by a cyclone (Deltares, 2014). The selection of “Draw Track” is used to trace a particular cyclone’s trajectory, then defining its respective time step in hours, maximum wind speed (Vmax) in knots, maximum radius wind speed (Rmax) in nautical miles, and pressure drop (Pdrop) in Pascal. The intensity or maximum wind speed is defined as the system's maximum sustained winds. The World Meteorological Organization defines sustained winds by measuring winds at a height of 10 meters and then taking the average. The United States National Weather Service, however, defines sustained winds within a tropical cyclone by averaging winds over a period of one-minute, measuring at the same height of 10 meters. The radius of maximum winds is characterized as the distance from the center of the tropical cyclone to the location of the cyclone's maximum winds. In well-developed hurricanes, the radius is found in the inner eyewall, while in subtropical systems, the radius occurs very frequently far away from the center. Lastly, the pressure drop represents the difference between the ambient and central pressures of a tropical system. The ambient pressure at sea level can be represented as 1 atmosphere, equivalent to 1,01345 bar, or 101325 Pascal.

The space varying wind and pressure on a spiderweb grid is added to the wind input which is then interpolated and combined in and around the cyclone. In Figure 3-7, the wind definition according to the nautical convention is illustrated, that is, the wind from the true North has direction zero and the wind turns clockwise with an increasing angle (Deltares, 2011).

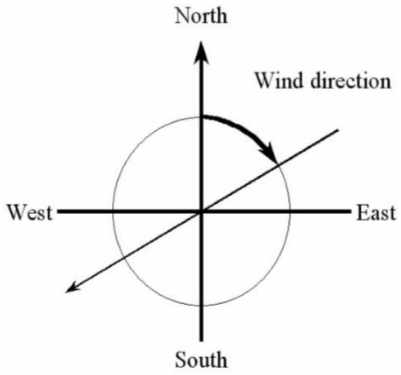

Figure 3-7 - Wind Definition according to Nautical Convention (Deltares, 2011).

When computing the cyclone, a Spiderweb file (*.spw file) is created containing wind field and pressure drop. Before computing, a number of parameters related to the spiderweb, which follows the cyclone in the computation can be defined, under “Spiderweb Parameters”, such as, the directional bins, “Dir bins”, and radial bins, “Radial bins” (Deltares, 2014).

The spiderweb grid is circular in which the number of rows, "n_rows", and number of columns, "n_cols", must be defined. The number of rows determine the grid size in a radial direction, while the number of columns define the grid size in an angular direction (Deltares, 2011). An example is shown in Figure 3-8. In Table 3-3, the header description of the spiderweb file is given, describing the values and respective meaning for the keywords found in the created spiderweb wind and pressure file.

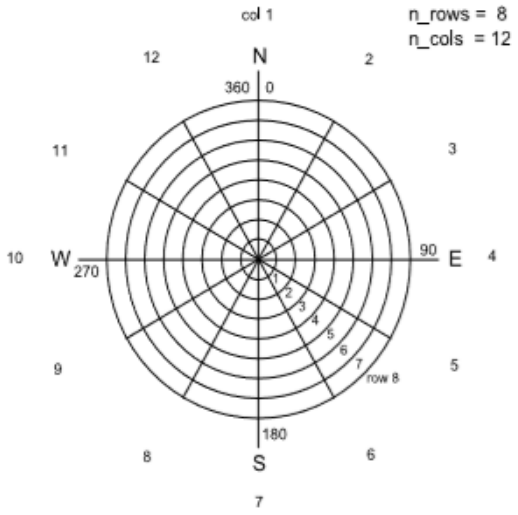

Figure 3-8 - Example of Spiderweb Grid Definition (Deltares, 2011).

Table 3-3 - Header Description of Spiderweb Wind and Pressure File (Deltares, 2011).

Keywords	Value	Description
FileVersion	1.03	version of file format
Filetype	meteo_on_spiderweb_grid #from TRACKfile: trackfile.trk	meteo input on Spiderweb grid
NODATA_value	free	value used for input that is to be neglected
n_cols	free	number of gridpoints in angular direction
n_rows	free	number of gridpoints in radial direction
grid.unit	m or degree	unit of Spiderweb grid
spw_radius	free	radius of the Spiderweb radius given in units given by spw_rad_unit
spw_rad_unit	m	unit of the Spiderweb radius
n_quantity	3	number of quantities specified in the file
quantity1	wind_speed	wind speed given in unit unit1
quantity2	wind_from_direction	direction where the wind is coming from given in unit unit2
quantity3	p_drop	drop in atmospheric pressure given in unit unit3
unit1	m s-1	unit of quantity1: meters/second
unit2	degree	unit of quantity2: degrees
unit3	Pa or mbar	unit of quantity3:Pascal or millibar

For each defined time step, the cyclone eye's position is given in the x and y direction, as well as its atmospheric pressure drop. In Figure 3-9, an example of the created spiderweb file for a spiderweb grid is given, corresponding to the "n_col" and "n_rows" portrayed in Figure 3-8.

```
FileVersion     = 1.03
filetype        = meteo_on_spiderweb_grid #from TRACK file: trackfile.trk
NODATA_value    = -999.000
n_cols          =    12
n_rows          =     8
grid_unit       = degree
spw_radius      =         500000.00
spw_rad_unit    = m
n_quantity      = 3
quantity1       = wind_speed
quantity2       = wind_from_direction
quantity3       = p_drop
unit1           = m s-1
unit2           = degree
unit3           = Pa
TIME            =           0.00 hours since 2014-08-06 00:00:00 +00:00
x_spw_eye       =      -72.39
y_spw_eye       =       38.35
pdrop_spw_eye   =          3000.00
   25.30   25.30   25.31   25.32   25.33   25.34   25.34   25.34   25.33   25.32   25.31   25.30
   16.36   16.37   16.39   16.43   16.47   16.50   16.51   16.50   16.47   16.43   16.39   16.37
   11.23   11.25   11.30   11.38   11.45   11.50   11.52   11.50   11.45   11.38   11.30   11.25
    7.93    7.95    8.02    8.12    8.22    8.30    8.32    8.30    8.22    8.12    8.02    7.95
    5.71    5.73    5.81    5.93    6.04    6.13    6.16    6.13    6.04    5.93    5.81    5.73
    4.19    4.22    4.31    4.42    4.55    4.64    4.67    4.64    4.55    4.42    4.31    4.22
    3.15    3.18    3.26    3.38    3.50    3.59    3.63    3.59    3.50    3.38    3.26    3.18
    2.43    2.45    2.53    2.63    2.75    2.84    2.88    2.84    2.75    2.63    2.53    2.45
   65.00   95.00  125.00  155.00  185.00  215.00  245.00  275.00  305.00  335.00    5.00   35.00
   65.00   95.00  125.00  155.00  185.00  215.00  245.00  275.00  305.00  335.00    5.00   35.00
   65.00   95.00  125.00  155.00  185.00  215.00  245.00  275.00  305.00  335.00    5.00   35.00
   65.00   95.00  125.00  155.00  185.00  215.00  245.00  275.00  305.00  335.00    5.00   35.00
   65.00   95.00  125.00  155.00  185.00  215.00  245.00  275.00  305.00  335.00    5.00   35.00
   65.00   95.00  125.00  155.00  185.00  215.00  245.00  275.00  305.00  335.00    5.00   35.00
   65.00   95.00  125.00  155.00  185.00  215.00  245.00  275.00  305.00  335.00    5.00   35.00
   65.00   95.00  125.00  155.00  185.00  215.00  245.00  275.00  305.00  335.00    5.00   35.00
   872.9   872.9   872.9   872.9   872.9   872.9   872.9   872.9   872.9   872.9   872.9   872.9
   426.5   426.5   426.5   426.5   426.5   426.5   426.5   426.5   426.5   426.5   426.5   426.5
   273.5   273.5   273.5   273.5   273.5   273.5   273.5   273.5   273.5   273.5   273.5   273.5
   198.3   198.3   198.3   198.3   198.3   198.3   198.3   198.3   198.3   198.3   198.3   198.3
   154.1   154.1   154.1   154.1   154.1   154.1   154.1   154.1   154.1   154.1   154.1   154.1
   125.2   125.2   125.2   125.2   125.2   125.2   125.2   125.2   125.2   125.2   125.2   125.2
   105.0   105.0   105.0   105.0   105.0   105.0   105.0   105.0   105.0   105.0   105.0   105.0
    90.1    90.1    90.1    90.1    90.1    90.1    90.1    90.1    90.1    90.1    90.1    90.1
TIME            =           6.00 hours since 2014-08-06 00:00:00 +00:00
x_spw_eye       =      -73.83
y_spw_eye       =       41.32
pdrop_spw_eye   =          1500.00
   21.12   23.73   24.98   24.74   23.03   20.03   16.09   11.90    9.00    9.66   13.22   17.43
   12.17   13.95   14.80   14.66   13.53   11.48    8.65    5.27    1.91    2.94    6.41    9.60
    9.56   10.57   11.08   11.01   10.36    9.19    7.67    6.15    5.21    5.45    6.65    8.17
    8.73    9.28    9.56    9.54    9.18    8.55    7.77    7.07    6.70    6.81    7.32    8.03
    8.44    8.75    8.91    8.90    8.70    8.34    7.91    7.55    7.37    7.42    7.69    8.06
    8.32    8.50    8.60    8.60    8.47    8.26    8.00    7.79    7.68    7.72    7.88    8.09
    8.26    8.37    8.44    8.44    8.36    8.22    8.05    7.92    7.85    7.88    7.98    8.11
    8.22    8.30    8.35    8.35    8.29    8.20    8.08    7.99    7.95    7.97    8.04    8.13
   86.29  107.78  128.26  148.54  169.27  191.36  216.55  248.85  295.91  351.76   33.18   62.43
  104.04  117.10  130.51  144.05  157.51  170.59  182.56  190.80  173.11   83.63   81.91   91.80
  118.35  124.77  132.37  140.35  147.94  154.09  157.02  153.63  140.84  124.25  115.17  114.37
  126.38  129.44  133.55  138.02  142.13  145.00  145.56  142.89  137.24  130.86  126.47  125.11
  130.27  131.87  134.18  136.76  139.10  140.60  140.68  139.05  136.13  132.97  130.67  129.77
  132.21  133.13  134.51  136.10  137.53  138.40  138.38  137.37  135.66  133.86  132.53  131.97
  133.24  133.81  134.70  135.72  136.66  137.22  137.18  136.52  135.43  134.30  133.47  133.10
  133.83  134.21  134.81  135.51  136.14  136.53  136.50  136.04  135.30  134.55  133.99  133.75
   224.5   224.5   224.5   224.5   224.5   224.5   224.5   224.5   224.5   224.5   224.5   224.5
    60.2    60.2    60.2    60.2    60.2    60.2    60.2    60.2    60.2    60.2    60.2    60.2
    27.2    27.2    27.2    27.2    27.2    27.2    27.2    27.2    27.2    27.2    27.2    27.2
    15.4    15.4    15.4    15.4    15.4    15.4    15.4    15.4    15.4    15.4    15.4    15.4
     9.9     9.9     9.9     9.9     9.9     9.9     9.9     9.9     9.9     9.9     9.9     9.9
     6.9     6.9     6.9     6.9     6.9     6.9     6.9     6.9     6.9     6.9     6.9     6.9
     5.1     5.1     5.1     5.1     5.1     5.1     5.1     5.1     5.1     5.1     5.1     5.1
     3.9     3.9     3.9     3.9     3.9     3.9     3.9     3.9     3.9     3.9     3.9     3.9
```

Figure 3-9 - Example of the spiderweb file on a 8x12 grid.

It is important to refer that the spiderweb grid has to be input in spherical coordinates, else it cannot be created. In the example shown in Figure 3-9, the cyclone and its respective spiderweb grid will have a radius of 500 kilometers. It is an 8x12 grid, meaning that the radius will be divided into 8 parts of 62,5 km each, and the 360 degrees of the respective circle divided into 12 parts of 30 degrees each. In this example, the wind speeds, wind directions, and pressure drops are given at two time steps. A shift of the cyclone's eye (latitude, longitude) can be observed from (-72,39, 38,35) to (-73,83, 41,32). Also, the pressure drop along the spiderweb wind field's eye decreases from 3000.0 Pa to 1500.0 Pa.

3.4. Processing and Post-Processing

In this chapter, a more entailed description of the processing (Delft3D-FLOW) and post-processing (QUICKPLOT) tools used will be given. In addition, a brief explanation of Delft3D-FLOW's numerical method – based on the finite difference method, will be addressed. The set of governing equations applied in Delft3D-FLOW for solving the Navier-Stokes equations for an incompressible fluid under shallow water will be described as well as the numerical aspects for a set of partial differential equations in combination with an appropriate set of initial and boundary conditions solved on a finite difference grid. The space discretization and time integration methods applied in Delft3D-FLOW will also be presented.

3.4.1. Delft3D-FLOW

With the application of Delft3D, it is possible to simulate the interaction of water, sediment, ecology, and water quality in time and space (Deltares, 2011). Delft3D simulates both two-dimensional and three-dimensional flow, sediment transport, morphology, waves, water quality, and ecology. This Delft3D collection is made up of D-Flow, D-Morphology, D-Wave, D-Water Quality, D-Ecology, and D-Particle Tracking. This compilation of modules is used for the modeling of the natural environments like coastal, river and estuarine zones.

D-Flow, the module used in this dissertation, is the standard processing program and covers curvilinear and rectilinear grids, full 2D hydrostatic flow, advection-diffusion module for salinity, temperature and substances, density driven flows, float (drogue) tracking, meteorological influences, on-line visualization and wave-current interaction. The D-Flow

includes 3D flow and turbulence modeling, spherical grids, domain decomposition (connect multiple grids; refinement in both horizontal and vertical direction allowed), structures (weirs, gates, floating structures, semi-transparent structures) and horizontal large eddy simulations (sub-grid turbulence in horizontal) (Deltares, 2011).

3.4.1.1. Finite Difference Method

Because the numerical method of Delft3D-FLOW is based on finite differences, this section will be dedicated to a brief summary of this method. The idea of this method is to replace the derivatives that appear in the differential equations by finite differences that approximate them. The finite difference method is the core of the Delft3D-FLOW program.

In order to obtain, for example, the physical quantity of a flow, the fluid's velocity can be measured at specific points. In order to obtain the flow quantities in between the points, they can be interpolated. The accuracy of the interpolation will depend on the distance in between the points. In this way, numerical techniques convert differential equations for finding the solution at discrete points in space which are referred to as "grid points". A holistic picture of the flow is created from the solution at those points. The different discretization methods usually divide the domain to produce sets of discrete numerical approximations to the derivative.

On a set of grid points, there are values of the dependent variable which can replace the continuous information contained in the differential equations' discrete values. This is said to discretize the distribution of the dependent variable in the domain of interest. The algebraic equations that involve the unknown values of the functions at the grid points are derived from the governing differential equations by transferring the spatial derivatives to their discrete approximations. These discretized equations are, in a way, the algebraic relations connecting the approximations of the values of the dependent variable at the grid points. Because the algebraic equations are derived from differential equation, they express the same physical information as the differential equation (Sayma, 2009).

The finite difference method is an especially simple procedure when used on meshes with a high degree of regularity, for example, uniform grids. This method consists of approximating the derivatives in the differential equation using a truncated Taylor series. The mesh should be

set up in a structured way, where its points should be located at the intersection points of families of rectilinear curves. This method is greatly useful for solution procedures which require higher order derivatives or high order of accuracy.

The finite difference approximation is described as the following,

$$\frac{\delta u}{\delta x} \approx \frac{u(x+\Delta x,y,z,t)-u(x,y,z,t)}{\Delta x} \tag{34}$$

in which for an approximation of u, the x, y, and z variables correspond to the Cartesian grid coordinates, and t variable corresponds to the time. From the many ways to approximate the first derivative, only the three basic difference schemes will be presented. They are the forward, backward, and central difference approximations (Petrovic, 2005).

The forward difference approximation:

$$\frac{\delta u}{\delta x} \approx \frac{u(x+\Delta x,y,z,t)-u(x,y,z,t)}{\Delta x} + O(\Delta x) \tag{35}$$

The backward difference approximation:

$$\frac{\delta u}{\delta x} \approx \frac{u(x,y,z,t)-u(x-\Delta x,y,z,t)}{\Delta x} + O(\Delta x) \tag{36}$$

The central difference approximation:

$$\frac{\delta u}{\delta x} \approx \frac{u(x+\Delta x,y,z,t)-u(x-\Delta x,y,z,t)}{2\Delta x} + O(\Delta x)^2 \tag{37}$$

The O given in each of the equations expresses the local truncation error from a single application of the method (Petrovic, 2005).

Since the second derivative is the first derivative of the first derivative,

$$\frac{\delta^2 u}{\delta x^2} \approx \frac{\frac{\delta u}{\delta x}(x+\Delta x/2,y,z,t)-\frac{\delta u}{\delta x}(x-\Delta x/2,y,z,t)}{\Delta x} \tag{38}$$

and,

$$\frac{\delta^2 u}{\delta x^2} \approx \frac{\frac{u(x+\Delta x,y,z,t)-u(x,y,z,t)}{\Delta x}-\frac{u(x,y,z,t)-u(x-\Delta x,y,z,t)}{\Delta x}}{\Delta x} \tag{39}$$

The second order derivative finite difference approximation is therefore:

$$\frac{\delta^2 u}{\delta x^2} \approx \frac{u(x+\Delta x,y,z,t)-2u(x,y,z,t)+u(x-\Delta x,y,z,t)}{(\Delta x)^2} \quad (40)$$

The spatial domain is discretized in equal space intervals of Δx. Evidently, however smaller the steps of Δx, the closer the values between the differential and difference of the rate of change of the function. The more nodes included in the calculation of the derivative, the higher the order of the scheme. The finite difference formulae for the first derivative can be formulated using any number of adjacent points with the order of approximation increasing with the number of points. A balance needs to be found between the order of accuracy and the number of grid points involved in the computation. This dictates the computational memory and effort needed. They both need to be kept to a minimum for a given overall solution accuracy. Boundary conditions can then be applied by setting known values at the end points. The system of algebraic equations can then be solved for the unknown quantities at the grid points (Sayma, 2009).

3.4.1.2. Staggered Grid

To discretize 3D shallow water equations, the variables (water level and velocity) must be arranged in a specific way. They must follow a pattern referred to as a staggered grid. A staggered grid allows for the natural and accurate formulation of partial differential equations with finite differences, as is the case of the Navier-Stokes and continuity equations. Not all quantities are defined in the same location in a numerical grid. They are stored in cell centers, not all in the same positions.

The arrangement used in Delft3D-FLOW is known as the Arakawa C-Grid. Commonly used in Earth system models for meteorology and oceanography, Arakawa grid systems portray several ways to represent and compute orthogonal physical qualities, such as velocity, pressure, etc. This type of grid (Arakawa C-Grid) allows for the evaluation of the u velocity components (east and west) at the grid center as well as the center of the left and right grid faces, and the evaluation of the v velocity components (north and south) at the grid center as well as at the centers of the upper and lower grid faces (Deltares, 2011). This is portrayed below in Figure 3-10.

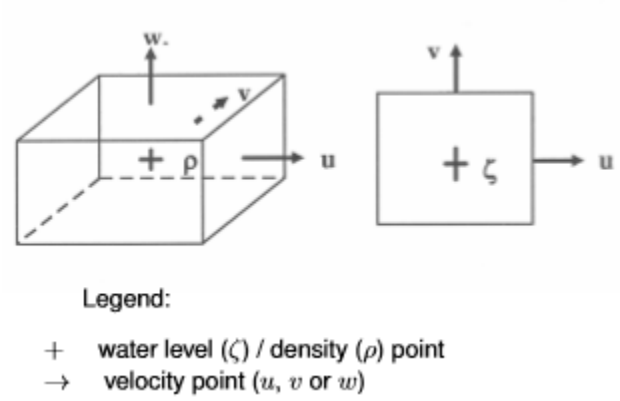

Figure 3-10 - Grid staggering: (left) 3D view, (right) top view (Deltares, 2011).

Using staggered grids has many benefits such as, avoiding the odd-even decoupling between pressure and velocity (Navier Stokes and continuity equations), easy boundary condition implementation, good accuracy with the reduced number of discrete state variables (compared to non-staggered grids), and prevents oscillations in water levels when dealing with shallow water solvers. A "simple" non staggered, rectangular grid can cause problems in formulating equations with finite differences because variables are not in optimal locations. This is an important disadvantage of this application because the fact that the variables are stored in different locations means it becomes more difficult to handle different control volumes (Gerya, 2010).

3.4.1.3. Boundary Conditions

The horizontal model area is defined by the grid enclosure (*.enc) which is made up of polygons that specify the boundaries of the model area. There are two types of boundaries: open and closed. The closed boundaries define "land-water" lines while the open boundaries define "water-water" lines. The open boundaries serve to represent the limit of the computational area. The polygons created are made up of line pieces connecting water level points on the numerical grid, with a direction parallel to the grid lines or diagonal through the grid.

The 3D and 2D depth-averaged shallow water or long-wave equations applied in Delft3D-FLOW represent a hyperbolic or parabolic set of partial differential equations (Deltares, 2011). Shallow water equations are divided into steady and transient state solutions. A transient state solution is a solution that is dependent of time, close to t=0, while a steady state

solution describes the behavior of the dependent variable of time as tending to infinity, $\frac{\delta x}{\delta t} = 0$. A steady state solution depends on the boundary conditions and the forcing terms. The transient state solution follows a deviation between initial conditions and steady state solutions at the beginning of the simulation, the reflection at open boundaries, and amount of dissipation (Deltares, 2011).

At the start up of a simulation, short waves develop with wavelengths coupled with the length of the model. A standing wave, which is a wave remaining in a constant position, can be generated when disturbances are reflected at the open boundaries. The transient solution can propagate out of the model, be reduced at the open boundaries (with α-coefficent), or die out due to bottom friction and viscosity. Steady state solution is reached once the transient state solution is completely vanished. Steady state is completely boundary conditions dependent (Deltares, 2011).

The number of boundary conditions being specified at any point of the boundary, should be equal to the number of characteristics entering the region at that same point. At the open boundaries, Delft3D-FLOW assumes that the flow is subcritical (or laminar) meaning that the flow is smaller than the velocity of the wave propagation (Deltares, 2011). What this suggests is that the Froude number is less than one, a speed-length ration with little resistance. The Froude number, Fr, is defined by the following,

$$Fr = \frac{|U|}{\sqrt{gH}} \tag{41}$$

This number determines the resistance of a partially submerged object moving through water. For a Fr less than one, the flow is considered subcritical. For a Fr greater than one, the flow is considered supercritical, and for a Fr equal to one, the flow is considered critical. Subcritical flows are commonly deep and slow, usually with depths greater than the critical depth. Supercritical flows are usually shallow and fast, with depths less than that of critical depths.

For subcritical flow, which is the case of the model's open boundaries, the inflow and the outflow must be specified. At inflow, the two boundary conditions must be defined and at the outflow one boundary condition needs to be defined. In the case of tidal flow, the number of required boundary conditions varies between the ebb and flood (Deltares, 2011).

3.4.1.4. Governing Equations

According to (Deltares, 2011), Delft3D uses nonlinear shallow water equations in two and three dimensions. The shallow water equations are derived by integrating the full Navier-Stokes equation in the vertical direction. As previously mentioned, these equations are based on the assumption that the horizontal scale is much larger than the vertical. The vertical accelerations are assumed to be much smaller than the horizontal ones, which reduces the vertical momentum equation to a hydrostatic pressure equation. In estuarine modeling, there is an approach to representing the horizontal direction and another representing the vertical one. Before presenting Delft3D's governing equations, it is important to refer to the different choices for each approach, available for the existing coordinate systems.

For the horizontal direction, Delft3D has two coordinate system options available. They are the Cartesian coordinate (ξ, η) and the spherical coordinates (λ,ϕ) (Deltares, 2011). Rectangular grids are considered special cases of Cartesian coordinates. In spherical coordinates λ is the longitude and φ is the latitude. Spherical coordinates are considered special cases as well, in which

$$\xi = \lambda \tag{42}$$

$$\eta = \phi \tag{43}$$

$$\sqrt{G_{\xi\xi}} = R cos\phi \tag{44}$$

$$\sqrt{G_{\eta\eta}} = R \tag{45}$$

in which R corresponds to the Earth's radius (6378,137 km) and $\sqrt{G_{\xi\xi}}$ and $\sqrt{G_{\eta\eta}}$ are coefficients used to transform curvilinear coordinates to rectangular coordinates. The numerical grid transformation is implicitly known by the mapping of the co-ordinates of the grid vertices from the physical to the computational space, Figure 3-11. The geometrical quantities $\sqrt{G_{\xi\xi}}$ and $\sqrt{G_{\eta\eta}}$ introduced in the transformed equations, Equation (44) and Equation (45), have to be discretized on the computational grid.

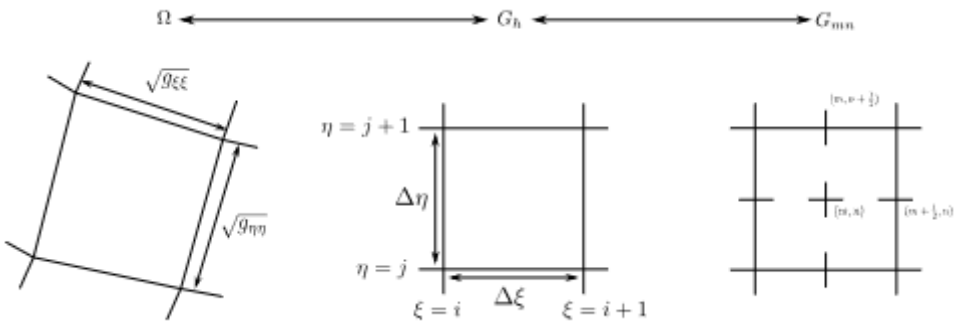

Figure 3-11 - Mapping of Physical Space to Computational Space (Deltares, 2011).

In terms of Delft3D's vertical direction, there are two coordinate options: the σ coordinate system and the Z model, seen in Figure 3-12 (Deltares, 2011).

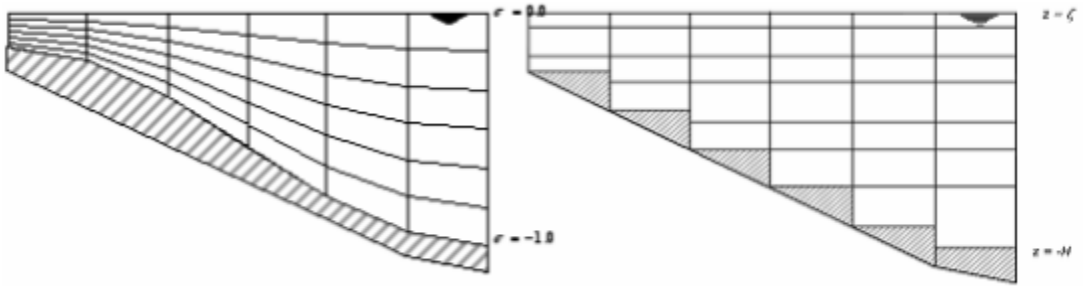

Figure 3-12 - Vertical Grid: (left) Sigma (σ) coordinate, (right) Z model (Deltares, 2011).

The sigma (σ) coordinate is designed so that $\sigma = 1$ corresponds to the bottom and $\sigma = 0$ corresponds to the surface. To solve the partial differential equations, the equations need to be transformed to the discrete space. The transformation from a physical z-coordinate to a σ-coordinate is done with the following equation,

$$\sigma = \frac{z-\zeta}{d+\zeta} = \frac{z-\zeta}{H} \tag{46}$$

in which z is the vertical coordinate in physical space, ζ is the free surface elevation above reference plane, d is the depth below that free surface, and H is the total water depth given by $(d + \zeta)$ (Deltares, 2011).

For a three dimensional shallow water model, the flow domain is made up of a horizontal plane of a limited area composed of open and closed boundaries, and in the vertical direction, a number of layers are defined. The governing equations of Deflt3D-FLOW according to (Deltares, 2011) are presented in detail as follows.

1. The depth-averaged continuity equation is given by,

$$\frac{\partial \zeta}{\partial t} + \frac{1}{\sqrt{G_{\xi\xi}}\sqrt{G_{\eta\eta}}}\frac{\partial[(d+\zeta)U\sqrt{G_{\eta\eta}}]}{\partial \xi} + \frac{1}{\sqrt{G_{\xi\xi}}\sqrt{G_{\eta\eta}}}\frac{\partial[(d+\zeta)U\sqrt{G_{\xi\xi}}]}{\partial \eta} = Q \quad (47)$$

where U and V are the depth-averaged velocity in a computational domain in the ξ- and η-direction, respectively and Q is the source or sink term (representing the contribution per unit area due to the discharge or withdrawal of water, precipitation, and evaporation) which is defined as,

$$Q = H\int_{-1}^{0}(q_{in} - q_{out})d\sigma + P - E \quad (48)$$

in which, $H = d + \zeta$, P is the precipitation, E is the evaporation, q_{in} is the source of water, and q_{out} is the sink for water.

2. The horizontal momentum equation in ξ- and η-direction are given by (Deltares, 2011),

$$\frac{\partial u}{\partial t} + \frac{u}{\sqrt{G_{\xi\xi}}}\frac{\partial u}{\partial \xi} + \frac{v}{\sqrt{G_{\eta\eta}}}\frac{\partial u}{\partial \eta} + \frac{\omega}{d+\zeta}\frac{\partial u}{\partial \sigma} - \frac{v^2}{\sqrt{G_{\xi\xi}}\sqrt{G_{\eta\eta}}}\frac{\partial\sqrt{G_{\eta\eta}}}{\partial \xi} + \frac{uv}{\sqrt{G_{\xi\xi}}\sqrt{G_{\eta\eta}}}\frac{\partial\sqrt{G_{\xi\xi}}}{\partial \eta} - fv =$$
$$-\frac{1}{p_o\sqrt{G_{\xi\xi}}}P_\xi + F_\xi + \frac{1}{(d+\zeta)^2}\frac{\partial}{\partial \sigma}(\nu_V\frac{\partial u}{\partial \sigma}) + M_\xi \quad (49)$$

and

$$\frac{\partial v}{\partial t} + \frac{u}{\sqrt{G_{\xi\xi}}}\frac{\partial v}{\partial \xi} + \frac{v}{\sqrt{G_{\eta\eta}}}\frac{\partial v}{\partial \eta} + \frac{\omega}{d+\zeta}\frac{\partial v}{\partial \sigma} + \frac{uv}{\sqrt{G_{\xi\xi}}\sqrt{G_{\eta\eta}}}\frac{\partial\sqrt{G_{\eta\eta}}}{\partial \xi} + \frac{u^2}{\sqrt{G_{\xi\xi}}\sqrt{G_{\eta\eta}}}\frac{\partial\sqrt{G_{\xi\xi}}}{\partial \eta} + fu =$$
$$-\frac{1}{p_o\sqrt{G_{\eta\eta}}}P_\eta + F_\eta + \frac{1}{(d+\zeta)^2}\frac{\partial}{\partial \sigma}(\nu_V\frac{\partial v}{\partial \sigma}) + M_\eta \quad (50)$$

where u and v are the eastward and northward velocity in the physical domain, respectively, ν_V is the vertical eddy velocity coefficient, P_ξ and P_η represent the pressure gradients, F_ξ and F_η represent the unbalance of horizontal Reynold's stresses, M_ξ and M_η are the contribution due to external sources or sinks, and f is the Coriolis coefficient.

3. The vertical velocity (ω) in the adapting σ-coordinate system is computed from the continuity equation (Deltares, 2011),

$$\frac{\partial \zeta}{\partial t} + \frac{1}{\sqrt{G_{\xi\xi}}\sqrt{G_{\eta\eta}}}\frac{\partial[(d+\zeta)u\sqrt{G_{\eta\eta}}]}{\partial \xi} + \frac{1}{\sqrt{G_{\xi\xi}}\sqrt{G_{\eta\eta}}}\frac{\partial[(d+\zeta)v\sqrt{G_{\xi\xi}}]}{\partial \eta} + \frac{\partial \omega}{\partial \sigma} = H(q_{in} - q_{out}) \quad (51)$$

The vertical velocity (ω) is defined at the iso σ-surfaces and is relative to the moving σ-plane. The "physical" vertical velocities (w) in the Cartesian coordinate system are not involved in

the model equations. The vertical physical velocity is utilized for post processing purposes. They can be expressed the horizontal velocities, water depths, water levels, and vertical ω-velocity according to (Deltares, 2011),

$$w = \omega + \frac{1}{\sqrt{G_{\xi\xi}}\sqrt{G_{\eta\eta}}}\left[u\sqrt{G_{\eta\eta}}\left(\sigma\frac{\partial H}{\partial \xi} + \frac{\partial \zeta}{\partial \xi}\right) + v\sqrt{G_{\xi\xi}}\left(\frac{\partial H}{\partial \eta} + \frac{\partial \zeta}{\partial \eta}\right)\right] + \left(\sigma\frac{\partial H}{\partial t} + \frac{\zeta}{\partial t}\right) \tag{52}$$

in which ω is the vertical velocity adapted to the σ-plane calculated in the previous continuity equation.

4. Considering the shallow water assumptions, in the momentum equations for the horizontal direction, the pressure is defined as hydrostatic. The vertical accelerations due to buoyancy effects and variations in the bottom topography are not considered. In the case of constant density and accounting for the atmospheric pressure, the pressure terms are defined as the following (Deltares, 2011),

$$\frac{1}{p_o\sqrt{G_{\xi\xi}}}P_\xi = \frac{g}{\sqrt{G_{\xi\xi}}}\frac{\partial \zeta}{\partial \xi} + \frac{1}{p_o\sqrt{G_{\xi\xi}}}\frac{\partial P_{atm}}{\partial \xi} \tag{53}$$

$$\frac{1}{p_o\sqrt{G_{\eta\eta}}}P_\eta = \frac{g}{\sqrt{G_{\eta\eta}}}\frac{\partial \zeta}{\partial \eta} + \frac{1}{p_o\sqrt{G_{\eta\eta}}}\frac{\partial P_{atm}}{\partial \eta} \tag{54}$$

The gradients of the free surface level are the barotropic pressure gradients. The atmospheric pressure is included in the system for storm surge simulations. The atmospheric pressure gradients dominate the external forcing at peak winds during storm events. Space and time varying wind and pressure fields are especially important when simulating storm surges.

For non-constant densities (Deltares, 2011),

$$\frac{1}{p_o\sqrt{G_{\xi\xi}}}P_\xi = \frac{g}{\sqrt{G_{\xi\xi}}}\frac{\partial \zeta}{\partial \xi} + g\frac{d+\zeta}{p_o\sqrt{G_{\xi\xi}}}\int_\sigma^0\left(\frac{\partial p}{\partial \xi} + \frac{\partial p}{\partial \sigma}\frac{\partial \sigma}{\partial \xi}\right)d\sigma' \tag{55}$$

$$\frac{1}{p_o\sqrt{G_{\eta\eta}}}P_\eta = \frac{g}{\sqrt{G_{\eta\eta}}}\frac{\partial \zeta}{\partial \eta} + g\frac{d+\zeta}{p_o\sqrt{G_{\eta\eta}}}\int_\sigma^0\left(\frac{\partial p}{\partial \eta} + \frac{\partial p}{\partial \sigma}\frac{\partial \sigma}{\partial \eta}\right)d\sigma' \tag{56}$$

5. The stress tensor is redefined in the σ-coordinate system assuming that the horizontal length scale is much larger than the water depth and that the flow is of boundary-layer type. The horizontal viscosity terms are reduced to a Laplace operator (Deltares, 2011),

$$-F_\xi = v_H\left(\frac{1}{\sqrt{G_{\xi\xi}}\sqrt{G_{\eta\eta}}}\frac{\partial^2 u}{\partial \xi^2} + \frac{1}{\sqrt{G_{\xi\xi}}\sqrt{G_{\eta\eta}}}\frac{\partial^2 u}{\partial \eta^2}\right) \tag{57}$$

$$F_\eta = v_H \left(\frac{1}{\sqrt{G_{\xi\xi}}\sqrt{G_{\eta\eta}}} \frac{\partial^2 v}{\partial \xi^2} + \frac{1}{\sqrt{G_{\xi\xi}}\sqrt{G_{\eta\eta}}} \frac{\partial^2 v}{\partial \eta^2} \right) \quad (58)$$

For large-scale flow, simulated with coarse horizontal grids, that is when shear stresses along closed boundaries can be neglected, the forces F_ξ and F_η are simplified.

6. The equation of state determines the density of the water as a function of salinity and temperature. In Delft3D-FLOW, there are two different formulations that can be chosen: the Eckhart or the UNESCO). The UNESCO, also known as the EOS80, is proved to have less error associated ($3{,}6 \cdot 10^{-3} kg/m^3$). Delft3D-FLOW uses the EOS80 as a default. The equation is written as follows (Deltares, 2011),

$$\rho = \rho_0 + A_s + B_s^{(3/2)} + C_s^2 \quad (59)$$

where

$$\rho_0 = 999.842594 + 6.793952 \cdot 10^{-2} t - 9.095290 \cdot 10^{-3} t^2 + 1.001685 \cdot 10^{-4} t^3 - 1.120083 \cdot 10^{-6} t^4 + 6.536332 \cdot 10^{-9} t^5 , \quad (60)$$

$$A = 8.24493 \cdot 10^{-1} - 4.0899 \cdot 10^{-3} t + 7.6438 \cdot 10^{-5} t^2 - 8.2467 \cdot 10^{-7} t^3 + 5.3875 \cdot 10^{-9} t^4, \quad (61)$$

$$B = -5.72466 \cdot 10^{-3} + 1.0227 \cdot 10^{-4} t - 1.6546 \cdot 10^{-6} t^2, \text{ and} \quad (62)$$

$$C = 4.8314 \cdot 10^{-4} t \quad (63)$$

The equation is valid for temperature, $t \in [0°C, 40°C]$ and salinity, $s \in [0{,}5\ ppt, 43\ ppt]$. The ppt stands for "part per thousands".

7. For 2D depth-averaged flow the shear stress at the bed induced by a turbulent flow is assumed to be given by a quadratic equation friction law (Deltares, 2011),

$$\overrightarrow{T_b} = \frac{\rho_0 g \overrightarrow{U} |\vec{U}|}{C_{2D}^2} \quad (64)$$

in which $|\vec{U}|$ is the magnitude of the horizontal velocity and C_{2D} is the 2D Chézy coefficient. Delft3D-FLOW provides three options for determining the Chézy coefficient.

The first is the Chézy Formulation, in which the value is user defined given in $(m^{1/2}/s)$.

The second is the Manning's Formulation which states that,

$$C_{2D} = \frac{\sqrt[6]{H}}{n} \tag{65}$$

in which H is the total water depth and n is Manning's coefficient given in $(m^{-1/3}/s)$.

Lastly, is the White Colebrook's Formulation in which,

$$C_{2D} = 18\, log_{10}\left(\frac{12H}{k_s}\right) \tag{66}$$

in which H is the total water depth and $k_s$is Nikuradse' roughness length.

8. To calculate bed shear stress, Delft3D-FLOW uses the logarithmic law of the wall for 3D models (Deltares, 2011),

$$T_{\xi\eta} = T_{\eta\xi} = \rho u_*^2 \tag{67}$$

In which the friction velocity u_* is determined by the logarithmic-law for a rough wall, with side wall roughness length z_{0n} and the velocity in the first grid point near the side wall. With Δx_s representing the grid size normal to the sidewall, then,

$$|\vec{u}_{sidewall}| = \frac{u_*}{\kappa} \ln\left(1 + \frac{\Delta x_s}{2z_{0n}}\right) \tag{68}$$

3.4.1.5. Time and Spatial Discretization

Delft3D-FLOW uses the alternating direction implicit (ADI) method to integrate shallow water equations in time. The ADI method splits one time step into two phases, in which each phase makes up half of a time step. In both the phases, all terms of the model equations are solved in a consistent way with at least second order accuracy in space (Deltares, 2011). It also uses three different spatial discretizations (in terms of advection): WAQUA-Scheme, Cyclic Method, and the Flooding Scheme. The choice of the spatial discretization has a big influence on the accuracy, monotony, and efficiency of the computational method. When using the finite differences method to calculate partial derivatives, it would be natural to place all variables on an equidistant grid and then use central differences as an approximation to the derivatives. This becomes a problem when applying this to two or three dimensional situations. In a two dimensional situation, four arbitrary values in a checkerboard layout

would be differentiated to zero. A grid with highly non-uniform values would be treated as if it had uniform values. Central differences are often second order accurate but can give rise to non physical spurious oscillations, called wiggles. Wiggles can arise near steep gradients of the quantity. They may also be introduced near closed boundaries in shallow water flows. In order to obtain a second order spatial accuracy with a compact stencil that excludes wiggles and facilitates accurate implementation of boundary conditions, the staggered grid is used (Deltares, 2011).

The WAQUA scheme and the Cyclic method are higher-order dissipative approximations of the advection term, but neither of the two impose any time restrictions. The Flooding scheme was developed for the 2D simulation with a rectilinear grid of inundation of dry land with obstacles such as road banks and dikes. Because of this, the Flooding scheme is more adequate for rapidly varying flow problems, like hydraulic jumps; however, this scheme imposes a time step restriction by the Courant number for advection. The time integration for the WAQUA scheme and the Cyclic method are based on the ADI method, while the Flooding scheme's advection term is taken at each previous time and moved to the right-hand side (Deltares, 2011).

For water level gradient and advection terms, the time levels are alternating. If in one stage a term is taken implicitly in time, the term will be taken explicitly in time in the other stage. In the first stage in the ADI method, the time level proceeds from l to $l + \frac{1}{2}$ and the simulation time from $t = l\Delta t$ to $t = \left(l + \frac{1}{2}\right)\Delta t$. The V-momentum equation is solved, followed by the U-momentum equation, which is implicitly coupled with the continuity equation by the free surface gradient. As the time continues from $l + \frac{1}{2}$ to $l + 1$, first the U-momentum equation is solved, followed by the V-momentum equation which is implicitly coupled with the continuity equation by the free gradient. In the second stage, the grid coefficients, direction dependent roughness coefficients, and the u-velocity and v-velocity are interchanged. The u and v momentum equations only varying in the sign of the Coriolis term. For the complete time step, each separate term is still integrated second order accurate in time (Deltares, 2011).

The advantages of the ADI method is that the implicitly integrated water levels and velocities are couples along the grid lines leading to system of equations with a small bandwidth. Substitution of the discrete momentum equations in the continuity equation leads to a tri-diagonal system of equations for the water levels. After the water levels are computed, the

velocities can be obtained by back substitution of the water levels in the discrete momentum equations (Wesseling, 2009).

The disadvantaged of the ADI method is that its efficiency can be lost if the time step is too constrained. Depending on the problem's geometry, to achieve sufficient accuracy, the time step must be "small" for the ADI method. However, if the shape of the domain does not inhibit signal propagation, or if the time step has to be limited for other reason anyway, the ADI scheme is the ideal choice (Wesseling, 2009).

3.4.2. QUICKPLOT

Common outputs of hydrodynamic modeling are predictions in water levels, tidal currents, and waves resulting from tidal currents, meteorological and density forces. The standard post-processing tools are the Delft3D-QUICKPLOT and MUPPET. The post-processing tool chosen for this dissertation was Delft3D-QUICKPLOT. QUICKPLOT is a program, developed with Matlab, used to visualize and animate numerical results produced by the Delft3D modules (Deltares, 2013).

There are five basic steps to attaining "plots" using this software. Once the program has started, one has to first select the file, select the data field, select the time, select the location (M and N values), and proceed to the "Quick View" to see the plotted results. The Delft3D-QUICKPLOT interface is shown in Figure 3-13.

The Delft3D output file containing the data information is the "trim" (*.dat) file. The data fields that can usually be studied are the model region's air pressure, wind speed, water levels, water depth, depth averaged velocities, Froude number, horizontal viscosity, bed shear stress, among many others. After the selection of the data file and data field, one must select the time step and which location to plot. As default, QUICKPLOT is set to plot the last given time step for the entire domain. If instead of a 2D plot of the whole domain, one wants a plot of, for example, a cross section along the N grid line, one could uncheck the checkboxes associated with the N line and the specified N-values can be inputted. If only certain zones within the grid are needed, the selecting of a block of M and N indices can become very useful in the analysis of simulated results. The M and N pairs must be separated with colons.

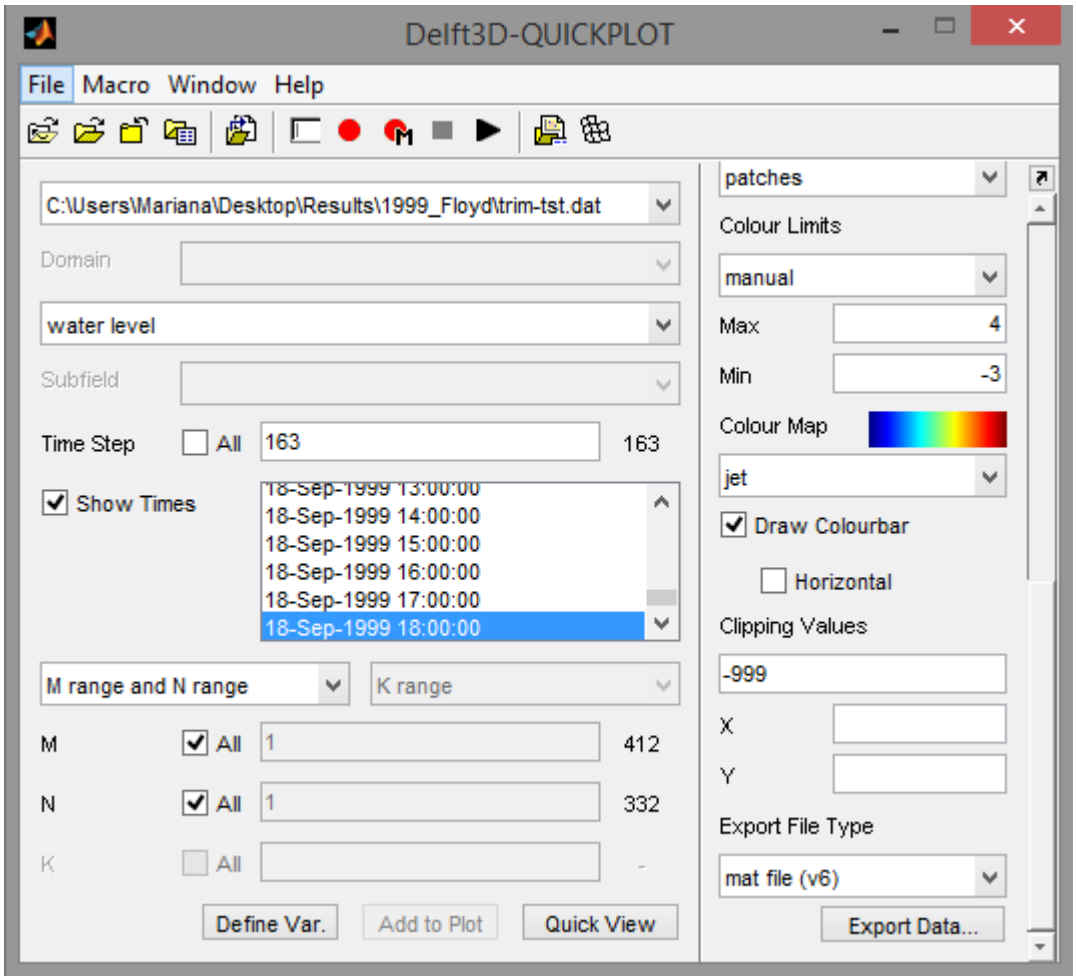

Figure 3-13 - Delft3D-QUICKPLOT Graphical User Interface.

After all the information is defined, one can then plot the data by selecting the "Quick View" option. Different quantities allow for different types of plots and, therefore, the lists of plot and export options in the right part of the window will adapt to one's selection. Depending on the data field that is chosen, one can obtain a 2D plot, a cross sectional plot, or a time-series plot. At the end of the list of plotting options, there will always be an option to export data to a number of file formats. This is especially useful for the purposes of this dissertation because it is possible to export the information obtained in a Matlab file (*.mat). The stand-alone version of Delft3D-QUICKPLOT writes the data in Matlab files compatible with Matlab version 6. QUICKPLOT versions running within Matlab as part of the Delft3D-MATLAB toolbox can also export to Matlab files native to version 7 and up (Deltares, 2013).

4. CASE STUDIES

4.1. The Battery, New York - Case Study

The New York county of Manhattan is the most densely populated county in the United States. Southern Manhattan for example, has a population density greater than the citywide average, containing a population of nearly 200,000 inhabitants. This densely developed region encloses a total of 26,5 million built square meters, in which 16,7 million square meters correspond to commercial areas and 9,8 million square meters to residential areas. At the water's edge, Southern Manhattan is rimmed by a bulkhead wall, which generally borders on public spaces. These spaces range from the East River Park and East River Esplanade on the East Side to Battery Park City in the south, to the public spaces of Battery Park City and Hudson River on the West Side (Bloomberg, 2013). The Battery, New York is the first area being studied in this dissertation, depicted in Figure 4-1.

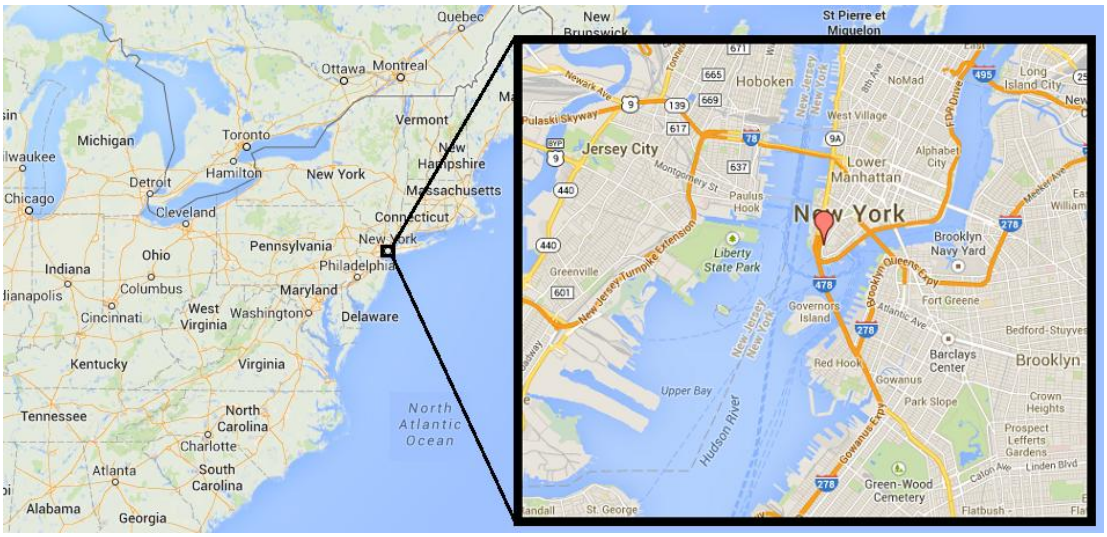

Figure 4-1 - Location of The Battery, New York (Google Maps, 2014).

The Battery is located at the southern tip of Manhattan, facing the New York/New Jersey Harbor. In 2009, this harbor was ranked the twenty third largest port in the world based on total cargo volume. In 2013, the American Association of Port Authorities (AAPA), ranked the Port of New York/New Jersey as the second busiest port in the United Stated, based on

total imports and exports by weight (American Association of Port Authorities, 2014). The New York Harbor is the largest port on the eastern seaboard of the United States, supporting the most densely populated metropolitan area in the United States. This harbor is the "backbone" of the northeast region of the United States, considered a port of critical importance for commerce and national security by the US. Federal Government (Walsh, 2011). Almost 80% of the imported cargo into the port is marketed to consumers within 100 miles of the port, making it a critical element in the regional economy (Walsh, 2011).

In 2007, the PlaNYC was launched as a long-term sustainability plan providing protection against the effects of tropical storms. In lieu of Hurricane Sandy's effects on New York City in 2012, as the probability of more severe weather becomes a reality, the bar must be set even higher. In December of 2012 the formation of a Special Initiative for Rebuilding and Resiliency produced a plan to provide additional protection for New York's infrastructure, building, and communities. *A Stronger, More Resilient New York* is a product of that, fundamentally a "roadmap" for a more sustainable 21st century New York (Bloomberg, 2013).

The NYC Panel on Climate Change, NPCC, projects that New York City could see up to 0,76 meter of sea level rise by the 2050s as well as triple the number of days above 90°F (Bloomberg, 2013). Below, in Figure 4-2, are the Preliminary Work Maps, PWM, released in June 2013 by the Federal Emergency Management Agency for the 2020s and 2050s.

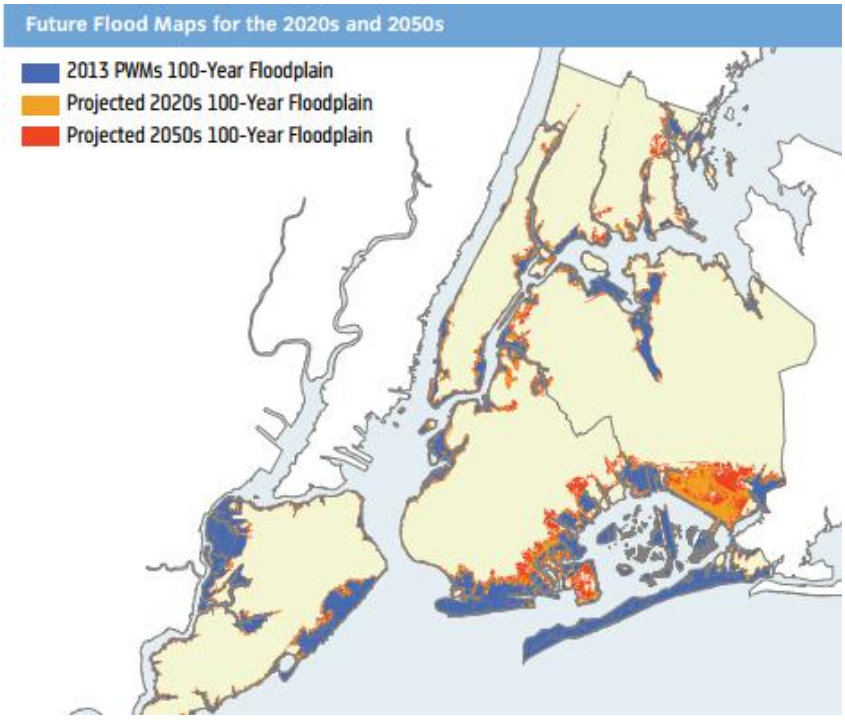

Figure 4-2 - New York's Future Flood Maps for the 2020s and 2050s (Bloomberg, 2013).

The area that might be flooded in the 2020s could expand to 152,81 square kilometers, encompassing about 88,0000 buildings. The NPCC's projected 2050 sea level rise can threaten communities residing in low-lying New York areas and make flooding as severe as today's 100-year storm at The Battery up to five times more likely. It also predicts that there is more than 50 percent probability that there will be an increase in the most intense hurricane in the North Atlantic Basin. The 2050s map could be 186,48 square kilometers about 24 percent of the city, an area encompassing 114,000 buildings. New York City in collaboration with the Swiss Reinsurance Company has performed an initial loss-modeling, which indicates that due to sea level rise, NYC is 17% more likely in the 2020s and 40% in the 2050s to see a storm that causes nineteen billion dollars in damages, as Superstorm Sandy did (Bloomberg, 2013).

Southern Manhattan's coastal areas are crucial to New York's evolution as a global city. Its waterfront can become a valuable asset, as home for residential and commercial office development; nevertheless, its low-lying coastal edges remain vulnerable to extreme weather. Southern Manhattan contains the fourth largest business district in the United States. It is positioned at the heart of the New York's transportation networks, such as subway lines, heliports, ferry landings, power facilities, healthcare institutions, and much more. A surge similar to the one experienced with Sandy can easily breach bulkheads and bring floodwaters one or two blocks inland, if not even farther. The waters can course into residential buildings, stores, office building, damaging interiors and even damaging critical infrastructure arrayed all along the coast (Bloomberg, 2013).

4.1.1. Historic Vulnerability

According to the National Ocean Service's *Quality Assessment of Sea Level Data* for the observation station 8518750 - The Battery, NY located at 40°42'0"N 74°00'9"W, the obtained sea level heights have all been referred to the station tide staff zero which is linked to fixed bench marks (UHSLC, 2014). While the standard mechanical or analog-to-digital recorder instrument was the primary gauge, the instrument type currently used is the Aquatrak acoustic sensor/protective well. Leveling calibration factors were applied monthly, based on tide staff comparisons (UHSLC, 2014).

The hourly tide gauge data for The Battery's station was acquired from the University of Hawaii Sea Level Center's, UHSLC, Global Sea Level Observing System (GLOSS) database.

The GLOSS network is an international program aimed at the establishment of high quality global and regional sea level networks for climate, oceanographic and coastal sea level research. Its principal component is the 290 sea level stations located around the world for long term climate change and oceanographic sea level monitoring (UHSLC, 2014).

The referenced bench marks are all located in the area around Battery Park. The information obtained for observation stations' bench marks is provided by the United States' Department of Commerce. In the case of The Battery's observation station, the tide gauge and staff are located on the pier behind the Inspection Office. The primary bench mark, which will be used as a reference in this dissertation, is a disk set in a concrete loading dock, (NOAA Datums Page, 2014) in which the elevations of tidal datums are all referred to the Mean Low Lower Water (MLLW) set at 0,000m, as seen in Figure 4-3. The National Oceanic and Atmospheric Administration defines the Mean Lower Low Water as the average of the lower low water height of each tidal day observed over the National Tidal Datum Epoch. For situations with shorter series, comparisons of simultaneous observations with a control tide station is made in order to derive the equivalent datum of the National Tidal Datum Epoch. The Mean Sea Level (MSL) is at an elevation of 0.783 meter (NOAA - Tides and Currents, 2014). This adjustment has to be made when comparing the historic data from the UHSLC database to the predicted, simulated data obtained from Delft3D-FLOW because QUICKPLOT's output data yields the water level in reference to the Mean Sea Level. The comparison of The Battery's observation station tide datums is given below in Figure 4-3.

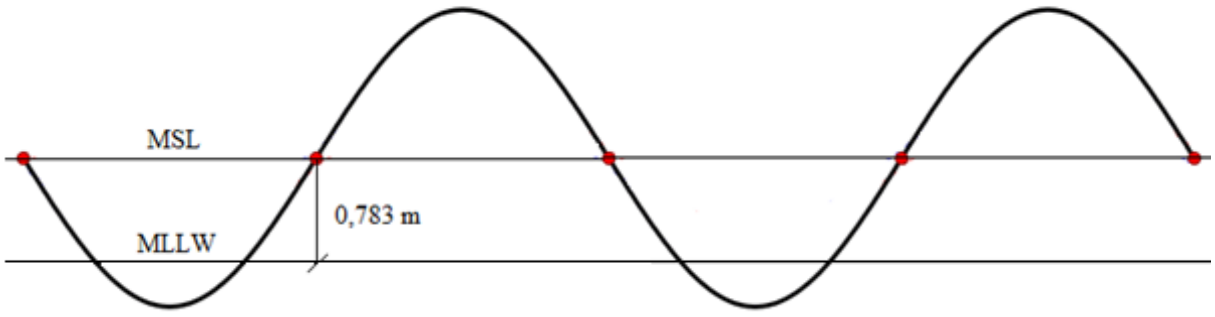

Figure 4-3 - Difference in Reference Data for The Battery, New York.

Utilizing the UHSLC's database information, it was possible to have some perception of the storm tide heights expected in the midst of a tropical storm occurring in the New York/New Jersey Harbor. The first step was identifying the most influential tropical cyclones to occur within an 100 kilometer radius around The Battery, New York. This was done using NOAA's

interactive historical hurricane track mapping application shown in Figure 4-4. The National Oceanic and Atmospheric Administration's Historical Hurricane tracker allows a user to search and display hurricane date by storm name, latitude, and longitude coordinates, or geographic region. The various colors seen below in Figure 4-4 represent the different categories of the tropical cyclones. It is clear that in this particular region the most common occurrence is of tropical storms, referred to as TS/SS in the caption. Analyzing all the historical tropical cyclones that have passed through the area, one can have an understanding of the worst possible scenarios expected of a storm surge for that location.

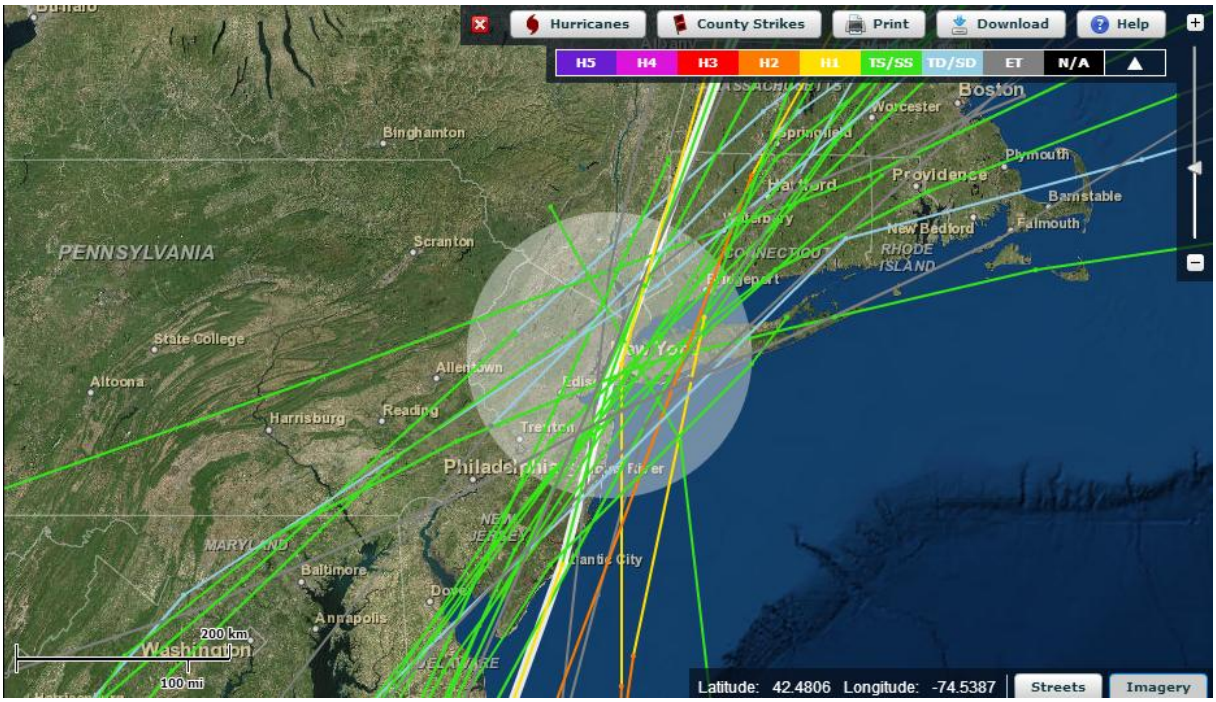

Figure 4-4 - Historical Tropical Cyclones within an 100 km radius of The Battery, NY (Historical Hurricane Tracks, 2014).

In Table 4-1 the tropical cyclone tracks that struck The Battery's observation station for which there is existing data to compare with are presented, each with their corresponding Start and End dates. When consulting the UHSLC's historic data, it was found that there were no records documented for any sea level data for The Battery's observation station before June 1st, 1920. Like this observation station, many others contained sea level records beginning only from the start of the 20th century. While NOAA's Historical Hurricane Track database recognizes tropical systems dating back to the 1800s, there would be no historical information with which to validate the simulations.

Table 4-1 - Historical Tropical Cyclones' corresponding Start and End Dates (The Battery, NY) (Tropical Cyclone Model & Best Track Archive: Storm Archive, 2014).

No.	Year	Name	Start Date	End Date
1	2011	Irene	21/8/2011	28/8/2011
2	2008	Hanna	28/8/2008	7/9/2008
3	2000	Gordon	14/9/2000	18/9/2000
4	1999	Floyd	7/9/1999	17/9/1999
5	1996	Bertha	5/7/1996	14/7/1996
6	1988	Chris	21/8/1988	30/8/1988
7	1985	Gloria	16/9/1985	2/10/1985
8	1976	Belle	6/8/1976	10/8/1976
9	1972	Agnes	14/6/1972	23/6/1972
10	1971	Doria	20/8/1971	29/8/1971
11	1961	Unnamed	12/9/1961	15/9/1961
12	1960	Brenda	28/7/1960	1/8/1960
13	1955	Diane	7/8/1955	21/8/1955
14	1952	Able	18/8/1952	2/9/1952
15	1945	Unnamed	12/9/1945	20/9/1945
16	1934	Unnamed	4/6/1934	21/6/1934
17	1924	Unnamed	27/9/1924	1/10/1924
18	1915	Unnamed	31/7/1915	5/8/1915

In Figure 4-5, for each of the analyzed tropical cyclones, the intensity, or maximum wind velocity, at the moment the system hits the study area, was recorded. Seen in both Figure 4-5 and in NOAA's tracks portrayed in Figure 4-4, the occurrence of tropical storms is most probable, i.e. tropical cyclones able to sustain winds from 62 to 118 km/h (33,5 to 63,7 knots).

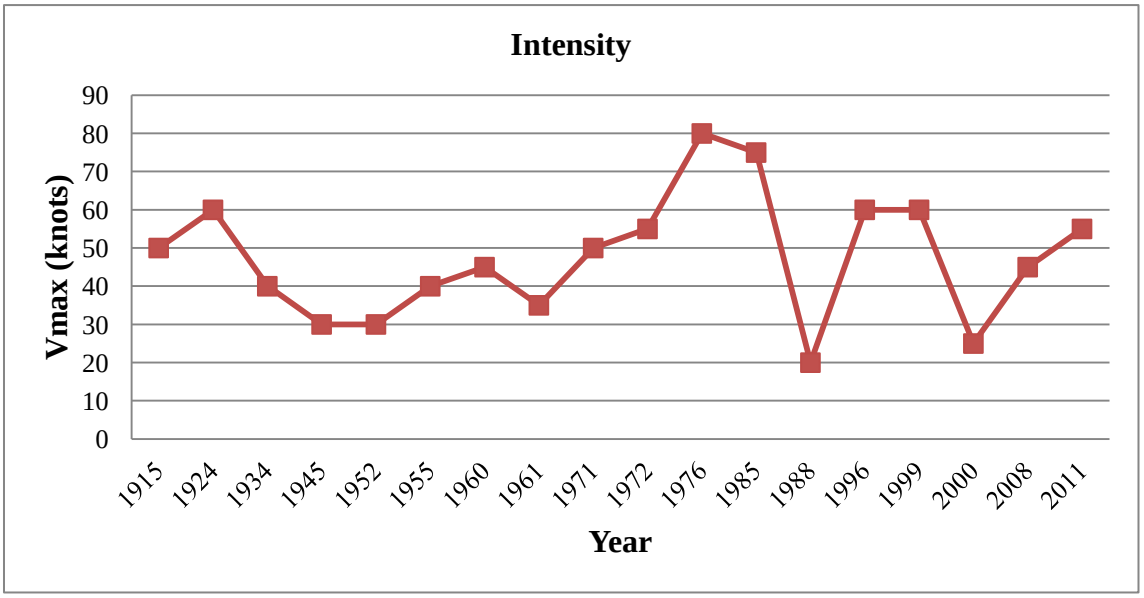

Figure 4-5 - Variation of the Storms' Intensities (The Battery, NY).

Applying a standard normal distribution, the function (Figure 4-6) gives the probability that any real observation will fall between any two real limits, i.e. intensity values. The variable μ stands for the mean or average expected value for the parameter, which in this case is the Vmax of 47,55 knots (87,04 km/h). The parameter σ represents the standard deviation, the unit of normal distribution, corresponding to 14,63. This information is useful in this kind of study because it allows for a better perception of a variable for which distribution is unknown. It is especially of utmost importance in terms of tropical cyclone forecasting. One has to base future previsions on observed historical trends. This will be further explore in Section 4.3.

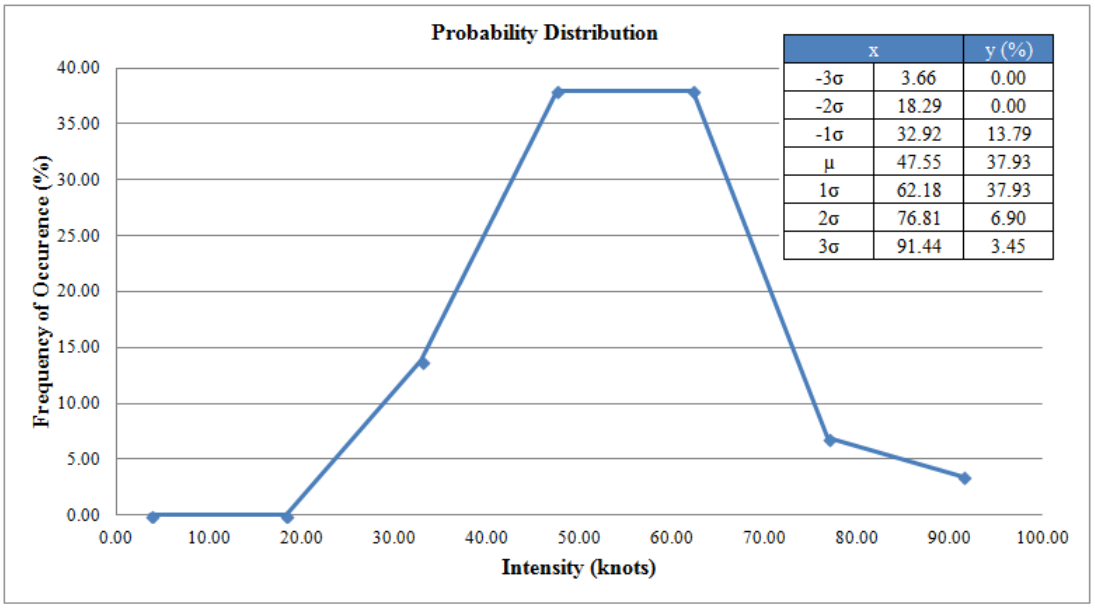

Figure 4-6 - Probability Distribution of a Storm's Intensity (The Battery, NY).

For an understanding of how the tropical cyclones' affect The Battery's surrounding environment, eight different observation stations (Figure 4-7), all relatively near The Battery, were gathered and the peaks of each station's sea level for the time interval of each of the given storms was obtained. This "peak", otherwise known as a maximum sea level, was registered as the maximum envelope of water in that location for each particular tropical storm. The maximum envelope of water, also known as the MEOW, of The Battery's observation station along with other adjacent observation stations were found.

After all the MEOWs are acquired for each historical storm, the maximum of the MEOWs, also known as the MOM, can be identified. The MOM is composed of the maximum storm tide heights for all the tropical storms of each category, that is, hurricanes, tropical storms, and tropical depressions. The values of the MOMs show the flooding possibility from a threatening tropical storm of any given category.

Figure 4-7 - Observation Stations for the US' Northeastern Coast Analysis (Google Maps, 2014).

The peaks are obtained, creating a kind of "wraparound" of the various categories. As the probability of worsening weather increases, it is essential to anticipate the occurrence of higher sea levels and their repercussions. In Table 4-2 are the eight analyzed observation stations with their respective elevation of the tidal datum, or Mean Sea Level, in reference to the Mean Lower Low Water (0,000 m) in meters. The same type of adjustment that was explained for The Battery's observation station data also had to be made for the remaining observation stations.

Table 4-2 - Analyzed Observation Stations and their respective MSL (The Battery, NY).

Stations	Locale	MSL (m)
A	Cape May	0.783
B	Atlantic City	0.675
C	The Battery	0.783
D	Montauk	0.357
E	New London	0.468
F	Newport	0.529
G	Woods Hole	0.300
H	Nantucket Is.	0.539

After analyzing the historic data, the MEOWs and MOMs were obtained for each of the stations, portrayed in Table 4-3 and Table 4-4 respectively. Table 4-3 represents each of the tropical cyclones' MEOWs for the eight observation stations represented in Figure 4-7. The values obtained from the UHSLC database were adjusted to correspond to the mean sea level

value of each location. The Mean Sea Level is a tide datum determined over a 19-year National Tidal Datum Epoch between 1983 and 2001 (NOAA Datums Page, 2014). It pertains to local mean sea level and should not be confused with the fixed datums of North American Vertical Datum of 1988 (NAVD88). The NAVD88 elevations are derived from an average of several bench mark elevations relative to tide station datum and their relationships to local MSL and other tidal datums relative may not be consistent from one location to another (NOAA Datums Page, 2014).

Table 4-3 - Maximum Envelope of Water - MEOW (The Battery, NY).

Maximum Envelope of Water - MEOW (m)										
Type	Name	Year	Observation stations							
			A	B	C	D	E	F	G	H
Hurricane	Gloria	1985	2,606	3,312		2,027	2,428	1,583	1,888	1,467
	Belle	1976	1,835	2,356		1,752	1,730	1,379	1,343	1,530
Tropical Storm	Irene	2011	2,541	2,743	3,090	2,375	2,547	2,017	1,860	1,757
	Hanna	2008	1,804	1,989	1,359	1,707	1,598	1,239	1,258	1,396
	Floyd	1999	2,111	2,579	2,125	1,787	1,791	1,204		1,502
	Bertha	1996	1,755	2,412		1,846	1,859	1,540	1,583	1,494
	Agnes	1972	1,677	2,282	2,164		2,123	1,727	1,681	1,552
	Doria	1971		1,874	1,936	1,505	1,541	1,150	1,136	1,281
	Unnamed	1961	-	2,068	1,655	1,441	1,513	1,178	1,133	-
	Brenda	1960	-	2,007	1,899	1,889	1,940	1,544	1,437	-
	Diane	1955	-	2,282	2,015	-	1,727	1,452	-	-
	Unnamed	1934	-	1,885	1,655	-	-		-	-
	Unnamed	1924	-	2,251		-	-	-	-	-
	Unnamed	1915	-	1,891	-	-	-	-	-	-
Tropical Depression	Gordon	2000	1,699	2,441	1,635	1,538	1,485	1,151	1,098	
	Chris	1988	1,744	2,630		1,649	1,565	1,413	1,285	1,454
	Able	1952	-	2,478	1,899	-	1,757	1,330	-	-
	Unnamed	1945	-	2,904	2,125	-	1,696	1,288	-	-
	Missing gauge									
-	No gauge data									

Below, Table 4-4 shows the station's MOM, for the three categories: hurricane, tropical storm, and tropical depression. This parameter, maximum sea level height, is chosen for this dissertation's analysis of a location's vulnerability because it is easily linked to potential areas that could be affected by waves overtopping, flooding, and coastal erosion. The comparison of historically observed sea levels gives important information for the expected effects of the various degrees of tropical cyclones.

Table 4-4 - Maximum of the MEOW - MOM (The Battery, NY).

Maximum of MEOW - MOM (m)								
Type								
	A	B	C	D	E	F	G	H
Hurricane	2.606	3.312		2.027	2.428	1.583	1.888	1.530
Tropical Storm	2.541	2.743	3.090	2.375	2.547	2.017	1.860	1.757
Tropical Depression	1.744	2.904	2.125	1.649	1.757	1.413	1.285	1.454
	Missing gauge							

As seen in Table 4-4, the regions experiencing the highest sea levels are the lower New Jersey region and the New York/New Jersey Harbor, corresponding to observation stations A, B, and C. While The Battery's observation station (C) is not in direct contact with the Atlantic Ocean, as is the case of observation stations A and B, it does still experience very high sea level heights. This could be due to the fact that this observation station is enclosed and the energy from the waves can refract around the barriers or can dissipate significantly as the wave breaks in the shallow waters (COMET, 2006). Observation stations D, E, F, G and H are located farther from the usual impact zone, therefore experiencing smaller storm tides.

4.1.2. Application

One of the main purposes of this dissertation is to replicate the height, evolution and extent of the storm tide that occurs for all the historical tropical storms referred to in the last section. For each of the historical tropical cyclones abovementioned, the same grid was utilized. The grid, shown in Figure 4-8, contains 412 points in the M direction and 332 points in the N direction.

The coordinate system used in all of the simulations was the WGS 84 (World Geodetic System) coordinate system. The WGS 83 is an Earth-centered, Earth-fixed terrestrial reference system and geodetic datum. A consistent set of constants and model parameters describe the Earth's size, shape, and geomagnetic fields. This is the standard US Department of Defense's definition of a global reference system for geospatial information. It is the reference system for Global Positioning System (GPS) and is compatible with the International Terrestrial Reference System (ITRS).

One of the main reasons for maintaining the default coordinate system is because the Tropical Cyclone Toolbox is not yet supported by projected coordinate systems, that is, Cartesian coordinate systems. The WGS 84 is a geographic coordinate system, meaning that it uses a three-dimensional spherical surface to define locations on Earth. This kind of system includes an angular unit of measure, a prime meridian, and a datum with a spheroidal reference. A point is referenced by its latitude and longitude values. The longitude and latitude are angles measured from the Earth's center to a point on the surface. The spheroid defines the size and shape of the Earth's model, as the datum connects the spheroid to the earth's surface. For most geographic coordinate systems, the prime meridian, the line of 0° longitude, passes through Greenwich, England (ArcGIS 9.3 , 2014).

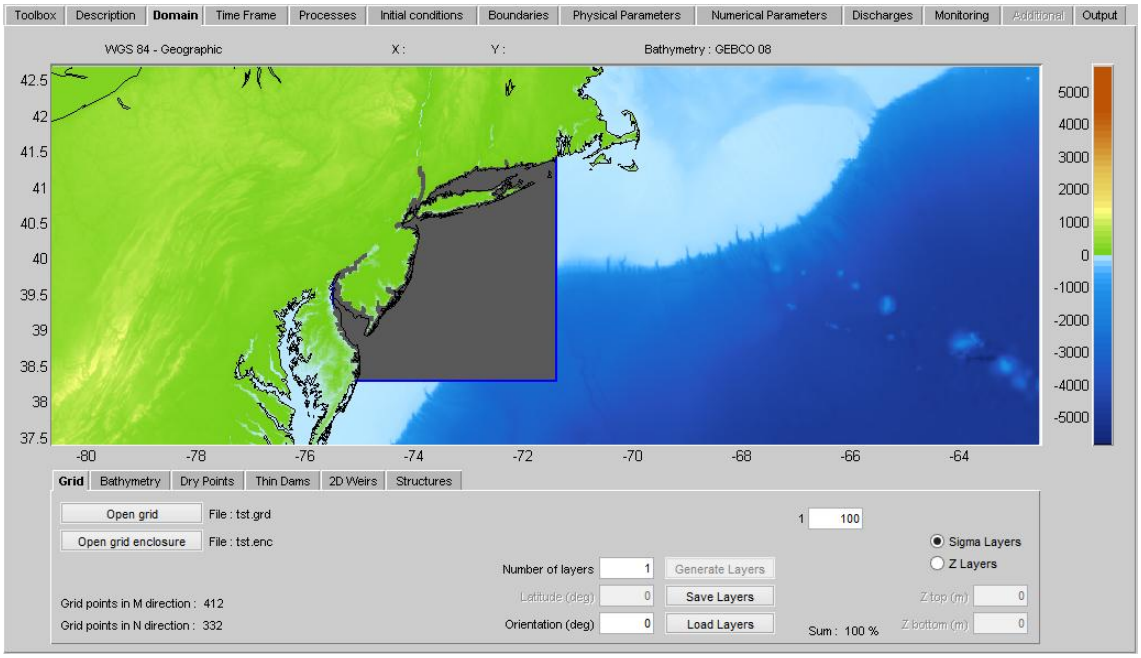

Figure 4-8 - Grid Definition for The Battery, NY.

The bathymetry data utilized was the GEBCO 08 bathymetry. It is largely generated by combining quality-controlled ship depth soundings with interpolation between sounding points guided by satellite-derived gravity data (GEBCO gridded bathymetry data, 2014). The General Bathymetric Chart of the Oceans (GEBCO) had the initial aim of preparing global series of charts showing the general shape of the ocean floor. It now operates under the joint auspices of the Intergovernmental Oceanographic Commission (IOC) and the International Hydrographic Organization (IHO). In the GEBCO 08 grid, there is also land data which is mainly based on the shuttle Radar Topography Mission (SRTM30) gridded digital elevation model (General Bathymetric Chart of the Oceans at BODC, 2014).

Once the coordinate system and bathymetry were chosen, the boundary conditions of the model had to be defined, seen in Figure 4-9. The boundaries of a river, an estuary or a coastal sea are generally curved and are not smoothly represented on a rectangular grid, which was the case of the simulations executed in this dissertation. The boundary becomes irregular and may introduce discretization errors. When defining the boundaries as water level boundary conditions, one must keep in mind that it is a globally varying quantity. According to the Delft3D-FLOW Manual, a small error in the prescription of water levels can only be compensated by a large response in the velocity components (Deltares, 2011). The area of influence of this phenomenon is not limited to a certain number of grid points near the boundary, but instead to the whole physical area. In order for these small errors not to influence the model results, one should locate the boundaries as far away from the areas of interest as possible (Deltares, 2011). This can be verified in the defined model grid, shown in Figure 4-9.

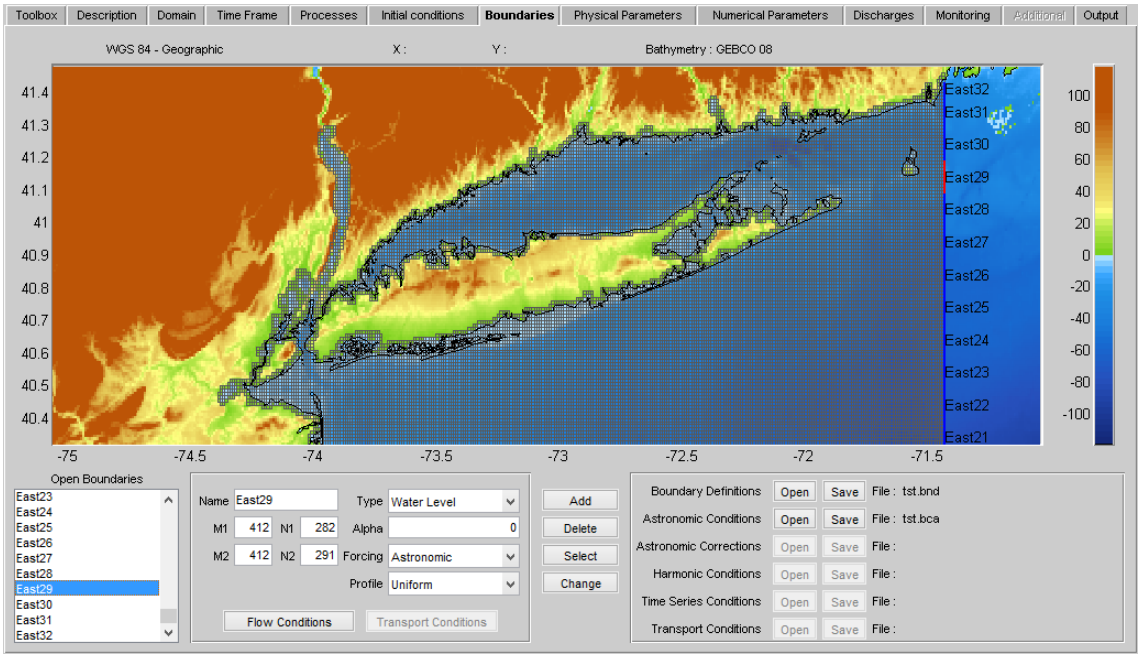

Figure 4-9 - East Boundary Conditions' Definition for The Battery, NY. Identical boundaries were defined for South and West open boundaries.

In this case study, the hydrodynamic forcing was set as using astronomic components. The astronomic option means the flow conditions are specified using tidal constituents, amplitudes, and phases. The interpolation between the two end points of a boundary section are obtained by linear interpolation of the values at these points. For boundary conditions expressed in amplitudes and phases, the interpolation is executed on these quantities. The observed tidal motion can be described in a series of simple harmonic constituent motions,

each with its own characteristic frequency, its angular velocity. The amplitudes and phases of the constituents vary with the positions where the tide is observed (Deltares, 2011).

With data available through Tropical Atlantic's Best Track Data, the simulations ran using storm track information that include, the latitude and longitude of the storm's eye, the intensity (maximum sustained 1-min wind speed), pressure drop, and radius of maximum winds, for 6-hour intervals, depicted in Figure 4-10. With more recent occurring tropical cyclones, one has access to more information about the system, making it much easier to reproduce accurately. At present, there are details on the tropical cyclones' isobar information, their wind field for each of the specific quadrants, and wave height details corresponding to the different quadrants. However, this kind of information is typically only available for the tropical systems occurring in the last decade. The further back, the harder it becomes to find data. In some instances, the only information available is the maximum sustained wind speed.

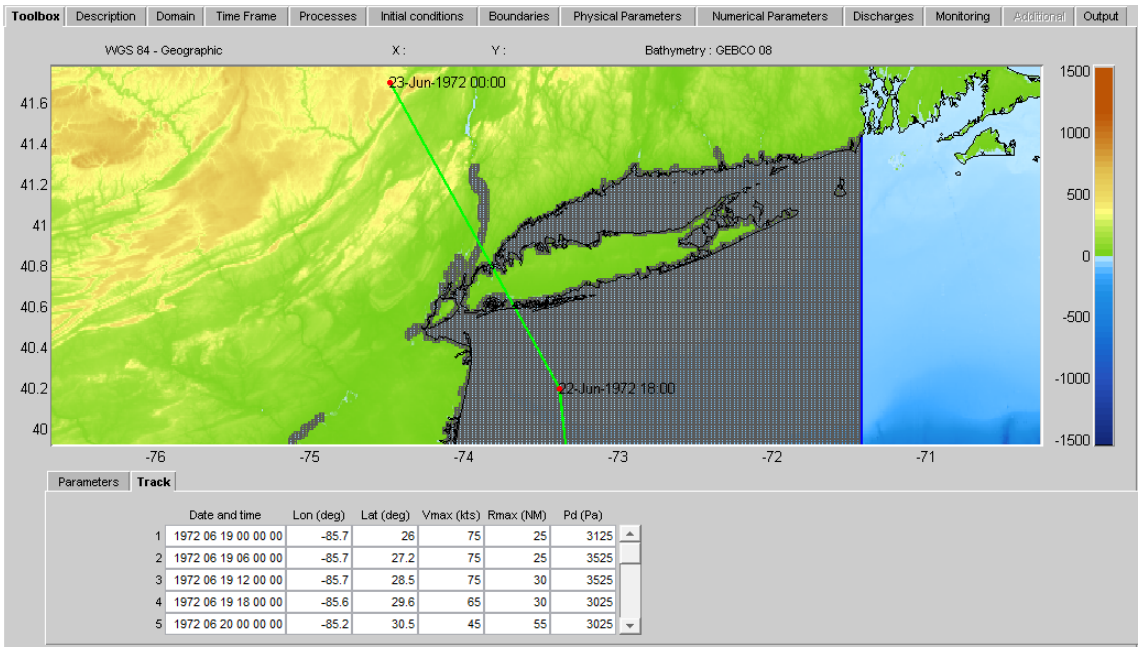

Figure 4-10 - Example of input data for tropical cyclones' track - Tropical Storm Hanna, 2008.

After the results of the simulated tropical cyclones are gathered, they are then compared to the observed hourly data collected from the University of Hawaii Sea Level Center's, UHSLC, Global Sea Level Observing System (GLOSS) database. The global tide data is supplemented by contributions of hourly data from agencies around the world on a monthly basis in support of the GLOSS Fast-Delivery (FD) System. The UHSLC datasets are used in combination with operational numerical models, for calibration of satellite altimeter data, the production of

oceanographic products, and research on inter-annual to decadal climate fluctuation and short-term extreme events (UHSLC, 2014).

4.1.3. Results

The resulting models of the various historical coastal storms affecting the US' eastern coast were a success. As previously explained in Section 3.3, when developing the spiderweb wind field in Delft Dashboard, if the maximum wind speed is below 25 knots (46,2 km/h) the generated spiderweb wind field will correspond to null speed at that time step, and time steps thereafter. Because of this, historic tropical depressions are very rarely able to be recreated with the same precision as hurricanes or tropical storms. A tropical cyclone categorized as a tropical depression can only sustain winds up to 33 knots, or 62 km/h. Most often than not, because the area of The Battery is so far north, the tropical systems are leading to becoming extratropical and also have a bigger tendency to decrease in wind speed and thus have more of a probability of arriving as tropical depressions. Also, as seen in Table 4-3, the gauge data for the two biggest hurricanes that struck The Battery are missing. This could be because the equipment is simply not capable of bearing such a large impact. As a result, the only models capable of being validated were the tropical storms.

It is important to remember that not all tropical cyclones were created with the input of the maximum sustained surface winds, pressure drop, and radius of maximum winds. The available data for each of the tropical storms is displayed in Table 4-5. While studying the tropical cyclones, as the research reached storms of later years, for example, the Unnamed Tropical Storm of 1934, the only available data was the maximum sustained surface winds (wind speed). The input of the radius of maximum winds (Rmax) proved to be especially difficult to obtain. The only tropical storms to have this data available were the two most recent tropical storms, 2008's Tropical Storm Hanna and 2011's Tropical Storm Irene. Because the Rmax is said to not have as big of an influence as the storm's pressure drop or its maximum wind speed, one could simply ignore it and Delft Dashboard would maintain the default 20 knots (37,04 km/h) throughout the tropical cyclones' tracks. Nevertheless, however "less" important it is than the other two variables, it was verified that it could mean the difference between a close to accurate storm reproduction and a mediocre one. This will be confirmed later on in this section.

Table 4-5 - Simulated Tropical Storms and respective available data (The Battery, NY).

Name	Year	Vmax (kts)	Rmax (n mi)	Pdrop (Pa)
Unnamed	1934	x		
Diane	1955	x		x
Brenda	1960	x		
Unnamed	1961	x		
Doria	1971	x		x
Agnes	1972	x		x
Floyd	1999	x		x
Hanna	2008	x	x	x
Irene	2011	x	x	x

Table 4-6 describes the exact hour at which the simulation reaches its peak water level height. The storm peaks appear to occur roughly around the same time step. The slight differences observed can possibly be due to the fact that data is not always retrieved with precision, or that wind fields are not always symmetric which can hinder the results.

Table 4-6 - Observed vs. Predicted Maximum Surge Heights' Time Step (The Battery, NY).

Name	Year	Observed		Predicted	
		Date	Hour	Date	Hour
Unnamed	1934	19/6/1934	16:00	19/6/1934	16:00
Diane	1955	19/8/1955	2:00	19/8/1955	1:00
Brenda	1960	30/7/1960	18:00	30/7/1960	15:00
Unnamed	1961	15/9/1961	4:00	15/9/1961	4:00
Doria	1971	28/8/1971	9:00	28/8/1971	9:00
Agnes	1972	22/6/1972	21:00	22/6/1972	19:00
Floyd	1999	16/9/1999	18:00	16/9/1999	23:00
Hanna	2008	7/9/2008	7:00	7/9/2008	2:00
Irene	2011	28/8/2011	13:00	28/8/2011	12:00

For the sake of keeping the results from being long-winded, only one of the tropical cyclones' QUICKPLOT output data will be presented - Tropical Storm Floyd. The remaining output information can be found in Appendix I. Below, in Figure 4-11, Tropical Storm Floyd's water levels is presented for the study area, where only the tidal influences are considered.

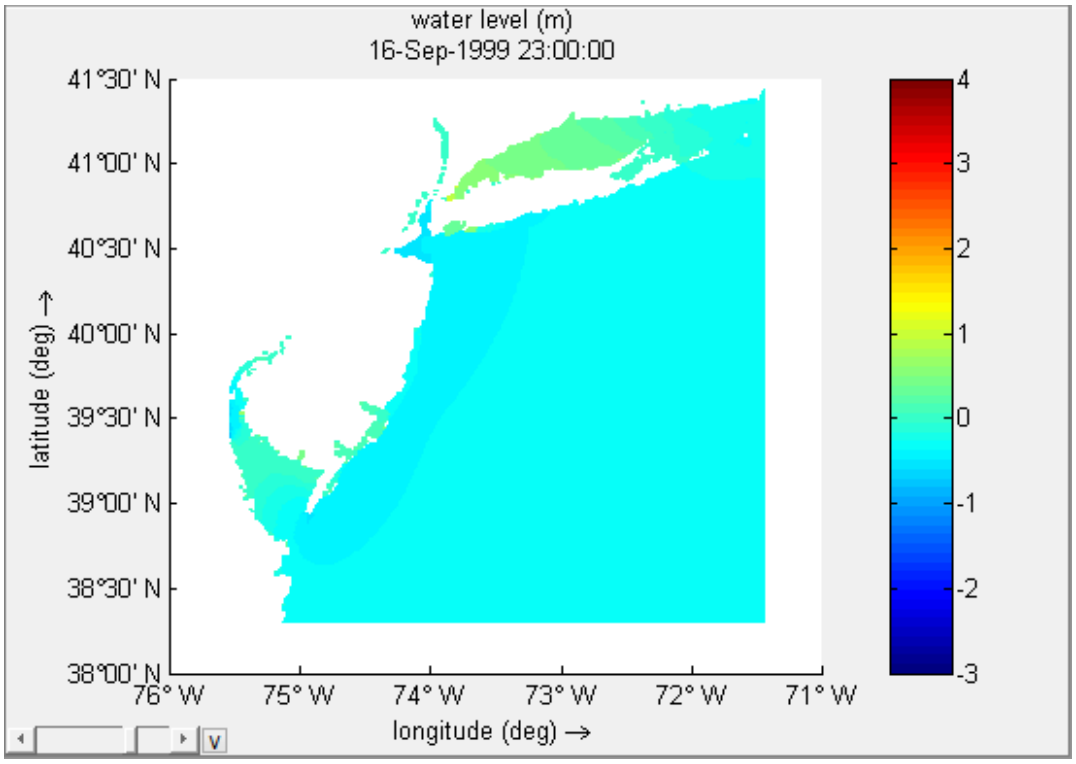

Figure 4-11 - Tropical Storm Floyd's water levels without spiderweb wind field (m).

In Figure 4-12, the result of the simulation of the water levels for the study area with the introduction of the storm's spiderweb wind field is given.

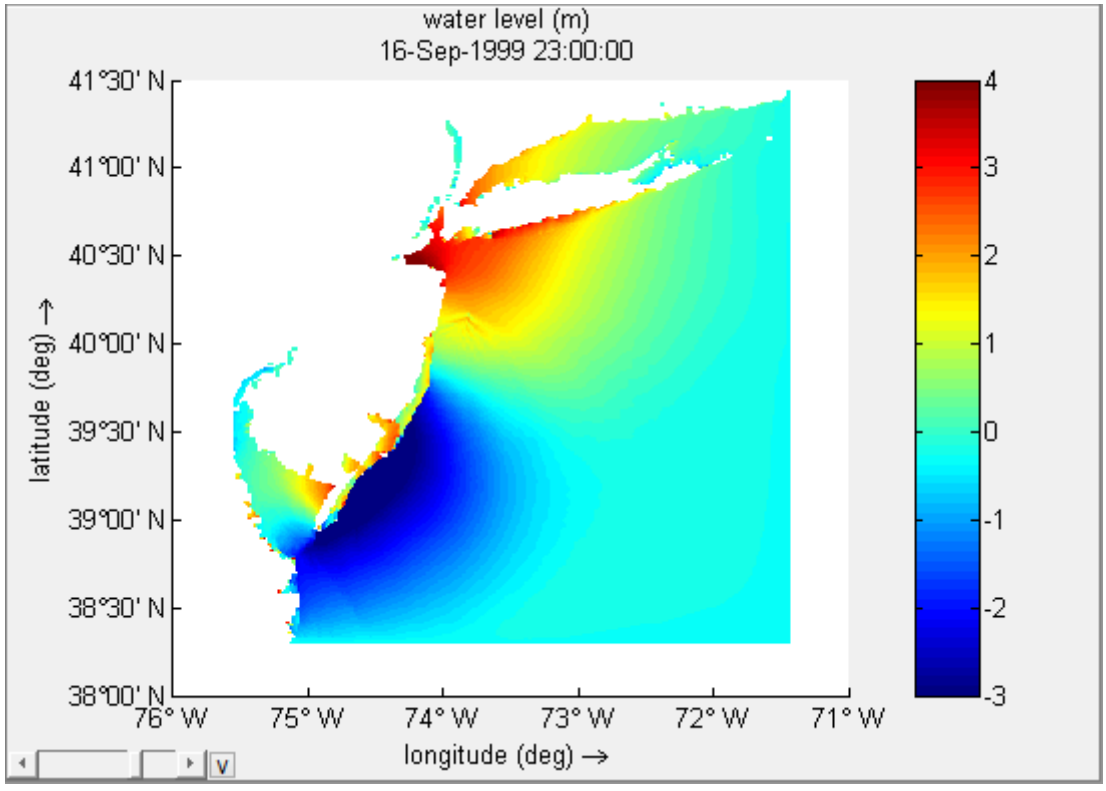

Figure 4-12 - Tropical Storm Floyd's water levels with spiderweb wind field (m).

As was previously mentioned, the radius of maximum winds (Rmax) is usually not given as much importance as the intensity (wind speed) or the pressure drop of a tropical storm. Because the region being studied can be the transition zone for tropical systems becoming extratropical systems, the radius of maximum winds can be a significant factor. The term extratropical means that there is polarward displacement. This implies that the main source of energy becomes "baroclinic". This means that the energy is obtained from horizontal temperature contrasts between cold and warm air (Weather Underground, 2014).

In this location, there is also the possibility that the system approaching is neither a tropical cyclone nor an extratropical storm. It can be a subtropical system. The National Hurricane Center, NHC, defines a subtropical storm as a non-frontal low-pressure system that has characteristics of both tropical and extratropical cyclones (Weather Underground, 2014). Like tropical cyclones, they have closed surface wind circulation about a well-defined center but lack a central dense overcast. Unlike tropical cyclones, subtropical cyclones derive a significant proportion of their energy from baroclinic sources (like extratropical storms), and are generally cold-core in the upper troposphere. In comparison to tropical cyclones, these systems normally have radius of maximum winds occurring relatively far from the center, usually greater than 60 nautical miles, with less symmetric wind fields and convection distribution. Because of this, the radius of maximum winds can play a big role in the simulated results! The NHC only began naming storms in 2002. Previous to that, from 1968 to 2001, the subtropical storms were just given numbers. Before 1968 some subtropical storms were not documented and those that were, were not even given names, simply referring to them as "Unnamed Storms". This is the case for a couple of the tropical systems simulated in this study. Also, between 1987 and 1995, the director of the NHC at the time declared that these systems should not be recognized. It is estimated that at least 10 storms are missing from that time period (Weather Underground, 2014).

The application of radius of maximum winds was considered essential to the tropical systems being analyzed. Unfortunately, this data is not easily found, so an estimate of the Rmax was given for all the tropical cyclones that did not have that information available. As each system reached the area of The Battery, the Rmax generally considered was between 65 and 100 nautical miles (120,38 to 185,20 km). An example of Tropical Storm Floyd's water levels with the absence of the Rmax is shown in Figure 4-13.

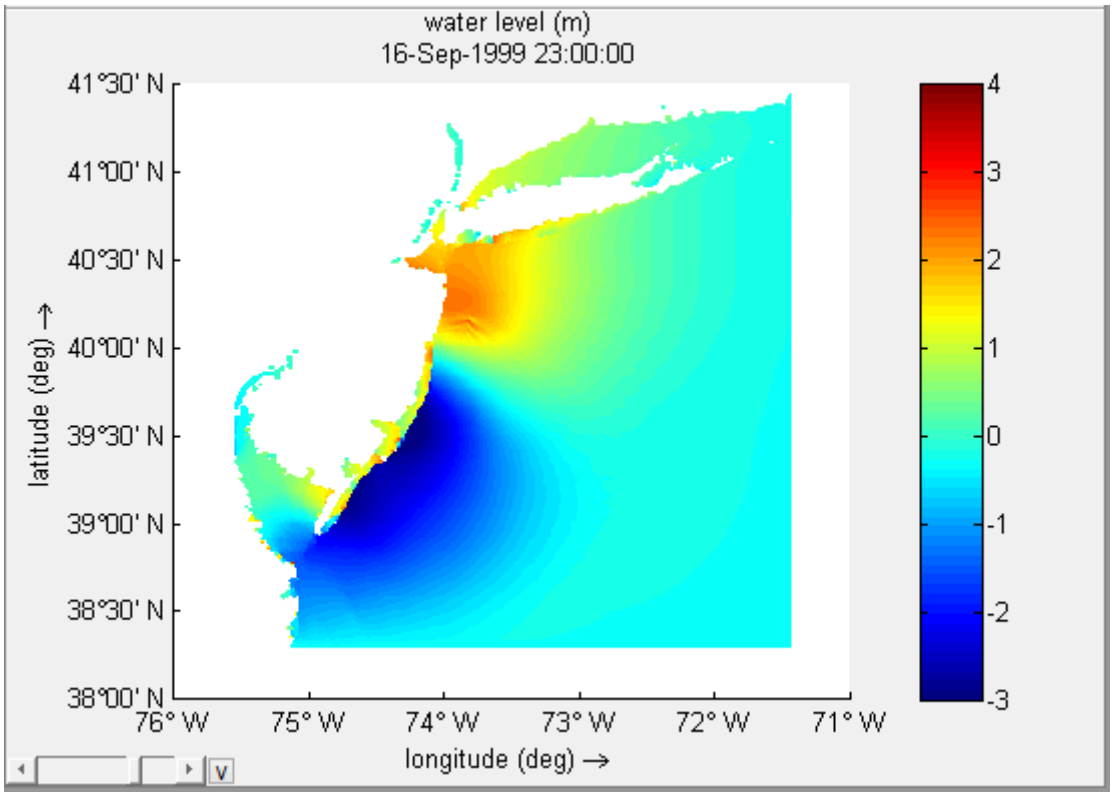

Figure 4-13 - Tropical Storm Floyd's water levels without a user-defined Rmax (m).

This simulation proves that the radius of maximum winds can make a significant difference in the final result. The difference between the default of 20 nautical miles (37,04 km) for radius of maximum winds and the usual 65 to 100 nautical miles (120,38 to 185,20 km) typically observed in this region (observed in Tropical Storms Irene and Hanna) can be the feature that can almost triplicate the intensity of the winds when the spiderweb wind field is created! There is a difference of almost three meters between the simulation with a user-defined Rmax (Figure 4-12) and the simulation with the Rmax default setting (Figure 4-13).

For the comparison of the two aforementioned simulations, QUICKPLOT produces a representation of the water levels associated with the storm surge, Figure 4-14. Knowing the exact location of The Battery's observation station, in other words, the M and N coordinates of the created grid point nearest to The Battery, a selection of a block of M and N indices can be chosen to output the water level information in a Matlab file (*.mat). QUICKPLOT allows for the generation of this file which allows for the exact value of the water level reached in the most specific of areas.

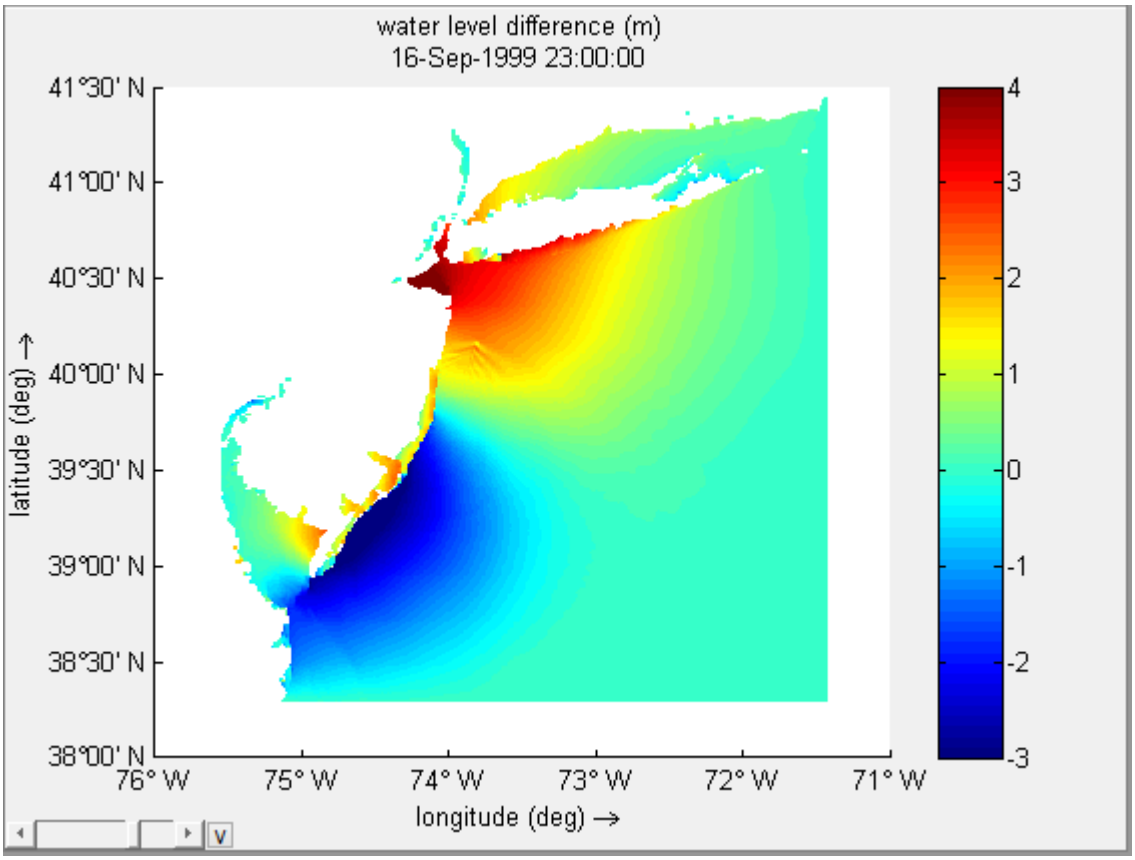

Figure 4-14 - Tropical Storm Floyd's water level difference - storm surge (m).

In Figure 4-15, one can better see the vectors corresponding to the created spiderweb wind field for the exact time step of the highest recorded water level.

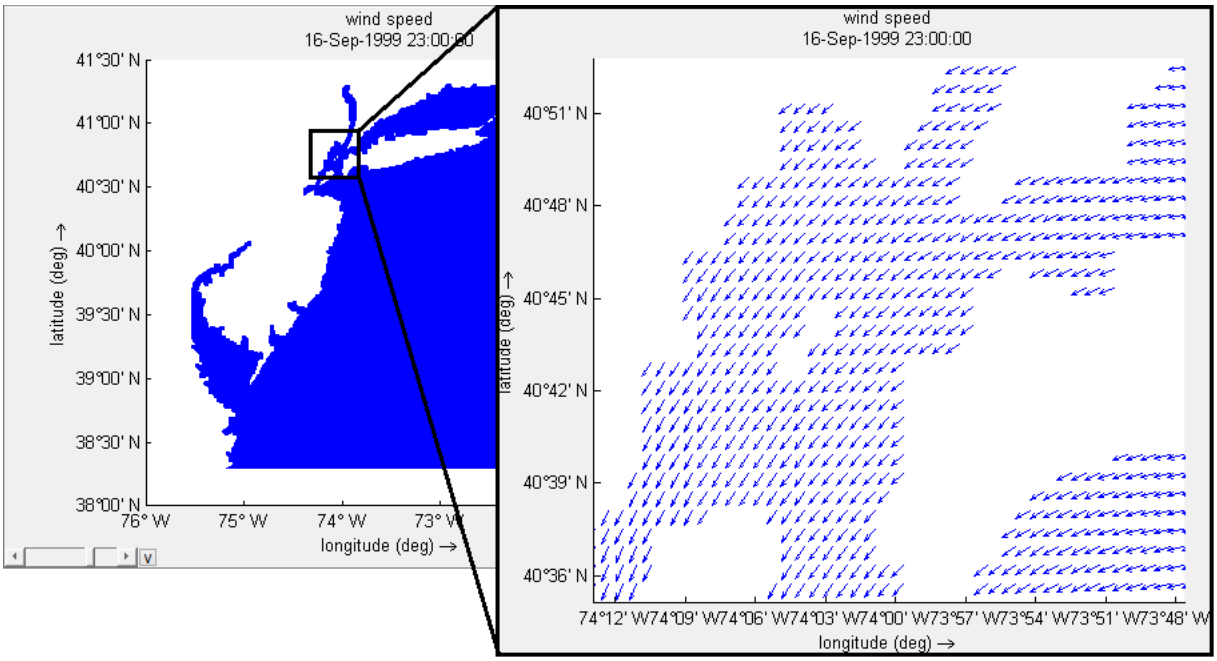

Figure 4-15 - Tropical Storm Floyd's spiderweb wind field.

In Figure 4-16, the predicted, or simulated, mean sea level for each of the tropical storms, with the addition of the spiderweb wind field, was compared to corresponding fictitious scenarios which only takes into account the tidal influences.

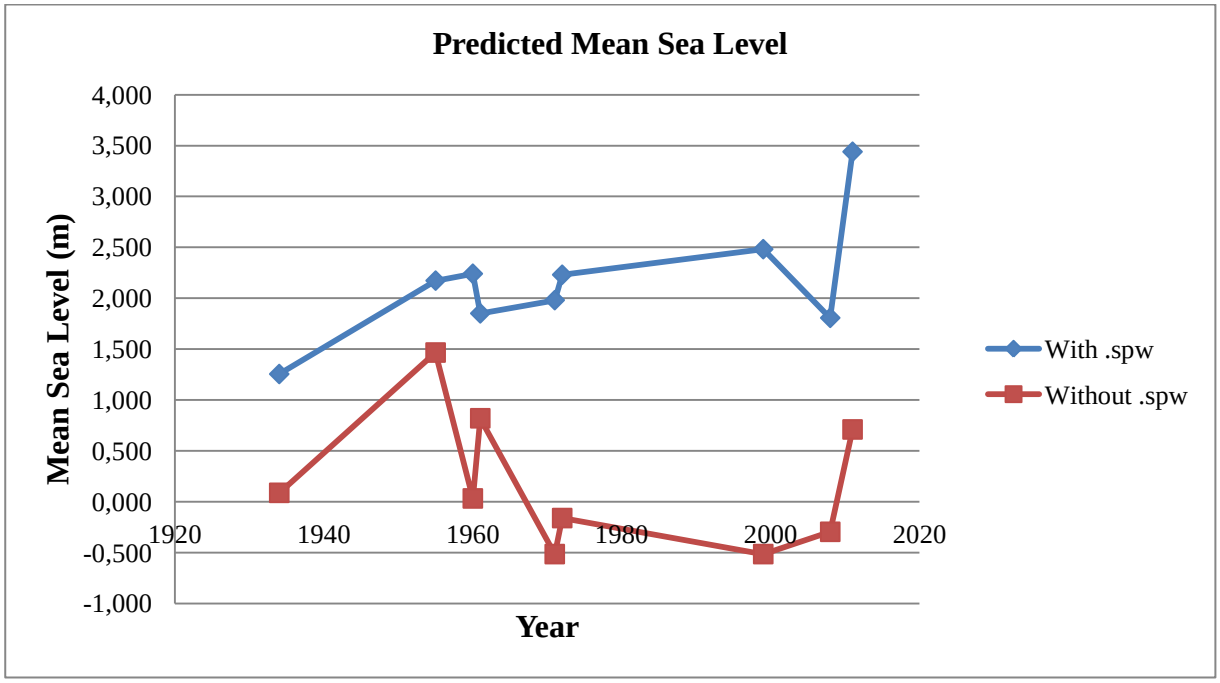

Figure 4-16 - Predicted Mean Sea Level (The Battery, NY).

When comparing the predicted values with the realistic, observed historic sea levels obtained from the UHSLC, the graph seen in Figure 4-17 was obtained.

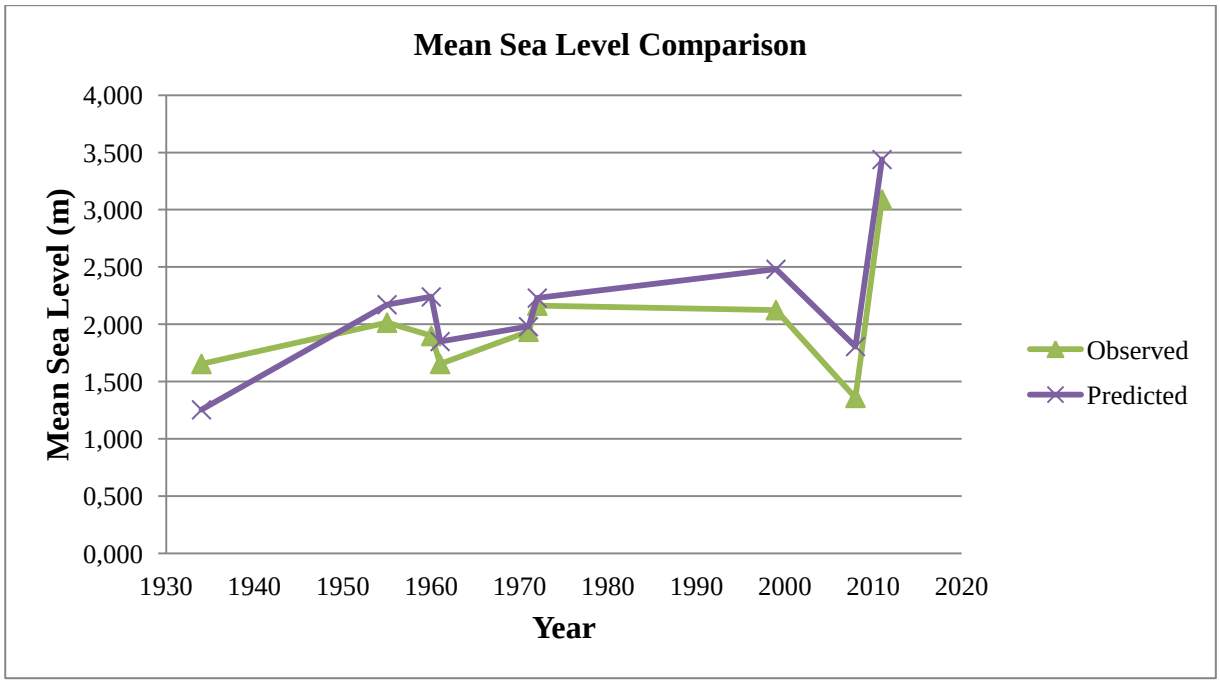

Figure 4-17 - Observed vs. Predicted Mean Sea Level (The Battery, NY).

Analyzing the results seen in Table 4-7, most of the simulation outputs averaged between a 13 to 28 percent error. Two simulations, 1971's Tropical Storm Doria and 1972's Tropical Storm Agnes, were able to reproduce the storm surge with high accuracy. Tropical Storm Doria and Tropical Storm Agnes produced storm surges with 1,79 and 2,84 percent error respectively. With the application of Delft Dashboard and Delft3D-FLOW, Tropical Storm Doria's predicted storm surge reached 2,496m, a value exceptionally close to the actually observed storm surge of 2,452m. The maximum resulting percent error was of 28,55% for the 1934 Unnamed Tropical Storm. This can be due to the fact that the available intensity data or atmospheric pressure data was not taken with great accuracy. It can also be due to an incorrect definition of the radius of maximum winds data. The lack of information, especially when dealing with systems dating back many years, increases the difficulty of recreating these tropical storms. Another suggestion to the elevated percent error can be due to discretization errors. Nevertheless, it is clear that for the most part, the application of Delft Dashboard's Tropical Cyclone's Toolbox does in fact produce valid tropical storm simulation. With such a user-friendly interface and relatively quick simulation times, one can reproduce a tropical storm and assess the outputting water levels, contributing in the planning and management of the coastal zones.

Table 4-7 - Values of Observed Surge vs. Predicted Surge and respective Simulated Percent Error (The Battery, NY).

Name	Year	Observed MSL (m)	Predicted MSL (m)	Without *.spw(m)	Observed Surge m)	Predicted Surge(m)	Percent Error (%)
Unnamed	1934	1,655	1,254	0,086	1,569	1,168	25,558
Diane	1955	2,015	2,172	1,465	0,550	0,707	28,545
Brenda	1960	1,899	2,240	0,031	1,868	2,209	18,255
Unnamed	1961	1,655	1,850	0,819	0,836	1,031	23,325
Doria	1971	1,936	1,980	-0,516	2,452	2,496	1,794
Agnes	1972	2,164	2,230	-0,162	2,326	2,392	2,837
Floyd	1999	2,125	2,481	-0,516	2,641	2,997	13,480
Hanna	2008	1,359	1,806	-0,297	1,656	2,103	26,993
Irene	2011	3,090	3,439	0,709	2,381	2,730	14,658

The use of a very dense grid can make it as though the discretization error is minimized. Of course, the use of a small curvilinear grid in the area of interest nested into a coarser model would produce better and faster results, but as it is witnessed in Figure 4-18, the results can come quite close regardless of that fact. Subtracting the values of the tidal influences at the point of each storm's occurrence from the observed and predicted mean seal level, the

observed and predicted storm surge can be compared. (Figure 4-18) In all the simulated storms except the 1934 Unnamed Tropical Storm, the predicted storm surge was superior to the historically observed surge. In a way these are conservative outcomes, the impact being always lesser than what is expected. This way, the results are always slightly in our favor.

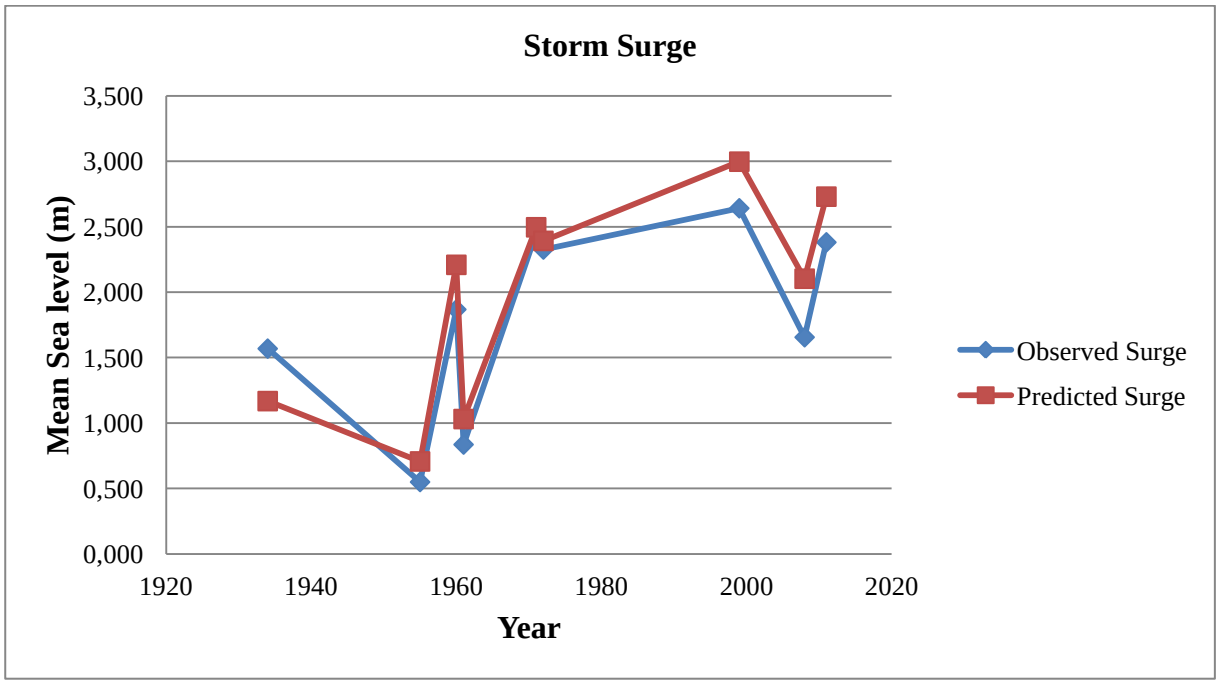

Figure 4-18 - Graphed Values of Observed vs. Predicted Storm Surge (The Battery, NY).

4.2. Northwestern Portuguese Coast - Case Study

This dissertation's second case study area is situated on other side of the North Atlantic Basin, specifically off the northwestern coast of Portugal. The region of interest, shown in Figure 4-19, will be focused on the coastline between the Douro estuary, located in the city of Porto, and the Lima estuary, found further north in the city of Viana do Castelo. According to the Portuguese Instituto Nacional de Estatistica, INE, the 2011 census records the metropolitan area of Porto with 1,758,531 inhabitants. This being the second most populated region in Portugal, second to the country's capital - Lisbon. The other extremity of the case study area is Viana do Castelo, one of the northernmost located districts in Portugal. The 2011 census records Viana do Castelo's urbanized area as having a population consisting of about 36,148 inhabitants.

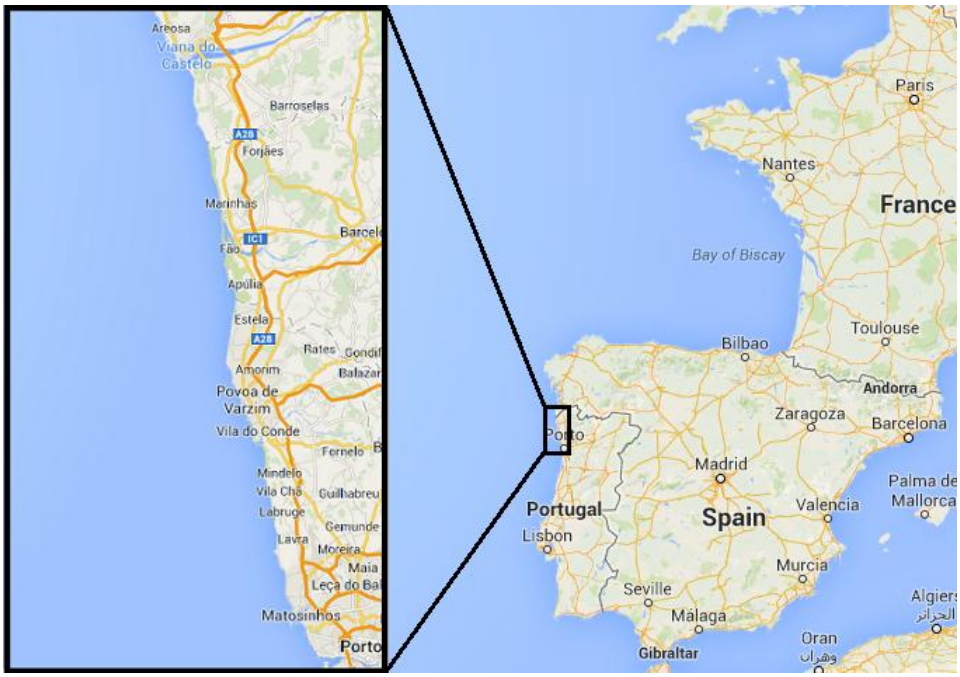

Figure 4-19 - Location of Portugal's Northwestern Coast (Google Maps, 2014).

The Douro estuary is a small deep estuary, embedded in a deep valley of granite and migmatite, containing a sandbank in its mouth. It is an estuary of a funnel type configuration with its coastal front measuring of about 1,4 km and with a narrowing of 6 km from the mouth of the Douro River (Dinis & Tavares, 2005). This configuration has a great potential for high wave elevations, potentially tsunami waves from a southwest to northwest direction (Dinis & Tavares, 2005). The Lima estuary, also a small estuary, is classified as a special conservation zone. This estuary occupies about 1,5 km of the seafront, very much tailored to port means, containing jetties (about 1,1 km). Its sandbank, enlarged by the construction of the southern jetty of about 280 m including conglomeratic sections. The river's mouth is slightly convergent, and the estuary's sandy bay is located at a distance of about 2,5 km (Dinis & Tavares, 2005).

In the last decade, the successive breaking of high temperature records has been a growing concern at a global level. Climate change has become a high priority global problem. Portugal is a country with mild Mediterranean climate, which is well known for their vulnerability to climate variability. The mean annual precipitation in mainland Portugal is around 900 mm, with a very high degree of spatial variation. In the region of the highlands of the northwest region (Minho, Portugal), the highest values, above 3000 mm, for the annual precipitation are recorded. On average, about 42% of the annual precipitation falls during the 3-month winter season, between December and February, while the lowest values occur during the summer

from June to August, corresponding to merely 6% of the annual mean (Miranda, et al., 2002). Average global surface temperatures have increased by approximately 0,6°C since the late 19th century with a 95% confidence limits of near 0,4 and 0,8°C. In the period between 1930 and 2000, the analysis of the climatological series of air temperatures in Portugal shows that beginning in 1972, there was a general trend towards an increase in the annual near surface air temperature. In Portugal, 1997 was the hottest recorded year of the last 70 years, while the six warmest years occurred in the last 12 years. The year 2000 was the 14th consecutive year with an above normal minimum air temperature. The changes in the frequency or intensity of extreme weather and climate weather and climate events are likely to have great effects on the environment and consequently on the society itself (Miranda, et al., 2002).

In terms of Portugal's wind characteristics, during "hurricane season" (specifically during the summer months), Portuguese Trade Winds blow more strongly in the afternoon from 6pm to about 7pm. Both in the summer and the winter, early morning wind tendencies indicate a direction from east to south, whereas towards the afternoon (after 3:00 PM) they change direction, traveling from west to north (Manor Houses of Portugal, 2014). According to wind speed statistics observed daily from 7am to 7pm, between November of 2000 and August of 2014, for the region of Porto, the months with the highest recorded averages averaged between 14,82 and 16,67 km/h respectively (Windfinder, 2014). These values are of little importance in terms of storm simulation. The importance lies in the swells created by wind speed observed farther off the coast of Portugal. During the winter, the Portuguese coast is affected by heavy swell for about 30% of the time, extending to about 20°W (Manor Houses of Portugal, 2014). Despite this climate wave and wind characteristics, intense winds can also treat the European western coast.

The National Strategy for the Sustainable Development - ENDS (*Estratégia Nacional para o Desenvolvimento Sustentável, Resol. Cons. Ministros, nº 180/2004*) values the diversity of the Portuguese natural heritage, national wealth of biodiversity, and the importance of coastal areas, suggesting for an appreciation and protection of these, particularly in relation to the erosive dynamics and climate changes. The Portuguese oceanic front is also considered of great significance due to its scientific, economic and military resources, and crucial for maritime safety and pollution control (Dinis & Tavares, 2005).

The National Program of Policy Planning - PNPOT (*Programa Nacional da Política de Ordenamento do Território, Resol. Cons. Ministros, nº76/2002*) in its strategic objectives,

protects the need to adopt a model of spatial organization of the coastlines, assuming resource recovery and heritage protection. With the Special Plans of Coastal Boundary - POOC (*Planos especiais de Ordenamento da Orla Costeira, Decreto-Lei n.º 309/93*) and the sectoral plan for the regime that defines the rules for the National Ecological Reserve - REN (*Reserva Ecológica Nacional, Decreto-Lei n.º 93/90*) which define the objectives and instruments for the protection and recovery of the Portuguese coastline (Dinis & Tavares, 2005).

The adoption of structural measures of rehabilitation and redevelopment of the coastline is proposed through the program, FINISTERRA (*Resol. Cons. Ministros, nº22/2003*). This program seeks to implement a policy and management of the coastal zones, namely the treatment of the critical areas and the stabilization of natural processes. Crucial aspects in implementing this program are the problem of erosion, the rising sea level, and the reduction of sediments supplied to the coast, anthropogenic degradation of natural systems, the need to carry out structural projects, and the implementation of monitoring system (Dinis & Tavares, 2005).

4.2.1. Historic Vulnerability

This second case study area usually experiences the trailing end of the tropical and extratropical systems described in this dissertation. During the summer, Portugal is usually more affected with droughts than storm crises. It is during the winter months that Western Europe, as a whole, suffers the most in terms of storm disasters. Particularly from December to February, Portugal experiences the worst kind of storms. In this time period, the large scale circulation is driven by the position and intensity of the Icelandic low, combined with a contrast of warm tropical Atlantic air masses. Portugal is gravely affected by westerly winds that carry moist air and produces rainfall events most typically observed in northern Portugal. This is a lot different from what occurs during the summer months, where northeasterly winds of either continental or maritime origins, typically bring warm and dry air into Portugal (Centre for Climate Adaptation, 2014). Because this dissertation deals with tropical cyclone occurrences during "hurricane season", that is between June 1st and November 30th, there will be no recreation of the winter storms. This is also due to the fact that obtaining information for this purpose is extremely difficult, especially in this case study region. The

development of Portuguese winter storms for future projects would greatly benefit research purposes in this area, seeing as it is a field with very limited information.

In this dissertation, the most importance is given to tropical cyclones formed in the Atlantic Ocean which typically have no temperature differences throughout the storm's surface and their winds usually derive from the release of energy due to cloud formation from the warm moist atmosphere of the tropic Atlantic. As the tropical cyclones curve polarward and to the east, normally they will transform into extratropical cyclones. As is has been previously described, extratropical cyclones get their energies from contrasts in horizontal temperatures. Extratropical cyclones have a "warm core" in the stratosphere (below the troposphere) and a "cold core" in the troposphere. There are instances in which extratropical cyclones can lose their frontal characteristics and develop convection near the center of the storm. This means the extratropical cyclone can convert to a tropical cyclone. This is a very common issue in this particular study area. The transformation of tropical cyclone to extratropical cyclones and vice versa continues to be a very difficult task for forecasters (NOAA - Hurricane Research Division, 2014).

The probability of the transitioning tropical cyclones shows a gradual rising transition probability, peaking during the months of September and October when 50% of all Atlantic tropical cyclones transition. Landfalling of a cyclone is most likely early in the season, and the transition of a cyclone is most likely late in the season. While this transitioning becomes more likely at the end of the season, this does not account for the fact that a significant number of storms that transition do not impact land. As the landfalling probability decreases with the progression of the season, when a storm eventually hits land, it is much more likely that it ultimately undergoes transitioning. October is the month in which the percentage of tropical cyclones undergoing transition is at its maximum (Hart & Evans, 2000).

According to the Europe's Centre for Climate Adaptation, an increase in severe storms of prevailing tropic origin reaching Western Europe is anticipated as a part of the 21st century global warming. An extended eastward extension of tropical storm development is projected. The vulnerability of countries to the effects of climate changes differs. The temperatures are increasing, but not in the same amount throughout Europe. Southern Europe seems to be the most vulnerable, experiencing more droughts and floods more often because of increasing climate variability (Centre for Climate Adaptation, 2014).

Tropical cyclones typically move in a north-westerly direction originating in the tropical Atlantic, and catching predominately westerly winds. This wind veers their track in a north-easterly direction, with the possibility of reaching Western Europe. If the region's genesis in the tropical Atlantic is further to the east, the possibility of reaching Western Europe increases. In addition, a resulting shorter distance traveled can allow for the tropical characteristics of hurricanes to be maintained, with less time allowed for the dissipation to occur (Hart & Evans, 2000). With the aid of model simulations, one can conclude that the consequences of such occurrences can have truly disastrous effects. With the projected rise in sea surface temperature, the frequency in severe winds and a resulting shift in the projected season of storm occurrences could be observed. What is considered as the season of highest occurrence, winter, could be replaced by the autumn season.

Just last year, Portugal was hit with giant waves from the St. Jude storm in the last week of October of 2013. According to Bill Sharp, the director of the Billabong XXL Big Wave Awards, the Atlantic Ocean experienced what was considered the most consistent string of radical storms seen in modern era of big wave surfing (TransWorld SURF, 2014). The more exposed areas of Portugal, such as Nazaré, are subject to brutal winds that can reach more protected shorelines with potential record-breaking power. In the case of the St. Jude storm, the wave reached to about 80 feet, about 24,3 meters, in height, coming close to the record breaking 30-meter wave surfed by McNamara in January of that same year (TransWorld SURF, 2014).

At present, many hurricanes wander away from the tropics and a small number of them have an impact on the Western European weather. When they do, the effects come in the form of high winds and rainfall events. When the hurricanes reach Western Europe, it should be noted that they are no longer true hurricane systems, seeing as they lack in high wind speeds and possess very low barometric pressures in comparison to true hurricanes (Hickey, 2011). The effects of these tropical systems have much to be explored and this chapter seeks to analyze the impact of the few tropical systems that do in fact arrive at the northern Portuguese shore. Similar to what was done for the US eastern coast, the databases of the National Oceanic and Atmospheric Administration, NOAA, were consulted to collect the various historical coastal storms affecting the Iberian Peninsula's coast, seen in Figure 4-20.

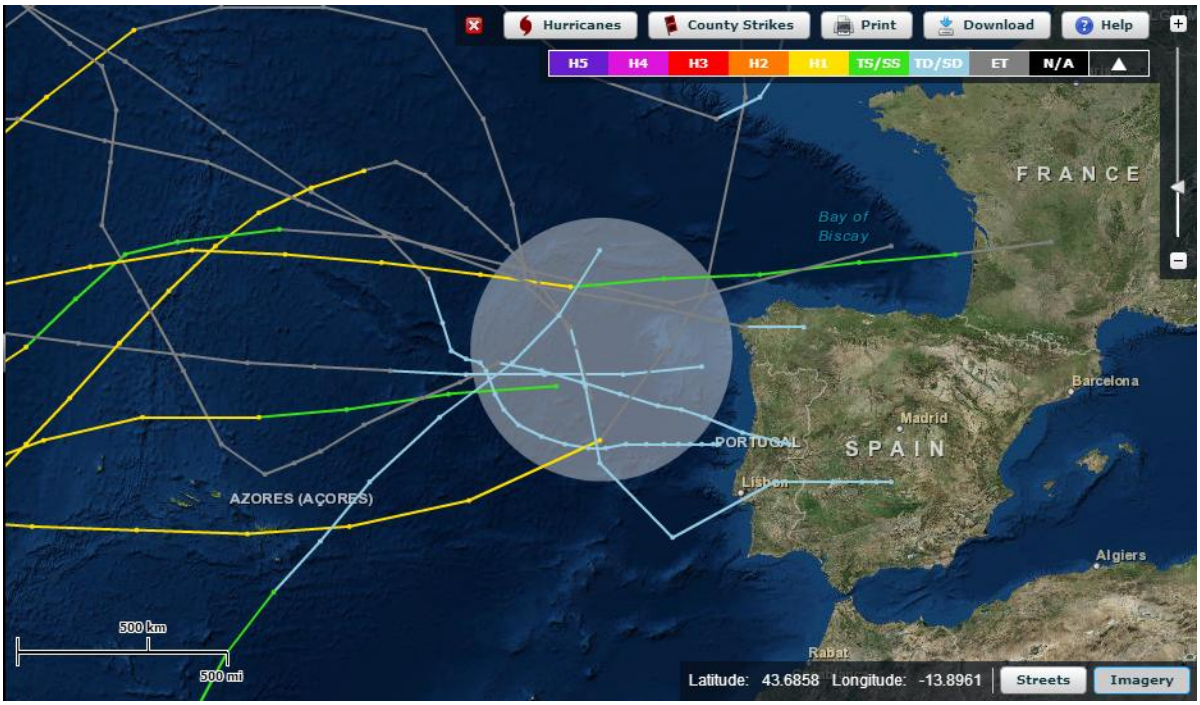

Figure 4-20 - Historical Tropical Cylones off the coast of Portugal (Historical Hurricane Tracks, 2014).

Unfortunately, the UHSLC's database does not have any information for northern Portuguese observation stations. Attaining hourly tide gauge data for the needed Portuguese stations proved to be an impossible task during the available time to develop the dissertation. Due to the lack of tide gauge information, there was no way to validate the storm surge heights expected for tropical storms affecting this region.

The second difficulty was related to the simulation of storms occurring at great distances of the case study region. The wave energies produced by tropical storms are not distributed evenly along its significant width at the fetch exit region. As a wave train leaves the fetch, it may leave at an angle to the main direction, thus arriving at a forecast point but lying to one side of the mainline of direction of the wind. The problem in swell forecasting is determining how much of the swell will reach the forecast point after the waves have spread out at all angles. Maximum wave heights will occur along the centerline of the fetch. The result is that the largest swell impact will occur where the great circle path of the centerline of the fetch intersects the final destination. Due to angular spreading, portrayed in Figure 4-21, the swell radiating from the fetch centerline can have a wide impact (COMET, 2006).

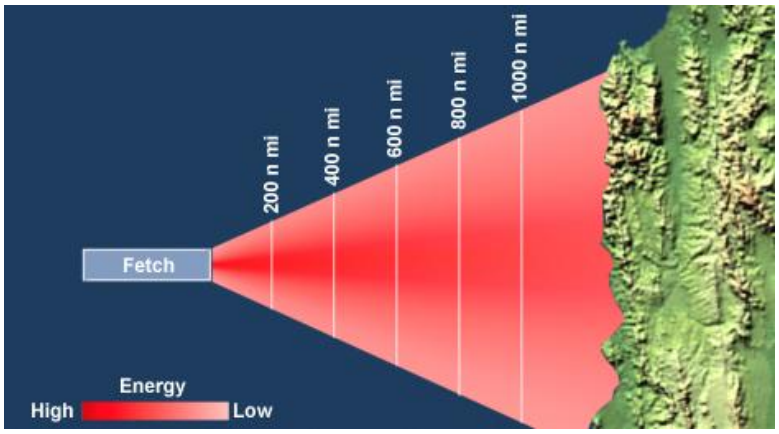

Figure 4-21 - Lateral Energy Spreading (COMET, 2006).

This is the case of many of the systems that affect the Portuguese coast. Because this side of the Northern Atlantic Basin usually gets hit with the tail-end of these tropical systems, it is very frequent that their impact is more due to swells than the actual strike of the storm against the shoreline. It is very hard to correctly simulate storms' swells with the Delft Dashboard application. Because of this, all the storms that are situated excessively far, did not result in any change in sea water level. Below, in Figure 4-22 are the tropical cyclone tracks that struck or came close to the northwestern Iberian Peninsula coast. For each of the analyzed tropical storms, the intensity, or maximum wind velocity, at the moment the system strikes the study area, is recorded. Contrary to the previous case study, there were no tropical cyclones identified in this region.

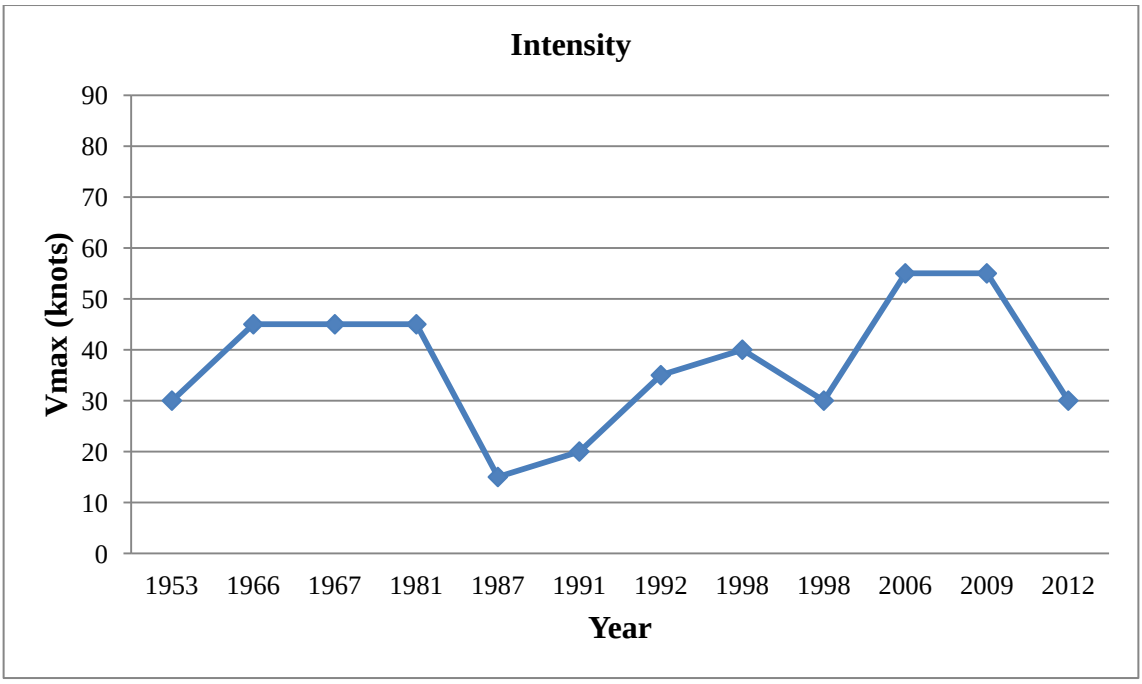

Figure 4-22 - Variation of the Storms' Intensities (Northern Portuguese coast).

The following table indicates the tropical systems that struck or whose effects come relatively close to the study area. They are given with their corresponding Start and End dates. Of the twelve tropical systems found, shown in Table 4-8, not all were simulated.

Table 4-8 - Historical Tropical Cyclones striking the Portuguese Coast and their respective Start and End Dates.

Name	Year	Start Date	End Date
Dolly	1953	8/9/1953	17/9/1953
Lois	1966	4/11/1966	14/11/1966
Chloe	1967	5/9/1967	21/9/1967
Irene	1981	21/9/1981	3/10/1981
Arlene	1987	8/8/1987	28/8/1987
Bob	1991	16/8/1991	29/8/1991
Frances	1992	22/10/1992	30/10/1992
Ivan	1998	19/9/1998	27/9/1998
Jeanne	1998	21/9/1998	4/10/1998
Gordon	2006	10/9/2006	24/9/2006
Grace	2009	27/09/2009	6/10/2009
Rafael	2012	12/10/2012	26/10/2012

To begin with, most of the storms with wind velocity properties of tropical depressions were eliminated due to the fact that Delft Dashboard simply cannot simulate an adequate spiderweb wind field. Tropical Depressions Dolly [1953], Arlene [1987], and Bob [1991] produced wind speed below 25 knots (46,30 km/h), therefore were unable to recreate; however, both Tropical Depressions Jeanne [1998] and Rafael [2012] struck the Iberian Peninsula's coast with a maximum sustained wind velocity of 30 knots (55,56 km/h). Because the velocities were above the 25-knot limit, it was possible to recreate. The tropical storms that were found much too far-away from the Portuguese coast were Tropical Storms Lois [1966], Ivan [1998], and Grace [2009]. As a result, the tropical storms that were simulated were Tropical Storms Chloe [1967], Irene [1981], Frances [1992], Jeanne [1998], Gordon [2006], and Rafael [2012].

As it is seen in Figure 4-22 and in NOAA's historical tropical cyclone tracks in Figure 4-20, the occurrence of a tropical storm is once again the most probable, with a greater tendency towards a tropical storm occurrence with very low wind speed, almost on the border between tropical storm and tropical depression. Applying a standard normal distribution, function seen in Figure 4-23, the probability that any real observation will fall between any two real

intensity values in the case of northwestern Portugal is shown. The average storm intensity, μ, was found to be of 37,08 knots (68,52 km/h) and the unit standard deviation, σ, of 12,16.

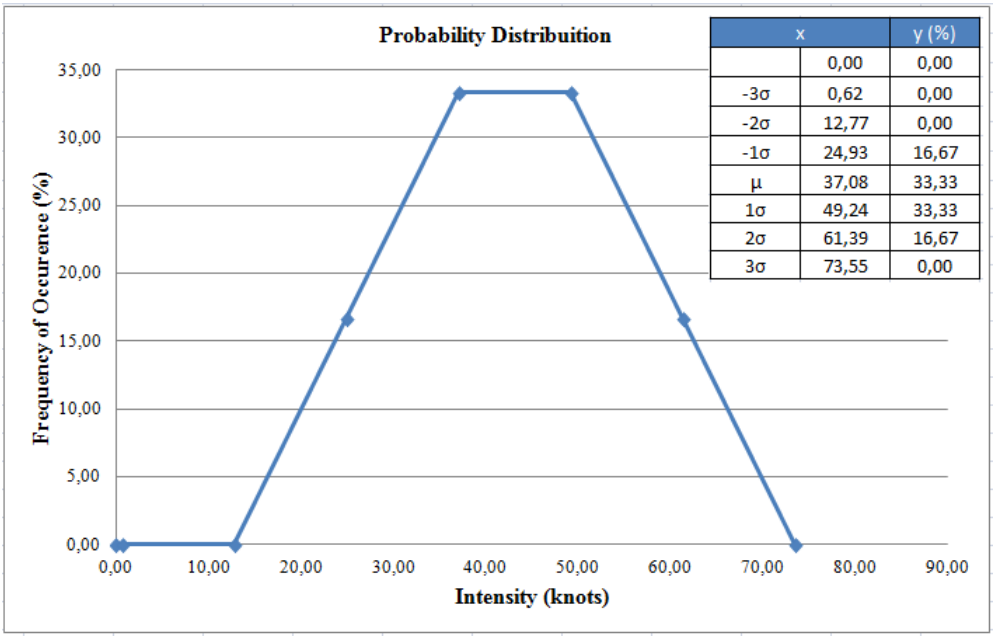

x		y (%)
	0,00	0,00
-3σ	0,62	0,00
-2σ	12,77	0,00
-1σ	24,93	16,67
μ	37,08	33,33
1σ	49,24	33,33
2σ	61,39	16,67
3σ	73,55	0,00

Figure 4-23 - Probability Distribuition of a Storm's Intensity (NW Portuguese coast).

Once again, this analysis proved to be useful as it allows for a better perception of the variables expected in this case study region. The next step would have been to analyze hourly tide gauge data for the time intervals of interest for each of the storm occurrences, and compare predicted data to real recorded data. This, due to the lack of available data, was not possible for this region. Since the tropical storms for The Battery, New York were validated, one assumes that with the correct application of the tropical storms' variables in this location, the results produced will be just as adequate. The tropical systems recreated for the Portuguese coast should be considered acceptable representations of the real tropical storms.

Because there is no accessible data with which to compare, the ensemble forecasting aspect of this dissertation, which will be presented in Section 4.3, is of more significance in this region. The application of fictitious trajectories will show how the area will be affected by varying the intensities, pressure drops, radii, and positions of possible future tropical systems. From that data, the MOMs obtained are of great value because it provides a real analysis of the vulnerability of that location to eventual storminess.

4.2.2. Application

The same grid was applied for the six analyzed historical tropical storms. The grid, seen in Figure 4-24, contains 329 points in the M direction and 232 points in the N direction.

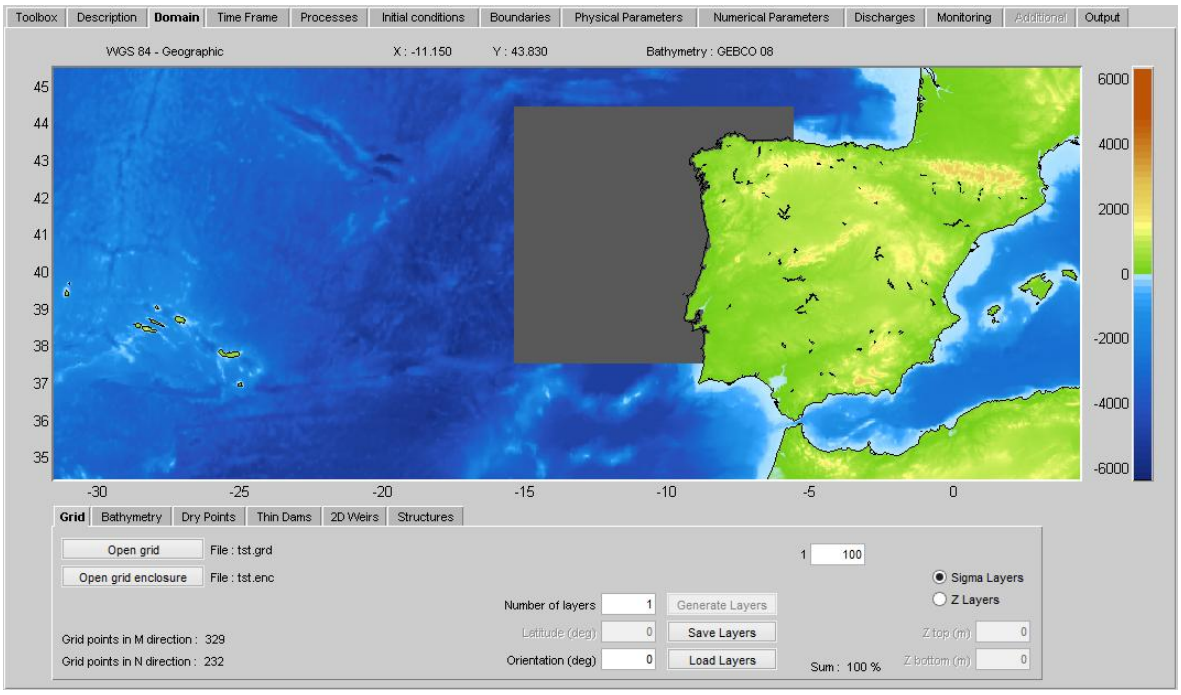

Figure 4-24 - Grid Definition for Northwestern Portuguese Coast Scenarios.

The coordinate system used in all of the simulations was, once again, the Delft Dashboard default, WGS 84 (World Geodetic System) coordinate system. The bathymetry data utilized was also the Delft Dashboard default selection, the GEBCO 08 bathymetry. It is important to refer that because any slight irregularity in the boundary conditions definition can introduce discretization errors, the area of influence created was large, with boundaries defined as far away from the case study as possible. The hydrodynamic forcing established was of astronomic components, meaning that the flow conditions are specified using tidal constituents, amplitudes, and phases. As previously explained, the interpolation between the two end points of a boundary section linearly interpolated to obtain the values at these points.

Accessing data available in the Tropical Atlantic's Best Track Data database, the Portuguese simulations ran using storm track information that include, the latitude and longitude of the storm's eye, the maximum sustained 1-min wind speed, pressure drop, and radius of maximum winds. Once again, the more recent tropical systems had more available data in comparison to the older ones.

4.2.3. Results

Because The Battery, New York's models were so successful, one would assume that applying the same methodology would result in equally successful simulations in other locations. As expected, no historical hurricanes were found to have passed directly in this area of interest. In this locale, only tropical storms and tropical depressions hit the coast. Since the area chosen is normally hit with the trailing end of these tropical systems, the more frequent occurrences are of tropical storms and depressions. Because of Delft Dashboard's spiderweb wind field limitations, more often than not, tropical depressions are unable to be recreated in this setting. Unlike the US models, a couple of the identified tropical depressions were effectively simulated seeing that tropical depression can sustain winds up to 33 knots (61,12 km/h), still within the possible parameters for the creation of a spiderweb wind field.

In this location, the tropical systems do not follow a normal pattern, contrary to the case study area on the other side of the Atlantic Ocean. There are tropical systems that proceed more northward affecting England and Ireland, while others curve polarward much earlier in its development and lean eastward affecting the Azores Island and consequently traveling towards the Iberian Peninsula's direction, portrayed in Figure 4-25. Many of these systems do affect the Portuguese coast via their big swells. Swells, however, are very difficult to reproduce with Delft Dashboard. After carrying out hundreds of simulations, it can be concluded that the systems that produce the best results are those that strike the shoreline directly, in a perpendicular manner.

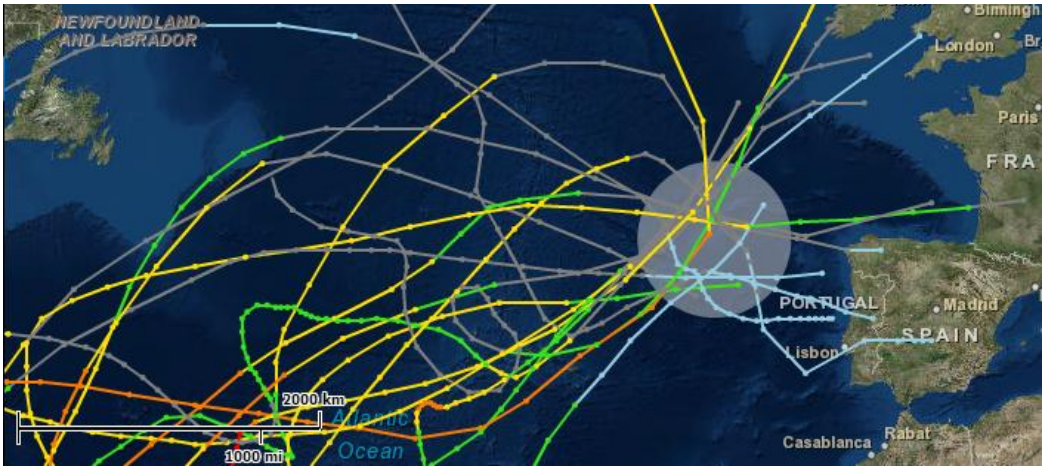

Figure 4-25 - Tropical Cyclone Tracks Striking Western Europe (Historical Hurricane Tracks, 2014).

The input of the radius of maximum winds once again proved to be a challenge to perfect. Seen in Table 4-9, the only tropical systems to have radius of maximum winds available data were the two more recent ones, 2006's Tropical Storm Gordon and 2012's Tropical Depression Rafael. However, in both cases, this Rmax data does not exist for the time steps pertinent to the region being analyzed. The Rmax is unavailable for the ending fraction of the tropical systems, i.e. when the systems have transitioned to extratropical.

Table 4-9 - Simulated Tropical Storms and respective available data (NW Portuguese coast).

Name	Year	Vmax (kts)	Rmax (n mi)	Pdrop (Pa)
Chloe	1967	x		x
Irene	1981	x		x
Frances	1992	x		x
Jeanne	1998	x		x
Gordon	2006	x	x	x
Rafael	2012	x	x	x

As it was proven in the previous case study, the Rmax does have a big influence in a storm's simulation. Delft Dashboard's default is normally not enough to result in the expected impact on the coast. Table 4-10 shows the exact time at which the simulations reach their peak water level height. There is no registered historical data with which to compare the obtained data.

Table 4-10 - Predicted Maximum Surge Height's Time Step (NW Portuguese Coast).

Name	Year	Predicted	
		Date	Hour
Chloe	1967	21/9/1967	3:00
Irene	1981	3/10/1981	5:00
Frances	1992	29/10/1992	17:00
Jeanne	1998	4/10/1998	2:00
Gordon	2006	21/9/2006	3:00
Rafael	2012	26/10/2012	1:00

Once again, in order to avoid a drawn-out Results section, only Tropical Storm Gordon's QUICKPLOT output data will be presented as an example. The remaining tropical cyclone output information can be found in Appendix II. Figure 4-26 shows Tropical Storm Gordon's water levels resulting from the consideration of only the tidal influences, while Figure 4-27 shows the result of the simulation of the water levels for the northwestern coast after the introduction of Tropical Storm Gordon's spiderweb wind field.

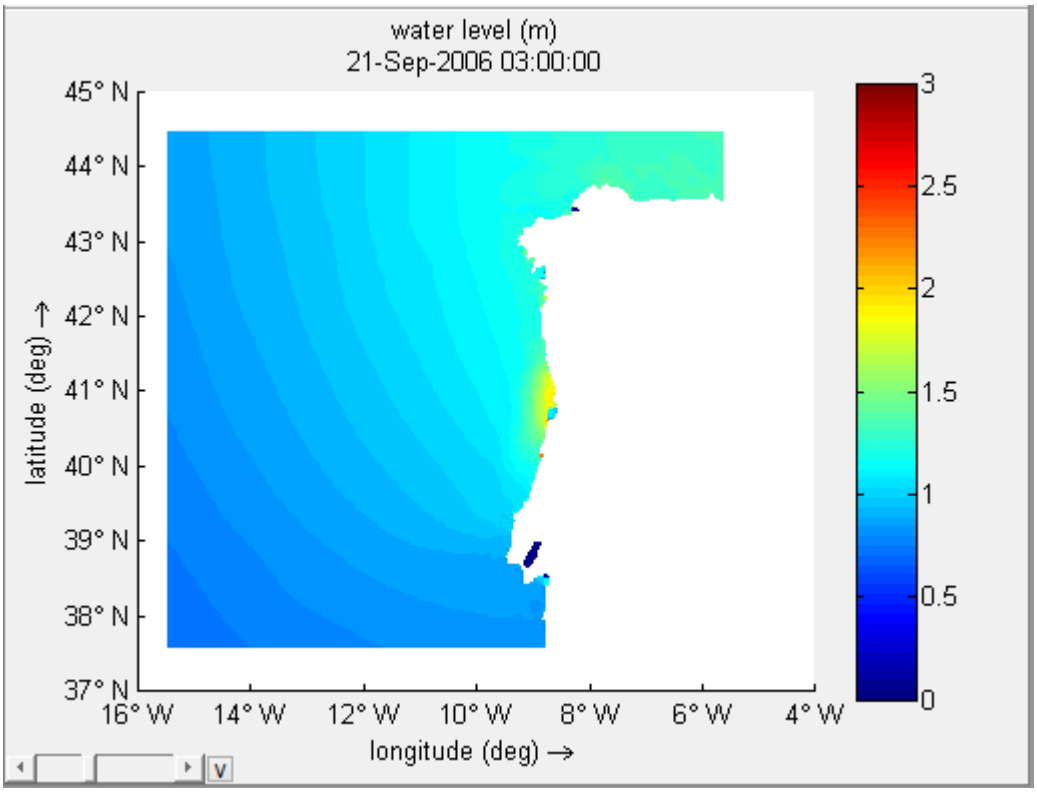

Figure 4-26 - Tropical Storm Gordon's water levels without spiderweb wind field (m).

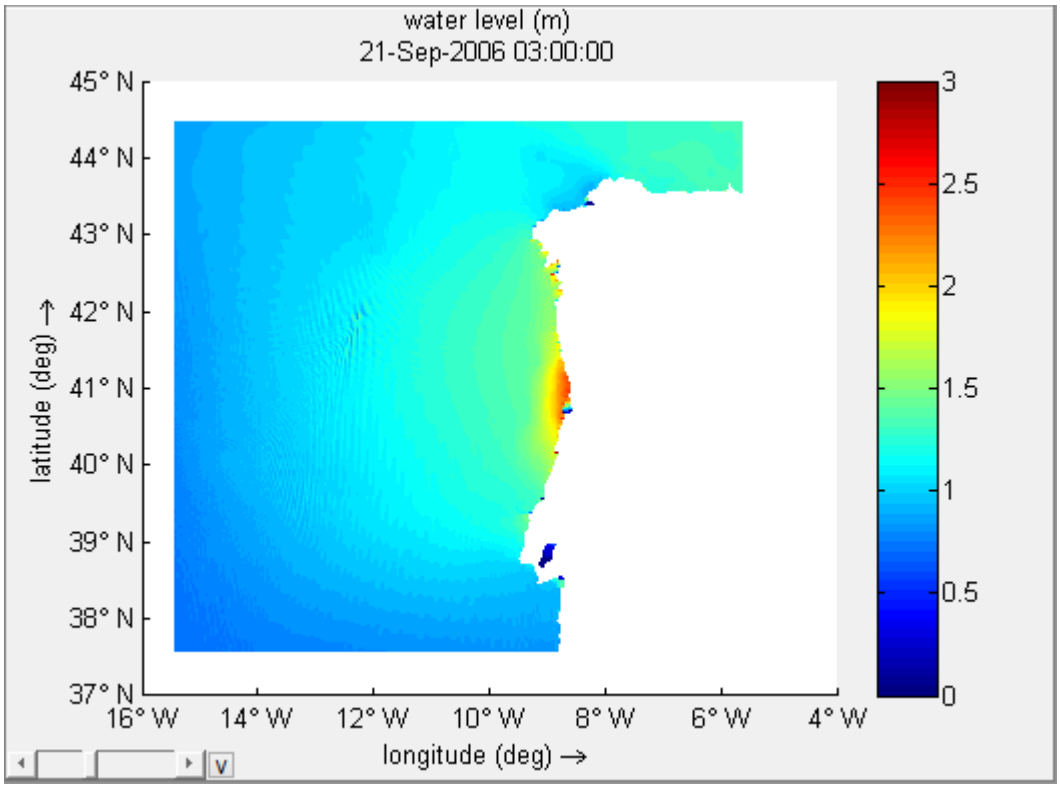

Figure 4-27 - Tropical Storm Gordon's water levels with spiderweb wind field (m).

Each of the occurrences found in Appendix II coincide at about the same time as the high tides observed in the simulations produced from the only tidal influences. Like in the previous case study, comparing the file containing the cyclone's wind field and the file without its wind field, QUICKPLOT outputs the resulting effect of the tropical storm, that is the storm surge, as portrayed below in Figure 4-28.

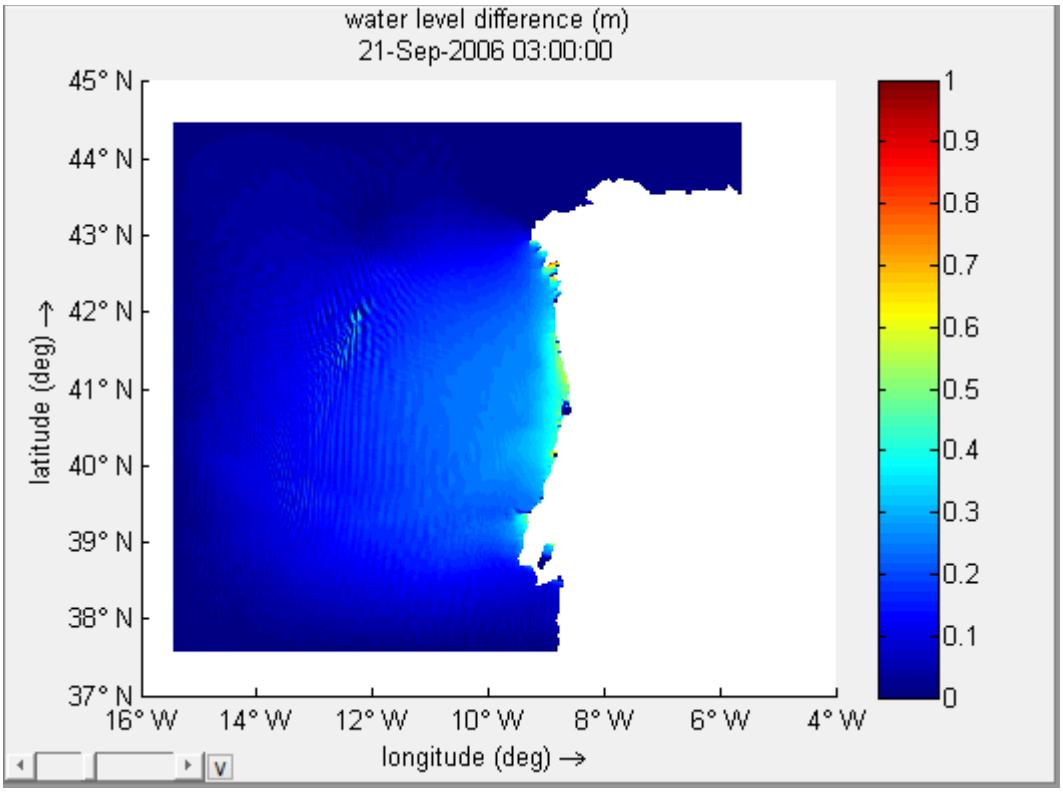

Figure 4-28 - Tropical Storm Gordon's water level difference bewteen the situation without a wind field (considering tidal effects only) and with a spiderweb wind field (m).

The application of a defined Rmax is very important in the Portuguese case studies. Because the storms do not always strike the coast directly, the impact that is usually felt is due to swells resulting of nearby tropical systems. Also, because the tropical cyclones are more prone to have transitioned into extratropical systems, the radius of maximum winds are even greater, impacting much bigger areas. Unfortunately, this data is not always readily available, having to consider various different scenarios until a change is observed in the mean sea level.

In Figure 4-29, one can distinguish the vectors corresponding to the created spiderweb wind field for Tropical Storm Gordon's particular case. The figure corresponds to the exact time step of the maximum predicted sea level.

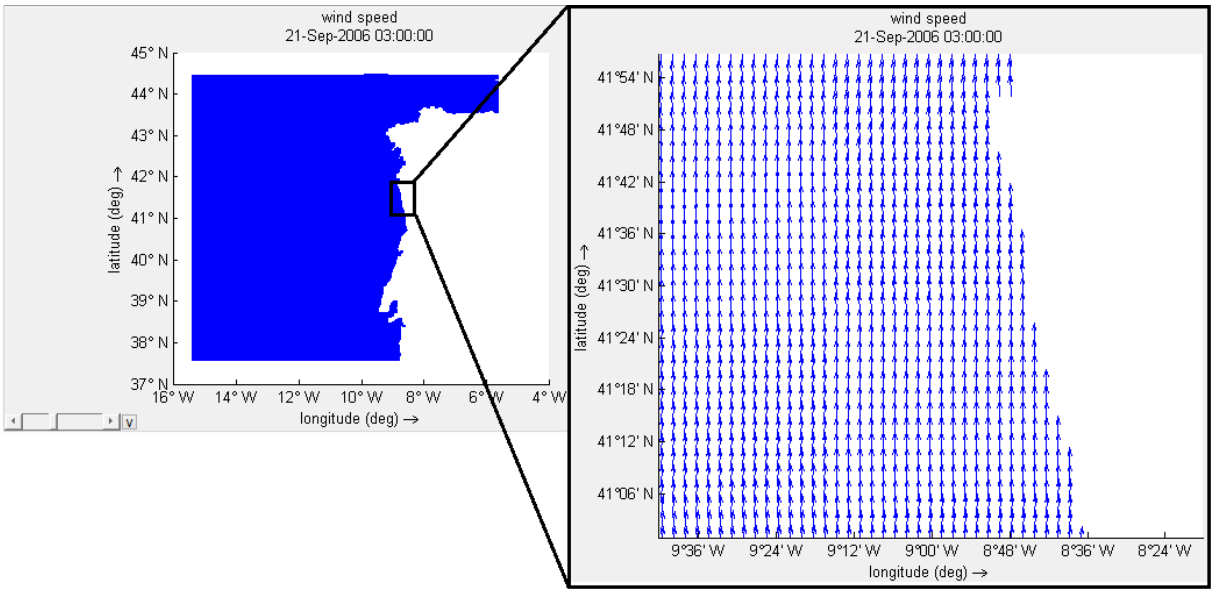

Figure 4-29 - Tropical Storm Gordon's spiderweb wind field.

The simulated mean sea level results are obtained by uploading an exportable Matlab file from QUICKPLOT onto Matlab. Knowing the exact location of the area of interest and selecting the corresponding M and N indices, the maximum water levels of that particular region were obtained. The exact location lies between the Leixões port located at 41°183'N and 8°700'W, and the Viana do Castelo port located at 41°42'N and 8°49'W. With this, it was possible to know the exact value of the height of the water level and the respective storm surge produced in that specific area. The results of the simulations are shown in Table 4-11.

Table 4-11 - Values of the Predicted Surge.

Name	Year	Predicted MSL (m)	Without *.spw(m)	Predicted Surge(m)
Chloe	1967	1,242	1,322	-0,080
Irene	1981	1,318	1,306	0,012
Frances	1992	1,451	1,277	0,174
Jeanne	1998	1,434	1,387	0,047
Gordon	2006	2,068	1,541	0,527
Rafael	2012	1,066	1,040	0,026

The predicted surge values are much smaller when compared to the results seen for The Battery, New York in Table 4-7. The maximum predicted storm surge predicted for The Battery, NY was 1999's Tropical Storm Floyd that produced a 2,997-meter storm surge. Tropical Storm Irene from 2011 also reproduced a fairly great storm surge of 2,730 meters. None of the predicted storm surges observed in the Portuguese coast come close to those

values. The maximum observed storm surge in this case is Tropical Storm Gordon's 2006 storm which produced a surge of 0,527 meter. The storm surges mostly vary between 0,01 and 0,60 meter in height. As it has been explained, this is a region more afflicted by winter storms. It is a region that is not greatly affected during the hurricane season. Even considering the Portuguese coast in its entirety, the northern shore is not even the most gravely affected region in the country. The Portuguese central region's shore is prone to very wave heights. It is progressively becoming better known for this characteristic, increasingly attracting the surfing community, especially during the winter months.

The simulated storm surge values were then compared to identical fictitious situations which did not implement the spiderweb wind field, taking into account merely the tidal influences. The comparison is shown in Figure 4-30. The difference between the two is the referred storm surge. The predicted, or simulated, mean sea level for each of the tropical storms was compared to a corresponding fictitious scenario at the point of its high tide.

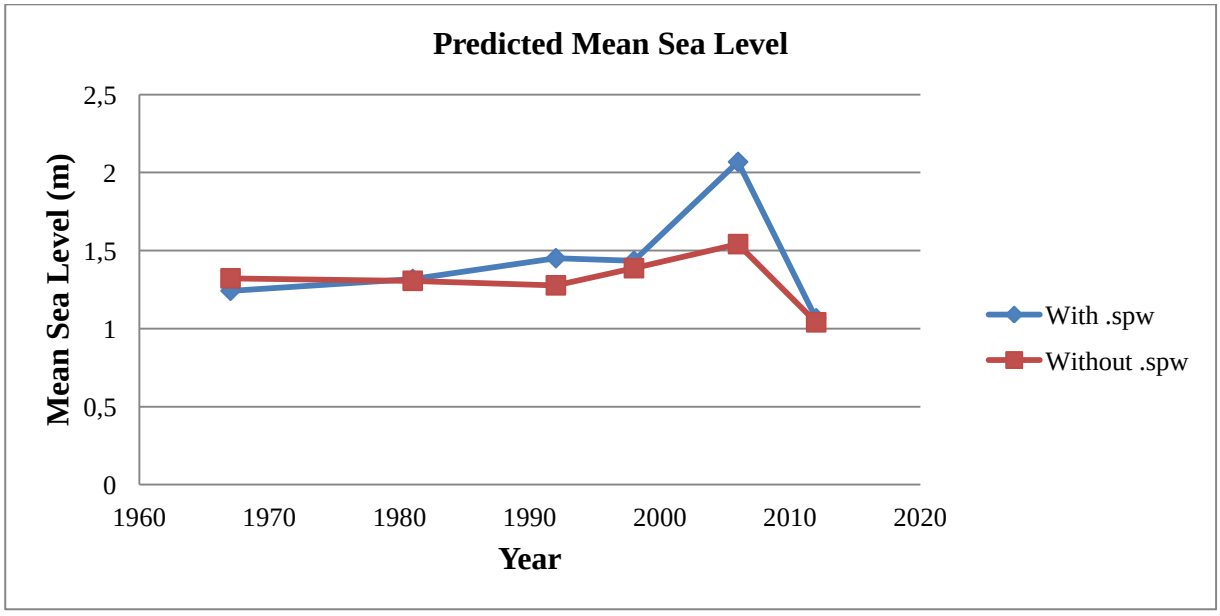

Figure 4-30 - Predicted Mean Sea Level (NW Portuguese Coast).

In order to validate these results, one would need actual measured tide gauge data at a nearby observation station. In the case of Portugal as a whole, there is very little hourly tide gauge information found. Consulting the UHSLC database, there is only one observation station with available research quality data. This station is located in the city of Cascais, Portugal, located much too far from our area of interest. Because the application of Delft Dashboard proved to have such successful results, with the given careful consideration, these results were also deemed to be just as accurate.

4.3. Ensemble Forecasting

In a subsequent phase, after the analysis of the hydrodynamic models, both case studies' storm vulnerability will be evaluated. Considering results from changes in the trajectories of the various historical storms, the vulnerability of the coast to storminess can be measured with the execution of different hypothetical scenarios. Simulations under conditions of uncertainty will be generated, in other words, ensemble forecasting will be projected. An ensemble forecast is an estimate of the future state of the atmosphere (Ensemble Forecasting, 2014). Results from the general circulation models, GCMs, about future tropical cyclone climatology are mixed, suggesting that overall frequencies of tropical storms could decrease slightly, but that there is potential for the generation of more intense hurricanes. There is also a strong suggestion that extratropical systems in the North Atlantic Basin have declined overall over the past 50 to 100 years, but there is an increase in frequency of really powerful storms (Keim, Muller, & Stone, 2004). Because of this, ensemble forecasting becomes more and more an essential tool for the proper planning and management of coastal regions.

By comparing the different possible outcomes, one can examine how likely a particular weather event will be. Using Numerical Weather Predictions (NWP), forecast models can calculate how atmospheric state will evolve based on its actual state. It provides predictions on variables like the temperature, pressure, wind, and rainfall. The downsides in this kind of model are the imprecision of the equations and the uncertainty in receiving weather observations, especially in difficult locations like for example, over mountains and oceans.

At present, there are many ensemble forecasting systems in practice, especially in the case of the United States' eastern coast as a whole. For example, the Global Ensemble Forecast System, GEFS, is a global coverage weather forecast model made up of 21 separate forecasts, used to quantify the amount of uncertainty in a forecast (NCDC & US Department of Commerce, 2014). GEFS are produced four times a day with forecasts going out to 16 days. The NOAA National Operational Model Archive Distribution System's (NOMADS) Ensemble Probability Tool allows a user to generate the multiple forecast ensemble to determine the probability that a set of conditions will occur at a given location using the GEFS ensemble near real-time (National Climatic Data Center, 2014).

4.3.1. Motivation

In essence, ensemble forecasting is a form of Monte Carlo analysis, in which numerical results are obtained based on the repeated random sampling of various variables. The Monte Carlo method is an application of the chaos theory, that is, it deals with the study of dynamical systems, i.e. tropical cyclones, that are greatly sensitive to initial condition. This paradigm is commonly known as the "butterfly effect." The initial conditions differences between various ensemble forecasts are very small, but when observing the results several days ahead, the forecast can vary greatly. The not catching of the "flutter of the butterfly" can generate a deviation of the initial state from reality. This method is used when deterministic approaches are impossible to apply.

The term deterministic means that the future behavior is completely dependent on initial conditions, a situation in which no random variables are involved. The deterministic approach in terms of numerical weather predictions refers to a single forecast obtained from a single established initial state of the atmosphere (NOAA NWS NCEPS - Ensemble Training Page, 2014). Based on observational data, once the initial state of the atmosphere is established, the model simulates its evolution from that initial state. This kind of approach will always produce the same result from the given initial conditions. According to NOAA's National Centers for Environment Prediction, NCEP, the deterministic will never yield the perfect forecast because of the following four aspects:

1. Equations used by a model do not fully capture processes in the atmosphere
2. Model resolution is not sufficient to capture all features in the atmosphere
3. Initial observations are not available at every point in the atmosphere
4. Observational data cannot be measured to an infinite degree of precision.

Since one cannot avoid observational errors in the initial analysis, these initial errors will grow with time integration through a self-applied mechanism (Zhang & Krishnamurti, 1997). Basically, these tiny, barely noticeable differences of initial state conditions do have a great influence in the outcome of these dynamical systems. In a chaotic system, like an atmosphere model, nonlinear errors can grow quickly. There can be great differences between what a weather model predicts and what truly occurs, resulting in an essentially useless model forecast. When dealing with natural systems, like weather and climatic conditions, they should be treated as a more statistical system rather than a deterministic one. Because of this,

the Monte Carlo method produces much better results. According to NOAA's National Centers for Environment Prediction, the application of a statistical analysis follows the subsequent pattern,

1. Domain definition along with all possible inputs (initial conditions)
2. Random inputs generated with a probability distribution over the domain (assigning a probability to each subset of possible outcomes)
3. Performance of a deterministic analysis
4. Analysis of results

Since the true state of the atmosphere can only be approximately observed, a statistical mean of a set of model forecasts, starting from slightly different initial states, reduces the impact of initial data uncertainties on the final forecast (Zhang & Krishnamurti, 1997). It has been proven that the Monte Carlo prediction results in a practical approximation to the stochastic dynamical technique and that an ensemble mean provides a more skillful forecast than the control run (Wesseling, 2009). The ensemble mean refers to the average of the ensemble members, which are individual solutions in the ensemble. The control run is the member of the ensemble obtained from the best initial analysis. The control is what is usually perturbed to produce the remaining members in the ensemble (NOAA NWS NCEPS - Ensemble Training Page, 2014).

In ensemble forecasting, the factors to be studied that are influential in the accuracy of a tropical cyclone prediction are the cyclone's track (position), the intensity of the cyclone, the radius of maximum winds, and its atmospheric pressure drop. It is important to keep in mind that it is not enough to have 10,000 ensemble members if they all produce the same solution. Also, having 10 ensemble members with solutions exhibiting no correlation between them, is equally futile. Ideally, the output will produce significant differences in solutions whose forecast distribution matches the actual frequency of occurrence (NOAA NWS NCEPS - Ensemble Training Page, 2014).

The idea for this phase of the dissertation is to assess the vulnerability of the coasts of the two case studies previously analyzed. Various scenarios of tropical cyclones affecting the northeastern United States coast (New York/New Jersey area) and the northwestern Portuguese coast (between Viana do Castelo and Leixões, Porto) are to be considered, resulting from a geographical shift of the "normal" trajectories of the tropical cyclones while varying their meteorological variables. This is an especially tedious task if done manually,

therefore, the application of a "Mouse Macro Recorder" is employed. The mouse macro recorder chosen was the Asoftech Automation Macro Recorder. The Asoftech Automation application allows for the automating of a series of computer tasks which can then be replayed. One can simulate or mimic mouse clicks and movements, keyboard presses, among other computer tasks. Another significant feature is its 'Schedule' feature, which allows the macro to run at a pre-defined time and even repeat infinitely (Asoftech, 2014). With the use of this recorder, the process of creating a randomized tropical cyclone can be repeated numerous times, without much effort. The problem now lies in how to have the computer create a fictitious trajectory and corresponding randomized variables associated to it.

A Microsoft Excel sheet (which later can be saved as *.spw file) will be created to define certain reasonable limits for the values of the variables (latitude, longitude, Vmax, Rmax, and Pdrop) witnessed in each of the case study areas. The variables will then be randomized according to these limits. This is to make sure that the ensemble members display correlations between them but at the same time, result in different outcomes. The limit restrictions imposed in each of the case study areas' Excel sheets will each be described in detail in the subsequent sections. After all the ensemble members are analyzed, the results need to be assessed. Applying the same idea that was executed in the two case studies, the Maximum Envelope of Water, MEOW, will be obtained for each storm for the location of interest. Then, taking the Maximum of the MEOWs (MOM) for each category, the worst possible scenarios expected of storm tides for that location is generated. The values of the MOM will indicate the location's vulnerability in terms of tropical depressions, tropical storms, and hurricanes.

4.3.2. Northeastern United States Coast (New York/New Jersey) - Case Study 1

The ensemble forecasts for the US coast ran from July 31, 2014 at 00:00AM to August 6, 2014 at 18:00PM. The Delft3D models ran for this defined period and each simulation lasted from about 10 to 15 minutes. The simulations were carried out with the use of an Intel Core i7-4700MQ, 2.40GHz processor. The grid dimensions were defined as 88 points in the M direction and 65 points in the N direction. An illustration of the created Delft Dashboard ensemble grid is shown in Figure 4-31.

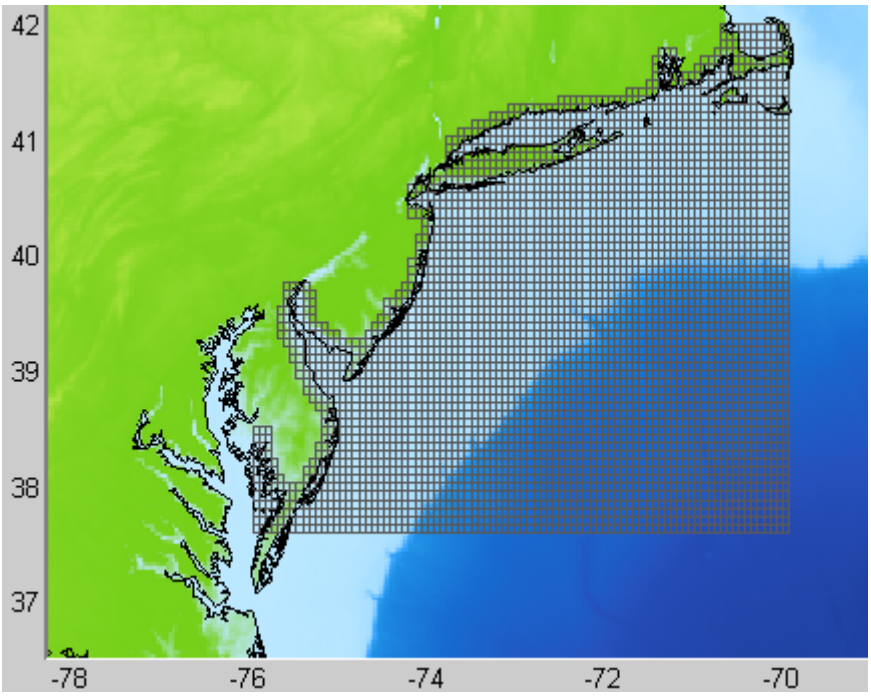

Figure 4-31 - Ensemble Grid Definition (New York/New Jersey, US).

The coordinate system used was Delft Dashboard's default setting, the WGS 64 coordinate system. The bathymetry applied was also the Delft Dashboard default setting, the GEBCO 08 bathymetry. The considered ensemble members' conditions in the creation of the Microsoft Office Excel sheet for the automatic generation of the tropical cyclone tracks are presented next.

The first variable established was the tropical cyclones' track position, the latitudes and longitudes, that typically originate in the eastern tropic Atlantic Ocean and then tend to curve polarward with a later period of possible extratropical transitioning. As explained in Section 2.3.3, the seasonal distribution of the tracks of extratropically transitioning cyclones is broken down into three periods: a low-latitude quiet early season, a high-latitude active mid season, and a mid-latitude active late season. Seeing that the simulations were executed from the end of July to beginning of August, corresponding to the beginning of the high-latitude active mid season, a transition needed to occur between the 40°N and 45°N latitude.

In order to create this curved trajectory, the first imposed limitation was that the longitude not surpass a longitudinal limit, selected between -76°W and -74°W. For each ensemble member simulation, a randomly selected value between this interval was considered as the tropical cyclones' turning point. The beginning of the cyclone path was selected to occur in any random value between -61,5°W and -77,5°W longitude. If perhaps, the increasing longitude

reaches this "peak", or turning point, the point following the turning point would continue in the opposite direction, that is, with a descending longitudinal value. This restriction forces the fictitious trajectories to curve toward the New York coastline before going too far westward, in order to simulate more "Sandy-like" cyclone trajectories. There is the possibility that the peak is never reached. In these instances, the trajectories resemble "straight lines" traveling in a northeastward direction. The longitudinal values were set to increase in random intervals between 0,5° and 1,0° if the point's longitudinal value occurs before reaching the turning point and between 0,1° and 0,5° if the longitudinal value in question occurs after the turning point.

The latitude for the beginning of the trajectories was selected to begin at any random value between the 19,5°N and 23,1°N. For trajectory points situated before the longitudinal turning point, the increments were of random values between 0,2° and 0,5°. For points located after the longitudinal turning point, the increments were of random values between 1,5° and 2,0°. This is so that before the curving northward of the cyclone's path, towards the study area, the increments are smaller, having lesser displacements, therefore guaranteeing that the tropical cyclone does not travel too far. This is very commonly observed in tropical cyclone paths of the Northern Atlantic Basin. The trajectory points of the storm's path before turning northward, are more tightly spaced. The larger increments defined after the turning point are so that the cyclone path is certain to go through the case study's general area.

The following variable, the maximum sustained winds, i.e. the maximum velocity, was selected to begin at a random value between 26 and 45 knots (48,15 and 83,34 km/h), in the lower easterly tropics of the Northern Atlantic Basin, as is commonly observed in this general region. In terms of the attributed values for the Vmax, while the tropical cyclone is approaching the United States' coast, before reaching the longitudinal turning point, the Vmax was increased in random intervals between 2 and 10 knots (3,70 and 18,52 km/h). This is true, only if, the previous Vmax value results in a value below 130 knots (240,76 km/h). If the Vmax reaches 130 knots (240,76 km/h) before the turning point, the value attributed to that point was of 130 knots (240,76 km/h) until the selected longitudinal peak. This is to avoid that the simulated hurricanes reach unrealistically high wind speeds, not normally observed in this region. Once the path reaches its westerly peak, the Vmax values were set to decrease in random intervals between 2 and 7 knots (3,70 and 12,96 km/h), as to simulate normally observed tropical cyclone behavior. As the cyclone travels northward, the velocity typically begins to decline and the other variables have more of an influence on water level effects. In

decreasing the values of the Vmax, there was careful consideration taken in averting that the wind speed reach below the 25 knot mark (46,30 km/h), which would lead to the non generation of a spiderweb wind field. This would be equivalent to having a simulation with just the tidal influences acting upon the study area, rendering the simulation useless for ensemble forecasting purposes.

The radius of maximum winds, Rmax, once again was a much more difficult factor to define because of the lack of available data. The Rmax was selected to begin with a random value between 25 and 60 nautical miles (46,30 and 111,12 km), normally observed in the lower easterly tropics of the Northern Atlantic Basin. It was detected that as the tropical system moves northward, the higher the probability of its transitioning to an extratropical system; therefore, defining a latitudinal maximum was the most rational approach. This latitudinal maximum was defined as 38°N latitude. Along the trajectory, it is usual for tropical cyclones to transform into extratropical systems around 35°N latitude (Hart & Evans, 2000). Although the transformed cyclones cannot have the same strengths witnessed earlier, over half of the systems undergo post-transitioning intensification and are most likely to impact the northeastern US and Canadian Maritimes (Hart & Evans, 2000). If the generated ensemble tropical cyclones path's latitude were positioned below the established 38°N latitude mark and the previously defined radius of maximum winds was selected with a value below or equal to 80 nautical miles (148,16 km), the Rmax was set to increased in random intervals between 2 and 5 nautical miles (3,70 and 9,26 km). If the ensemble tropical cyclone path's point were positioned above the 38°N latitude mark and the previously defined radius was selected above 80 nautical miles (148,16 km), the Rmax was set to increase in random intervals between 10 and 20 nautical miles (18,52 and 37,04 km), certifying that the input value not exceed 150 nautical miles (277,80 km). This is because, as the tropical cyclones transition to extratropical systems, the radius of maximum winds typically do not exceed 150 nautical miles (277,80 km).

Lastly, the ensemble members' pressure drop was defined. The pressure drop, Pdrop, was set to begin with a random value between 2500 and 6000 Pascal. In the ensemble tropical cyclone path's region before the considered longitudinal turning point, the Pdrop was set to increase in random intervals between 100 and 500 Pa, with an imposed limit of 8500 Pa. After the longitudinal turning point, if the previous randomized Pdrop input was greater than 1500 Pa, then it was set to decrease in random intervals between 100 and 500 Pa. If the previous

randomized Pdrop input was found to be below 1500 Pa, then the resultant Pdrop was set to increase.

Since the problem at hand (tropical storms) is of a very chaotic nature, nonlinear errors are common and the application of an ensemble forecast can be of great importance. The alteration of the initial values significantly influence the results; therefore, a statistical mean of a set of model forecasts can reduce the impact of the initial data uncertainties on the final result. With the application of the abovementioned conditions inputted onto a randomized Excel sheet, the outputs produced significant differences in solutions whose distributions do in fact match actual frequency of occurrence.

4.3.2.1. Results

With the application of the mouse recorder, after recording the first simulation, the program ran for 241 times. With the elimination of dubious data, 232 of the 241 created ensemble members were successfully analyzed. Considering a small area within the grid corresponding to the NY/NJ Harbor, with the application of a simple Matlab script found in Appendix III, the maximum of the mean sea level was obtained for all of the ensemble members for the specific area of interest. The graph depicted in Figure 4-32 shows the results for the maximum mean sea levels for the area surrounding the New York/New Jersey Harbor for the duration of the simulation.

Of the 232 ensemble members, 175 members resulted in less than 7 meters of mean sea level, 149 members resulted in less than 6 meters of mean sea level, 120 members resulted in less than 5 meters, and 109 members resulted in less than 4 meters of mean sea level. This means that the 7, 6, 5, and 4-meter mean sea level limit resulted in enclosing 75,43%, 64,22%, 51,72%, and 46,98% of the total ensemble members respectively.

In the situations where the randomly created tropical cyclone trajectory did not even come close to the case study area, the resulting mean sea level was of about 1,272 meter. An example of the outputted water level data for this type of situation is portrayed in Figure 4-33. Only 4 of the total 232 ensemble members (1,72%) were unaffected by the simulated tropical cyclones.

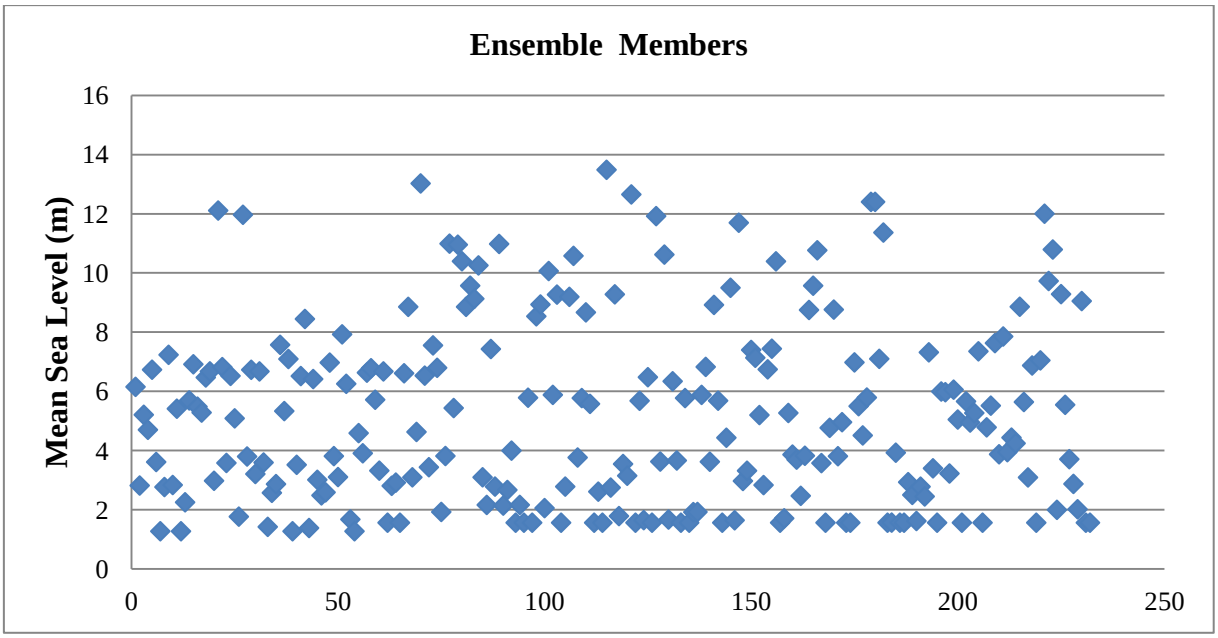

Figure 4-32 - Ensemble Members' Results for the Northeastern United States' Coast.

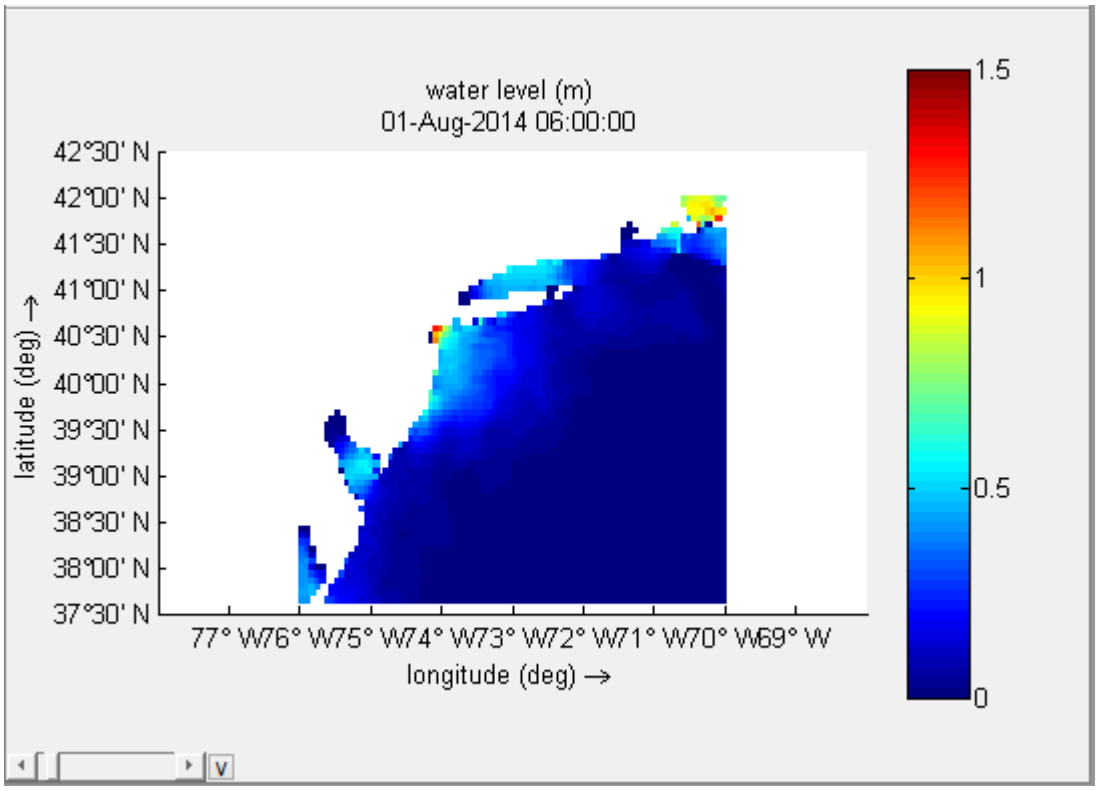

Figure 4-33 - Example of an ensemble member in which the spiderweb wind field does not occur within the grid; only tidal effects considered (New York).

The details for the tropical cyclone with the worst simulation scenario, i.e. the maximum predicted mean sea level, will be presented. This "worst case scenario" storm track (track no. 126 in Appendix IV) is shown in Figure 4-34, where one can see that the path hits the area of the New York/New Jersey Harbor in a perpendicular fashion, resulting in a maximum mean

sea level of 13,483 meters on August 6th, 2014 at 7:00AM. Because the trajectory's points are only defined every six hours, the closest time step found for the 7:00AM occurrence was the 6:00AM time step. At the 6:00AM time step, the following data information was randomly generated: a latitude of 38,8°N, a longitude of 74,5°W, a Vmax of 109,0 knots (201,87 km/h), a Rmax of about 100 nautical miles (185,2 km), and a Pdrop of about 6000 Pascal. This storm trajectory did at one point reach up to 130 knots (240,76 km/h) a couple of days preceding its arrival to the New York/New Jersey coast, classifying it as a Category 4 hurricane,.

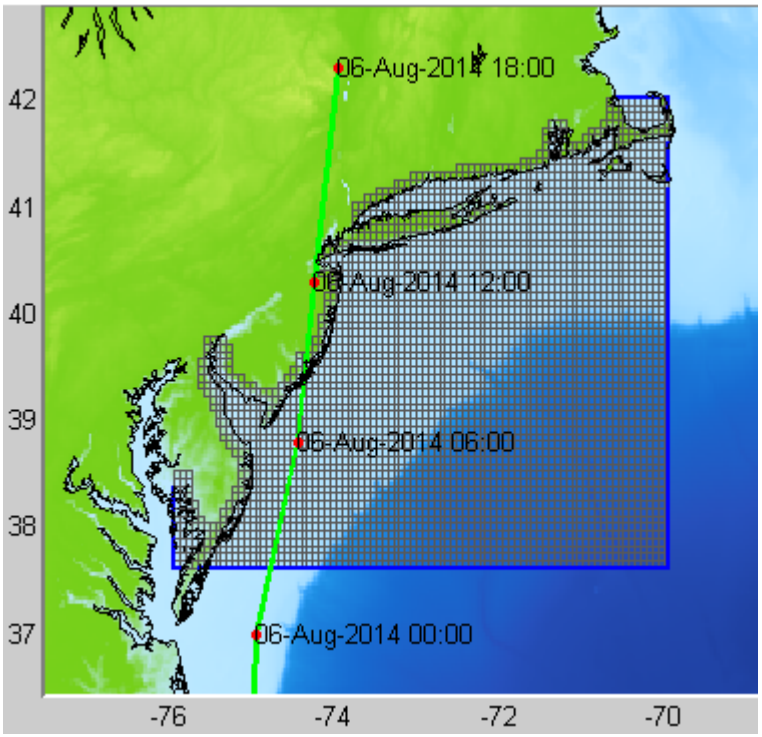

Figure 4-34 - Worst Case Scenario - Tropical Cyclone Trajectory for the NE United States' Coast.

The data for the generation of these storms was derived from historic initial conditions which were then randomized, as described in the previous subsection. The aggravation of the wind speed and the atmospheric pressure can potentially reach these limits, resulting in truly daunting effects. The resulting ensemble members had 22 tropical cyclone trajectories that surpassed 10 meters in height (9,48%). One can conclude that while the probability is small, the danger is still existent. If the mere swell from Hurricane Sandy was able to produce wave heights of almost 10 meters, resulting in damages that to date are still not fully recovered, the recorded 13,483-meter wave resulting from a direct hit can have even worse catastrophic consequences. The maximum mean sea level and the storm's corresponding spiderweb wind field is presented in Figure 4-35 and Figure 4-36 respectively.

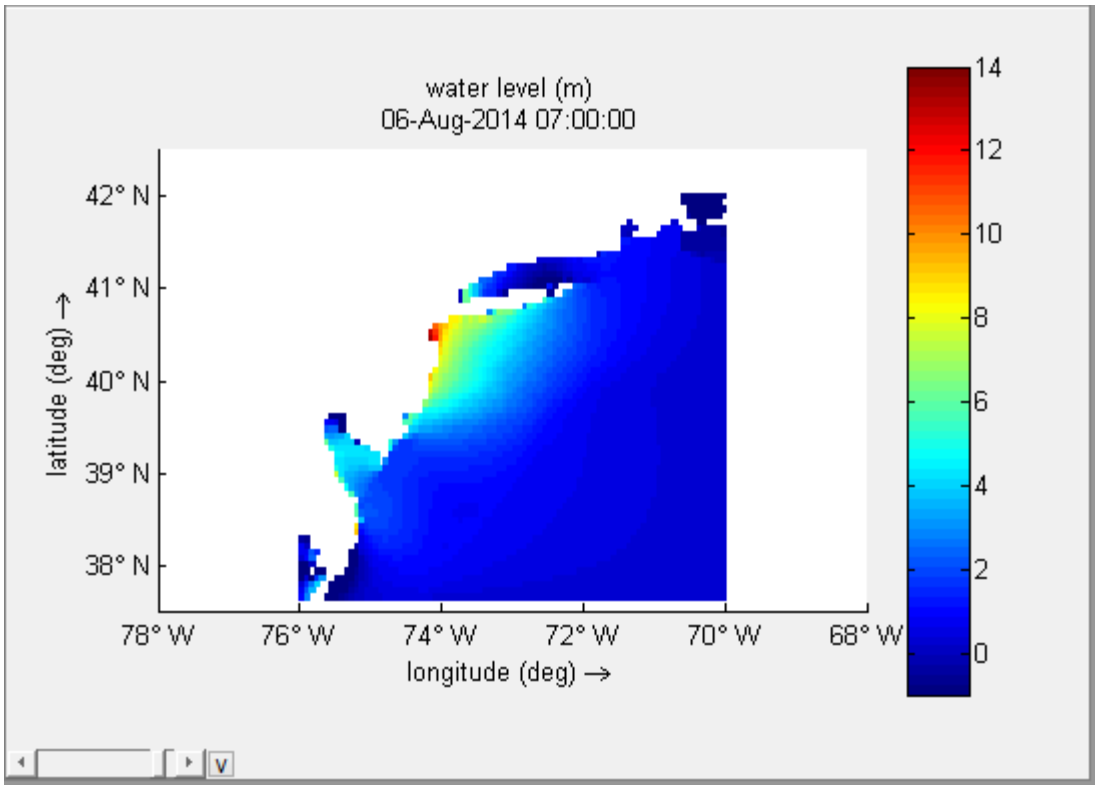

Figure 4-35 - Worst Case Scenario - Maximum Mean Water Level for the NE United States' Coast (m).

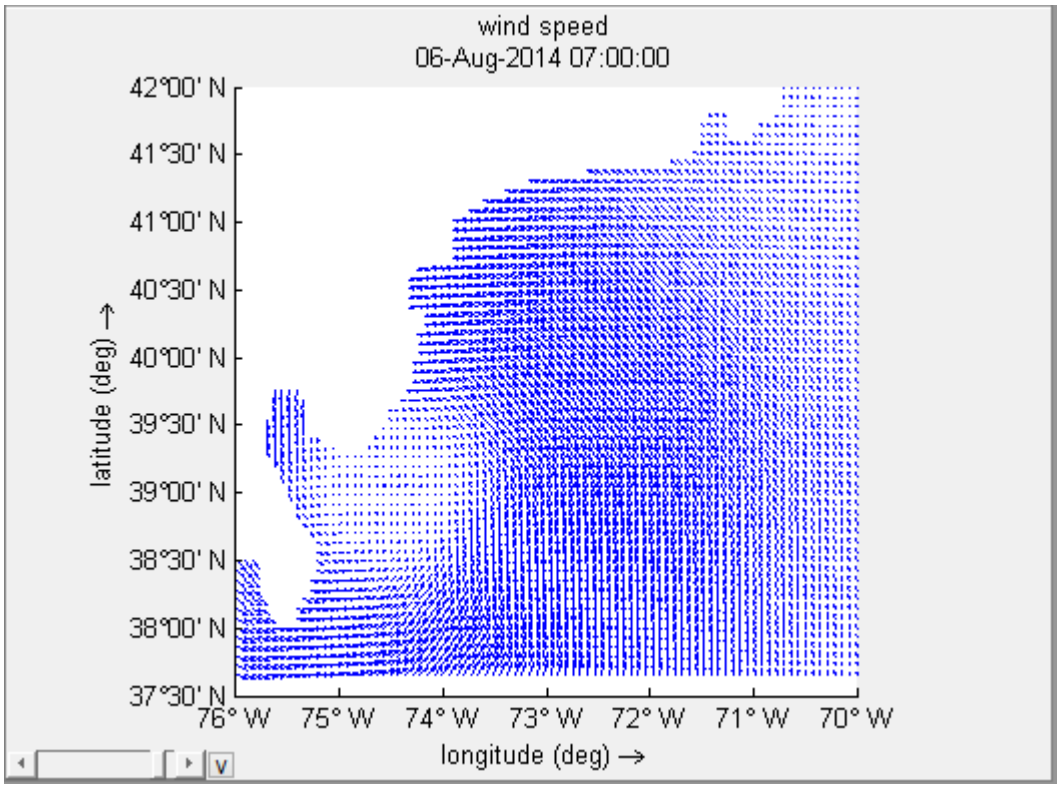

Figure 4-36 - Worst Case Scenario - spiderweb wind field (NE United States' coast).

It is important to note that the ensemble members' grid is not as refined as the one for the recreated historic simulations from Section 4.1.2. Because of this, the exact water level can be slightly different. A quick simulation of the same tropical cyclone track (no. 126) during the same, originally considered time period ran for a grid of much smaller size, but with a much greater degree of refinement. This grid contained 140 points in the M direction and 122 points in the N direction. As seen in Figure 4-37, there is a slight difference in maximum mean sea level. The maximum does not reach the supposed 13-meter mark as depicted in Figure 4-35, but the applied coarse grid is a close enough approximation nonetheless.

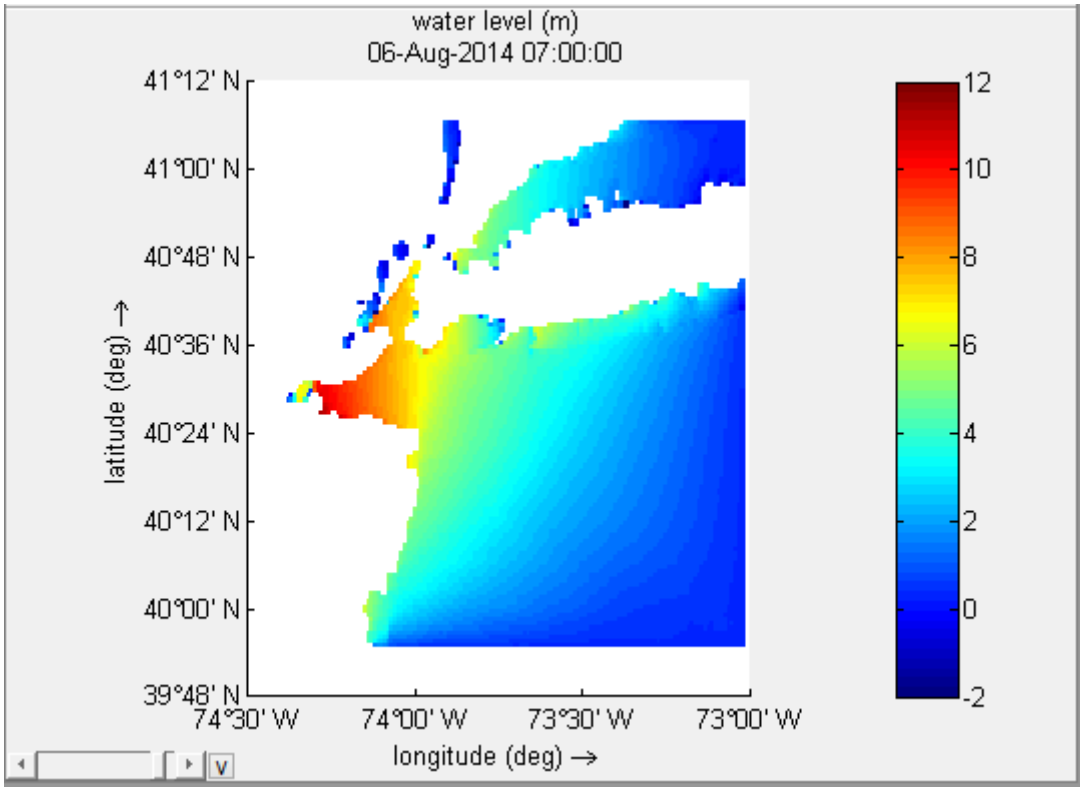

Figure 4-37 - Worst Case Scenario - Maximum Mean Water Level for the NE United States' Coast with a more refined grid (m).

For the purpose of the ensemble forecasting aspect of this dissertation, the error does not cause any concern. The ensemble forecasting executed is at a very small scale. There are programs better capable for analyzing this topic. For example, the United States' National Weather Service's Sea, Lake, and Overland Surges from Hurricanes (SLOSH) program has a Probabilistic Surge (P-Surge) application that incorporates statistics of past forecast performances automatically and generates an ensemble of SLOSH runs based on distributions of track, intensity, and size errors (NOAA - National Hurricane Division, 2014). These models, of course, are a lot more computationally efficient and are able to resolve complex

intricacies like inland flooding, the overtopping of barrier systems, deep passes between bodies of water, etc.

Nevertheless, the application of this kind of ensemble forecasting does contribute for a comprehensive view of the vulnerability of the coastal regions being studied. The vulnerability of the coast was evaluated by finding the maximum envelope of water (MEOW) for each of the ensemble storm simulations and consequently obtaining the maximum of each category (MOM). The MOMs for each of the categories are indicators of the location's vulnerability (maximum sea level expected). Because the number of ensemble members is quite extensive, they are given in Appendix IV each with their maximum MSL and respective category. The resulting Maximum of the MEOWs, MOMs, of each category are shown below in Table 4-12.

As seen in Appendix IV, in this analysis there were 147 hurricanes, 55 tropical storms, and 30 tropical depressions produced. These are the categories which the wind speed reached in the entire grid at the same time step that the MEOW was observed for the specific area. Because the tropical cyclones were "forced" to pass directly through the desired area of interest, it was expected that there would be more observed hurricanes than usual. The purpose of this application is just that - to study how the water levels correspond to an exacerbation of typically observed data, predicting potentially catastrophic tropical cyclones. This intensification resulted in a Maximum of the MEOW of 13,483 meters. For the Tropical Storm category, the maximum mean sea level for the MEOWs resulted in 6,339 meters. This is double the mean sea level of the results analyzed for Tropical Storm Irene given in Table 4-7. Tropical Storm Irene resulted in the highest observed MSL of 3,090 meters, for The Battery, NY in Section 4.1.3. Evidently, the utilized ensemble forecasting grid is coarser and encompasses a slightly wider area; nevertheless, the simple change in the direction of the tropical cyclone hit, produces two times the MSL! Lastly, the Tropical Depression category resulted in a maximum mean sea level of 1,562 meter. The tropical depressions in this analysis represent the results of tropical systems observed outside the grid area, generating results with merely tidal influences, or very small water level variations due to swells.

Table 4-12 - Ensemble Maximum of the MEOWs (NE United States' coast).

Type	No. of Occurrences	MOM (m)
Hurricane	147	13,483
Tropical Storm	55	6,339
Tropical Depression	30	1,562

4.3.3. Northwestern Portuguese coast (Porto) - Case Study 2

For the Portuguese northwestern coast, the ensemble forecasts ran from August 17, 2014 at 00:00AM to August 23, 2014 at 00:00AM. The Delft3D models ran for this defined period and each simulation also lasted from about 10 to 15 minutes. Again, the simulations were carried out with the use of an Intel Core i7-4700MQ, 2.40GHz processor. The grid dimensions were defined with 117 points in the M direction and 67 points in the N direction. Figure 4-38 portrays the ensemble grid created in the Delft Dashboard interface. Again, the coordinate system used was Delft Dashboard's default coordinate system setting, WGS 64 coordinate system, and the bathymetry applied was also Delft Dashboard's default bathymetry setting, GEBCO 08. The considered ensemble members' tropical cyclone conditions in the creation of the Microsoft Office Excel sheet for the automatic generation of the tropical cyclone tracks for the Portuguese coast will be presented below.

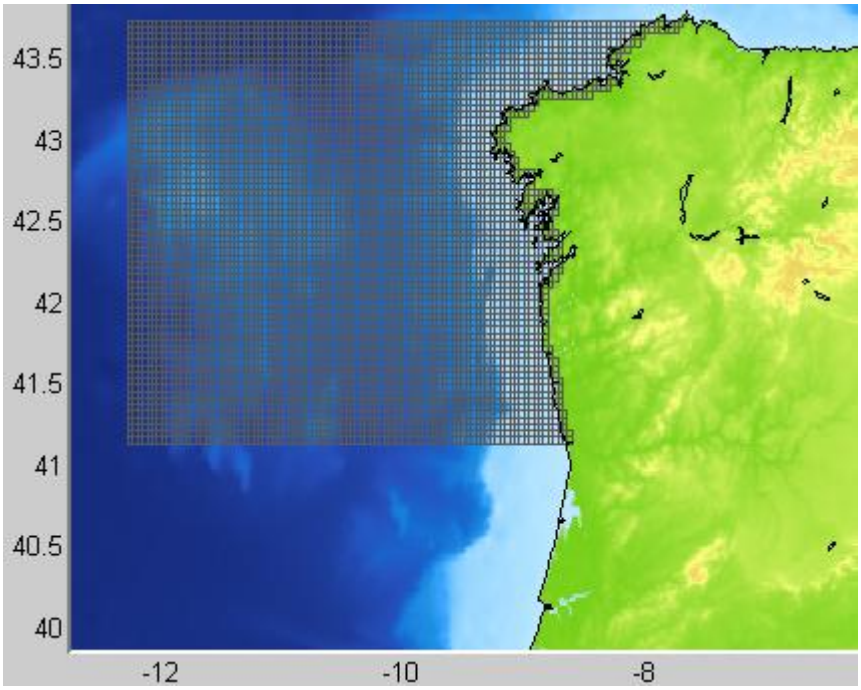

Figure 4-38 - Ensemble Grid Definition (NW Portuguese coast).

The first variable to establish is the tropical cyclones' track position, that is, how its longitude and latitude progresses throughout the given time. Normally, as tropical cyclones travel westward, they tend to curve polarward with a continued period of transitioning of tropical systems to extratropical. At the beginning of the season, the delayed warming of the oceans tend to force the location of transition northward, since the critical threshold for tropical

development is pushed northward. As the season progresses, after the month of August, the climatologically favored region for baroclinic development expands southward (Hart & Evans, 2000). It is at this point where the trailing ends of tropical cyclones become most threatening in Portugal's case.

In order to imitate trajectories that reach Western Europe, specifically the northern Portuguese coast, the first imposed limitation was that the latitude not surpass a certain limit, selected as 45°N. Contrary to the New York/New Jersey coast case study, the peak was found in the latitudinal direction because during high "hurricane season", occurring between August and October, the transition occurs between 40°N and 50°N (Hart & Evans, 2000). The cyclones' paths were selected to begin at a random value between 36,5°N and 44,8°N latitude. The values were set to increase in random intervals between 0,1° and 0,3° if the point's latitude occurred before reaching the turning point. At this point, the trajectory was forced southward so as to hit the Iberian Peninsula. If the point reached the established latitudinal peak, at 45°N, the values were set to subsequently decrease in random intervals between 0,1° and 0,5°. The very small variance in the paths' latitudes was to ensure a somewhat direct, or "straight", cyclonic trajectory towards the coast, similar to what is usually witnessed in this region.

For the paths' longitudinal values, the tropical cyclone trajectories were set to begin at a random value between -27,0°W and -22,5°W longitude. The following points were then set to increase in random increments between 0,5° and 1,0°. Again, the very small variance is due to trying to maintain the tropical cyclone path as straight as possible. With the combination of the longitude and latitude origins, the beginning of the trajectories was established in the region of the Portuguese Azores Islands. This is because it is usually at this point that a lot of the tropical cyclones travel towards Western Europe. There are a variety of different tropical cyclone paths that pass through this point. There are tropical cyclones that reach the United States' coast and continue to gain strength and travel across the Atlantic Ocean, and in contrast, there are tropical cyclones that begin in the lower tropics and curve polarward in the mid-Atlantic very early in their development. The different types of paths are portrayed in Figure 4-39. Because it is so hard to characterize a "typical" tropical cyclone path, it was opted to simulate the small part of the tropical cyclone that would reach the Portuguese coast, i.e. their tail-ends. It seemed as though it was the component that the tropical cyclones, as a group, had in common.

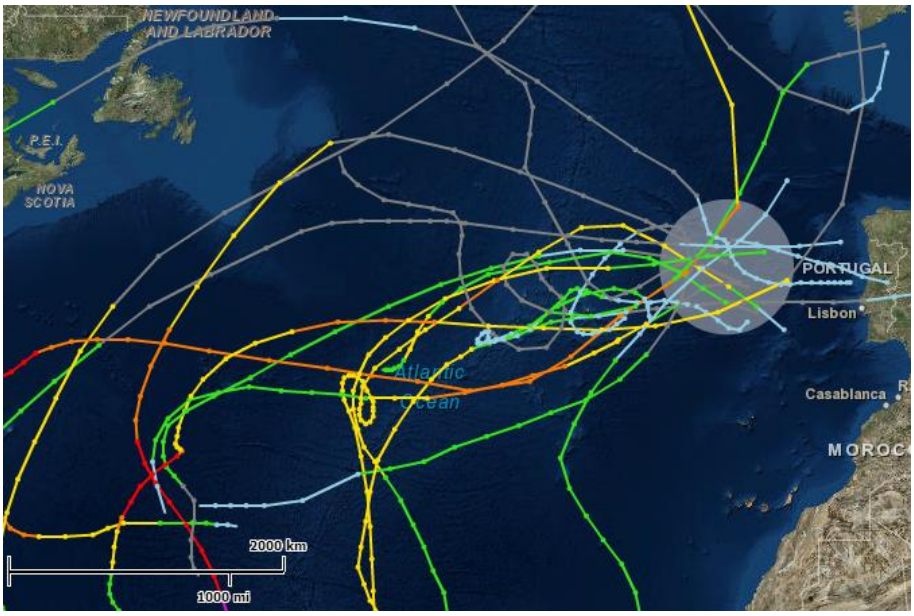

Figure 4-39 - Mid-Atlantic Historic Tropical Cyclones (Historical Hurricane Tracks, 2014).

The next variable was the maximum sustained winds, Vmax. In the region of the Azores Islands, this variable was selected to begin with a random value between 55,0 and 98,0 knots (101,86 and 181,50 km/h) with the attempt to span the various values historically recorded in that area. Because the tropical cyclones that approach the Portuguese coast are typically already transitioning extratropical cyclones with very low intensities, the main particularity to apply to the intensity's definition was that the cyclones' Vmax not reach values below 30 knots (55,56 km/h) because of Delft Dashboard's tropical depression wind field creation limitation. The analysis made in this ensemble forecasting is the coast's vulnerability to coastal storms, in other words, coastal storms that will truly impact the shorelines. Because of this, each point's intensity in the storm trajectory was set to decrease in random intervals between 1,0 and 1,5 knots (1,85 and 2,78 km/h) if the previous point was greater than or equal to 30 knots (55,56 km/h). If the value decreased so much that it reached 30 knots (55,56 km/h), the following point was set to decrease in smaller random intervals between 0,5 and 1,0 knots (0,93and 1,85 km/h).

The radius of maximum winds was a factor of utmost difficulty to define, especially in this specific region. In the middle of the Atlantic Ocean, there are instances in which the tropical systems can sustain wind speeds of up to 95 knots (175,94 km/h), corresponding to a Category 2 Hurricane, as well as, tropical systems with very weak wind speeds, not even reaching 30 knots (55,56 km/h). Because the storm's intensity is so varied in this area, specifically around the Azores Islands, the initial attributed Rmax of the tropical cyclone path

also needs to greatly vary. A tropical system with a small Rmax produces much more disastrous effects versus a same tropical system with a much larger Rmax. The Rmax for the ensemble members was set to begin at any random value between 50 and 125 nautical miles (92,6 and 231,5 km). It was then set to increase in random intervals between 0,5 and 1,0 nautical mile (0,93 and 1,85 km). Because of this great variation, different classes of tropical systems would be observed.

Last of all, the pressure drop, Pdrop, was selected to begin with a random value between 2500 and 6000 Pascal. The subsequent points were then set to decrease in random intervals between 100 and 500 Pascal, avoiding that the pressure drop reach values below 1000 Pascal. If the Pdrop decreased too much, the value was set to consider 2200 Pascal as the value instead, and the process would resume from that value. This way, the value attributed at the beginning of the trajectory would be very varied, capable of reaching up to 6000 Pascal, but when reaching closer to the Portuguese coast, the value would never exceed the 2000 Pascal mark. With all these randomized variables in the Microsoft Excel sheet defined for this location, the different tropical cyclones' outputs then produced very different mean sea level results, ideal for ensemble forecasting purposes. The results of the ensemble members will be discussed next.

4.3.3.1. Results

Like the case of the northeastern New York coast, the mouse recorder was again used to record the first simulation, and subsequently the program repeated that sequence and ran for 211 simulations. Eliminating simulation that produced dubious data, 209 of the 211 created ensemble members were analyzed. Again, considering a small area within the grid corresponding to the area of interest (between Porto and Viana do Castelo), the Matlab script given in Appendix III was used to obtain the maximum of the mean sea level for all of the ensemble members for that specific area. Figure 4-40 displays the graphed results for each of the ensemble members for the region of the Portuguese northwestern coast.

Of the 209 ensemble members, 197 members resulted in less than 2 meters of mean sea level, 152 members resulted in less than 1,5 meter of mean sea level, 91 members resulted in less than 1,3 meter, and 25 members resulted in less than 1,2 meter of mean sea level. This means that the 2, 1,5, 1,3, and 1,2-meter mean sea level limit resulted in enclosing 94,26%, 72,73%, 43,54%, and 11,96% of the total ensemble members respectively.

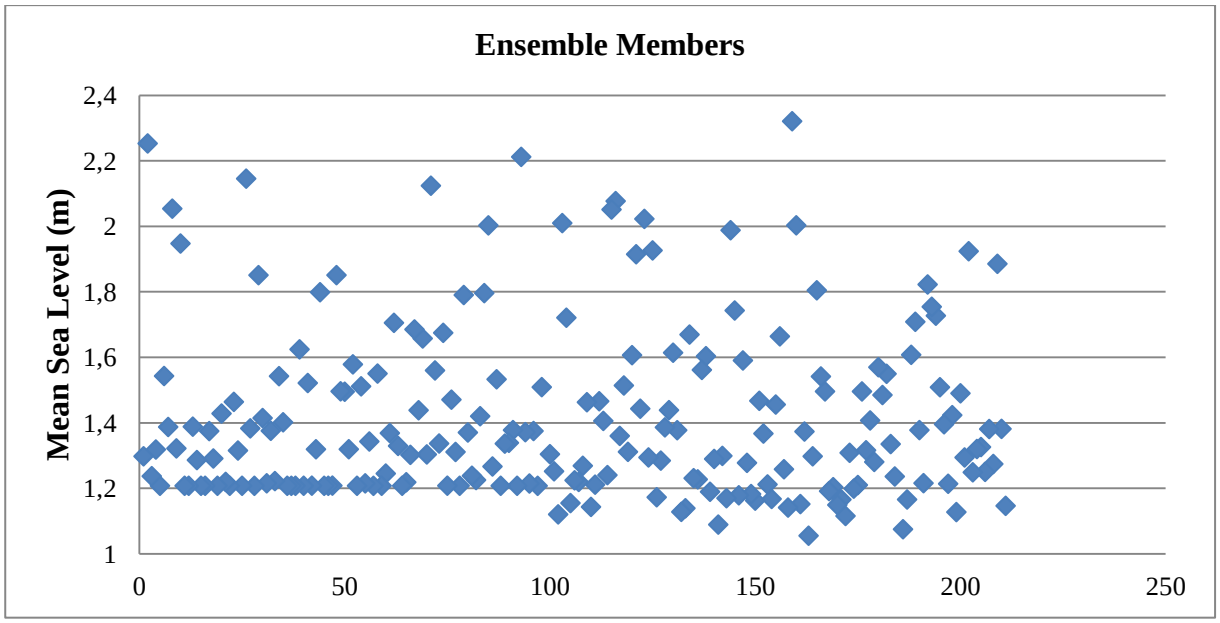

Figure 4-40 - Ensemble Members' Results for the NW Portuguese Coast.

For situations in which the randomly created tropical cyclone trajectory did not reach the region, the resulting mean sea level was of 1,208 meter as seen in Figure 4-41. Seventeen of the 209 ensemble members created were unaffected by the tropical cyclone simulations, corresponding to 8,13% of the total.

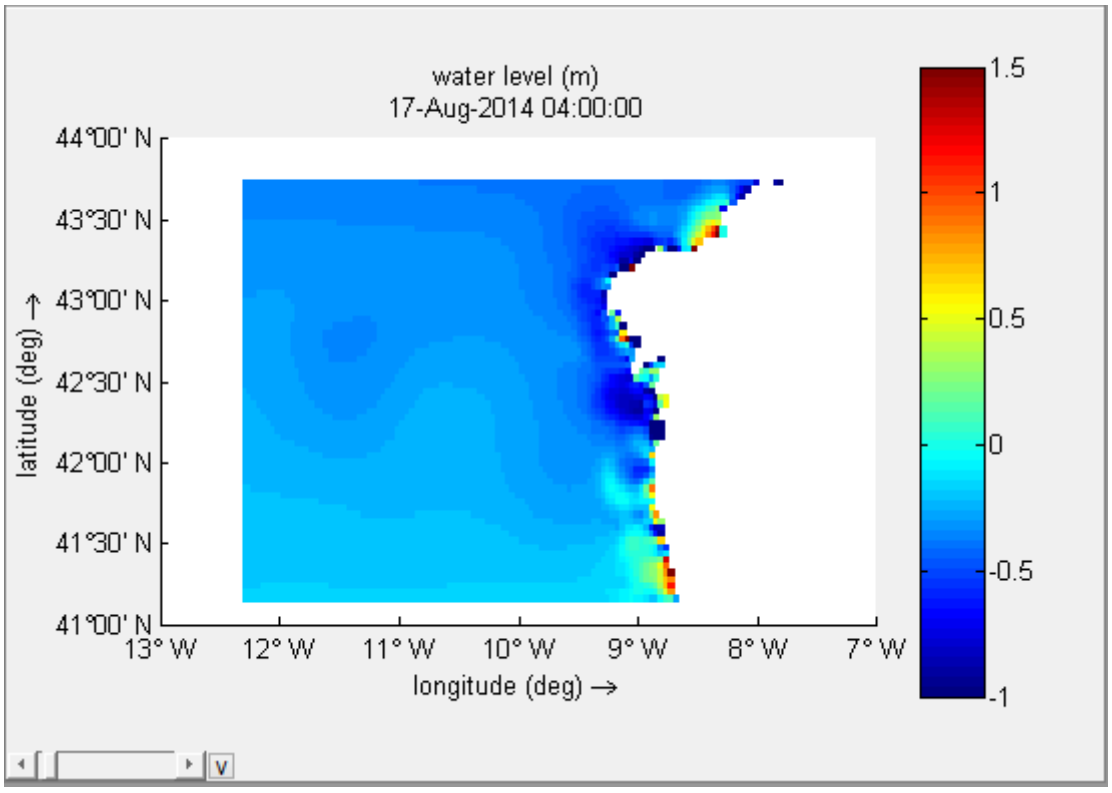

Figure 4-41 - Example of an ensemble memeber in which the spiderweb wind field does not occur within the grid; only tidal effects considered (Portuguese coast).

The details for the tropical cyclone with the worst simulation scenario outcome will be also presented. The worst scenario tropical cyclone (track no. 159 in Appendix V) corresponds to the simulation that resulted in the greatest predicted sea level. In this case, the worst scenario's storm track, seen in Figure 4-42, directly hits the northwestern corner of the Iberian Peninsula. The resulting maximum sea level of the worst case scenario, Figure 4-42, is of 2,320 meters on August 22, 2014 at 14:00PM, in the area encompassing northern Portugal. Because the trajectory's points are only defined every six hours, the closest time step to the maximum predicted sea level found at 14:00PM was the 12:00PM time step, two hours before the defined storm variables. At the 12:00PM time step, the following was randomly generated: a latitude of 43,4°N, a longitude of 9,2°W, a Vmax velocity of 68,1 knots (126,12 km/h), a Rmax of about 80,2 nautical miles (148,53 km), and a Pdrop of about 2200 Pascal.

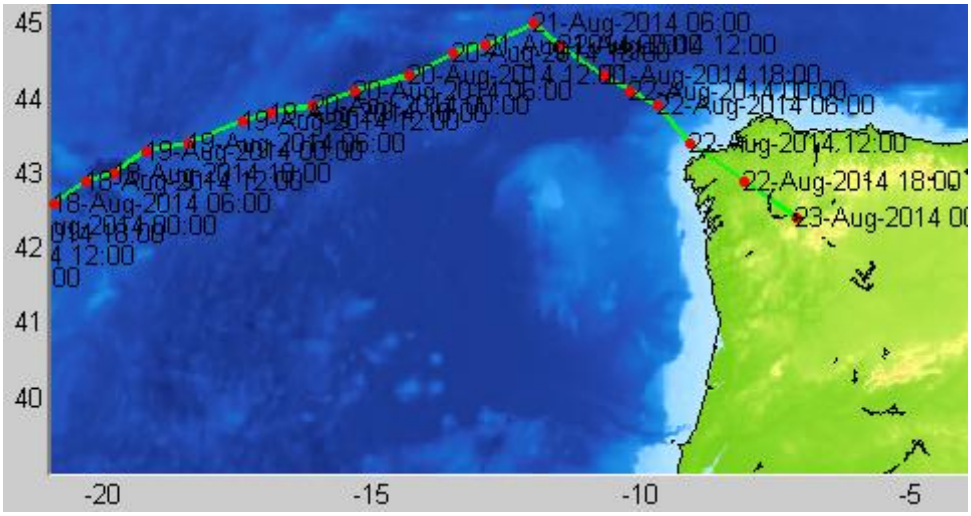

Figure 4-42 - Worst Case Scenario - Tropical Cyclone Trajectory for the NW Portuguese Coast.

The resulting ensemble members had 12 tropical cyclone trajectories that surpassed 2 meters in height, that is 5,74% of the total. These results are in no way similar to the results obtained for the other side of the Northern Atlantic Basin. There is a much bigger tendency for more disastrous provoking storms on the western side of the Atlantic Ocean during the summertime. Considering the historic initial conditions observed for these ensemble members, the most exacerbated situation was only able to produce a sea level height of 2,320 meters. As climate change continues to become a worrying factor, these rising storm tides are a great probability. The maximum mean sea level and the storm's corresponding spiderweb wind field are presented in Figure 4-43 and Figure 4-44 respectively.

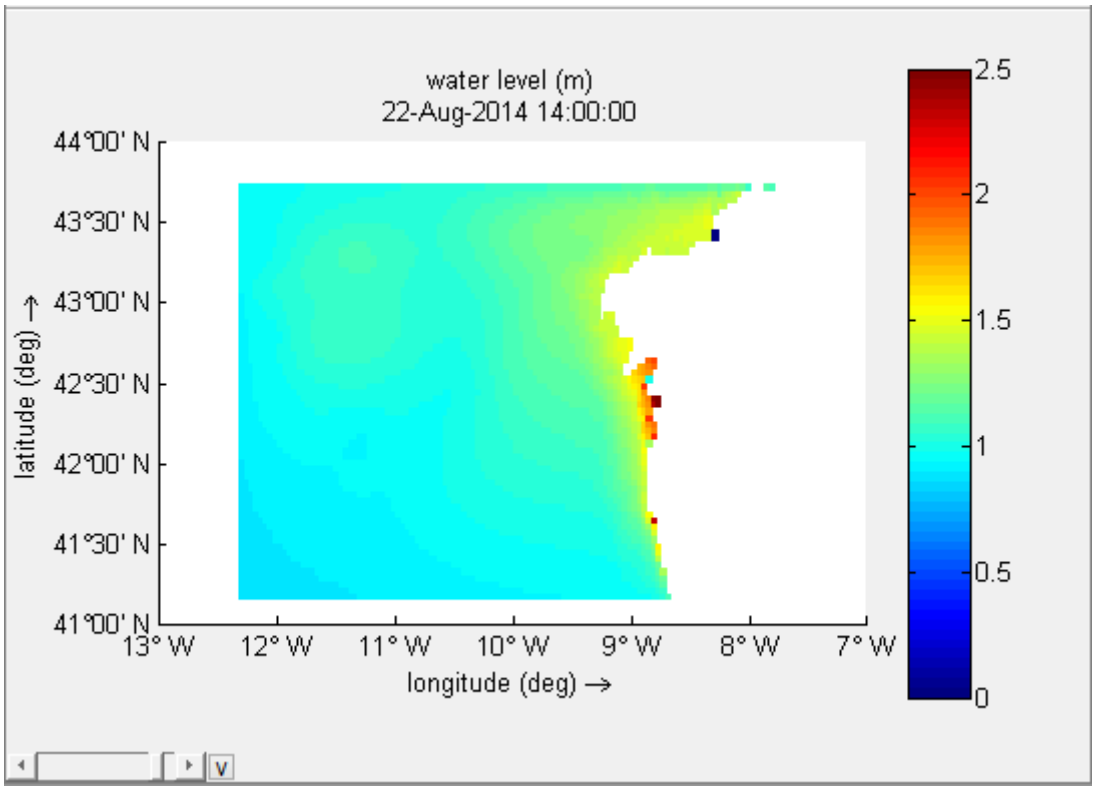

Figure 4-43 - Worst Case Scenario - Maximum Mean Water Level for the NW Portuguese Coast (m).

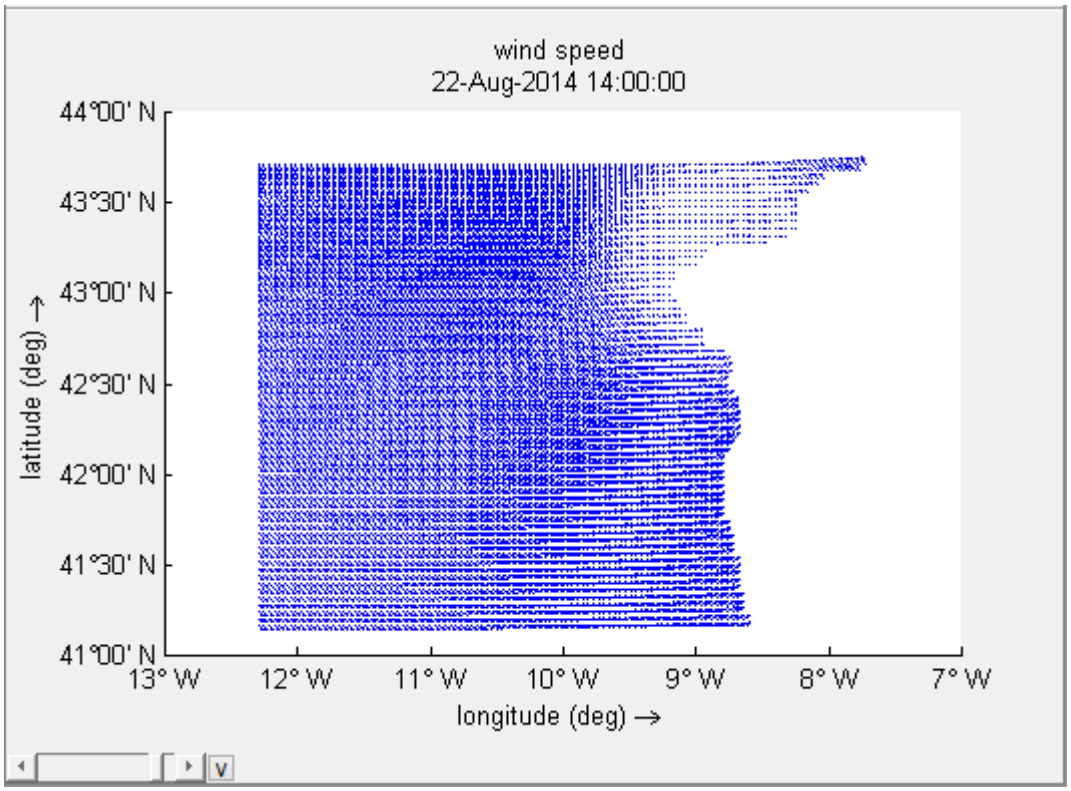

Figure 4-44 - Worst Case Scenario - Spiderweb Wind Field (NW Portuguese coast).

The application of ensemble forecasting for this case study area is of great use. Because of the tremendous lack of information available in this field of study, this type of study becomes very valuable in terms of characterization of the coast. The vulnerability of this part of the coast can be evaluated. The resulting MOMs (maximum sea level expected) for each type of storm can be indicators of the location's susceptibility. Like in the previous case study, because the number of ensemble members can be extensive, the MEOW values are given in Appendix V. The resulting Maximum of the MEOWs are given below in Table 4-13.

In this analysis, there were 3 hurricanes (all Category 1 hurricanes), 177 tropical storms, and 29 tropical depressions produced. Seen in Section 4.2.1, the most commonly observed occurrences in this region are of tropical depressions and tropical storms with very low sustained winds. A tropical storm is able to sustained winds from 62 to 118 km/h. Contrary to what is normally observed, there were a greater amount of observed tropical storms and even a few Category 1 hurricanes. With the intensification of typically observed results in this case study area, 37,29% of all the ensemble tropical storms experienced wind speed of 90 km/h or higher. The Maximum of the MEOW for the three simulated hurricanes resulted in 2,253 meters. For the Tropical Storm category, the maximum sea level for the MEOWs resulted in 2,321 meters and for the Tropical Depression category, the maximum sea level for the MEOWs produced a maximum of 1,208 meter. The tropical depressions, unlike in the NY/NJ area, did directly strike the coast.

Table 4-13 - Ensemble Maximum of the MEOWs (NW Portuguese coast).

Type	No. of Occurrences	MOM (m)
Hurricane	3	2,253
Tropical Storm	177	2,321
Tropical Depression	29	1,208

5. CONCLUSION

5.1. General Conclusions

Coastal storm impacts are among the most significant in terms of environment and economy. Although a coastal storm's wind speed is lesser when compared to tornadoes, their scale and duration are much larger, which are compounded by the generation of damaging waves that propagate far beyond the region of wind stress. The impacts of these storms are significant to both the coastal morphodynamics and the large population base that inhabit the coastal zone (Keim, Muller, & Stone, 2004). During the development of tropical systems in the North Atlantic Basin, the storms drift westward at tropical latitudes within the easterly trade winds, then often turn northward, tracking around the Atlantic Subtropical High to affect the eastern United States and occasionally even western Europe (Keim, Muller, & Stone, 2004).

In this dissertation, two high resolution models were created for simulation of hydrodynamics associated with coastal storms: one for the area surrounding The Battery, New York and the other for the northwestern Portuguese coast. In the case of The Battery, New York, it is a site that is well shielded by its surrounding topography, which can cause a reduction of the wind stress, which is why the resulting water levels obtained, especially when evaluating the general area of New York/ New Jersey with ensemble forecasting, are smaller when compared to the New Jersey coast that is in direct contact with the Atlantic Ocean. The northwestern Portuguese coast is a region that is not as affected in terms of evaluating cyclones occurring during "hurricane season", however, research suggests that the potential for the generation of more intense hurricanes is a growing reality.

The models created were based on available free software and data sets, and can be executed on a regular desktop. Models with much higher resolutions require much more powerful computers with excessive demonstration costs. The available historical data obtained shows that the occurrence of tropical storms are much more frequent than tropical depressions or tropical cyclones in both case study regions.

The simulations performed for The Battery, New York were successful in estimating water levels values, verified when compared to historically recorded water levels. Most of the simulations' outputs averaged between a 13 and 28 percent error. In a couple of the simulated tropical storms, the storm surges were produced with great accuracy. In one case, the storm surge produced resulted in a mere 1,79 percent error. With the aid of Delft Dashboard, the implementation of these models were attained with a reasonably high resolution grid. Usually, in coastal seas, estuaries, lakes, and other locations with steep topography or bathymetry, the sigma coordinate system can produce numerical errors. The sigma coordinate system, despite being boundary-fitted, does not necessarily have enough resolution around the pycnocline (Deltares, 2011). An approach to overcoming the issue is the application of the curvilinear coordinates in the vertical direction. Another shortcoming of this model creation is the possible discretization errors due to boundary conditions not being provided properly. The solution would be for the application of a nested smaller curvilinear grid within a larger, coarser grid. Nevertheless, the results obtained in this first case study were very close to reality. Why build a more complicated, nested model if the resulting values come so close?

Because the application of Delft Dashboard to the historical hurricane tracks for The Battery, New York was so successful, it is assumed that the application would have similar results in other locations. Therefore, an identical methodology was applied in the northwestern Portuguese coast. Several tropical storms were recreated, however, there was no historical data with which to compare it to. It is important that research in this area be explored because it is a rising issue. Even in terms of winter storms (a more common occurrence in this region), there is little existing data.

In a second phase of this dissertation, the forecasting of possible future tropical systems is executed. Ensemble forecasting was implemented by simply shifting trajectories of typically observed tropical cyclones, along with the randomizing of their initial conditions and subsequently the conditions of the trajectory points thereafter, to produce different realistic outcomes. Sometimes, the simple change in timing of a storm can imply very different flooding scenarios. For example, the forcing of Hurricane Sandy's storm to begin several hours earlier, so that it may coincide with high tide in Long Island Sound, would have worsened the flooding in the areas. Because such little information is provided in regions like the northwestern coast of Portugal, this kind of forecasting proves to be significant to this case study. The results are a valuable contribution to estimate storm tide heights, for each storm category, so as to support planning and management of this coastal zone and to assist in the

preparation of emergency plans. With the use of computer modeling of storm surges, studies on coastal adaptations to reduce future flooding should explore the impact of protective measures such as walls, wetlands, storm surge barriers, sand dunes, and changes in the depths of shipping channels.

In the ensemble forecasting section, for the case of The Battery, New York, 63,36% of the 232 total ensemble members produced were hurricanes, 23,71% were tropical storms, and 12,93% were tropical depressions. This intensification of the typically observed data resulted in a Maximum of the MEOW value of 13,483 meters for the hurricane category, 6,339 meters for the tropical storm category, and lastly 1,562 meter for the tropical depression category. In the northwestern Portuguese coast, 1,44% of the total 209 ensemble members produced were hurricanes, 84,69% were tropical storms, and 13,88% were tropical depressions. These values resulted in a Maximum of MEOW of 2,253 meters for the hurricane category, 2,321meters for the tropical storm category, and 1,208 meter for the tropical depression category. Forcing of the tropical cyclones to pass directly through the desired area made it possible to study how the water levels correspond to an exacerbation of the typically observed data.

The results obtained in this dissertation serve as significant implications for the short-term evolution of coasts particularly if an increase in frequency or intensity of hurricanes occurs. While barriers and beach ridge coasts demonstrate stability and protection over past decades, significant erosion trends can be observed with an increased onset of tropical systems. Similarly, over longer timescales, the incidence and intensity of storms plays an important role in the evolution of coastal morphodynamics.

5.2. Future Challenges

For future modeling efforts, there is need for high quality measurements of water level spread across the Portuguese coast. These measurements should be repeated for a few years in order to take into account annual variations and so models can be validated. Model validation is impossible without such high quality, consistent data. A more complete study of the future scenarios can be made with the same ensemble forecasting method for winter storms. This information can be greatly valuable for means of protecting our shorelines, cities, and even the inhabitants that are ever more susceptible to storm surge risks. A vertical resolution for future models should be explored, in order to better understand the impacts of these storm

surges. More in depth research in how the storm surges can increase rate of exchange with the ocean and consequently the flushing rate and salinity of rivers, lagoons, etc. can be affected should also be studied. Further research to characterize the intensity of coastal storms based on readily available parameters such as wind and pressure so that a physical or climatic rather than a socioeconomic evaluation of severity should be encouraged. Over half of all Americans live in coastal states (NOAA - Coastal Decison-making Tools, 2014). This is a phenomena also existing in the Portuguese community. Each year people are flocking to the coasts. With the growing of coastal populations comes more development, such as new homes, roads, and so on. They do enrich the economy, but also place pressure on the environment, which can potentially diminish the aesthetic and economic value of living in a coastal area.

There are also growing tools to help in terms of costal management and planning. NOAA's Digital Coast Impact Viewer allows for the visualization of potential impacts due to sea level rise. This viewer can display potential future sea levels, provide simulations of sea level rise at local landmarks, communicates spatial uncertainty of mapped sea levels, models potential marsh migration due to sea level rise, overlays social and economic data onto potential sea level rise, examines how tidal flooding will becomes more frequent with sea level rise (NOAA - Digital Coast, 2014). Tools such as the one described can help in balancing the health of the coasts and ensued by a balance in the health in the economy (NOAA - Coastal Decison-making Tools, 2014).

As the effort for better coastal preparation with the application of coastal decision-making tools become more and more widespread, an interesting question persists: Could preventing a hurricane be possible? This is an ambitious task already explored in the past. From 1962 to 1983, the United States Government attempted to weaken tropical cyclones by flying aircrafts into the cyclones, and "seeding" them with silver iodine. This was known as Project Stormfury. The silver iodine would cause the supercooled water from the storm to freeze, disturbing the structure of the hurricane. This hypothesis, however, was discredited after the discovery that tropical cyclones' have very little supercooled water and instead, a great amount of ice crystals (Levitt, 2012). In the National Geographic documentary, *Preventing Armageddon*, a innovative solution to the attempt of preventing these tropical systems was put to the test by Professor Alan Blumberg of Stevens Institute of Technology. Blumberg proposed a hurricane prevention method with the application of pumps, vertically inserted at sea. The idea of the pump is similar to that of a straw. When one holds the top of the straw, the liquid from the bottom can be transported upwards. The pump, one meter in width and

300 meters deep with a float on top to keep from sinking, would have the same effect as the straw. These pumps would have to be dropped 48 hours in advance and the action of bringing the cooler water from the bottom of the sea towards the top can potentially make a difference. The premise of the hypothesis is that the hurricane can be weakened by lessening the heat uptake into the storm or modifying the precipitation processes that occur within the hurricane. The simple cooling of the water of a mere two degrees can reduce the intensity by 50%. This would mean transforming a Category 5 Hurricane to a Category 3 Hurricane, or a Category 3 Hurricane to a Category 1 Hurricane. Unfortunately, there is a downside. For the two degree decrease in temperature, it is estimated that 200 pumps are required. Also, to treat just one hurricane, an investment of 100 million dollars is necessary. There is the added unknown of how this can affect a tropical system at this large scale. There is the possibility that because the cold water is heavier than warm water that it would sink too quickly for it to effect the hurricane. Also, who is to say that with the switch of the cool path onto a warm path the tropical system would just dislocate, and simply threaten a different region (Levitt, 2012)?

A second proposed idea of Blumberg's is even more ambitious. The idea is to develop three sets of islands at the mouth of New York Bay to bear the impact of any oncoming storm surge, creating a calmer beach region, offering new ecosystems and lessening the need for coastal protection projects. Because most of the tropical systems experienced in that region landfall parallel to the coastline, there is no need to implement the islands right at the mouth of the bay. The ideal position would be a concave position along the shorelines. The islands are proposed to be constructed by navel engineers using sand from 5000 year old glacial deposits further offshore. Again, the downside is the enormous investment required. The islands cost between 5,6 and 12,2 billion dollars to build. According to Blumberg, they could save the region up to 12 billion dollars in damage on one storm alone. Besides the price, there is the possibility for unforeseeable effects in the nutrients of the region's water which could affect commercial and recreational fishing as well as enclose other ecological concerns (DeChiaro, 2014).

However incredulous and ambitious the previous ideas were, one can conclude that this is an important topic that is worth investing in. Climate change is a growing issue and one must prepare and not abandon the city waterfronts. The objective should be to build and invest in creating stronger more resilient cities. This is a worldwide issue. This depends on the safety of millions of people all over the world that inhabit coastal cities (Gregory, 2014).

REFERENCES

American Association of Port Authorities. (2014). *Port Industry Statistics - Port Industry Information - AAPA*. Retrieved September 26, 2014, from Aapa-ports.org: http://www.aapa-ports.org/Industry/content.cfm?ItemNumber=900

ArcGIS 9.3 . (2014). *Coordinate systems, map projections, and geographic (datum) transformations*. Retrieved from Resources.esri.com: http://resources.esri.com/help/9.3/arcgisengine/dotnet/89b720a5-7339-44b0-8b58-0f5bf2843393.htm

Asoftech. (2014). *Mouse Keyboard Macro Recorder - Automation Software*. Retrieved July 29, 2014, from Asoftech.com: http://www.asoftech.com/ata/

Bloomberg, T. C. (2013). *A Stronger, More Resilient New York.* Long-term Sustainability Plan, plaNYC, New York.

Briney, A. (2014). *How Does the Coriolis Effect Impact Earth?* Retrieved from About.com: http://geography.about.com/od/physicalgeography/a/coriolis.htm

Celik, I. B. (1999, December). *West Virginia University - Introductory Trubulence Modeling.* Retrieved January 15, 2015, from Fem.unicamp.br: http://www.fem.unicamp.br/~im450/palestras%26artigos/ASME_Tubulence/cds13workbook.pdf

Centre for Climate Adaptation. (2014). *Climate change - Portugal - Climate Adaptation*. Retrieved September 9, 2014, from Climateadaptation.eu: http://www.climateadaptation.eu/portugal/climate-change/

COMET. (2003, July 31). *Meterology Education and Training » Resource Description: Wave Types and Characteristics*. Retrieved January 29, 2014, from Meted.ucar.edu: https://www.meted.ucar.edu/training_module.php?id=126#.VBBIlfldV9o

COMET. (2005, July 14). *Meterology Education and Training » Resource Description: Wave Life Cycle I: Generation*. Retrieved January 30, 2014, from Meted.ucar.edu: https://www.meted.ucar.edu/training_module.php?id=172#.VBBIk_ldV9o

COMET. (2006, January 12). *Meterology Education and Training » Resource Description: Wave Life Cycle II: Propagation and Dispersion*. Retrieved February 13, 2014, from

Meted.ucar.edu: https://www.meted.ucar.edu/training_module.php?id=188#.VBBNI_ldV9p

COMET. (2010, November 15). *Meterology Education and Training » Resource Description: Tsunamis*. Retrieved February 4, 2014, from Meted.ucar.edu: https://www.meted.ucar.edu/training_module.php?id=831#.VBBIkfldV9o

COMET. (2013, January 9). *Meterology Education and Training » Resource Description: Tropical Severe Local Storms*. Retrieved February 7, 2014, from Meted.ucar.edu: https://www.meted.ucar.edu/training_module.php?id=995&tab=04#.VBBIsfldV9o

DeChiaro, D. (2014, March 9). *New way to fight hurricanes Stevens prof wants funding to build islands off NJ NY - A scientist at the Stevens Institute of Technology in Hoboken has applied for federal funding to build a series of islands off the coast of New York and New Jersey*. Retrieved July 17, 2014, from Hudsonreporter.com: http://www.hudsonreporter.com/view/full_story/24711067/article-New-way-to-fight-hurricanes--Stevens-prof-wants-funding-to-build-islands-off-NJ--NY--?instance=latest_story

Deltares. (2011). *User Manual Delft3D-FLOW. Simulation of multi-dimensional hydrodynamic flows and transport phenomena, including sediments* (Version 4.00 ed.). The Netherlands.

Deltares. (2011). *User Manual Delft3D-RGFGRID. Generation and manipulation of curvilinear grids for Delft3D-FLOW and Delft3D-WAVE* (Version 4.00 ed.). The Netherlands.

Deltares. (2013). *User Manual Delft3D-QUICKPLOT. Visualisation and animation program for analysis of simulation results* (Version 2.15.29963 ed.). The Netherlands.

Deltares. (2014). *Manual - Delft Dashboard - Deltares Public Wiki*. Retrieved February 5, 2014, from Publicwiki.deltares.nl: http://publicwiki.deltares.nl/display/ddb/Manual

Dinis, J. L., & Tavares, A. O. (2005). Susceptibility geomorphology of tsunamis in the Portuguese west coast. *Proceeding if the III Congress on planning and management of coastal areasof the Portuguese-speaking countries*, (pp. 1-17).

Ensemble Forecasting. (2014). Retrieved February 25, 2014, from Met Office: http://www.metoffice.gov.uk/research/areas/data-assimilation-and-ensembles/ensemble-forecasting

Federal Emergency Management Agency Review. (2014). New York City Hazard Mitigation Plan. In *6. Coastal Storms, Chapter 3: Risk Assessment.*

GEBCO gridded bathymetry data. (2014). Retrieved from GEBCO: http://www.gebco.net/data_and_products/gridded_bathymetry_data/

General Bathymetric Chart of the Oceans at BODC. (2014). Retrieved Abril 7, 2014, from British Oceanographic Data Centre: http://www.bodc.ac.uk/projects/international/gebco/

Gerya, T. (2010, May 8). *Why should we use staggered grid?* Retrieved from Introduction to numerical methods for geologists, mathematicians and physicists: http://numericalmethods.wordpress.com/2010/05/08/why-should-we-use-staggered-grid/

Google Maps. (2014). *Google Maps*. Retrieved from Maps.google.pt: http://maps.google.pt

Gordon, A. (2004). *The Climate System - Ocean Circulation Lecture.* Retrieved December 16, 2014, from Eesc.columbia.edu: http://eesc.columbia.edu/courses/ees/climate/lectures/o_circ.html

Gregory, J. (2014). *Climate Change 2013: The Physical Science Basis | Projections of sea level rise*. Retrieved March 5, 2014, from Ipcc.ch: http://www.ipcc.ch/pdf/unfccc/cop19/3_gregory13sbsta.pdf

Hart, R. E., & Evans, J. L. (2000, Abril 1). A Climatology of the Extratropical Transition of Atlantic Tropical Cyclones. *Journal of Climate, Volume 14*, 546-564.

Hasselmann, K., Barnett, T., Bouws, E., Carlson, H., Cartwright, D., Enke, K., . . . Walden, H. (1973). Measurements of wind-wave growth and swell decay during the Joint North Sea Wave Project (JONSWAP). *Deutches Hydrographisches Institut*.

Hickey, K. (2011). The Impact of Hurricanes on the Weather in Western Europe. In A. Lupo (Ed.), *Recent Hurricane Research - Climate, Dynamic, and Societal Impacts* (pp. 77-84). Intech.

Historical Hurricane Tracks. (2014). Retrieved from Csc.noaa.gov: http://csc.noaa.gov/hurricanes/#

Holweg, E. J. (2000). *Mariner's Guide For Hurricane Awareness in the North Atlantic Basin.*

Keim, B. D., Muller, R. A., & Stone, G. W. (2004). Spatial and temporal variability of coastal storms in the North Atlantic Basin. *Marine Geology*, 7-15.

Landsea, C. (2014). *TCFAQ G5) What determines the movement of tropical cyclones?* Retrieved 11 25, 2014, from Aoml.noaa.gov: http://www.aoml.noaa.gov/hrd/tcfaq/G5.html

Landsea, C., & Goldenberg, S. (2004, August 13). *Tropical Cyclone FAQ*. Retrieved February 27, 2014, from Aoml.noaa.gov: http://www.aoml.noaa.gov/hrd/weather_sub/faq.html

Levitt, D. (Producer), & Bouchardeau, C. (Director). (2012). *Naked Science: Preventing Armageddon* [Motion Picture].

Manor Houses of Portugal. (2014). *Sailing the Portuguese coast - General information - Portugal*. Retrieved September 29, 2014, from Manorhouses.com: http://www.manorhouses.com/ports/geninfo.htm

Miranda, P. M., Coelho, F. E., Tomé, A. R., Valente, M. A., Carvalho, A., Pires, C., . . . Ramalho, C. (2002). Chapter 2 - 20th Century Portuguese Climate and Climate Scenarios. In F. D. Santos, K. Forbes, & R. Moita (Eds.), *Climate Change in Portugal: Scenarios Impacts and Adaptation Measures (SLAM Project)* (pp. 23-83). Gradiva.

National Climatic Data Center. (2014). *Global Ensemble Forecast System (GEFS) | NCDC*. Retrieved February 26, 2014, from Ncdc.noaa.gov: http://www.ncdc.noaa.gov/data-access/model-data/model-datasets/global-ensemble-forecast-system-gefs

National Geographic. (2014). *Storm Surge - Encyclopedia Entry*. Retrieved December 19, 2014, from Education.nationalgeographic.com: http://education.nationalgeographic.com/education/encyclopedia/storm-surge/?ar_a=1

National Ocean Service. (2014, December 8). *How fast is the Gulf Stream?* Retrieved December 15, 2014, from Oceanservice.noaa.gov: http://oceanservice.noaa.gov/facts/gulfstreamspeed.html

National Weather Service. (2011, October 21). *NWS JetStream - The Jet Stream*. Retrieved November 25, 2014, from Srh.noaa.gov: http://www.srh.noaa.gov/jetstream/global/jet.htm

NCDC, N., & US Department of Commerce, N. (2014). *NOMADS | Ensemble Probability Tool | National Climatic Data Center (NCDC)*. Retrieved February 26, 2014, from Nomads.ncdc.noaa.gov: http://nomads.ncdc.noaa.gov/EnsProb/

Nelson, S. A. (2012, July 2). *Tulane University EENS 3050 - Tsunami Lecture*. Retrieved December 16, 2014, from Tulane.edu: http://www.tulane.edu/~sanelson/Natural_Disasters/tsunami.htm

NOAA - Coastal Decison-making Tools. (2014). *Coastal Decision-making Tools*. Retrieved July 5, 2014, from Oceanservice.noaa.gov: http://oceanservice.noaa.gov/tools/dmtools/

NOAA - Digital Coast. (2014). *Sea Level Rise and Coastal Flooding Impacts Viewer*. Retrieved July 15, 2014, from Csc.noaa.gov: http://csc.noaa.gov/digitalcoast/tools/slrviewer

NOAA - Hurricane Research Division. (2014, June 1). *TCFAQ A BASIC DEFINITIONS - Atlantic Oceanographic & Meterological Laboratory*. Retrieved from Aoml.noaa.gov: http://www.aoml.noaa.gov/hrd/tcfaq/tcfaqA.html

NOAA - National Hurricane Center. (2013, May 24). *Saffir-Simpson Hurricane Wind Scale*. Retrieved from Nhc.noaa.gov: http://www.nhc.noaa.gov/aboutsshws.php

NOAA - National Hurricane Division. (2014, September 5). *Storm Surge Overview*. Retrieved February 13, 2014, from NHc.noaa.gov: http://www.nhc.noaa.gov/surge/

NOAA - Tides and Currents. (2014). *Station Home Page - The Battery, NY*. Retrieved Abril 25, 2014, from Tidesandcurrents.noaa.gov: http://tidesandcurrents.noaa.gov/stationhome.html?id=8518750

NOAA Datums Page. (2014). *Published Bench Mark Sheet for 8518750 THE BATTERY, NEW YORK HARBOR NEW YORK*. Retrieved Abril 25, 2014, from Co-ops.nos.noaa.gov: http://co-ops.nos.noaa.gov/benchmarks/8518750.html

NOAA NWS NCEPS - Ensemble Training Page. (2014). Retrieved February 26, 2014, from Hpc.ncep.noaa.gov: http://www.hpc.ncep.noaa.gov/ensembletraining/

NOAA Office of Coast Survey. (2014). *How Hydrodynamic Models Are Used*. Retrieved February 26, 2014, from NOAA's Office of Coast Survey: http://www.nauticalcharts.noaa.gov/csdl/learn_models.html

NWS JetStream - Types of Thunderstorms. (2014). Retrieved from Srh.noaa.gov: http://www.srh.noaa.gov/jetstream/tstorms/tstrmtypes.htm

NWS National Hurricane Center. (2012, May 30). *Hurricanes in History*. Retrieved November 25, 2014, from Nhc.noaa.gov: http://www.nhc.noaa.gov/outreach/history/

Ormondt, M. v. (2012, May 9). How to set up a Delft3D model with Delft Dashboard? | Webinar. Netherlands: Deltares.

Petrovic, Z. (2005, October 5). Simulation of Fluid Flows . University of Belgrade - Factulty of Mechanical Engineering.

Pinho, J. L. (2000). *Application of mathematical modeling to the study of hydrodynamics and water quality in coastal areas.* Ph.D, Minho University, Guimarães.

Rappaport, E. N., & Fernandez-Partagas, J. (1995). *The Deadlist Atlantic Tropical Cyclones, 1492-1996.* National Weather Service NHC.

Sayma, A. (2009). *Computational Fluid Dynamics.* Abdulnasser Sayma & Ventus Publishing ApS.

Stewart, R. (2006, November 15). *Introduction to Physical Oceanography : Chapter 16 - Ocean Waves - Ocean-Wave Spectra*. Retrieved November 25, 2014, from Oceanworld.tamu.edu: http://oceanworld.tamu.edu/resources/ocng_textbook/chapter16/chapter16_04.htm

TransWorld SURF. (2014). *Winter Storm Hercules Slams Europe With XXL Surf - Transworld Surf*. Retrieved September 15, 2014, from Surf.transworld.net: http://surf.transworld.net/1000166456/photos/winter-storm-hercules-slams-europe-xxl-surf/

Tropical Cyclone Climatology. (2014). Retrieved August 20, 2014, from Nhc.noaa.gov: http://www.nhc.noaa.gov/climo/

Tropical Cyclone Model & Best Track Archive: Storm Archive. (2014). Retrieved from Tropicalatlantic.com: http://www.tropicalatlantic.com/modelsOLD/data.cgi?archive=1

UHSLC. (2014). Retrieved from Uhslc.soest.hawaii.edu: http://uhslc.soest.hawaii.edu/data/faq

University of Tennessee. (2014). *Conservation of Angular Momentum*. Retrieved from Csep10.phys.utk.edu: http://csep10.phys.utk.edu/astr161/lect/solarsys/angmom.html

Walsh, K. J. (2011, October 25). *The Port of New York and New Jersey, a Critical Hub of Global Commerce*. Retrieved September 26, 2014, from Forbes: http://www.forbes.com/sites/gcaptain/2011/10/25/the-port-of-new-york-and-new-jersey-a-critical-hub-of-global-commerce/

Weather FAQs. (2008). *CAPE, Shear, and the Thunderstorms | Weather FAQs*. Retrieved February 24, 2014, from Weatherfaqs.org.uk: http://www.weatherfaqs.org.uk/node/172

Weather Online. (2014). *Weather Facts: North Atlantic Drift (Gulf Stream)*. Retrieved December 15, 2014, from Weatheronline.co.uk: http://www.weatheronline.co.uk/reports/wxfacts/North-Atlantic-Drift-Gulf-Stream.htm

Weather Underground. (2014). *Definition of Tropical, Subtropical, and Extratropical Storms | Weather Underground*. Retrieved March 2014, from Wunderground.com: http://www.wunderground.com/hurricane/subtropical.asp

Weisstein, E. W. (2014). *Navier-Stokes Equations - from Eric Weisstein's World of Physics*. Retrieved Abril 4, 2014, from Scienceworld.wolfram.com: http://www.gps.caltech.edu/~cdp/Desktop/Navier-Stokes%20Eqn.pdf

Wesseling, P. (2009). *Principles of computational fluid dynamics.* Berlin: Spinger-Verlag.

Willoughby, H. (2012). Distributions and Trends od Death and Destruction from Hurricanes in the United States, 1900-2008. *American Society of Civil Engineers*.

Windfinder. (2014). *Windfinder.com - Wind and weather statistic Porto*. Retrieved September 29, 2014, from Windfinder.com: http://www.windfinder.com/windstatistics/porto

Zhang, Z., & Krishnamurti, T. (1997). Ensemble forecasting of hurricane tracks. *Bulletin of the American Meterological Society, Volume 78*(Issue no. 12), 2785-2795.

APPENDIX I - SCENARIOS FOR THE BATTERY, NEW YORK

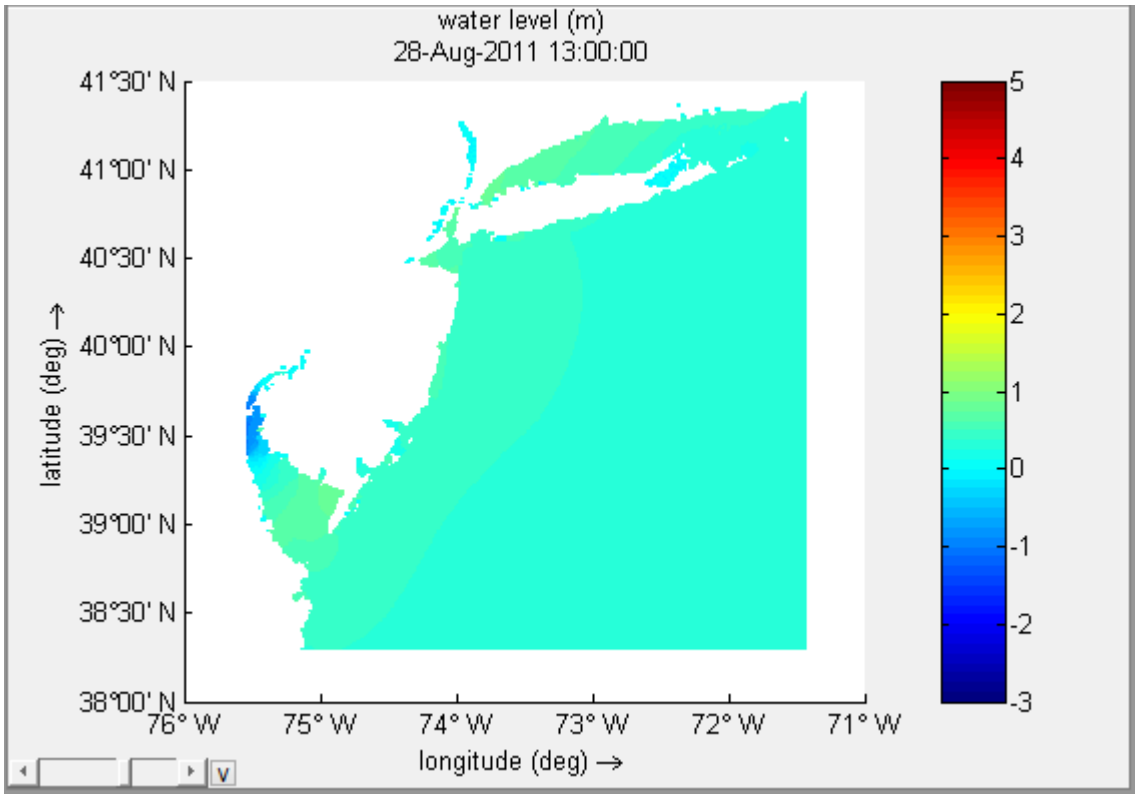

Figure I-1 - Tropical Storm Irene's water levels without spiderweb wind field (m)

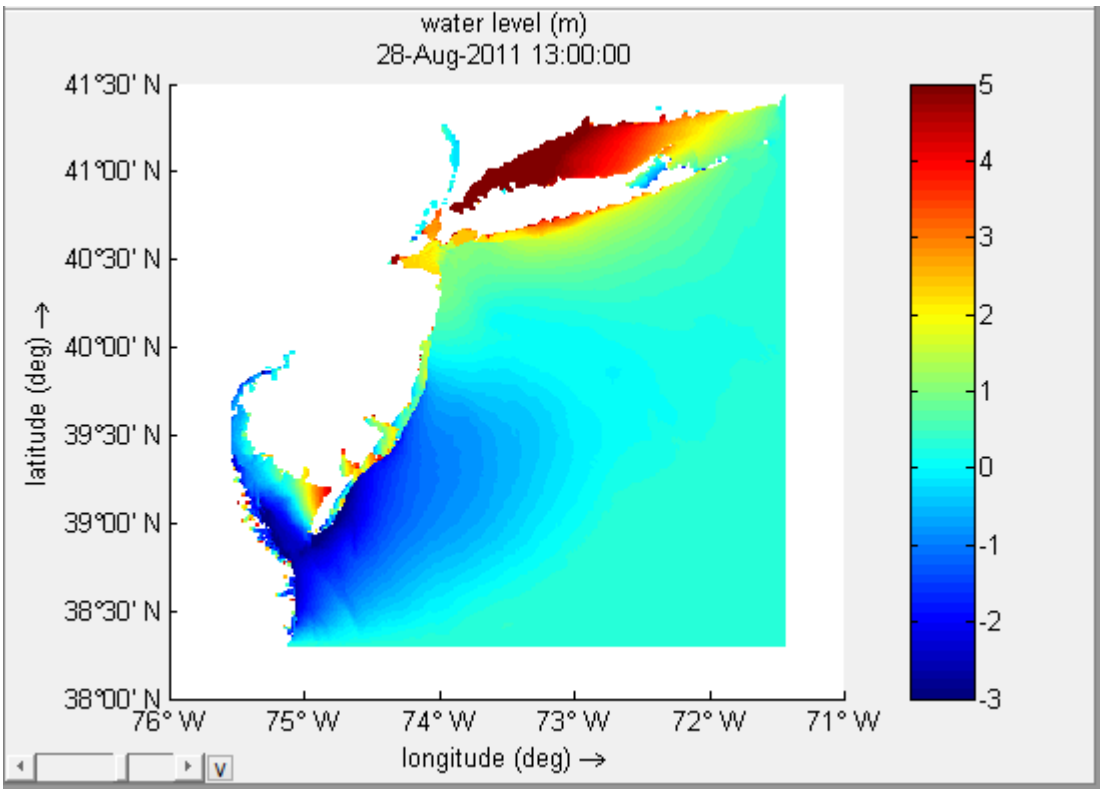

Figure I-2 - Tropical Storm Irene's water levels with spiderweb wind field (m)

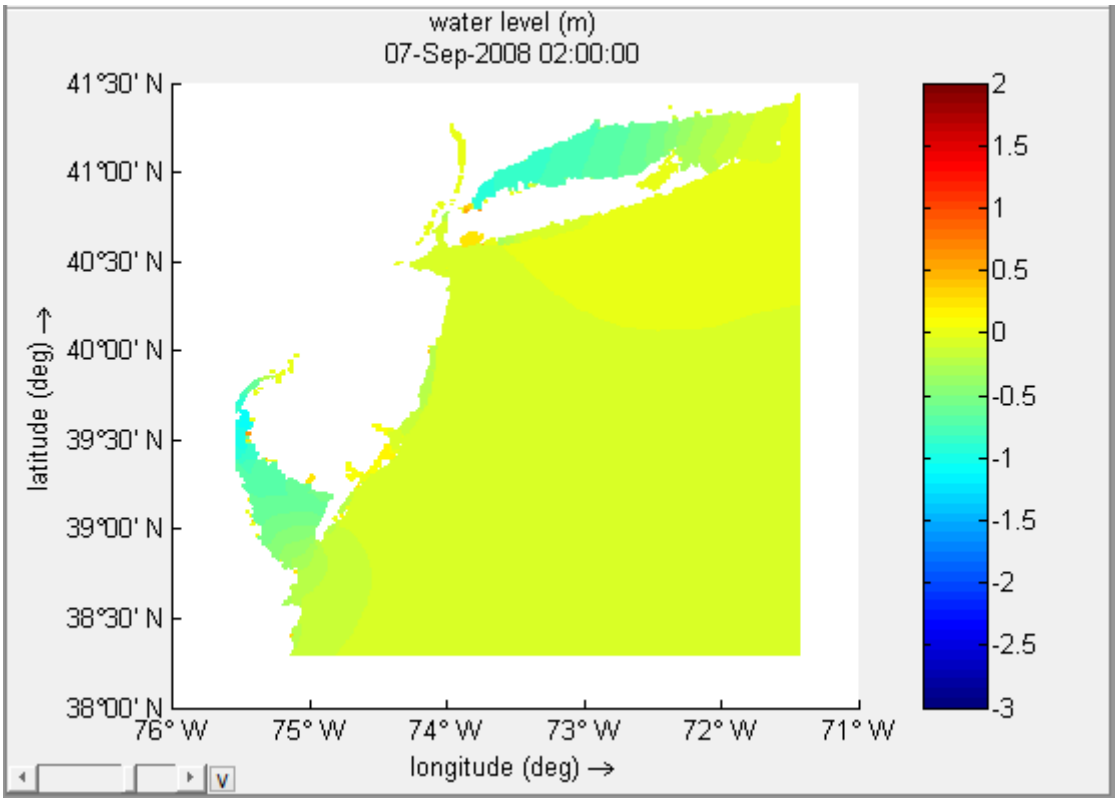

Figure I-3 - Tropical Storm Hanna's water levels without spiderweb wind field (m)

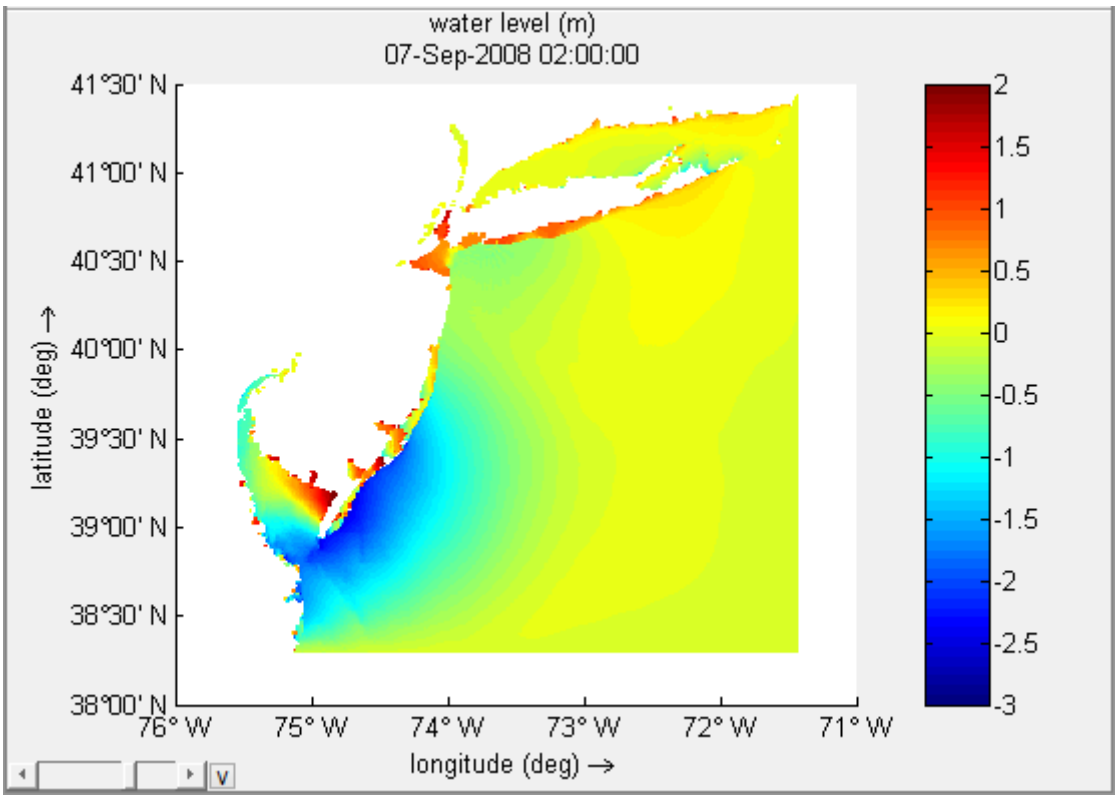

Figure I-4 Tropical Storm Hanna's water levels with spiderweb wind field (m)

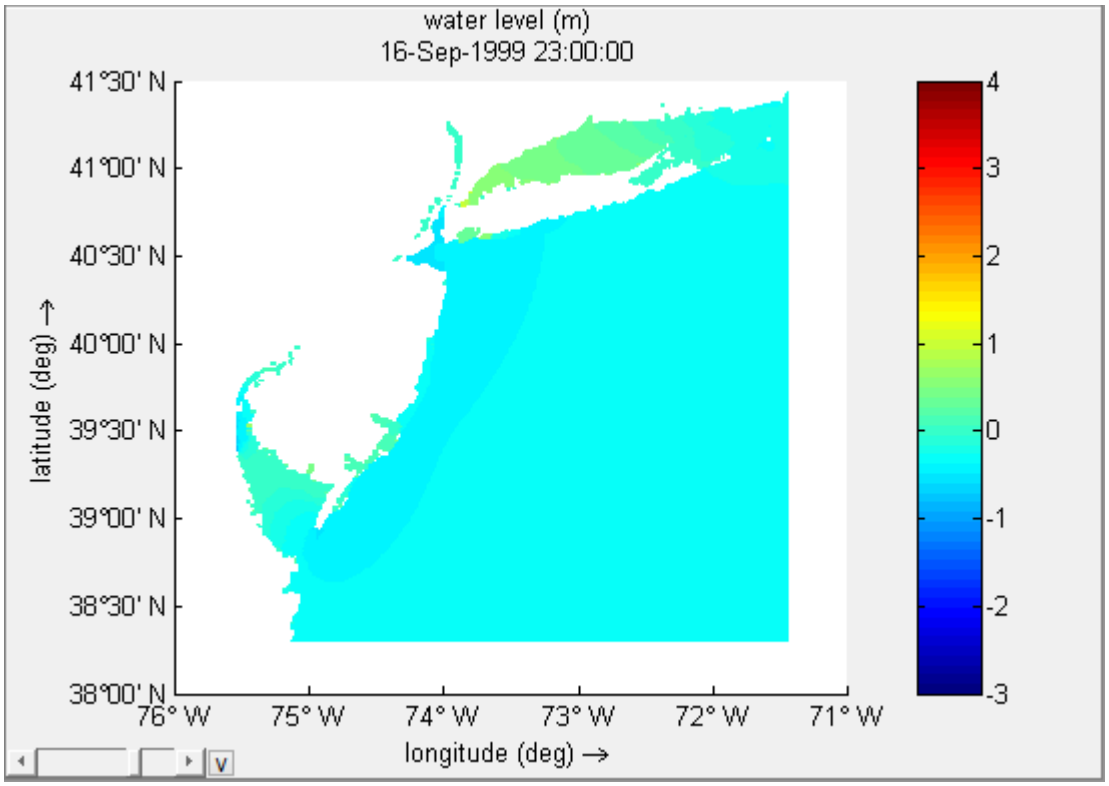

Figure I-5 - Tropical Storm Floyd's water levels without spiderweb wind field (m)

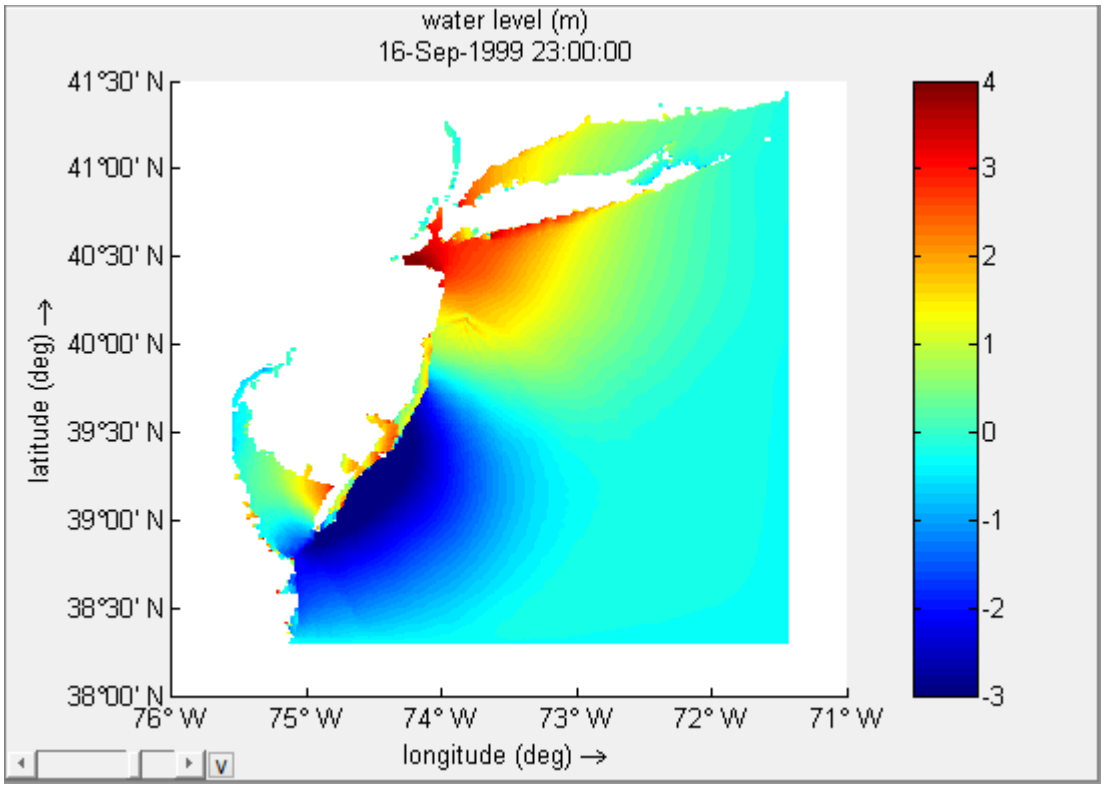

Figure I-6 - Tropical Storm Floyd's water levels with spiderweb wind field (m)

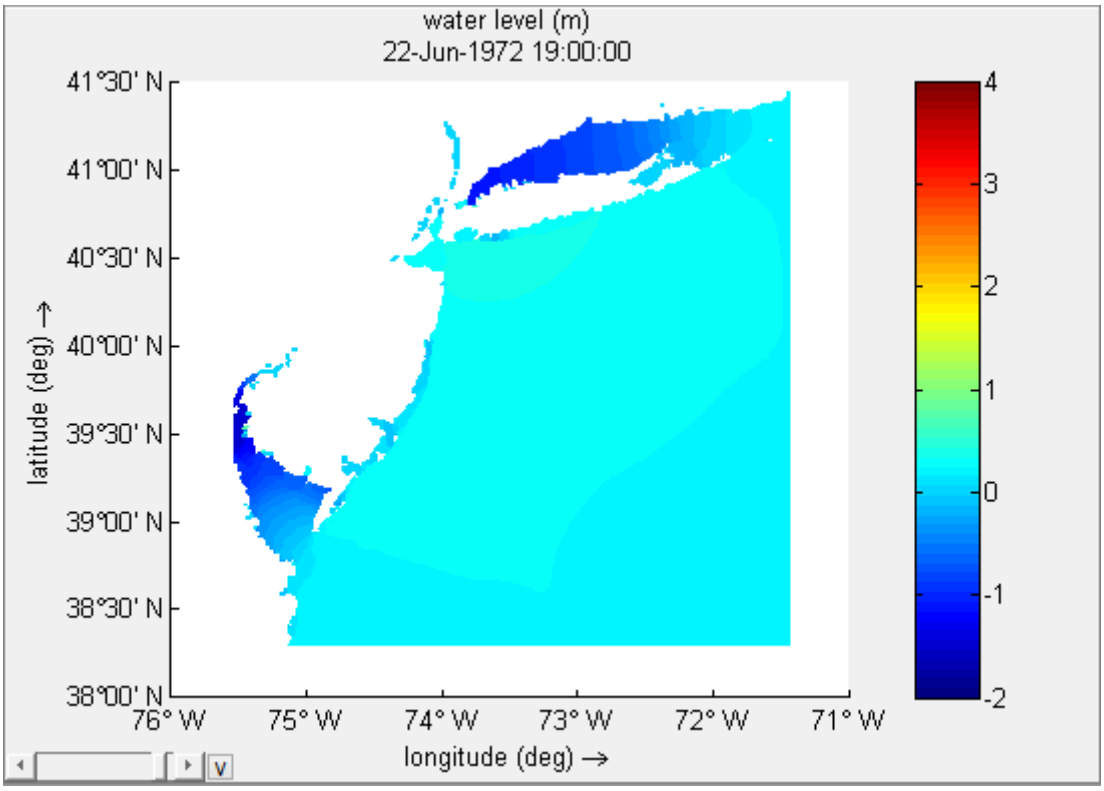

Figure I-7 - Tropical Storm Agnes' water levels without spiderweb wind field (m)

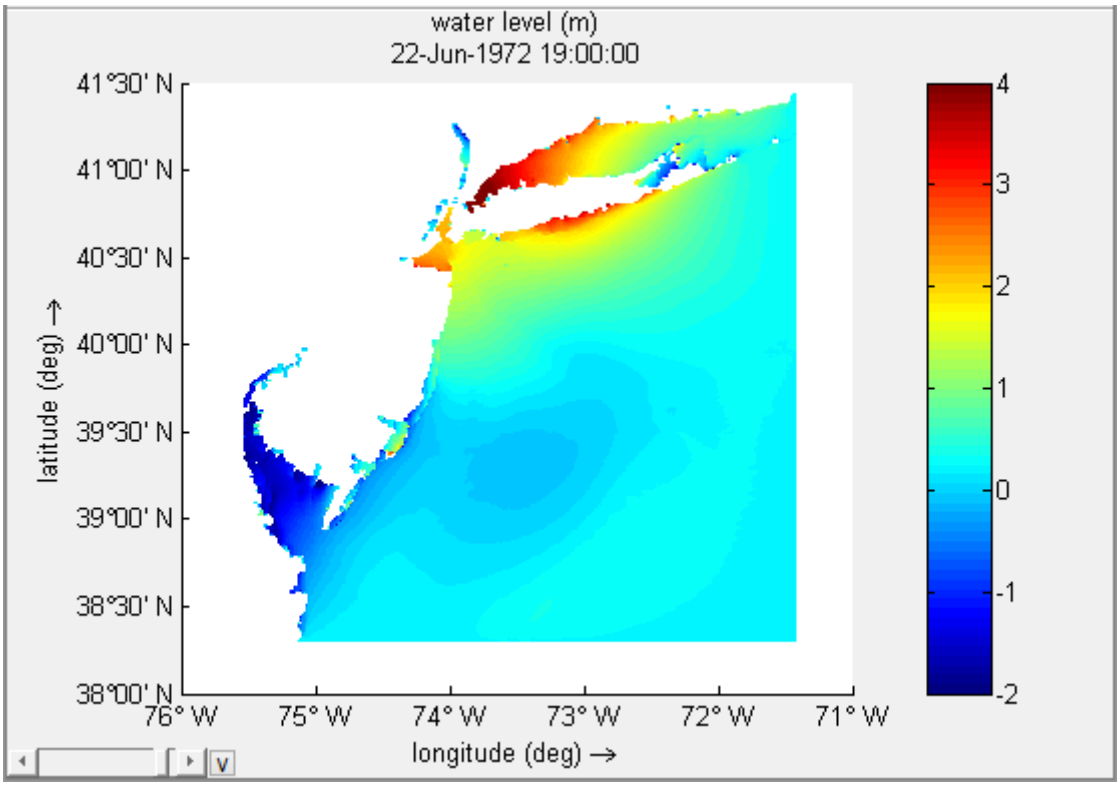

Figure I-8 -Tropical Storm Agnes' water levels with spiderweb wind field (m)

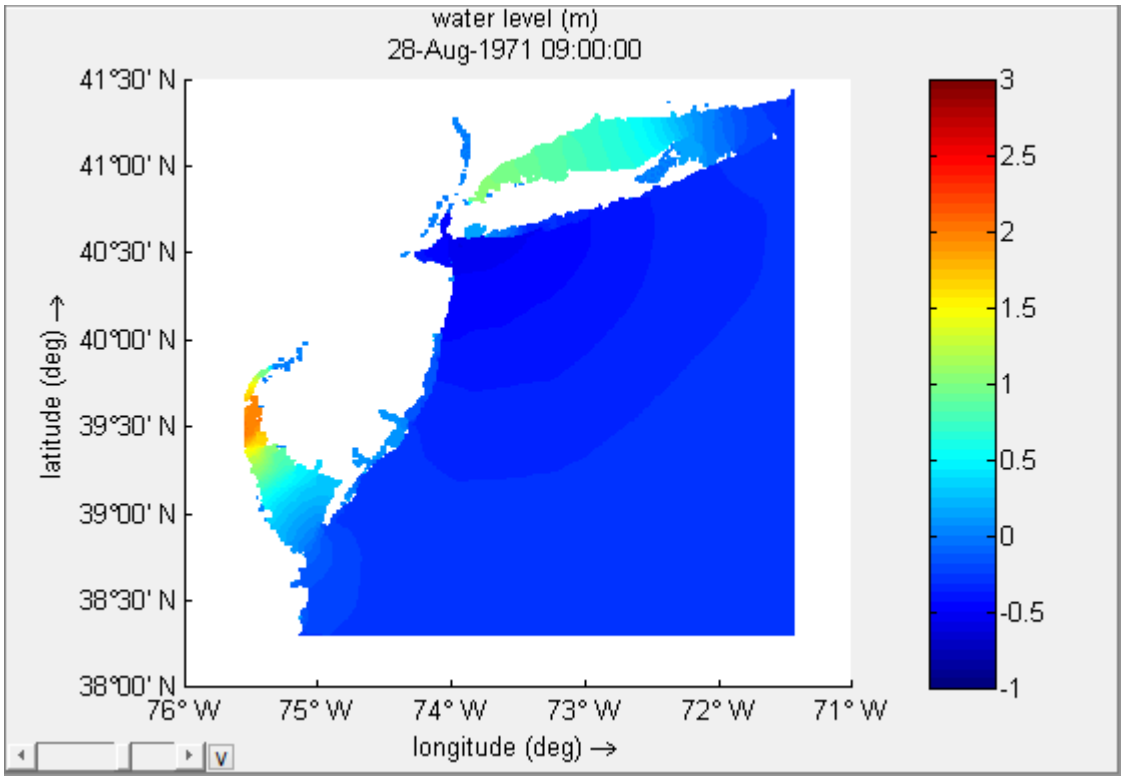

Figure I-9 - Tropical Storm Doria's water levels without spiderweb wind field (m)

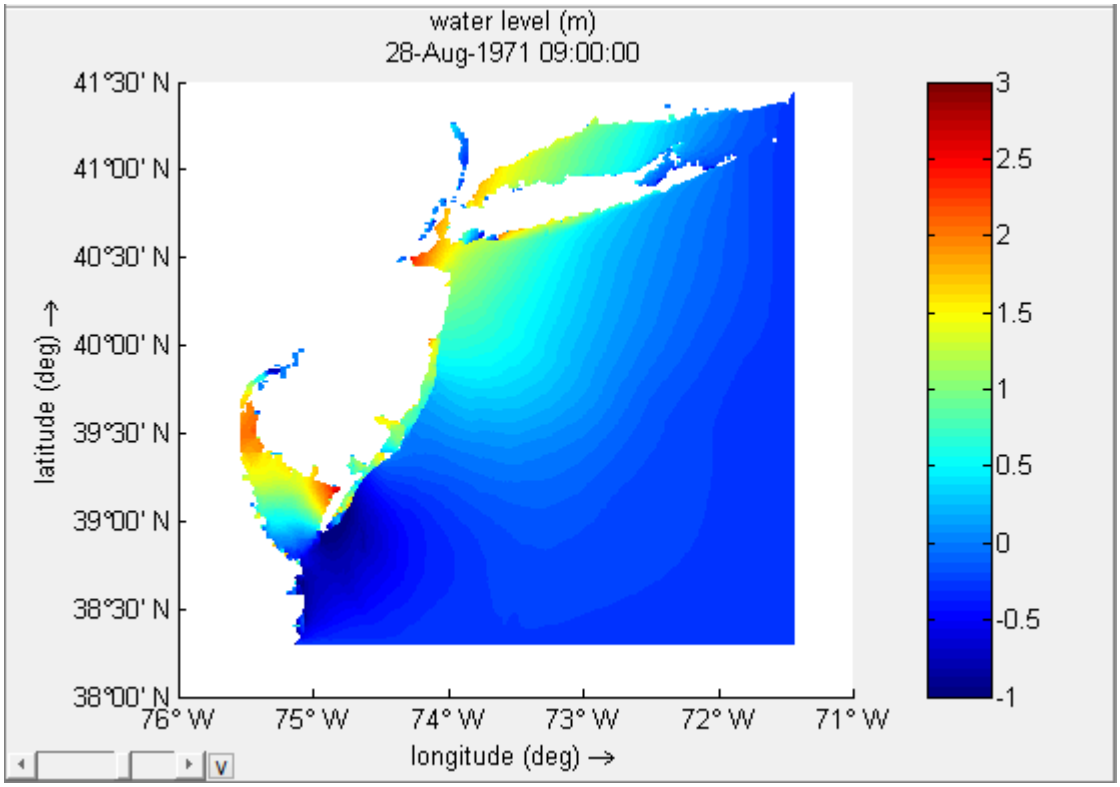

Figure I-10 - Tropical Storm Doria's water levels with spiderweb wind field (m)

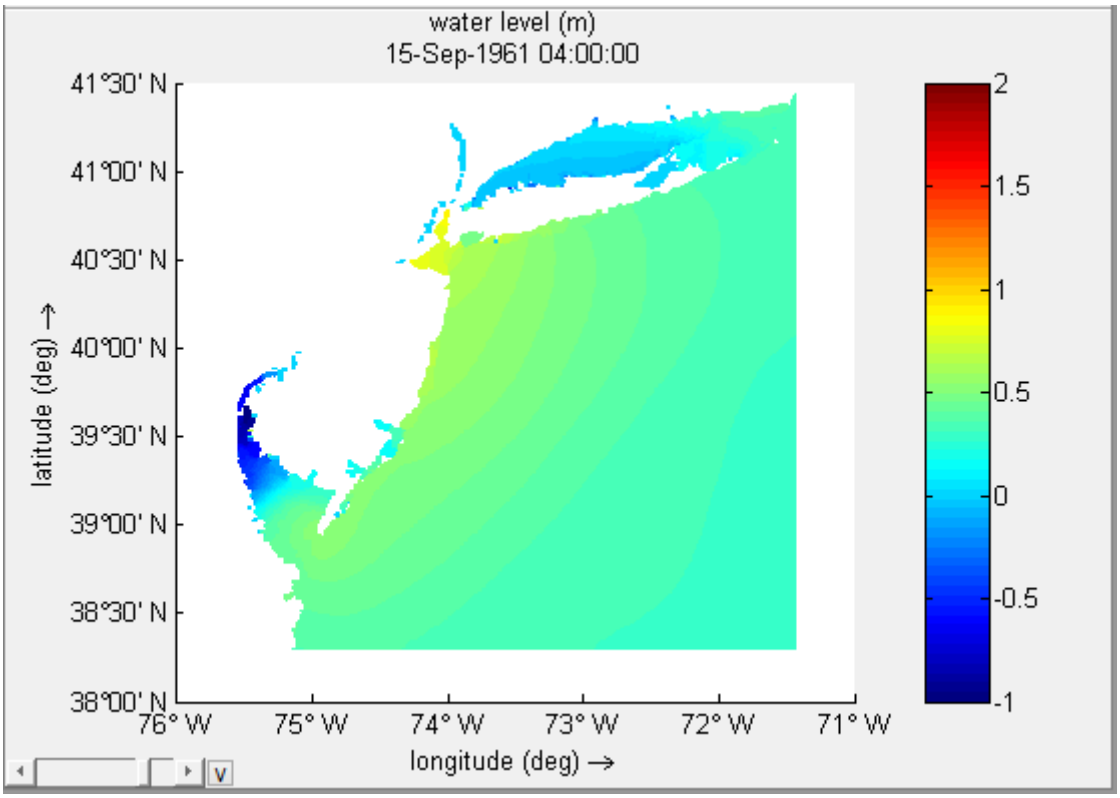

Figure I-11 - 1961 Unnamed Tropical Storm's water levels without spiderweb wind field (m)

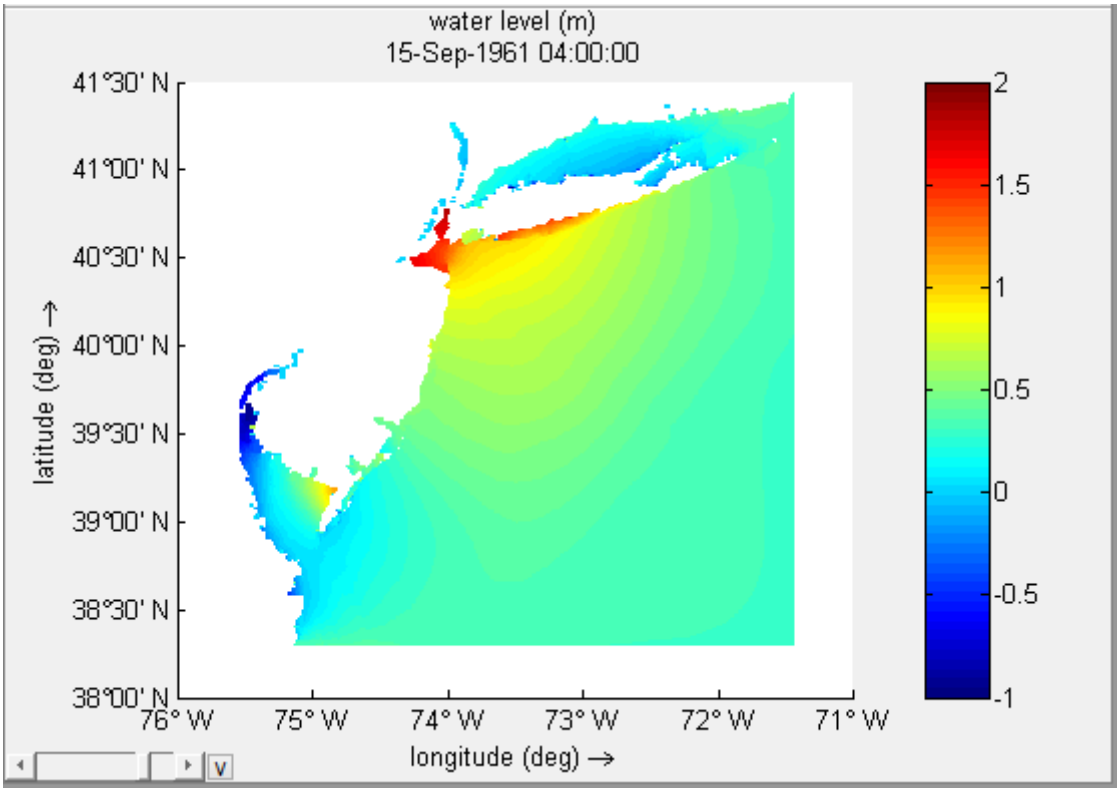

Figure I-12 - 1961 Unnamed Tropical Storm's water levels with spiderweb wind field (m)

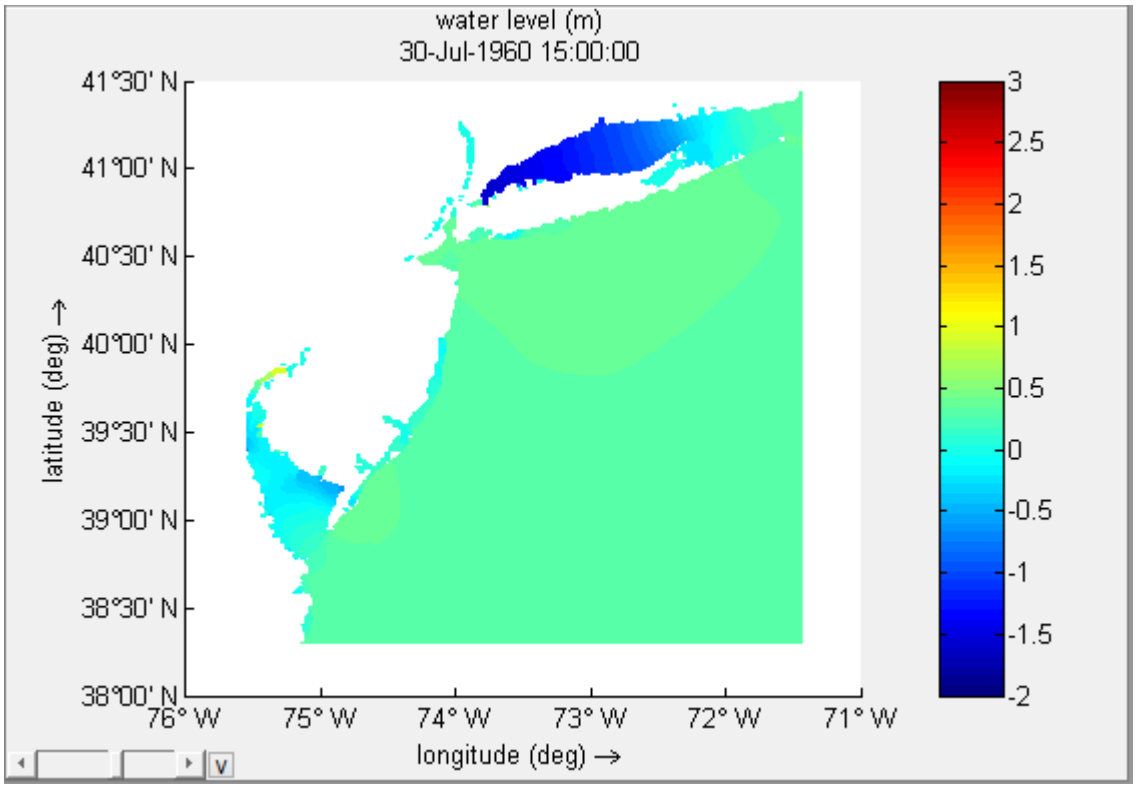

Figure I-13 - Tropical Storm Brenda's water levels without spiderweb wind field (m)

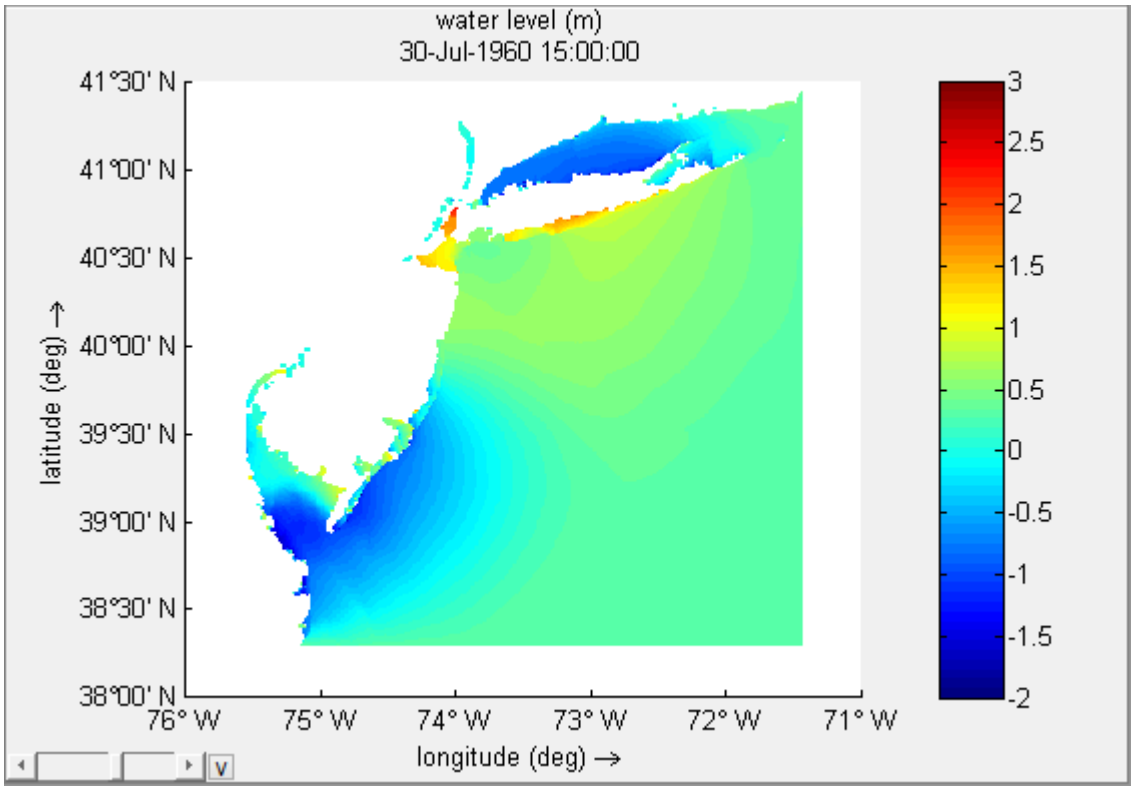

Figure I-14 - Tropical Storm Brenda's water levels with spiderweb wind field (m)

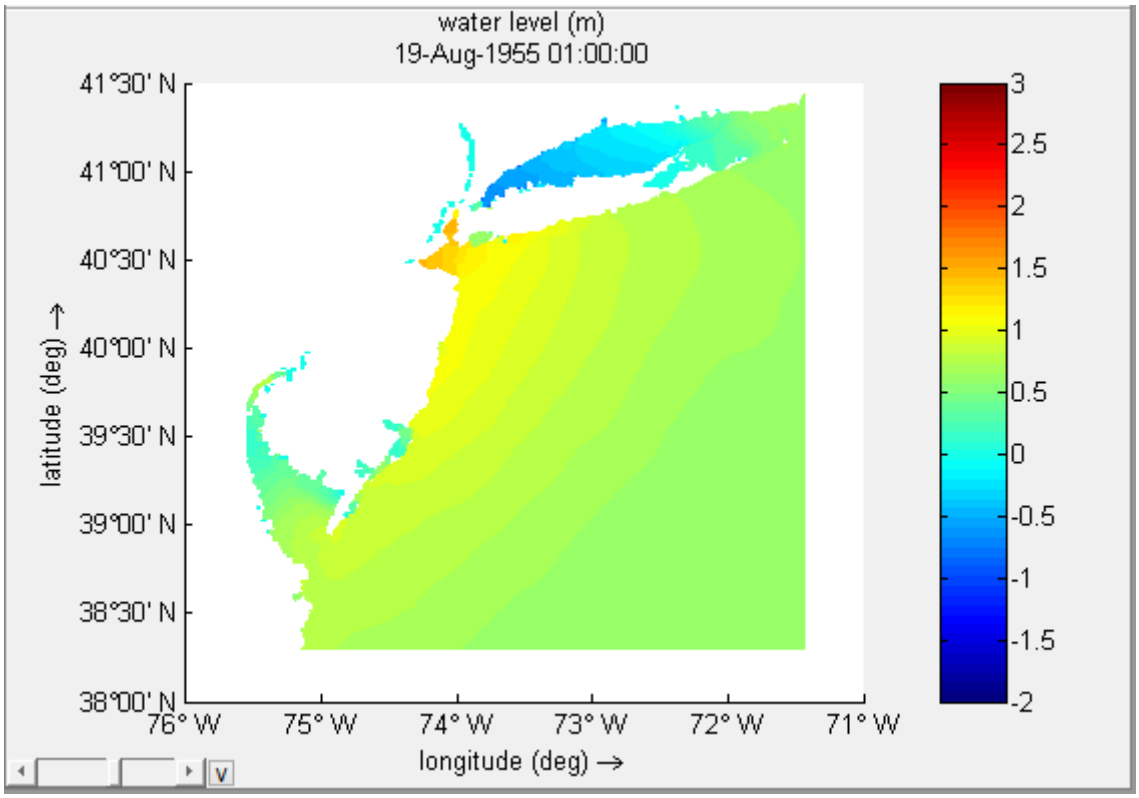

Figure I-15 - Tropical Storm Diane's water levels without spiderweb wind field (m)

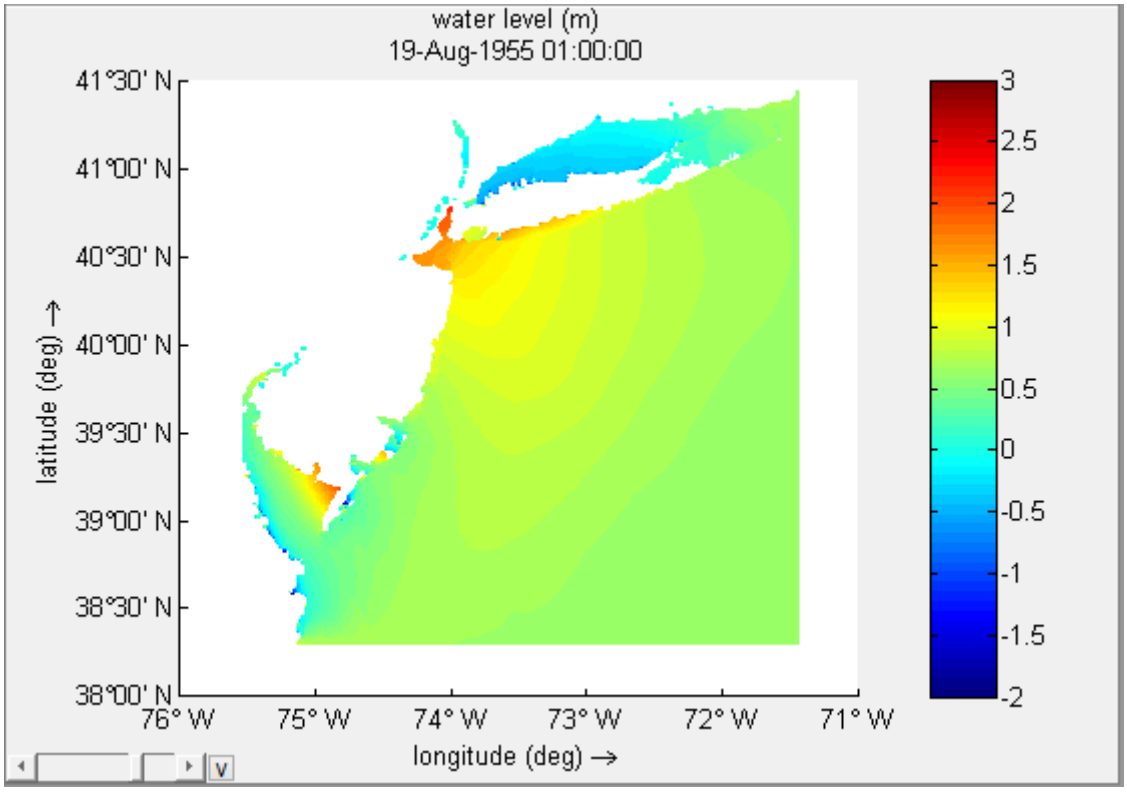

Figure I-16 - Tropical Storm Diane's water levels with spiderweb wind field (m)

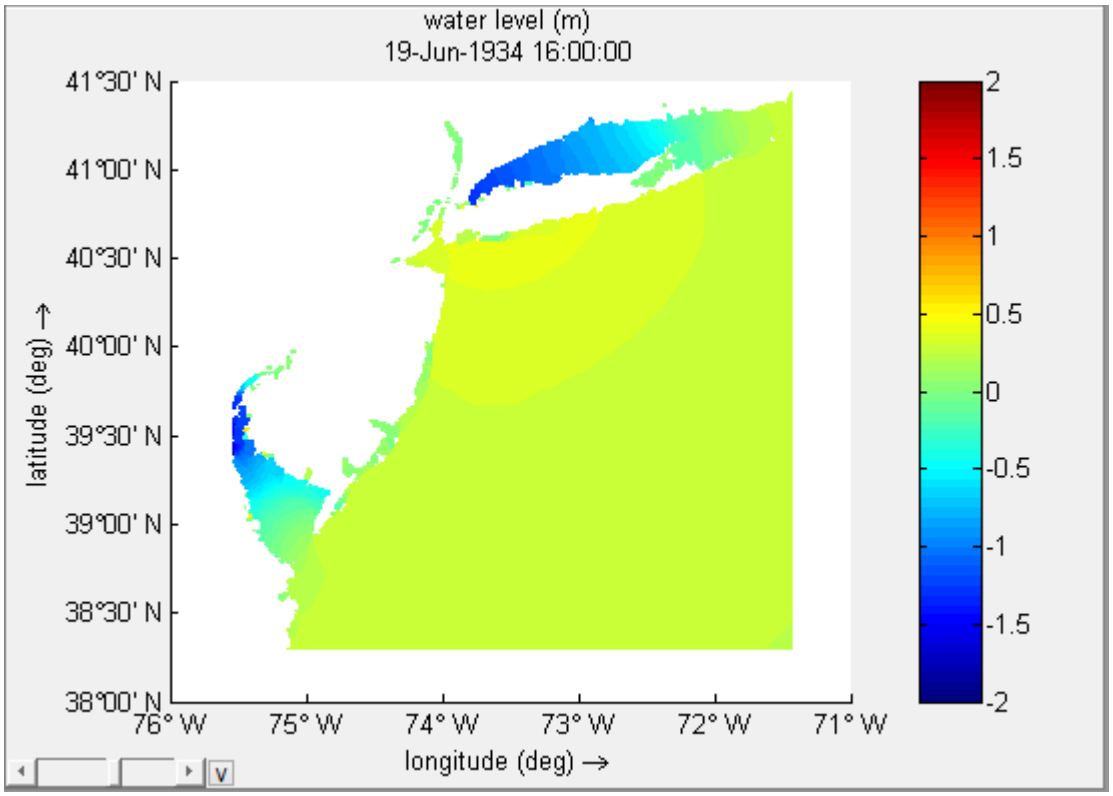

Figure I-17 -1934 Unnamed Tropical Storm's water levels without spiderweb wind field (m)

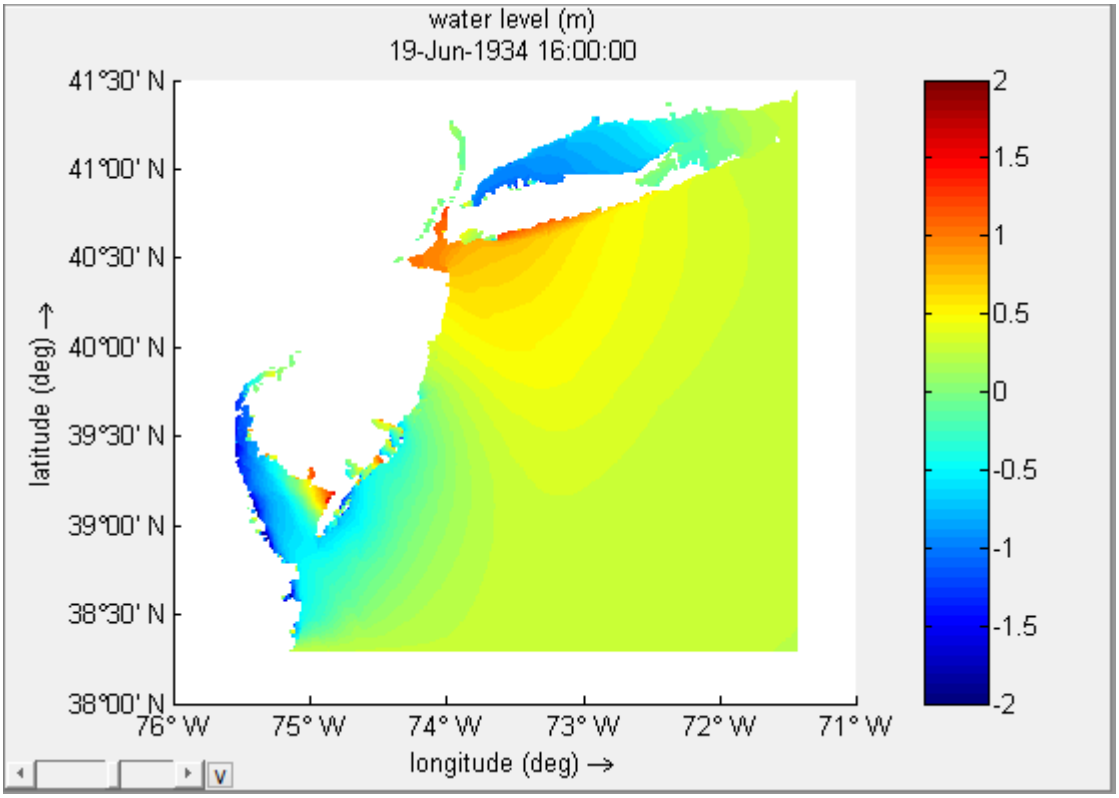

Figure I-18 - 1934 Unnamed Tropical Storm's water levels with spiderweb wind field (m)

APPENDIX II - SCENARIOS FOR PORTUGAL'S NW COAST

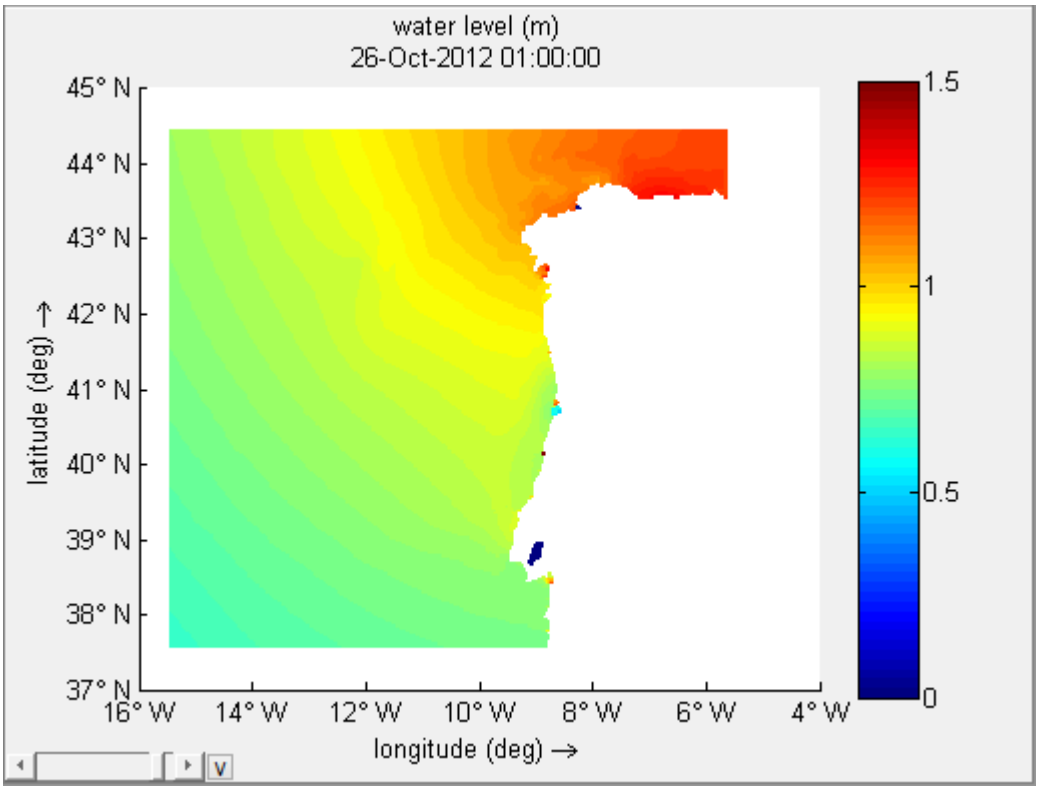

Figure II-1 - Tropical Storm Rafael's water levels without spiderweb wind field (m)

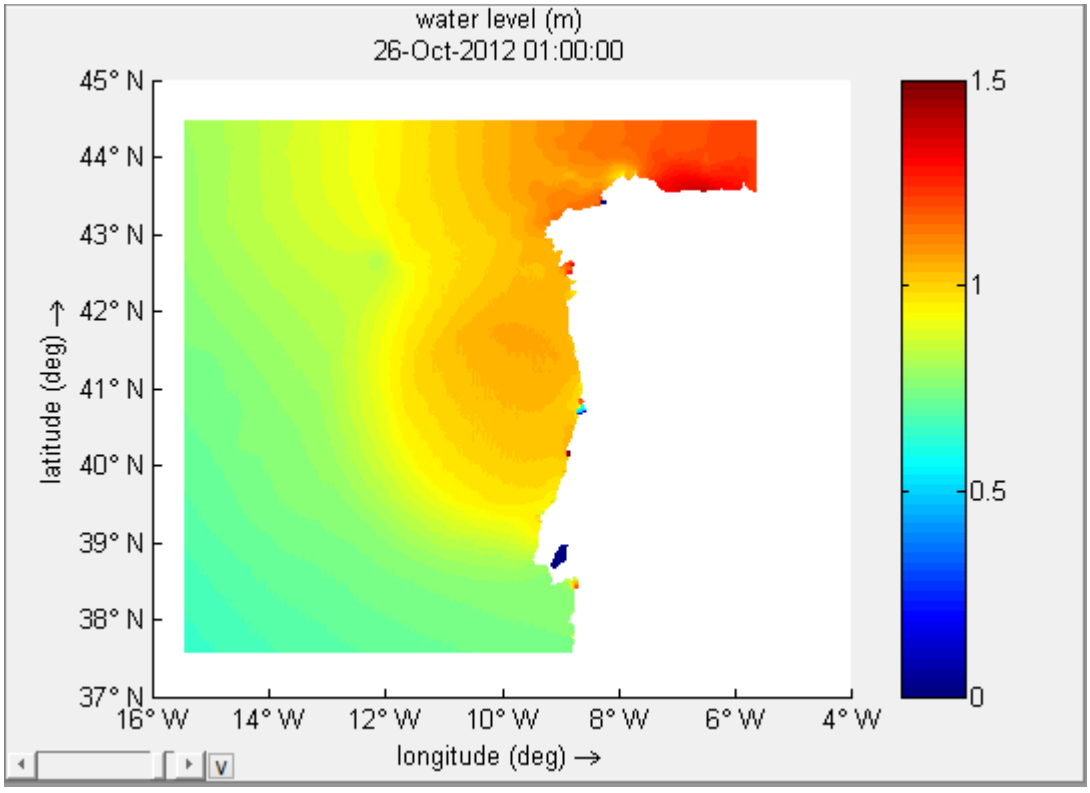

Figure II- 2 - Tropical Storm Rafael's water levels with spiderweb wind field (m)

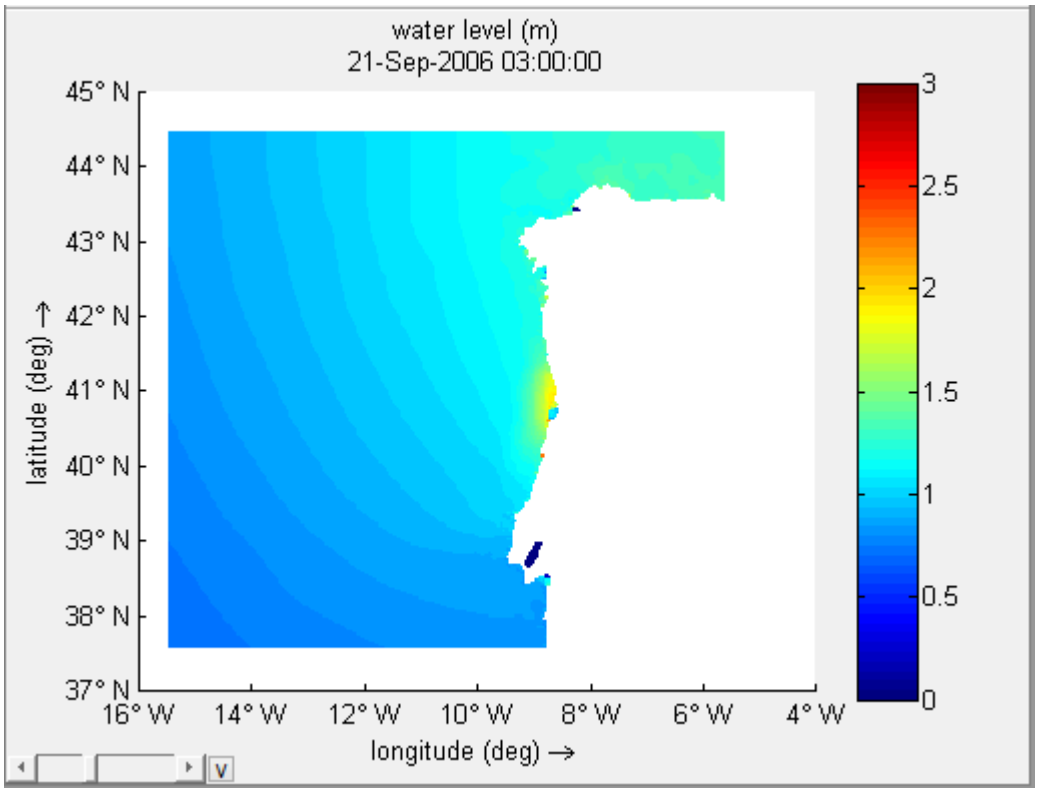

Figure II-3 - Tropical Storm Gordon's water levels without spiderweb wind field (m)

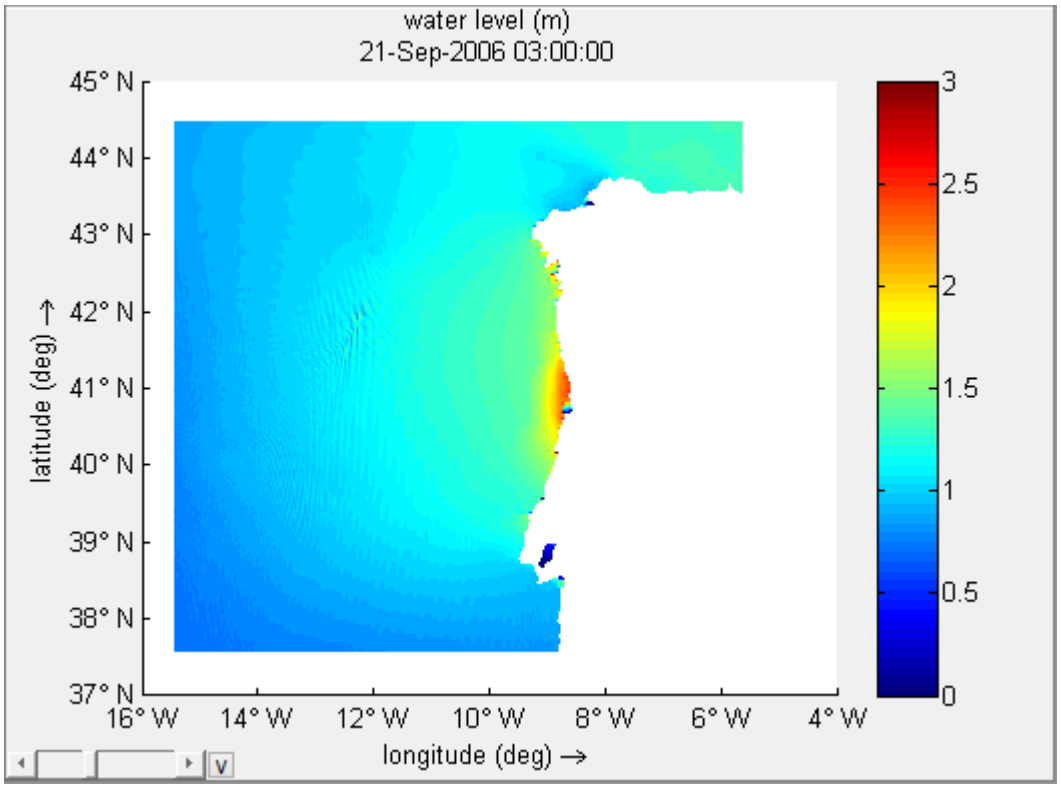

Figure II-4 - Tropical Storm Gordon's water levels with spiderweb wind field (m)

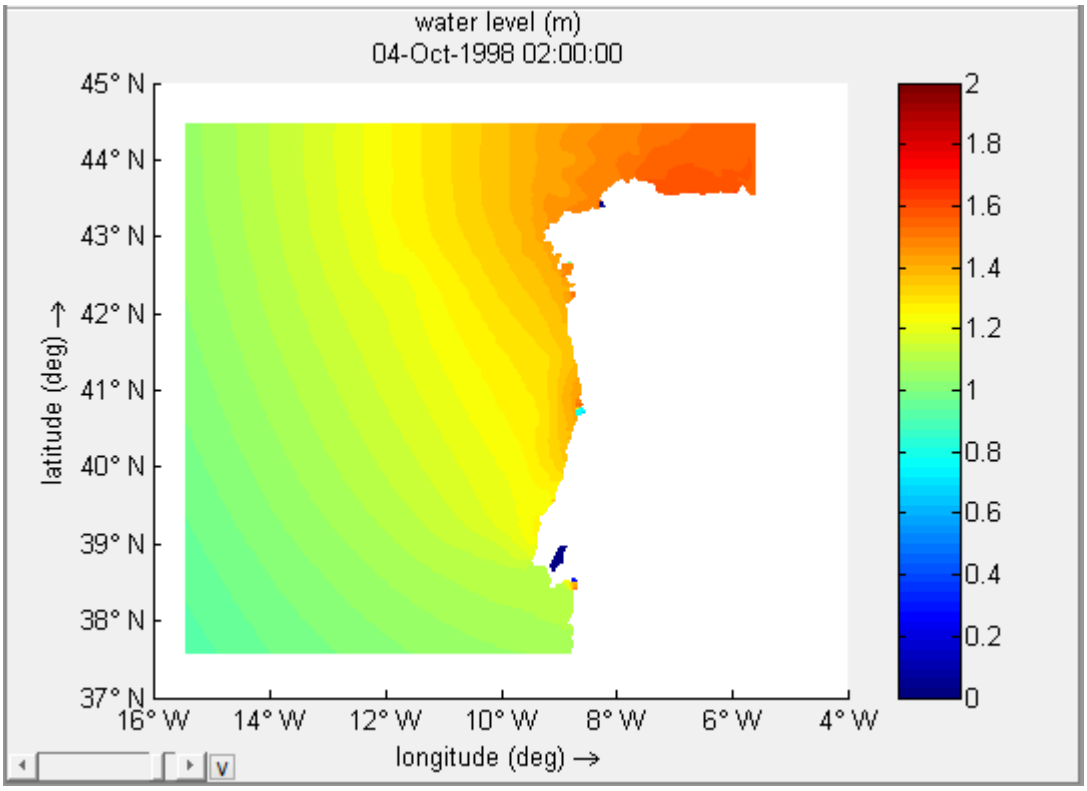

Figure II-5 - Tropical Storm Jeanne's water levels without spiderweb wind field (m)

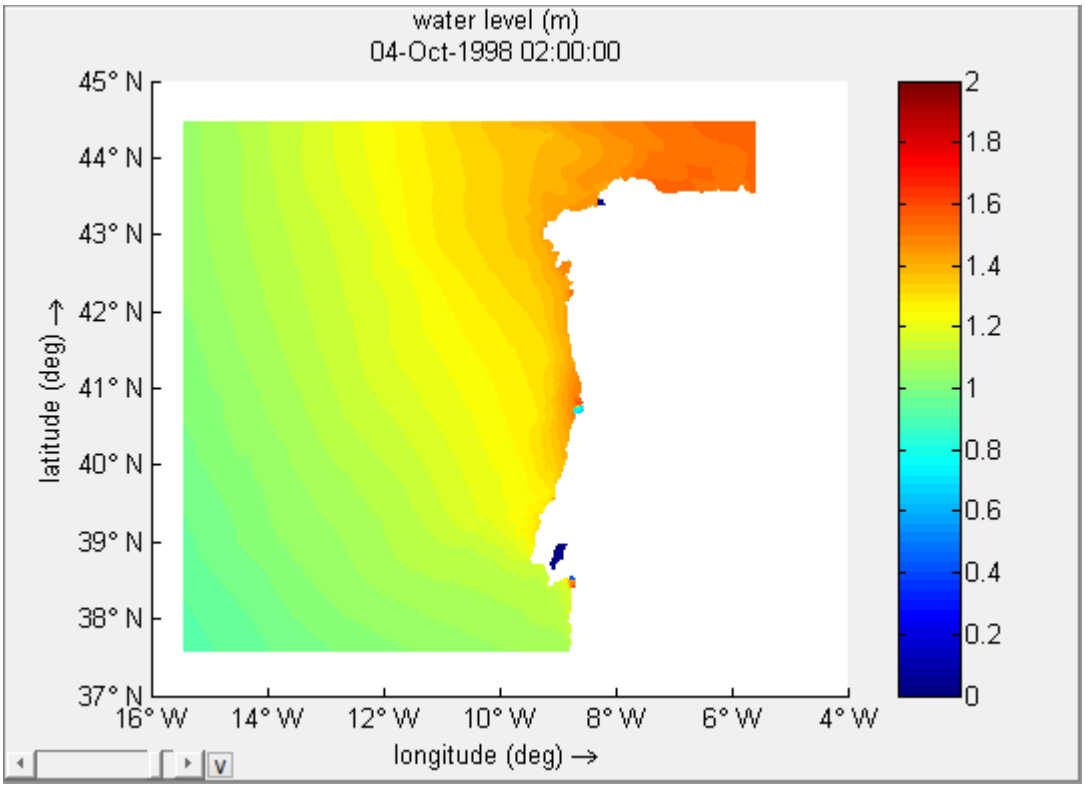

Figure II-6 - Tropical Storm Jeanne's water levels with spiderweb wind field (m)

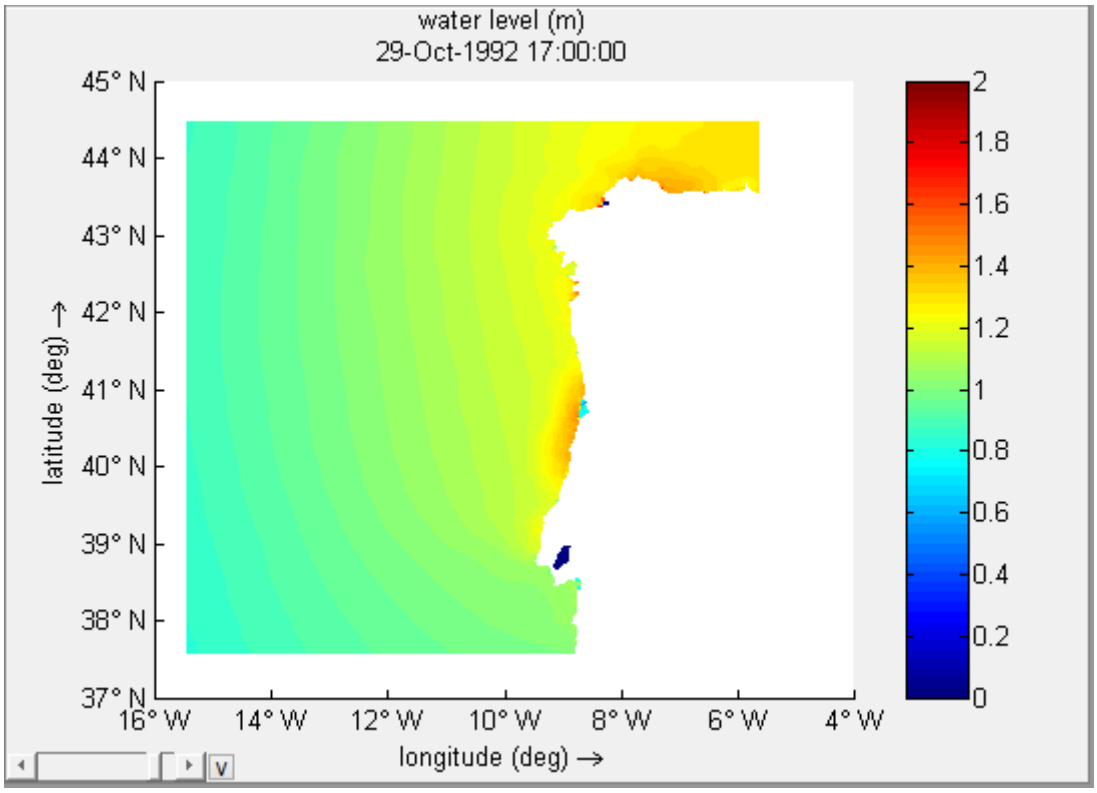

Figure II-7 - Tropical Storm Frances' water levels without spiderweb wind field (m)

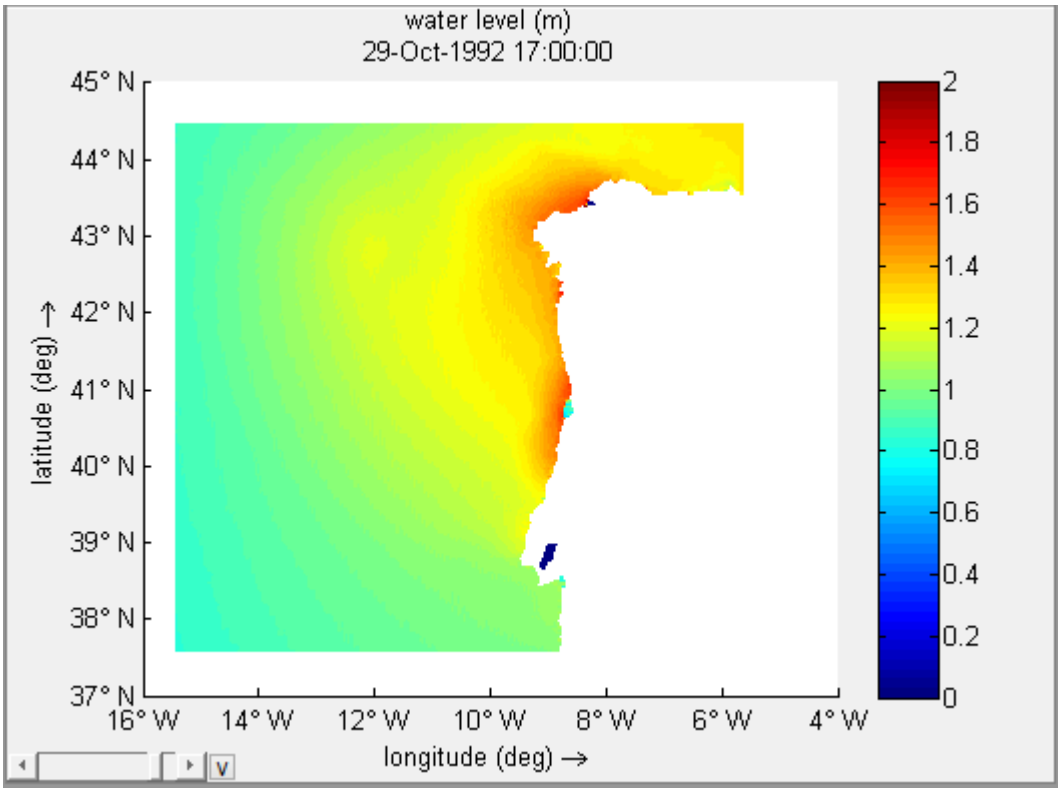

Figure II-8 - Tropical Storm Frances' water levels with spiderweb wind field (m)

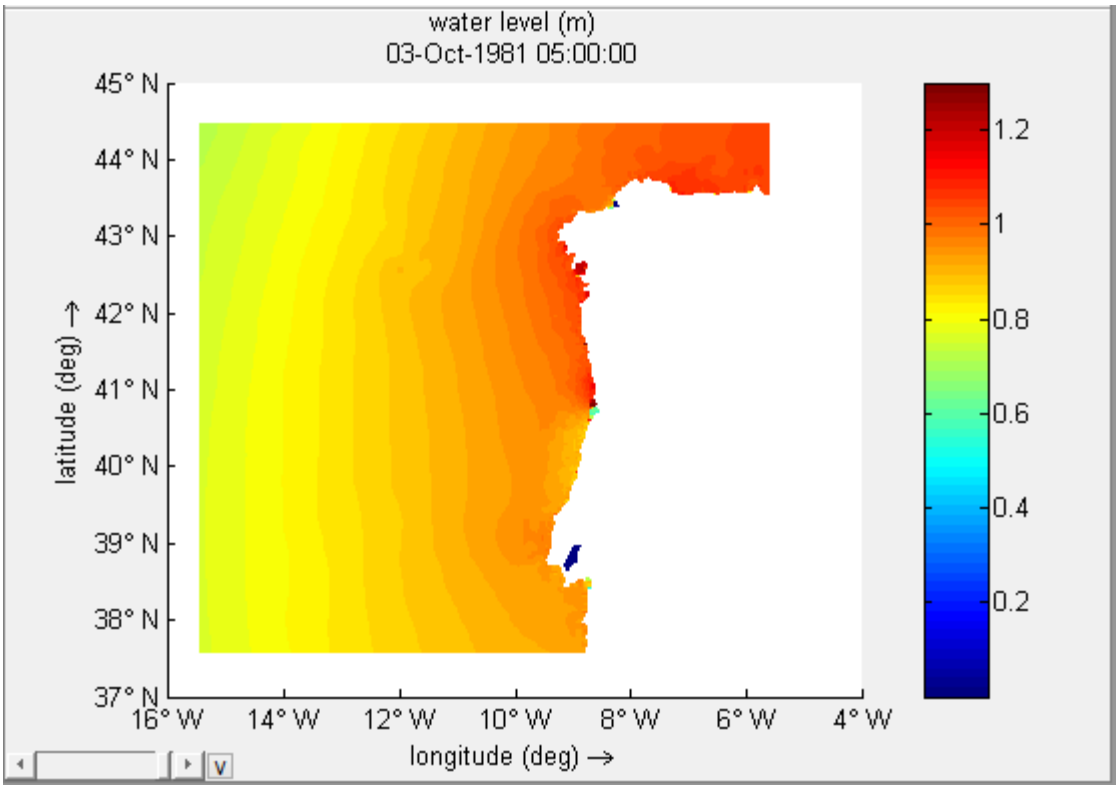

Figure II-9 - Tropical Storm Irene's water levels without spiderweb wind field (m)

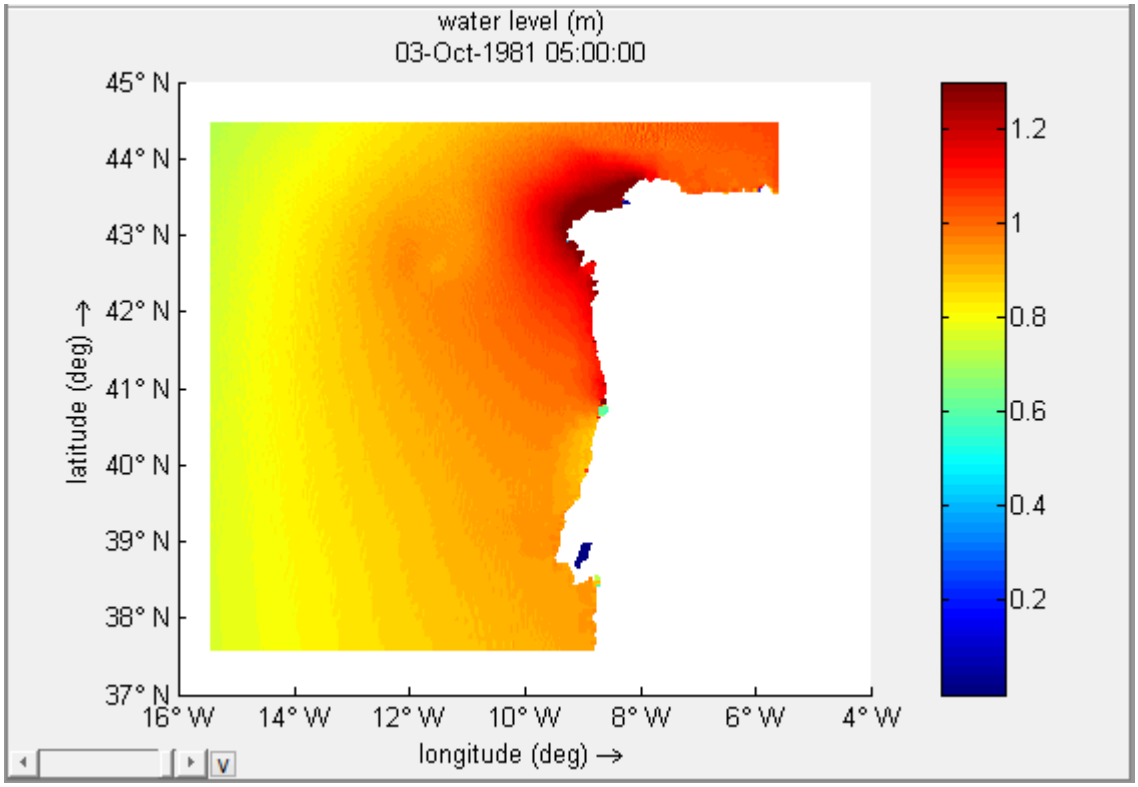

Figure II-10 - Tropical Storm Irene's water levels with spiderweb wind field (m)

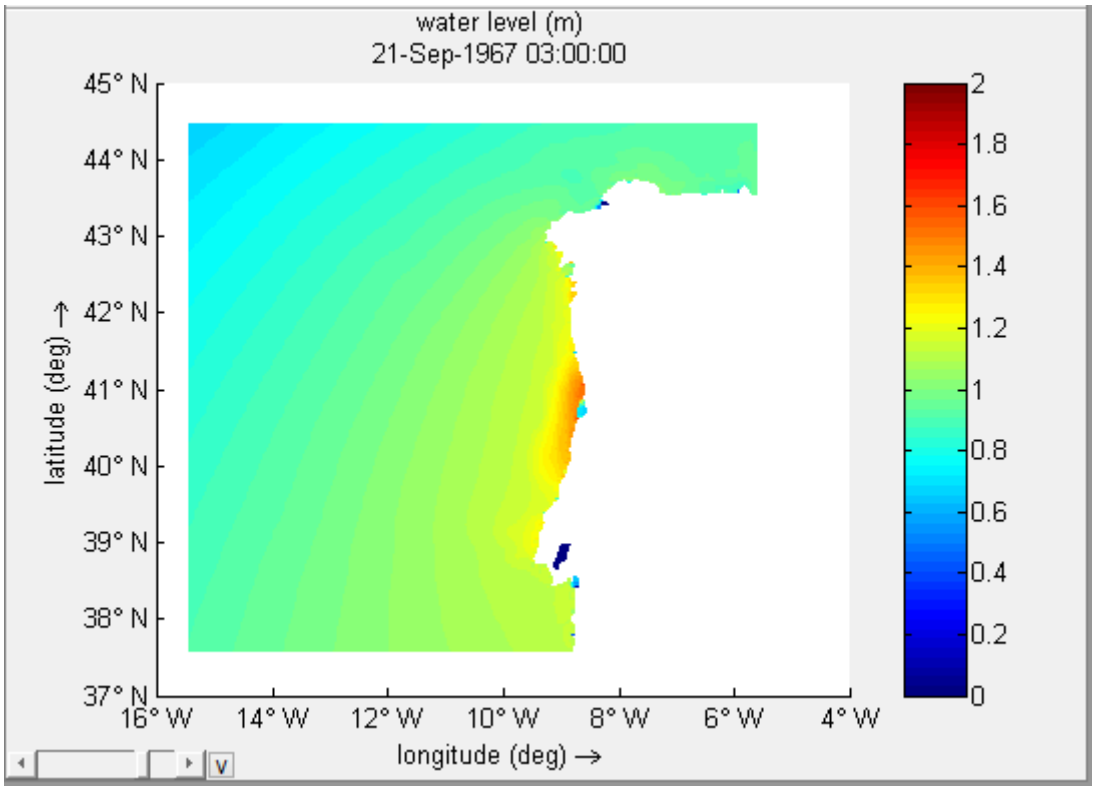

Figure II-11 - Tropical Storm Chloe's water levels without spiderweb wind field (m)

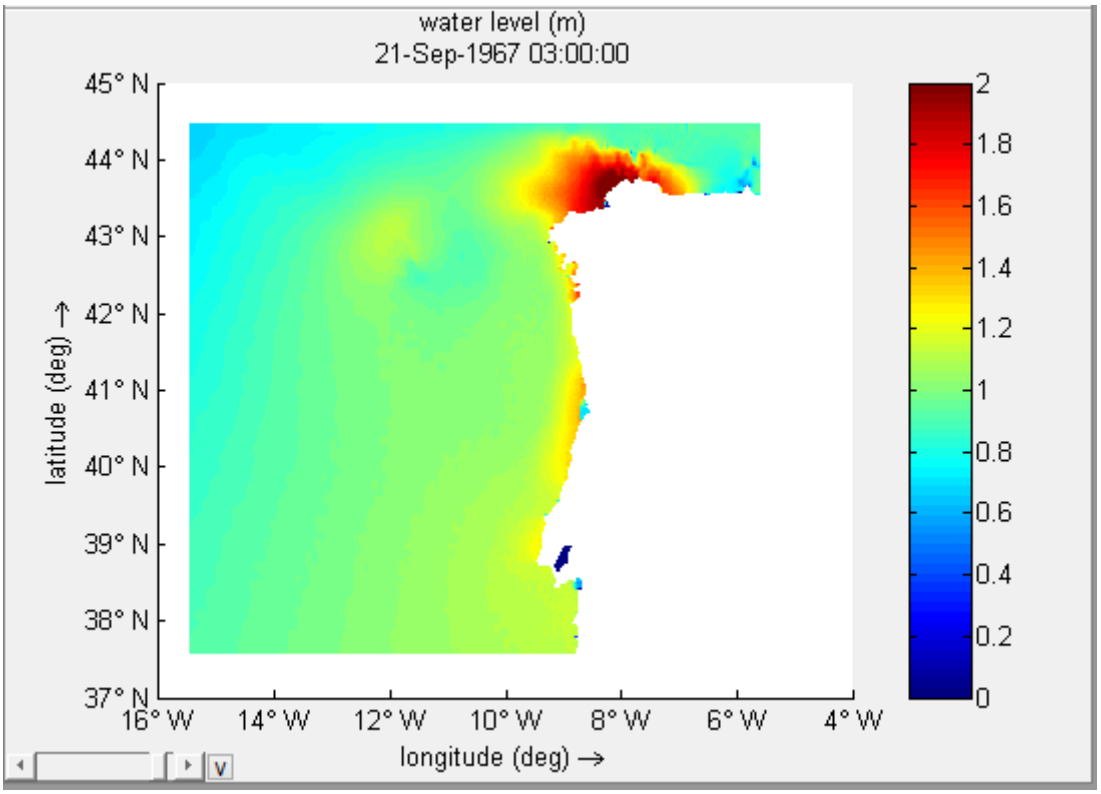

Figure II-12 - Tropical Storm Chloe's water levels with spiderweb wind field (m)

APPENDIX III - MATLAB SCRIPT (OBTAINING THE MAXIMUM MEAN SEA LEVEL)

```
maximo=0;
minimo=0;
celmax_i=0;
celmax_j=0;
celmin_i=0;
celmin_j=0;
tempo=0;
clc

ok=size(data.Val);
mm=ok(1);
ii=ok(2);
jj=ok(3);

for m=15:mm

    for i=1:ii
         for j=1:jj
            if data.Val(m,i,j)>maximo
            maximo=data.Val(m,i,j);
            celmax_i=i;
            celmax_j=j;
            tempo=m;
            end
         if data.Val(m,i,j)<minimo
           minimo=data.Val(m,i,j);
          celmin_i=i;
          celmin_j=j;
         end
        end
    end
end

plot(data.Val(:,celmax_i,celmax_j))
disp(' ');
disp('valor maximo positivo');
disp(maximo);
disp('celula do maximo positivo');
disp(celmax_i);
disp(celmax_j);
disp('valor maximo negativo');
disp(minimo);
disp('celula do maximo negativo');
disp(celmin_i);
disp(celmin_j);
disp('tempo');
disp(tempo);
```

APPENDIX IV - MEOW FOR NORTHEASTERN UNITED STATES COAST ENSEMBLE MEMBERS

Table IV-1 - MEOW for the NE United States coast ensemble members

No.	MEOW (m)	Vmax (km/h)	Category
241	6,151	140,337	Hurricane
240	2,817	101,655	TS
239	5,207	158,502	Hurricane
238	4,699	164,925	Hurricane
237	6,730	145,599	Hurricane
236	3,611	100,218	TS
235	1,272	0,000	TD
234	2,767	116,380	TS
233	7,233	157,274	Hurricane
232	2,835	92,631	TS
231	5,413	149,500	Hurricane
230	1,272	0,000	TD
229	2,251	109,818	TS
228	5,692	151,204	Hurricane
227	6,913	143,549	Hurricane
226	5,481	140,870	Hurricane
225	5,282	126,572	Hurricane
224	6,468	147,575	Hurricane
223	6,673	141,671	Hurricane
222	2,977	155,112	Hurricane
221	12,107	194,100	Hurricane
220	6,817	153,088	Hurricane
219	3,580	128,880	Hurricane
218	6,521	125,024	Hurricane
217	5,086	111,303	TS
216	1,766	168,044	Hurricane
215	11,963	190,648	Hurricane
214	3,797	149,567	Hurricane
213	6,728	187,515	Hurricane
212	3,207	104,013	TS
211	6,672	139,490	Hurricane
210	3,594	161,001	Hurricane
209	1,421	94,915	TS
208	2,571	120,652	Hurricane
207	2,865	111,932	TS
206	7,570	153,721	Hurricane
205	5,333	134,285	Hurricane
204	7,091	172,122	Hurricane
203	1,272	0,000	TD
202	3,517	153,179	Hurricane
201	6,515	159,051	Hurricane
200	8,444	151,933	Hurricane

199	1,382	148,194	Hurricane
198	6,415	131,435	Hurricane
197	3,011	94,604	TS
196	2,485	134,748	Hurricane
195	2,587	101,793	TS
194	6,970	145,240	Hurricane
193	3,811	99,007	TS
192	3,103	102,783	TS
191	7,924	168,017	Hurricane
190	6,253	168,588	Hurricane
189	1,673	82,254	TS
188	1,272	0,000	TD
187	4,588	109,604	TS
186	3,907	157,422	Hurricane
185	6,630	139,168	Hurricane
183	6,780	145,717	Hurricane
182	5,716	135,265	Hurricane
181	3,320	104,219	TS
180	6,672	127,697	Hurricane
179	1,562	0,000	TD
178	2,807	84,371	TS
177	2,916	111,526	TS
176	1,562	0,000	TD
175	6,609	184,752	Hurricane
174	8,853	168,071	Hurricane
173	3,094	92,342	TS
172	4,628	121,474	Hurricane
171	13,022	201,523	Hurricane
170	6,529	174,455	Hurricane
169	3,436	184,789	Hurricane
168	7,551	179,193	Hurricane
167	6,794	151,537	Hurricane
166	1,925	92,287	TS
165	3,815	131,760	Hurricane
164	10,988	189,210	Hurricane
163	5,435	132,890	Hurricane
162	10,953	181,246	Hurricane
161	10,395	160,953	Hurricane
160	8,854	175,213	Hurricane
159	9,568	176,723	Hurricane
158	9,126	166,938	Hurricane
157	10,253	169,380	Hurricane
156	3,095	123,647	Hurricane
155	2,162	93,708	TS
154	7,429	160,779	Hurricane
153	2,782	104,118	TS
152	10,979	180,421	Hurricane
151	2,139	100,000	TS

150	2,666	88,541	TS
149	3,995	142,982	Hurricane
148	1,562	0,000	TD
147	2,162	114,781	TS
146	1,562	0,000	TD
145	5,784	131,284	Hurricane
144	1,562	0,000	TD
143	8,534	186,942	Hurricane
142	8,932	189,396	Hurricane
141	2,055	97,553	TS
140	10,064	168,206	Hurricane
139	5,879	134,909	Hurricane
138	9,267	167,990	Hurricane
137	1,562	0,000	TD
136	2,781	109,772	TS
135	9,191	163,601	Hurricane
134	10,576	183,338	Hurricane
133	3,763	97,966	TS
132	5,772	145,066	Hurricane
131	8,667	179,782	Hurricane
130	5,575	133,266	Hurricane
129	1,562	0,000	TD
128	2,611	99,743	TS
127	1,562	0,000	TD
126	13,483	195,991	Hurricane
125	2,747	95,496	TS
124	9,276	162,302	Hurricane
123	1,785	112,706	TS
122	3,544	137,059	Hurricane
121	3,148	141,310	Hurricane
120	12,651	193,422	Hurricane
119	1,562	0,000	TD
118	5,680	132,934	Hurricane
117	1,648	110,331	TS
116	6,477	153,781	Hurricane
115	1,562	0,000	TD
114	11,918	189,173	Hurricane
113	3,627	103,075	TS
112	10,619	172,707	Hurricane
111	1,668	101,495	TS
110	6,339	115,741	TS
109	3,662	153,683	Hurricane
108	1,562	0,000	TD
107	5,772	139,717	Hurricane
106	1,562	0,000	TD
105	1,919	107,637	TS
104	1,924	116,513	TS
103	5,879	136,035	Hurricane

102	6,825	141,111	Hurricane
101	3,621	116,213	TS
100	8,919	176,303	Hurricane
99	5,683	136,480	Hurricane
98	1,562	0,000	TD
97	4,432	129,834	Hurricane
96	9,498	165,737	Hurricane
95	1,642	88,667	TS
94	11,695	182,841	Hurricane
93	2,971	129,322	Hurricane
92	3,317	194,680	Hurricane
91	7,397	165,512	Hurricane
90	7,133	161,766	Hurricane
89	5,198	141,767	Hurricane
88	2,832	123,909	Hurricane
87	6,742	142,123	Hurricane
86	7,439	167,672	Hurricane
85	10,391	172,159	Hurricane
84	1,562	0,000	TD
83	1,710	90,338	TS
82	5,268	139,625	Hurricane
81	3,862	113,012	TS
80	3,692	151,730	Hurricane
79	2,469	95,183	TS
78	3,822	153,969	Hurricane
77	8,748	171,945	Hurricane
76	9,567	162,525	Hurricane
68	10,764	179,626	Hurricane
67	3,575	155,250	Hurricane
66	1,562	0,000	TD
65	4,766	167,860	Hurricane
64	8,760	188,337	Hurricane
63	3,807	118,239	Hurricane
62	4,957	119,035	Hurricane
61	1,562	0,000	TD
60	1,562	0,000	TD
59	6,977	130,454	Hurricane
58	5,498	138,040	Hurricane
57	4,509	116,038	TS
56	5,789	182,654	Hurricane
55	12,400	186,327	Hurricane
54	12,400	186,327	Hurricane
53	7,097	189,532	Hurricane
52	11,363	180,851	Hurricane
51	1,562	0,000	TD
50	1,565	97,476	TS
49	3,927	124,446	Hurricane
48	1,562	0,000	TD

47	1,562	0,000	TD
46	2,930	104,623	TS
45	2,501	113,809	TS
44	1,619	92,353	TS
43	2,779	88,152	TS
42	2,449	130,639	Hurricane
41	7,317	168,647	Hurricane
40	3,398	151,573	Hurricane
39	1,562	0,000	TD
38	5,994	135,930	Hurricane
37	5,970	174,708	Hurricane
36	3,223	93,430	TS
35	6,056	151,394	Hurricane
34	5,047	125,435	Hurricane
33	1,562	0,000	TD
32	5,659	127,317	Hurricane
31	4,945	143,693	Hurricane
30	5,267	151,285	Hurricane
29	7,351	159,622	Hurricane
28	1,562	0,000	TD
27	4,783	144,377	Hurricane
26	5,515	150,017	Hurricane
25	7,628	160,444	Hurricane
24	3,873	152,447	Hurricane
23	7,852	185,336	Hurricane
22	3,945	169,187	Hurricane
20	4,435	114,885	TS
19	4,242	117,396	TS
18	8,857	154,320	Hurricane
17	5,639	164,922	Hurricane
16	3,091	92,197	TS
15	6,872	152,006	Hurricane
14	1,562	0,000	TD
13	7,045	139,782	Hurricane
12	11,999	191,655	Hurricane
11	9,726	160,940	Hurricane
10	10,790	194,452	Hurricane
9	1,996	171,851	Hurricane
8	9,284	182,855	Hurricane
7	5,544	172,686	Hurricane
6	3,707	111,284	TS
5	2,872	97,730	TS
4	2,014	82,872	TS
3	9,049	175,798	Hurricane
2	1,562	0,000	TD
1	1,562	0,000	TD

APPENDIX V - MEOW FOR NORTHWESTERN PORTUGUESE COAST ENSEMBLE MEMBERS

Table V- 1 - MEOW for the NW Portuguese coast ensemble members

No.	MEOW (m)	Vmax (km/h)	Category
211	1,146	73,870	TS
210	1,381	86,256	TS
209	1,885	99,683	TS
208	1,274	83,253	TS
207	1,381	77,093	TS
206	1,250	64,376	TS
205	1,326	95,887	TS
204	1,320	71,845	TS
203	1,249	81,976	TS
202	1,924	91,540	TS
201	1,294	69,229	TS
200	1,490	73,834	TS
199	1,127	65,473	TS
198	1,423	90,872	TS
197	1,214	102,304	TS
196	1,396	80,681	TS
195	1,509	75,007	TS
194	1,727	98,353	TS
193	1,754	98,668	TS
192	1,822	100,407	TS
191	1,216	76,554	TS
190	1,378	76,680	TS
189	1,708	102,490	TS
188	1,608	81,145	TS
187	1,166	102,537	TS
186	1,075	66,101	TS
184	1,236	74,417	TS
183	1,335	77,722	TS
182	1,550	80,089	TS
181	1,485	99,859	TS
180	1,570	99,032	TS
179	1,281	74,658	TS
178	1,407	84,214	TS
177	1,316	76,335	TS
176	1,496	99,071	TS
175	1,210	78,448	TS
174	1,199	70,651	TS
173	1,308	84,376	TS
172	1,116	62,115	TS
171	1,166	67,023	TS
170	1,149	55,509	TD
169	1,203	71,956	TS

168	1,191	105,669	TS
167	1,496	97,098	TS
166	1,541	82,162	TS
165	1,805	98,891	TS
164	1,298	97,115	TS
163	1,055	66,267	TS
162	1,373	82,246	TS
161	1,152	72,471	TS
160	2,003	102,809	TS
159	2,321	115,494	TS
158	1,141	75,976	TS
157	1,258	63,622	TS
156	1,664	79,765	TS
155	1,456	115,284	TS
154	1,168	64,269	TS
153	1,212	80,419	TS
152	1,367	79,862	TS
151	1,467	107,784	TS
150	1,162	94,095	TS
149	1,182	82,152	TS
148	1,278	90,879	TS
147	1,590	88,443	TS
146	1,179	85,139	TS
145	1,743	105,933	TS
144	1,988	105,125	TS
143	1,170	73,051	TS
142	1,299	78,118	TS
141	1,089	116,694	TS
140	1,290	81,819	TS
139	1,189	68,478	TS
138	1,603	89,744	TS
137	1,562	106,087	TS
136	1,227	73,705	TS
135	1,231	81,962	TS
134	1,669	87,261	TS
133	1,139	50,370	TD
132	1,128	64,143	TS
131	1,377	70,120	TS
130	1,614	96,781	TS
129	1,439	100,246	TS
128	1,386	111,797	TS
127	1,285	102,914	TS
126	1,173	66,698	TS
125	1,926	90,526	TS
124	1,294	108,048	TS
123	2,023	106,578	TS
122	1,443	103,191	TS
121	1,915	117,406	TS

120	1,607	104,751	TS
119	1,311	112,949	TS
118	1,514	72,461	TS
117	1,360	79,485	TS
116	2,077	111,905	TS
115	2,051	99,383	TS
114	1,240	72,173	TS
113	1,406	69,600	TS
112	1,466	77,836	TS
111	1,211	69,864	TS
110	1,143	81,359	TS
109	1,463	103,416	TS
108	1,269	78,290	TS
107	1,220	82,233	TS
106	1,224	81,300	TS
105	1,155	58,630	TD
104	1,721	85,281	TS
103	2,010	96,605	TS
102	1,120	74,795	TS
101	1,252	71,052	TS
100	1,304	83,300	TS
98	1,509	87,849	TS
97	1,208	7,241	TD
96	1,375	73,266	TS
95	1,215	87,953	TS
94	1,371	83,443	TS
93	2,212	124,902	Hurricane
92	1,208	0,000	TD
91	1,378	87,441	TS
90	1,339	84,033	TS
89	1,336	106,450	TS
88	1,208	0,000	TD
87	1,533	80,580	TS
86	1,267	81,810	TS
85	2,003	108,702	TS
84	1,796	92,694	TS
83	1,420	67,982	TS
82	1,225	99,567	TS
81	1,238	81,489	TS
80	1,370	70,597	TS
79	1,790	99,843	TS
78	1,208	0,000	TD
77	1,311	81,040	TS
76	1,471	78,077	TS
75	1,208	6,313	TD
74	1,675	101,084	TS
73	1,337	84,425	TS
72	1,560	82,361	TS

71	2,124	104,732	TS
70	1,303	69,161	TS
69	1,658	79,170	TS
68	1,438	108,156	TS
67	1,685	108,586	TS
66	1,302	80,837	TS
65	1,219	78,326	TS
64	1,208	0,000	TD
63	1,329	81,790	TS
62	1,705	86,683	TS
61	1,369	80,063	TS
60	1,245	65,862	TS
59	1,208	0,000	TD
58	1,550	83,771	TS
57	1,208	19,596	TD
56	1,343	74,772	TS
55	1,215	105,475	TS
54	1,511	82,636	TS
53	1,208	0,000	TD
52	1,578	124,183	Hurricane
51	1,319	83,020	TS
50	1,495	112,326	TS
49	1,496	77,603	TS
48	1,851	103,347	TS
47	1,208	15,502	TD
46	1,208	0,000	TD
45	1,208	5,731	TD
44	1,799	83,275	TS
43	1,319	94,334	TS
42	1,208	11,490	TD
41	1,522	81,053	TS
40	1,208	5,139	TD
39	1,624	80,184	TS
38	1,208	0,000	TD
37	1,208	2,934	TD
36	1,208	0,000	TD
35	1,402	93,790	TS
34	1,542	79,795	TS
33	1,222	72,638	TS
32	1,376	77,719	TS
31	1,215	75,422	TS
30	1,415	86,282	TS
29	1,851	94,165	TS
28	1,208	4,774	TD
27	1,383	80,846	TS
26	2,146	113,356	TS
25	1,208	0,000	TD
24	1,315	91,229	TS

23	1,464	82,256	TS
22	1,208	0,205	TD
21	1,220	85,046	TS
20	1,428	78,011	TS
19	1,208	0,000	TD
18	1,291	82,997	TS
17	1,375	92,730	TS
16	1,208	0,000	TD
15	1,208	2,285	TD
14	1,286	78,108	TS
13	1,388	98,271	TS
12	1,208	0,000	TD
11	1,208	0,105	TD
10	1,947	107,205	TS
9	1,322	64,108	TS
8	2,054	99,016	TS
7	1,387	81,089	TS
6	1,543	79,462	TS
5	1,208	0,000	TD
4	1,318	70,079	TS
3	1,237	78,116	TS
2	2,253	124,457	Hurricane
1	1,298	86,028	TS